JYU DISSERTATIONS 859

Emilia Virtanen

Recovery and Separation of Rare Earth Elements by Utilizing α-aminophosphonic Acids as Precipitants and Adsorbents

UNIVERSITY OF JYVÄSKYLÄ
FACULTY OF MATHEMATICS
AND SCIENCE

JYU DISSERTATIONS 859

Emilia Virtanen

Recovery and Separation of Rare Earth Elements by Utilizing α-aminophosphonic Acids as Precipitants and Adsorbents

Esitetään Jyväskylän yliopiston matemaattis-luonnontieteellisen tiedekunnan suostumuksella
julkisesti tarkastettavaksi Ylistönrinteen auditoriossa Fys1
joulukuun 11. päivänä 2024 kello 12.

Academic dissertation to be publicly discussed, by permission of
the Faculty of Mathematics and Science of the University of Jyväskylä,
in Ylistönrinne, auditorium Fys1, on December 11, 2024, at 12 o'clock.

JYVÄSKYLÄN YLIOPISTO
UNIVERSITY OF JYVÄSKYLÄ

JYVÄSKYLÄ 2024

Editors
Jani Moilanen
Department of Chemistry, University of Jyväskylä
Päivi Vuorio
Open Science Centre, University of Jyväskylä

ISBN 978-952-86-0432-7
ISSN 2489-9003

Permanent link to this publication: http://urn.fi/URN:ISBN:978-952-86-0432-7

ABSTRACT

Virtanen, Emilia
Recovery and separation of rare earth elements by utilizing α-aminophosphonic acids as precipitants and adsorbents
Jyväskylä: University of Jyväskylä, 2024, 83 p. + original articles
(JYU Dissertations
ISSN 2489-9003; 859)
ISBN 978-952-86-0432-7 (PDF)

Rare earth elements (REE) are essential elements in various modern technological applications and renewable energy production. As the world shifts towards greener technologies, the consumption of REEs is expected to rise. Therefore, their efficient separation from each other, as well as recovery from their minerals and waste streams, will be of great importance. During the past decade, aminophosphonates have attracted attention as extracting agents in liquid-liquid extraction and as adsorbents for REE separation and recovery. Their ability to act as precipitation agents, however, has yet to be studied. In this dissertation, the α-aminophosphonates were first investigated as precipitation agents for REEs and Th and U, which are present in the same ores. The precipitation agents were found to efficiently precipitate Sc, Th, and U at pH 1, whereas other REEs precipitated around pH 4. The separation between adjacent REEs was low. Second, the self-synthetized α-aminophosphonate was utilized as an additive in 3D-printed filters to recover REEs from mining wastewater. The recovery of REEs (Sc, Y, Nd, Dy) from the mining wastewater was the most effective at pH 2, as the adsorption of most non-target elements (Co, Cu, Al, Ca, K, Zn) was small. Overall, the developed recovery process for REEs yielded a final eluate containing 69.9% of REEs, a clear improvement over the initial concentration of 8.3%. Third, the separation process for separating REEs, B, Al, Fe, Co, and Cu from NdFeB magnets was developed by combining methanesulfonic acid (MSA) leaching, precipitation, and solid-phase extraction. In the solid-phase extraction step ecofriendly MSA, ammonium chloride and potassium oxalate were utilized as eluents and 3D-printed filters containing commercial α-aminophosphonate ion-exchanger (Lewatit TP260) as an adsorbent. With the developed separation process Fe and REEs were recovered with 97.6% and 99.4% purity, respectively. Furthermore, the other elements were separated into less complex fractions. The work presented in this dissertation provides new separation methods for REEs and other critical elements utilizing both precipitation and solid-phase extraction methods. Additionally, this dissertation contributes new information on separating REEs, Th, and U using α-aminophosphonic acid precipitants, which had yet to be investigated.

Keywords: Rare earth element, α-aminophosphonic acid, critical element, 3D printing, adsorption, precipitation, secondary source

TIIVISTELMÄ

Virtanen, Emilia
Harvinaisten maametallien talteenotto ja erottaminen sakkauttamalla ja adsorboimalla käyttäen α-aminofosfonaatteja.
Jyväskylä: Jyväskylän yliopisto, 2024, 83 s. + alkuperäiset artikkelit
(JYU Dissertations
ISSN 2489-9003; 859)
ISBN 978-952-86-0432-7 (PDF)

Harvinaisia maametalleja (Rare earth element, REE) hyödynnetään useissa nykyteknologian sovelluksissa ja uusiutuvan energian tuotannossa. Etenkin vihreiden teknologioiden lisääntyessä myös tarve REE:lle kasvaa tulevaisuudessa ja siten niiden tehokas talteenotto sekä niiden mineraaleista että jätevirroista tulee olemaan entistä tärkeämpää jatkossa. Etenkin viime vuosikymmenen aikana aminofosfonaattien on tutkittu olevan hyviä neste-nesteuuttoreagensseja ja adsorbenttejä REE:n talteenottamiseksi. REE:lle α-aminofosfonaatteja ei ole kuitenkaan vielä tutkittu sakkautusreagensseina. Tässä väitöskirjatyössä tutkimme α-aminofosfonaatteja ensin sakkautusreagensseina REE:n lisäksi samoissa mineraaleissa esiintyville Th:lle ja U:lle pH:n funktiona. pH 1:ssä havaittiin Sc, Th, ja U sakkautuvan tehokkaasti, kun taas REE:t sakkautuivat tehokkaammin pH 4:ssä. Vierekkäisten elementtien erottaminen oli kuitenkin tehotonta. Seuraavaksi itsesyntetisoitua α-aminofosfonaattia hyödynnettiin additiivinä 3D printatuissa suodattimissa, joita tutkittiin REE:n talteenottamiseksi happamista kaivosjätevesistä. REE:n (Sc, Y, Nd, Dy) talteenottoon pH 2 osoittautui parhaaksi, sillä suurin osa kaivosveden muista alkuaineista (Co, Cu, Al, Ca, K, Zn) ei adsorboitunut tässä pH:ssa. REE:n osuutta saatiin siten liuoksessa konsentroitua 8,3 prosentista 69,9 prosenttiin. Viimeisenä tutkittiin erotteluprosessia, jossa REE:t, B, Al, Fe, Co ja Cu talteenotetaan neodyymimagneeteista. Prosessissa yhdistettiin liuotus, sakkautus ja kiinteäfaasiuutto käyttäen 3D printattuja suodattimia, joissa adsorboivana aineena toimi kaupallinen α-aminofosfonaattia sisältävä ioninvaihtohartsi Lewatit TP260. 3D printattujen suodattimien kiinteäfaasiuutossa käytettiin eluentteina ympäristöystävällistä metaanisulfonihappoa, ammoniumkloridia ja kaliumoksalaattia. Erotusprosessilla Fe ja REE:t saatiin 97,6% ja 99,4% puhtaisiin fraktioihin. Muut alkuaineet saatiin omiin vähemmän monimutkaisiin fraktioihinsa. Tässä väitöskirjassa esitetty työ tuo uutta tietoa REE:n ja muiden kriittisten alkuaineiden erotteluun käyttäen joko sakkautus- tai adsorptiomenetelmää. Lisäksi α-aminofosfonaattien käyttämistä REE:n, Th ja U:n sakkauttamiseen tutkittiin ensimmäistä kertaa.

Asiasanat: Harvinaiset maametallit, α-aminofosfonaatit, kriittiset alkuaineet, 3D printatut materiaalit, adsorptio, sakkautus

Author

Emilia Virtanen
Department of Chemistry
University of Jyväskylä
emilia.j.virtanen@jyu.fi
ORCID 0000-0003-3856-914X

Supervisors

Assistant Professor Jani Moilanen
Department of Chemistry
University of Jyväskylä

Professor Ari Väisänen
Department of Chemistry
University of Jyväskylä

Assistant Professor Kaisa Helttunen
Department of Chemistry
University of Jyväskylä

Reviewers

Sami Virolainen
Unit of Separation Science
Lappeenranta University of Technology

Martina Petranikova
Department of Chemistry and Chemical Engineering
Chalmers University of Technology

Opponent

Ulla Lassi
Research Unit of Sustainable Chemistry
University of Oulu

PREFACE

The research presented in this dissertation was carried out at the University of Jyväskylä between 2020 and 2024.

When I started my studies at the Department of Chemistry, the head of the department at the time compared obtaining a bachelor's, master's, and PhD degrees to climbing the long set of stairs on the Ylistönrinne campus. Climbing the first three set of stairs is like getting your bachelor's degree. The next two set of stairs represents the time spent getting your master's, and the final steps that go all the way to the top are your PhD degree. Back then I thought to myself that I would never climb that last set of stairs, not because I lacked confidence about my ability to do so, but because I really detested public speaking, which the PhD journey culminates in. However, after being introduced to a welcoming research group, the staff of the department, and an interesting research topic during my master's studies, it was no wonder I challenged myself and chose to climb those stairs.

First, I would like to warmly thank my supervisors Assistant Professor Jani Moilanen, Professor Ari Väisänen, and Assistant Professor Kaisa Helttunen for providing me with invaluable help in their areas of expertise and supervising me for the past four years. I would especially like to thank Jani for his fast responses, availability for conversations, and various helpful comments regarding the research topic. You have helped me complete this dissertation faster than I would have without you. Thank you also for providing a working atmosphere for free and relaxed discussions. Sincere thanks also to the two reviewers of this dissertation, Associate Professors Sami Virolainen and Martina Petranikova, for taking the time to review it.

I would like to thank the Main Group Chemistry research group for generally being good company during lunch and coffee breaks over the past four years. My labmates Esa and Krista for either helping me with experimental work or just being there as mental support. Most of the days working together have been a joy, even when the chemistry in the lab did not go as planned.

I want to thank my family for being supportive, especially my mom, who has always been very excited about me earning a PhD. Last, I want to thank Kasperi for being there during the stressful days and understanding the difficulties of working towards a PhD. Your mental support has been irreplaceable.

Jyväskylä, 9 October 2024
Emilia Virtanen

LIST OF ORIGINAL PUBLICATIONS

(I) Virtanen, E. J., Perämäki, S., Helttunen, K., Väisänen, A. Moilanen, J. O. Alkyl-Substituted Aminobis(phosphonates)—Efficient Precipitating Agents for Rare Earth Elements, Thorium, and Uranium in Aqueous Solutions. *ACS Omega* **6**, 23977–23987 (2021).

(II) Virtanen, E. J. Kukkonen, E., Yliharju, J., Tuomisto, M., Frimodig, J., Kinnunen, K., Lahtinen, E., Hänninen, M. M., Väisänen, A., Haukka, M., Moilanen, J. O., Recovery of rare earth elements from mining wastewater with aminomethylphosphonic acid functionalized 3D-printed filters. *Separation and Purification Technology* **353**, 128599 (2025).

(III) Virtanen, E. J., Yliharju, J., Kukkonen, E., Christiansen, T., Tuomisto, M., Miettinen, A., Väisänen, A., Moilanen J. O., Separating critical elements from NdFeB magnets with aminophosphonic acid functionalised 3D printed filters and their detailed structural characterisation with X-ray tomography, *manuscript*

Author's contribution

The author has carried out all syntheses, and most of the spectroscopic studies, regarding chemical characterization of the complexes and the 3D-printed filters reported on in Papers **I–III**. For Paper **I**, the author conducted all complexation and precipitation studies, and for Papers **II** and **III**, nearly all the solid-phase–extraction studies. Apart from X-ray tomography data, all acquired data was primarily analyzed by the author. The author wrote the initial drafts of all three papers, prepared the figures, compiled the data, except for the X-ray tomography studies in Papers **I–III ,** and prepared the associated supporting information.

FIGURES

TABLES

CONTENTS

1 INTRODUCTION

Rare earth elements—commonly abbreviated as REE—consist of lanthanoids (La-Lu), Sc, and Y. REEs are extensively used in various modern applications such as mobile phones, catalysts, batteries of e-vehicles, and renewable energy production.[1–3] In particular, electric vehicles and the production of renewable energy play an important role in transition towards more sustainable technologies.[1] Consequently, the demand of REEs has been projected to increase considerably in the future. For example, new wind turbines alone can increase the demand of REEs up to threefold between 2020 and 2050,[4] whereas the EU has estimated that up to twelve and fourfold more Dy and Nd are needed by 2050.[5] REEs are classified as critical elements, due to their economic importance and the risks associated with their availability, with China producing over 70% of used REEs.[6,7] In 2017, an old REE mine was reopened in the US to not only meet the growing demand for REEs but also to increase production outside of China.[8] No REE-producing mine exists in Europe, although multiple promising sites have been discovered.[9] REEs are typically found in low concentrations in ores, but the most common REE-containing minerals are bastnäsite, monazite, and xenotime.[10] Monazite also contains radioactive elements like Th and U. Given the presence of radioactive elements, the low concentrations of REEs in various minerals, and their similar physiochemical properties, extracting REEs from their ores is challenging.[11] Therefore, it is important to develop novel efficient and environmentally friendly separation processes for REE ore concentrates that can also separate harmful and radioactive elements. Equally important, if not more so, is to enhance the recovery of REEs from secondary sources where the concentrations of REEs are relatively high.[2,12,13] In EU, the recycling rate of REEs is only 1%, and globally about 13%–14% of produced REEs were reported to be from recycled materials in 2022.[14] The low recycling rates can partly be explained by higher costs of recycling compared to primary production. However, with the effective recycling of wind turbines and electric car motors, 35% of the demand for REEs could potentially be supplied from secondary sources.[15] Other illustrative examples are mine tailings, mining raffinates, and acidic wastewaters that can contain REEs depending on the target metal of the process and the

mineral composition of the ores mined.[16] The potential is vast because mining waste is one of the largest waste streams in the EU with roughly 500 megatons produced in 2020,[17] and the annual production of tailings alone can be up to 13 gigatons globally.[18] For example, 24 t/year[19] or 985 kg/year[20] of REEs could be recovered from mining waste and residues, respectively. Waste electrical and electronic equipment (WEEE), which includes a wide range of devices, includes, for example, NdFeB magnets and phosphor materials which can contain up to approximately 30 wt% of REEs.[21,22] WEEE is a rather heterogenous secondary source for REEs consisting of plastic, glass, and/or metals from which the NdFeB magnets or LEDs need to be separated.[23–25] Although small NdFeB magnets are utilized in electric equipment, larger ones can be recovered from motors of electric cars and wind turbines.[26]

The first α-aminophosphonates with a general formula of $(RO)_2P(O)CR'_2NR''_2$ (R, R' R'' = H, organic substituent without or with functional group) were studied as liquid-liquid extractants for REEs as early as in the 1960s and 1970s.[27–30] However, the investigation of these compounds for REE recovery only truly began in the 2010s.[31] α-Aminophosphonates refer to organophosphorous compounds containing both a phosphonate and an amine group in the structure. The amine can be either primary, secondary, or tertiary amine. α-Aminophosphonic acids are acid derivatives of α-aminophosphonates and they have both an acidic phosphonate ($PO(OH)_x$) and a basic amine (NH) group which makes these acids versatile liquid-liquid extractants[32–39] and adsorption materials for REEs.[40–42] In liquid-liquid extraction, the reported α-aminophosphonic acids have enhanced separation between REEs compared to commercially used phosphonate-based liquid-liquid extractants.[32–39]. The ability of α-aminophosphonates to extract different metal ions can be tuned by varying the organic moiety and/or the number of phosphonate groups. The amount of binding sites which are available for coordination can be increased by synthetising multiple phosphonate groups to the recovery agent. This can be applied to the development of new liquid-liquid extractants, precipitants, or α-aminophosphonate-based adsorption materials.

α-Aminophosphonate adsorption materials have already been used as they are for metal recovery, and multiple commercial ion-exchangers containing an α-aminophosphonates as functional groups are available, including Lewatit TP260, MCR50, and Purolite S940. They could also be incorporated into 3D-printed (host) materials where they would function as adsorptive additives. Nowadays 3D-printed adsorption and ion-exchange materials can be easily manufactured, and consequently their utilization in the solid-phase extraction of metals has increased. The advantage is that their sizes and shapes can be customized for different applications, and the additives can readily be changed.[43–45] Thus, they can be adapted for a variety of different recovery and removal processes such as metal recovery,[44–50] analyte preconcentration,[51–53] and organic material capture.[54] Apart from Papers **II** and **III**, no literature on α-aminophosphonate additives in the 3D-printed adsorption material has been published for REE recovery. In

addition, α-aminophosphonic acids were investigated as precipitants for REEs for the first time in Paper **I**.

1.1 Aim of the work

Phosphonate-based extractants have been widely utilized in REE recovery and separation due to their good extraction properties.[55–57] Incorporating an amino group into the phosphonate framework opens new strategies to modify the molecular structures, coordination pockets, coordination affinities, and extraction properties of the phosphonate-based extractants.[31] This dissertation aimed to investigate recovery agents containing not only the phosphonate moiety but also a basic amine moiety, specifically α-aminophosphonic acids, for the recovery and separation of REEs using precipitation and solid-phase extraction methods. Thus, the discussion in this dissertation is limited to α-aminophosphonates, and the individual chapters are not comprehensive reviews of their topics, but only introduce the reader to the chosen topics. Moreover, the results and discussion only highlight the main outcomes of the experimental work carried out for the dissertation. For a detailed discussion, see Papers **I–III**.

In Paper **I**, α-aminophosphonic acids with different water solubilities were synthesized by varying the length of the alkyl chains. These acids were investigated as precipitants for REEs, Th, and U in acidic aqueous solutions. The pH ranged from 1 to 4 with the aim to separate REEs from Th and U as well as REEs from each other. The acid–base and complex formation properties were also investigated to get more insight into the precipitation process and structures of the formed complexes.

In Paper **II,** self-synthetized α-aminophosphonic acid was utilized as an additive in 3D-printed filters, which were investigated for the recovery of REE from acidic mining wastewater. The filters were thoroughly characterized using infrared spectroscopy, powder X-ray diffraction, and X-ray tomography to investigate their functional groups and micrometer-level structure. Because the author's contribution to the X-ray tomography studies is minimal, it is only briefly discussed in the dissertation.

In Paper **III**, work on the 3D-printed filters was continued by also utilizing a commercial α-aminophosphonate-functionalized additive (Lewatit TP260) in the filters. A comparison was conducted between the filters containing either self-synthesized or commercial additives for the recovery of elements from NdFeB magnet waste. Like in Paper **II**, detailed characterization was conducted for the filters containing the commercial additive using infrared spectroscopy, powder X-ray diffraction, and X-ray tomography to shed on light on their chemical and physical structures and adsorption mechanism.

2 RARE EARTH ELEMENTS

Rare earth elements are a group of elements which consist of lanthanoids (La–Lu) as well as Sc and Y. REEs have similar physio-chemical properties and because of this they have tendency to occur in the same mineral ores. The term *rare* in their name dates back to the 1800s, a time when the known minerals containing REEs were uncommon, and extracting and separating these elements from their minerals was a challenging and tedious task.[58] This led to the misconception that they were rare in nature. Additionally, REEs do not exist in veins like gold or iron but are dispersed throughout various minerals. This further accentuated their apparent rarity. Despite their name, REEs are not rare in the earth crust. In fact, cerium alone is the 25th most abundant element in the Earth's crust, being more abundant than copper. Nowadays, the term rare is more often interpreted to reflect the economic importance and extraction challenges of REEs rather than their actual abundance in the earth's crust.[59,60]

2.1 Properties and classification

REEs generally exist in the +3 oxidation state in nature, except for Ce, Pr, and Tb, which can also form complexes in the +4 oxidation state. In addition, Sm, Eu, Yb can form complexes in the +2 oxidation state.[57] The prevalent +3 oxidation state is based on their electron configurations in neutral forms, which are [Ar]3$d^1$4s^2 for Sc, [Kr]4$d^1$5s^2 for Y, and [Xe]4f^n6s^2 for lanthanoids, except for La, Ce, Gd, and Lu, in which the 5d orbital is singly occupied as well.[61] The 4f orbitals are positioned closer to the nucleus than the orbitals of shells 5 and 6, and, thus, they experience a stronger effective nuclear charge than electrons in higher orbitals. Because of this, the three electrons from the outermost 5d and 6s orbitals of lanthanoids are more easily removed than from the inner 4f orbitals, leading to a typical electron configuration of [Xe]4f^n in the +3 oxidation state. As the empty, half-filled, and full f-shells have exceptional stability, the formation of Ce^{4+} (f^0), Tb^{4+} (f^7), and Eu^{2+} (f^7), and Yb^{2+} (f^{14}) is possible.[61] The different oxidation states of

these few lanthanoids can be utilized in the separation of REEs. For example, Eu^{2+} and Ce^{4+} can be separated by selective reduction[62–64] and oxidation[65], respectively. Lanthanoids also exhibit a lanthanoid contraction which is a greater than expected decrease in ionic radii with the increasing atomic number. The contraction is caused by the poor shielding effect of the 4*f* orbitals against the increasing nuclear charge. Like the oxidation state, this contraction can be exploited in the separation of REEs.[11]

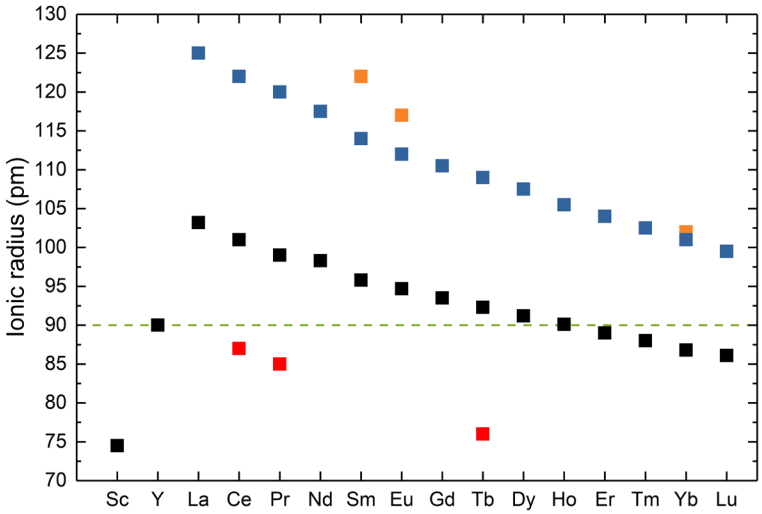

Figure 1. Ionic radii of REEs in oxidation state +4 (red), +3 (black), and +2 (orange). All the radii are for six-coordinate ions except for Sm^{2+} which is seven-coordinate. For comparison hydrated ionic radii (eight- and nine-coordinate) for lanthanoids are shown in blue. For comparison, an ionic radius of Y, which is classified as HREEs, is marked with a dashed line.[66]

Based on the electron configurations and atomic weights of REEs, they can be classified as light REEs (LREE) and heavy REEs (HREE). LREEs include lanthanoids with zero to seven 4*f* electrons (La–Gd), whereas heavy HREEs consist of lanthanoids with nine to fourteen 4*f* electrons (Tb – Lu).[67] Y, which has a similar ionic radius to heavy lanthanoids, is classified as HREE (Figure 1). The radii of the hydrated lanthanoid ions exhibit a similar declining trend in size, with the decrease being slightly more pronounced, especially for the LREEs.[68] The radii are also larger compared to the non-hydrated radii that should be taken into account when recovery studies are performed in aqueous solutions. Although Sc is classified as REE, it is not typically included in either of these subgroups due to its much smaller ionic radii. REEs can additionally be classified according to their ionic radii when it is necessary to emphasize size differences to explain variations in their properties. Usually, LREEs and HREEs are referred to as large and small REEs, respectively.

2.2 Primary sources, production, and separation

LREEs are mainly produced from two minerals, bastnäzite (RE)(CO_3)F and monazite (RE/Th)PO_4, while the main source of HREEs is xenotime YPO_4.[10] The minerals containing REEs, especially monazite, can also contain significant amounts of radioactive elements such as Th and U. For example, Monazite can contain up to 20 wt% of Th and 16 wt% of U, whereas bastnäsite and xenotime usually contain significantly lesser amounts of radioactive elements.[10] The high content of Th^{4+} stems from the fact that its ionic radii and oxidation state are similar to those of Ce^{4+}, thus allowing it easy substitution in the mineral lattices. During the processing of the ores, REEs are typically selectively leached with acid or base, leaving other elements present in the ore in undissolved residue, including Th and U. However, Th and U can also be leached with REEs with sulfuric acid,[11] from which they can then be separated via precipitation or liquid-liquid extraction.[69] In liquid-liquid extraction, Th and U are transferred from an aqueous phase to an organic phase utilizing amine- or phosphonate-based extractants that are selective for these elements.[11] The removal of Th, and U is crucial due to their radioactive nature, which poses environmental and safety hazards during REE processing.[70] After the removal of Th and U, an REE concentrate is obtained, where REEs can be separated from each other using liquid-liquid extraction. In addition to liquid-liquid extraction, REEs can be separated from each other by utilizing fractional crystallization, precipitation, or ion-exchange. These methods, however, are less widely used on a larger scale due to their lower efficiency compared to liquid-liquid extraction. Typically, they are utilized alongside liquid-liquid extraction to either pre-concentrate, purify fractions, or precipitate REEs out from the final REE-rich fraction. Before discussing the different separation methods of REEs in more detail, the separation factor (*SF*) is determined first. The parameter measures the separation efficiency for the utilized method.

2.2.1 Separation factor

The separation between two ions or metals can be measured through the separation factor. *SF* is determined from the distribution factors (*D*) of selected element pairs.[71] *D* indicates the amount of an element extracted from a solution compared to the amount of an element remaining in the solution as presented in Equation 1:

$$D = \frac{q}{c} \tag{1}$$

in which q is the concentration of an extracted element and c is the concentration of elements in a solution. *SF* can then be determined for chosen elements using

Equation 2:

$$SF_{\frac{1}{2}} = \frac{D_1}{D_2} \quad (2)$$

in which D_1 and D_2 are the distribution factors of the chosen elements. If two elements have a similar tendency to extract from the solution, the separation factor is 1 and indicates no separation between the elements. For clarity, *SF* is typically calculated so that the obtained value is ≥ 1. Thus, the higher the obtained value is, the higher the separation between the two elements is. Although *SF* was originally used to measure the distribution between two immiscible solvents, it has been applied for precipitation as well.[71–77]

2.2.2 Liquid-Liquid extraction

In liquid-liquid extraction, REEs are extracted from an acidic aqueous phase to an organic phase containing extractant(s). The classical extraction agents in liquid-liquid extraction for REEs are phosphonate-based compounds, di(2-ethylhexyl) phosphoric acid (DEHPA) and 2-ethylhexyl phosphonic acid mono-2-ethylhexyl ester (EHEHPA) (Figure 2).[11]

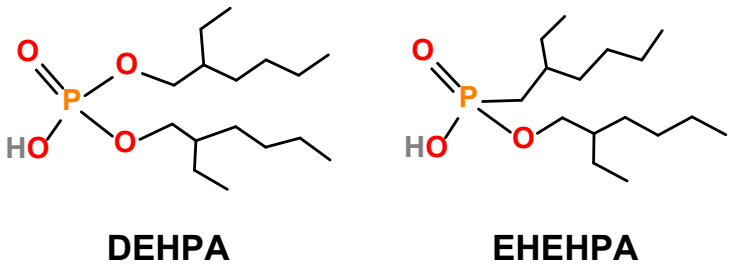

Figure 2. Structures of commonly used extraction agents for REEs di(2-ethylhexyl)phosphoric acid (DEHPA) and 2-ethylhexyl phosphonic acid mono-2-ethylhexyl ester (EHEHPA).

DEHPA and EHEHPA are widely used due to their good recyclability and robustness in acidic conditions. Out of these two extractants, DEHPA is usually more efficient at separating REEs as the separation factors range from 1.03 to 425 for DEHPA and from 1.09 to 199 for EHEHPA (Figure 3).[11] Even though large *SF*s have been reported for the HREE and LREE separation, the separation between adjacent lanthanoids remains low even with these two commercially utilized extractants. For DEHPA, the *SF*s between adjacent lanthanoids generally range from 1.03 to 2.23, except for the Sm/Nd pair, for which the *SF* is 4.86. For EHEHPA, the values of *SF*s range from 1.09 to 2.58. Given the poor *SF*s between adjacent lanthanoids, the complete separation of a single REE requires multiple separation stages with DEHPA and EHEHPA. Thus, more efficient ways to separate REEs have widely been investigated by improving the liquid-liquid extraction process.

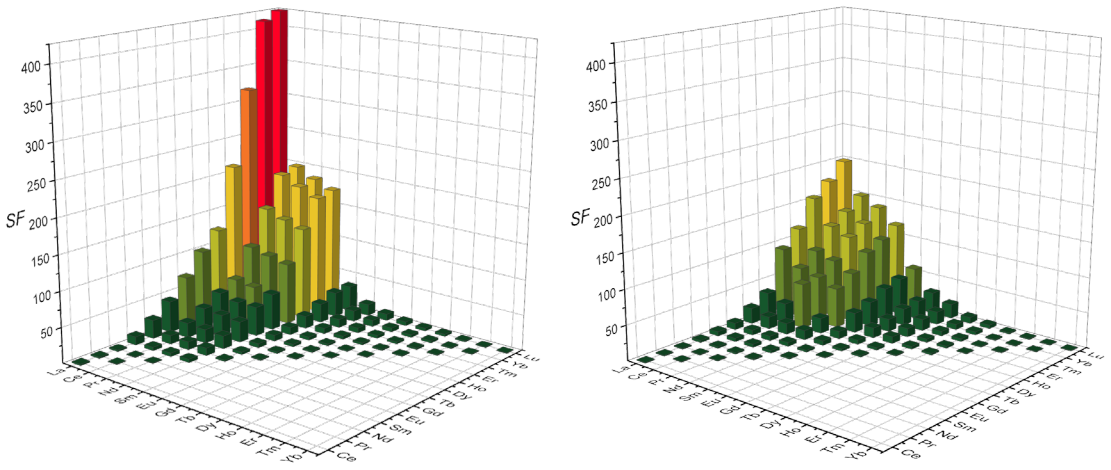

Figure 3. Separation factors of lanthanoids for DEHPA (left) and EHEHPA (right).[11]

One recent promising family of extractants is multidentate N,O-based extracting agents, which have demonstrated strong binding to both REEs and actinoids.[78-82] In contrast to acidic DEHPA and EHEPA, they are neutral extractants, meaning that they do not contain an acidic proton. These neutral extractants exploit the size difference of REEs to separate LREEs from HREEs.[83] For example, by varying the structure and rigidity of the tetradentate bis-lactam framework (Figure 4), its coordination pocket can be optimized for specific REEs, which further influences the stability of formed complexes.[84] The extraction was performed in an immiscible mixture of 1,2-dichloroethane and 0.9 M HNO_3, maintaining the concentration of lanthanoids at 1 mM and the concentration of the extractants at 7 mM. Organic phase extractants **1** and **3** preferred complexation with LREEs (La–Nd) due to the stable configuration of N donor atoms. **1** and **3** also separated LREEs from each other reasonably well as $SF_{La/Nd}$ was 21.4 and 17.4 for **1** and **3**, respectively. For **2**, the complexes of Nd and Sm were more stable than other LREE complexes in 0.9M HNO_3, yielding good recovery rates for them. However, when the acid concentration was increased from 0.9 M to 5 M HNO_3, **2** preferred HREEs over LREEs. In contrast to **1–3**, **4** extracted REEs poorly under the same conditions because of their flexible structure. In addition to the organic phase extractants **1–4**, a water-soluble bis-lactam extractant **5** was investigated with lipophilic diglycolamides (DGA) as a co-extractant, to improve separation between REEs. Like **1–4**, **5** showed a preference towards LREEs over HREEs. Thus, by combining water-soluble **5** with lipophilic DGAs, which prefer HREEs, the separation between different REE pairs was enhanced.[85] For example, $SF_{Nd/Pr}$ of 4.2, $SF_{Sm/Nd}$ of 20, and $SF_{Tb/Gd}$ of 5.8 were obtained for the chosen REE pairs.

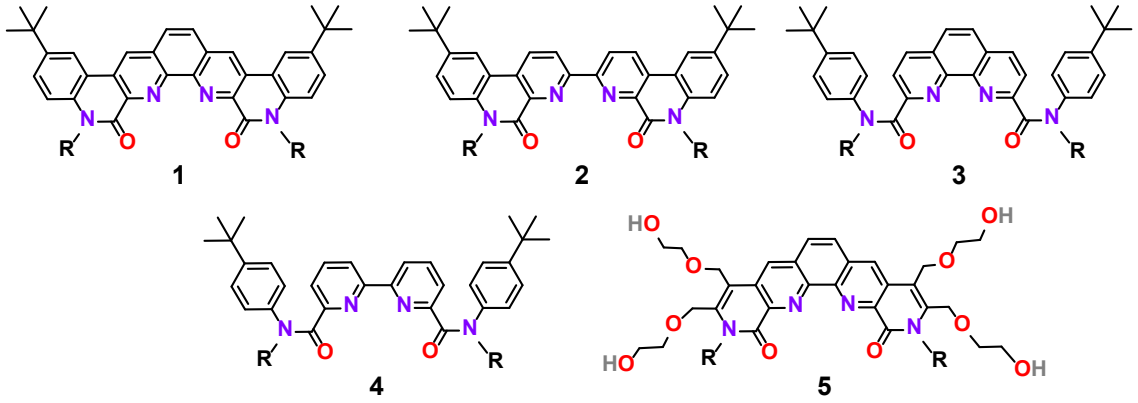

Figure 4. Structures of **1–5**. R = 2-octyldodecyl for **1–4** and R = H for **5**.

Although the aforementioned N,O-based extractants are among the most promising extraction agents, their synthesis is far from trivial. More straightforwardly synthesized α-aminophosphonates (see Chapter 3) have also been developed and investigated as extraction agents for REEs (Figure 5).[32–38] The earliest aminophosphonic acid extractants **6** and **7** were investigated in the extraction of LREEs, specifically Eu^{3+}, from varying concentrations of HCl media.[27–30] **7** was found to be generally a better extractant for lanthanoids compared to **6**, but it also extracted Sr^{2+} and Mn^{2+} better.[30] The separation between Ce^{3+} and Pr^{3+} was studied with both **6** and **7** from HCl media, but no significant differences could be achieved in their extraction.[28]

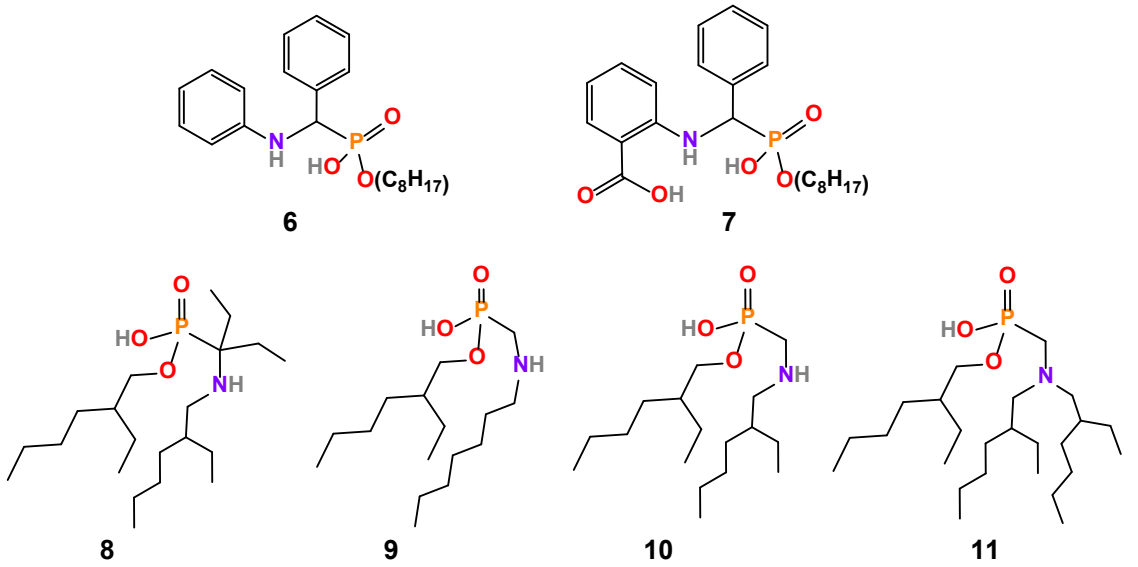

Figure 5. Structures of aminophosphonic acid extractants **6–11** studied for REE extraction.

Extractants **8–11** were found to improve the separation factors between the adjacent HREEs rather than LREEs. The organic phase used for **8–11** was *n*-heptane and the aqueous phase diluted HCl. Among the reported

aminophosphonates, extractant **8** was found to be a slightly better extraction agent for HREEs than EHEHPA from 1.0–4.1 M HCl aqueous phase.[32] The best determined *SF*s for adjacent HREEs (Ho–Lu and Y) were 1.36–3.22 in varying HCl concentrations (0.95–2.07 M). Extractants **9** and **10** showed similar separation efficiency for HREEs as their *SF*s ranged from 1.07 to 1.93 and 1.04 to 4.29, respectively.[34,36] Extractant **11** had similar extraction abilities to **9** and **10,** exceeding the *SF*s of both EHEHPA and DEHPA for the adjacent HREEs as the *SF*s ranged from 1.57 to 3.53 for Ho–Lu.[38] However, its extraction efficiency, which indicates the ratio of metal the extractant can extract from the aqueous phase to an organic phase, was smaller than that of EHEHPA. Only 50% Lu was extracted from 0.4 mM Lu^{3+} solution at maximum. Compared to N,O-donors (**1–5**), the selectivity of **8–11** towards either LREEs or HREEs is not as good, which likely results from their freely rotating bonds disabling the size-selective binding.

Separation studies were also performed for extractants **8** and **10** with DEHPA and EHEHPA, respectively, to reveal their synergistic effect in REE separation.[33,37] In synergistic extraction, two extractants are simultaneously used in the organic phase instead of one. It is assumed that the extractants form a more stable complex with the target element (REE) than alone, which can improve the selectivity towards specific REEs.[86] With two extractants the extraction efficiency can also be greater. Compared to **10** or DEHPA alone, the synergistic extraction of Lu^{3+} with **8** and DEHPA in a 1:1 molar ratio was more efficient.[33] The separation between adjacent REEs was also studied and it was found to be better for the synergistic system than for DEHPA alone but worse than for **10** as the *SF*s of a synergetic system varied from 1.01 to 2.77. Similar to **10** and DEHPA, the molar ratio of 1:1 was also optimal for **10** and EHEHPA in synergistic studies.[37] The obtained separation factors for adjacent REEs were close to those of sole **10** but showed improvement to the *SF*s of EHEHPA. However, the loading capacity of the 1:1 mixture in Yb and Lu extraction was smaller than EHEHPA. The loading capacity of the extractant refers to the total maximum amount of dissolved metal (solute) it is able to extract from the solution.

2.2.3 Precipitation and crystallization

One of the most traditional precipitation agents for REEs are oxalates which strongly bind to REEs even at low pH values, forming poorly water-soluble oxalates.[87–89] The general formula of the oxalate complexes is $REE_2(C_2O_4)_3 \cdot nH_2O$, in which n can vary from 7 to 10.[90,91] The solubilities of REE-oxalate complexes vary in a function of temperature and the amount of oxalate in the solution, enabling their fractional precipitation.[89,92] For example, 1M oxalic acid can separate Sm–Dy from other REEs at pH 7.3 at 90°C with recovery rate of 73%.[93] In general, oxalate precipitation has proven to be rather inefficient in REE separation and is more often utilized for precipitating all REEs at once. Precipitated oxalates can be converted to REE-oxides through calcination at high temperatures.[11,94] This step is commercially important because REE-oxides are used in various industrial applications and are starting materials for various REE compounds. Another traditional precipitation method for REEs is double

sulphates.[11] The double sulphate complexes are typically precipitated by adding Na^+, K^+, or NH_4^+ sulphate to an REE-containing solution to form $REE_2(SO_4)_3 \cdot M_2SO_4 \cdot H_2O$ (M = Na^+, K^+, or NH_4^+).[11,95] Generally, LREEs (La–Sm) form almost insoluble double sulphates, whereas HREEs (Ho–Lu, and Y) are rather soluble. The solubilities of the remaining "middle" REEs (Eu, Gd, and Dy) are between these two extremes. Thus, by using the double sulphate precipitation, the REE mixture can be separated into three different groups.[11]

Due to the traditional precipitation agents being inefficient in REE separation, new and more efficient precipitation agents have been widely investigated.[71–74,96] Since the liquid-liquid and solid-phase extraction are considered more effective methods for separating REEs on a large scale than precipitation, the latter has been mainly utilized for impurity removal, separating LREEs from HREEs,[72,96] or separating two REEs from each other.[73,74] Separation of Y from LREEs was studied from a carbonate solution containing 10 g/l of REEs.[96] Upon the addition of H_2O_2 to the solution, the LREEs readily precipitated from the solution as peroxycarbonates $REE_2(CO_4)_3$, leaving Y in the solution. Using this method, the share of Y was increased from 2.4% to 80% in the solution. The separation of LREEs with a tripodal amino arene precipitation agent was investigated in a toluene/8M HNO_3 system. While most of the *SF*s for adjacent pairs were similar to *SF*s obtained in liquid-liquid extraction (Chapter 2.2.2), $SF_{Sm/Nd}$ was 9, which is greater than what has been achieved in liquid-liquid extraction.[72] A tripodal nitrate ligand selectively precipitated Dy from a benzene solution containing only Nd and Dy with a $SF_{Nd/Dy}$ of 359.[73] The precipitation properties of the ligand were further studied with La, Nd, and Dy in aqueous acidic solutions and the following $SF_{Nd/Dy}$ of 213 and $SF_{La/Nd}$ of 16.2 were obtained.[71] Even better results were obtained for glycine substitued macropa (G-macropa) in Nd/Dy separation as it formed weaker complexes with HREEs than LREEs. By adding HCO_3^- to the water solution containing Nd, Dy, and the ligand, Dy was selectively precipitated out with a huge $SF_{Nd/Dy}$ of 741,[74] highlighting the efficiency of precipitation methods to separate binary mixtures of REEs.

Fractional crystallization is another less utilized separation method due to its relatively slow process. The crystallization is typically initiated either by different solubility of REE complexes as a function of temperature or by the slow evaporation of crystallization solvent. Older fractional crystallization methods have utilized double salts like precipitation. For example, double ammonium nitrates have been used to separate La, Pr, and Nd from LREE mixtures with high purities of 99.9%, 99.5%, and 99.9% respectively.[97,98] The formed complex is generally written as $REE(NO_3)_3 \cdot NH_4NO_3 \cdot 4H_2O$.[11] Double magnesium nitrates which form complex $2REE(NO_3)_3 \cdot 3Mg(NO_3)_2 \cdot 24H_2O$ have been utilized to separate Sm, Eu, and Gd. For the separation of La–Sm from the other REEs double manganese nitrates have been employed, forming a complex $2REE(NO_3)_3 \cdot 3Mn(NO_3)_2 \cdot 24H_2O$.[11] HREEs can be separated as a group with bromates forming $REE(BrO_3)_3 \cdot 9H_2O$, but many recrystallizations are required.[99] For example, to increase the purity of Nd from 88% to 99.9% required 138 recrystallizations,[97] whereas to obtain pure Ho bromate required roughly 1500

recrystallizations.[11] Probably, the most notorious example of bromate crystallization is the purification of Tm through 15,000 recrystallizations.[99]

Borate crystallization is one important example of an effective binary component fractional crystallization although crystallization conditions are harsh, requiring 3 days in water at 200°C.[75] Depending on the lanthanoid, different products can be formed. For example, with La, $LaB_4O_6(OH)_2Cl$ is formed whereas the product for Ce, Nd, and Pr is $REE_2B_{12}O_{18}Cl_2(OH)_4(H_2O)_4 \cdot nH_2O$. With Sm, Eu, and Gd, $REEB_6O_8(OH)_5 \cdot H_3BO_3 \cdot H_2O$ is obtained, but Eu, Gd, and Tb can also form $LnB_6O_8(OH)_5 \cdot H_3BO_3$ without the water of crystallization. Finally, Tb and the rest of the HREEs can form $REE_4B_{24}O_{36}(OH)_{12} \cdot H_2O$. Unfortunately, borate crystallization is not effective for separating the adjacent REEs because their *SF*s ranged from 1.22 to 1.51. Only $SF_{Nd/Sm}$ was a bit higher, with a value of 4.03, which is comparable to *SF*s obtained in liquid-liquid separation (Chapter 2.2.2). However, the separation between HREEs and LREEs was good because $SF_{Ce/Lu}$ and $SF_{Nd/Dy}$ were 716.85 and 67.76, respectively. Other fractional crystallization studies include coordination polymers[76,77], which have yielded good separation factors, especially for Nd/Dy separation ($SF_{Nd/Dy}$ > 300), and selective crystallization with an iodate-sulphate system that has been reported to separate efficiently LREEs from HREEs.[100]

2.2.4 Ion-exchange chromatography

Ion-exchange chromatography is a traditional method for the treatment of solutions containing trace amounts of rare earth elements (REEs) and it is particularly applied to obtain high purity levels of REEs.[101] During the 1950s, ion exchange chromatography was the predominant technique employed in the separation of REEs before liquid-liquid extraction replaced it due to its higher efficiency. All ion-exchange resins contain functional groups which can exchange positive or negative ions. In cation exchange resins, the ions that are exchanged, are positively charged, whereas in anion exchange resins, they are negatively charged.[102] When the ion-exchange resin interacts with a solution containing ions, the ions within the resin are exchanged for those present in the solution. Traditionally, ion exchange resins, such as sulfonic acid–functionalized Dowex 50, were utilized to adsorb REEs, and ammonium ethylenediaminetetraacetate (EDTA) or hydroxyisobutarate (HIBA) was used as the complexing agent during the elution step.[61,103] The underlying principle of this process is that HREEs form more stable complexes with EDTA and HIBA than LREEs. Thus, HREEs are first eluted out from a resin resulting in the separation of HREEs and LREEs via ion-exchange as depicted in Figure 6.[61] Nowadays different ion exchange materials are heavily investigated in recovery and separation of REEs either from each other or other elements.[104–109] Given the vast literature, only some illustrative examples are given below about ion exchange materials, whereas α-aminophosphonate-based ion exchange materials are discussed in detail in Chapter 3. For example, zeolite and bentonite ion exchange materials separated REEs from Co, Ni, Ca, Mg, Zn, and K, and the subsequent elution of the adsorbed

REEs with 1M $(NH_4)_2SO_4$ completely desorbed them.[104] The study illustrated well how REEs could be removed from other elements, but the separation of REEs from each other is more challenging. For instance, the separation of LREEs was studied using a dimethylethanolamine functionalized ion-exchange resin. The REEs were adsorbed as their methylglycine N,N-diacetate (MGDA) complexes, and could be separated due to the small differences in the stabilities of the REE-MDGA complexes when eluted with dilute mineral acids. Fractions of La, Nd, and Eu were obtained with the purities of 81%, 57%, and 76%, respectively.[105] A N,N-dioctyldiglycolic acid–functionalized acidic ion-exchanger was also studied for REE separation, and it was found that the separation of LREEs was more efficient than that of HREEs.[106] La-Nd showed separation in their elution curves, whereas little to no separation of HREEs was detected at pH 2 when HNO_3 was used as an eluent.

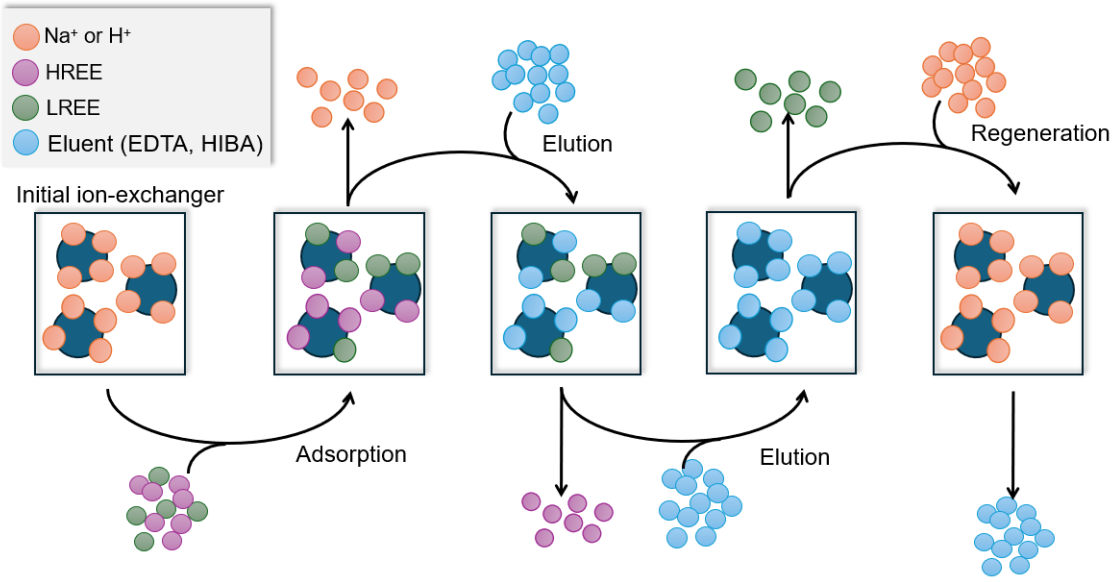

Figure 6. Principle of separating HREEs and LREEs with ion-exchange chromatography.

2.3 Secondary sources

Secondary sources for REEs include, for example, electronic waste, coal combustion products, and industrial byproducts. These sources are recognized as vital to meet the increasing future demand for REEs. For example, NiMH batteries can contain 9.23 and 4.56 wt% of La and Ce,[110] whereas mobile phones, computers, and speakers use neodymium magnets consisting of an alloy mainly made of Fe (60–70 wt%), Nd (20–30 wt%), Pr (0.5–7 wt%), and B (0.3–1 wt%).[26] In addition, NdFeB magnets can also contain Gd, Tb, Dy, and Ho to increase the coercivity and operating temperature of a magnet.[111–113] The total REE percentage

in the NdFeB magnets varies between 15–30 wt%.[21] NdFeB magnets are additionally obtained from electric cars and wind turbines. Industrial byproducts including mining residues, acidic aqueous waste, and waste generated in the metal smelting processes can show very high concentrations of REEs. For example, acid mine drainage can contain 5 to 25 mg/l of REEs,[114] whereas bauxite residue, a side product from aluminum production, contains 0.1 wt% of REEs.[12] Valorizing these secondary sources would not only address the current supply-demand gap but also significantly decrease demand for open (new) mining sites, making REE supply chains more sustainable.

2.3.1 Mining waste

Mining waste, consisting of topsoil material, sedimentary rocks, waste rocks, and tailings, is formed as a byproduct of the mining industry after the valuable targeted metals are extracted from minerals.[115,116] In addition to the solid mining waste, sulfide-rich mineral waste can result in aqueous acidic mining wastewaters. These are formed when the mineral is exposed to air and water. The wet and oxidative conditions convert sulfide-rich mineral to sulfuric acid, causing acid mine drainages (AMD). The drainages contain high concentration of metals, which are leached from not only the sulphide ores but also from the surrounding minerals.[117] The elemental composition of the mining waste is mining site dependent and thus highly influenced on the minerals mined and the target metals in the main extraction process.

Phosphogypsum, which is a mining waste of apatite ores, has been investigated to be a valuable sources for REEs as up to 80% of REEs can be leached out for further recovery processes.[118,119] In one study, 75% of REEs were recovered from phosphogypsum by utilizing a chelating aminophosphonate-functionalized ion-exchange resin.[120] With commercial ion-exchangers, REEs were recovered almost selectively from the acidic mine waters.[16,121–124] However, the adsorption of REEs from mining waste has been hindered by the existence of other co-adsorbing elements such as Ca and Al.[120,121] In addition to the ion-exchange, recovering REEs from mining wastewaters has been studied by precipitation by different precipitation agents as well. Introducing phosphate to a solution containing 230 mg/l of REEs and 75.0 g/l of Fe(II) resulted in 95% precipitation of REEs and <1% co-precipitation of Fe(II).[125] By applying Na_2CO_3 to acid mine drainage, 85% of REEs could be recovered by precipitation at pH 7 and the amount of REEs could be concentrated to 15 times.[126] Overall, mining wastewaters are a valuable secondary source for REEs if the challenges arising from the co-extraction of ions can be overcome.

2.3.2 Neodymium magnets

NdFeB magnets are an increasing secondary source for REEs as the amount of waste electric equipment as well as e-vehicles and wind turbines will increase in the future.[5,127] Multiple studies with a focus on the separation of the main components (Fe, Nd, Dy) from the magnets have been published during the past

decade.[21,26,73,111,128–134] The separation of Nd from Fe has been reported by double salt precipitation to yield 100% pure Nd.[128] First, a simulated roasted magnet is leached with $ZnCl_2$ to selectively dissolve Nd, obtaining a great $SF_{Nd/Fe}$ of 13,456. By traditional double salt precipitation with Na_2SO_4, Nd can be selectively precipitated as double sulfate. Separation of Nd and Dy has been studied by solvent extraction with neutral phosphine oxide extractant Cyanex 923 by replacing the aqueous phase with polyethylene glycol.[129] Three extraction stages were found to be required for the sufficient recovery of Dy. With a precipitation method, Nd can be separated from Nd/Fe[135] and Nd/Dy[73,134] systems. The separation from Fe can be simply performed by Fe precipitation at pH 4,[135] and separation between Nd and Dy can be achieved with tripodal ligands based on solubility differences of the formed complexes.[73,134] Additionally, with a quaternal ammonium ionic liquid, good separation of Nd from Fe, Co, and Ni has been achieved.[130]

Recovery of REEs from real NdFeB leachates typically combines selective leaching of REEs from the magnet with precipitation or solvent extraction.[136–139] However, it has been reported that by selective precipitation with tripodal amido ligand, a Nd/Pr mixture can be separated from heavier REEs.[140] Afterwards, 98% of Dy, Gd, and Ho can be recovered with solvent extraction by utilizing N,N,N,N-tetraoctyldiglycolamide. In another study, separation of REEs was achieved by first leaching magnet scrap at 80°C with a 1:1 combination of ionic liquids and water.[137] Fe was separated into the ionic liquid fraction whereas REEs and Co into the aqueous phase when the leachate cooled to room temperature. REEs and Co were then precipitated with oxalic acid, and Co was further separated from REEs by adding ammonia to form soluble Co ammonia complexes $[Co(NH_3)_6]C_2O_4$ resulting in a 99.9% pure REE fraction.[137] Another method describes alkali baking in which a magnet is leached with NaOH at 150–200°C.[136] REEs are transformed into soluble hydroxides while Fe remains in $NaFeO_2$ residue. REEs are then calcined and leached with versatic acid, from which they can be recovered by oxalic acid precipitation with 98.4% purity. 1.2% of Al and Co remain as impurities.[136] HCl has shown to be an efficient leaching agent for NdFeB magnets, as REEs and B can be selectively leached, separating them from Fe.[138,139] When oxalic acid is introduced to the leachate, REEs can be further recovered yielding 99% pure REEs (Nd, Dy, and Pr).

Overall recovery and separation of Nd, Dy, and Pr have been shown to be viable from NdFeB magnets with different methods. However, challenges remain in the purity of the acquired REE fraction and applying methods from the binary metal studies (Nd/Fe) to real leachates containing other elements.

3 α-AMINOPHOSPHONATES

α-Aminophosphonates have been investigated as the recovery agents for REEs already in 1960s, but the investigation of these compounds truly started after the 2010s.[31] The α-aminophosphonates have mainly been utilized as liquid-liquid extractants but in recent years also as adsorption materials. They contain a basic amine and (an acidic) phosphonate group(s), and are prepared via condensation reaction between amine, phosphonate and ketone or aldehyde.[141] As long as the α-aminophosphonate contains OH group, they can form zwitterionic structures, and act both as a base and an acid. The amount of amine or phosphonate groups can easily be varied by changing the starting materials in synthesis. The properties of the α-aminophosphonates can also be tuned by introducing different functional groups into the ligand framework or by varying lengths of the carbon chains of alkyl and aryl substituents. Compounds with long carbon chains or large aromatic moieties are insoluble in water and are suitable as extractants in liquid-liquid extraction or adsorbents in solid-phase extraction. In contrast, water-soluble α-aminophosphonates can be used as precipitation agents if their metal complexes are poorly soluble or insoluble in water. All of these properties make α-aminophosphonates suitable recovery agents for REEs. In this dissertation, only α-aminophosphonates are discussed.

3.1 Synthesis

The main reaction route used for the synthesis of α-aminophosphonates is the Kabachnik-Fields reaction (Figure 7). The compounds can also be synthesized via Pudovik[29,30] or Mannich[142,143] reactions. Kabachnik-Fields is a hydrophosphonylation reaction in which amine, aldehyde, or ketone and phosphonate react in the presence of an acid catalyst to yield an α-aminophosphonate.[144] The formed side product is water. The amine reagent can either be ammonia, primary amine, or secondary amine. By selecting different amines and altering the stoichiometry of phosphonate and aldehyde/ketone, the

amount of phosphonate moieties in the final product can be adjusted.[145] Generally, ammonia results in triphosphonates, a primary amine to bisphosphonates, and a secondary amine to monophosphonates.[145] The substituents R_1–R_6 can be vastly different in the reaction, which allows α-aminophosphonates with different properties to be synthetized. For example, utilizing salicylaldehyde and diphenylphosphite as the starting reagents, leads to α-aminophosphonates in which the large aryl moieties ensure non-water-solubility.[146,147] In addition to the above, the Kabachnik-Fields reaction has one more advantage over many other reactions. The synthesis can typically be performed in one pot without multiple reaction steps, making this reaction simple and "clean".

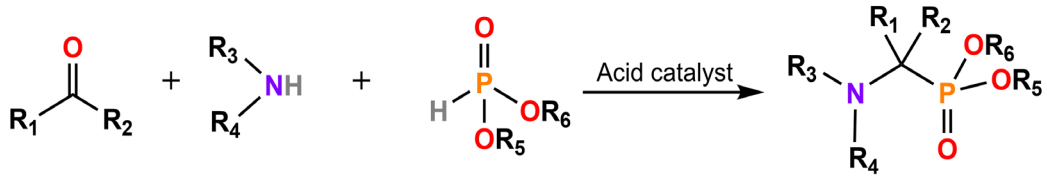

Figure 7. Kabachnik-Fields reaction for synthesizing α-aminophosphonates. $R_{1\text{-}6}$ can be hydrogen, alkyl or aryl substituents.

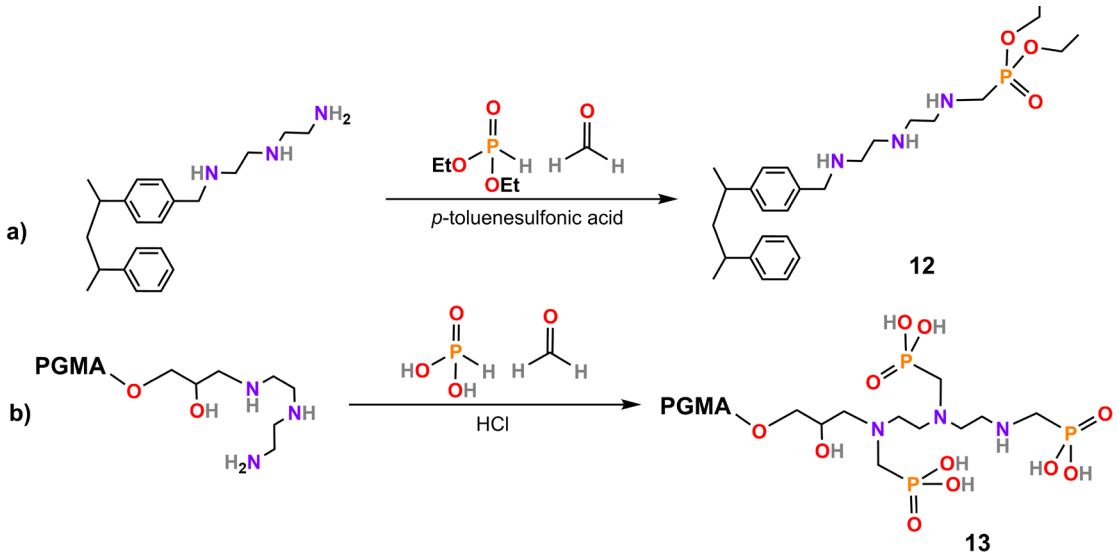

Figure 8. Functionalization of (a) styrene-divinylbenzene and (b) PGMA polymers with α-aminophosphonate functionality.

When α-aminophosphonate-based adsorbent materials are designed, the α-aminophosphonate functionality is typically incorporated into the polymer (chain). Another way is to synthesize large hydrophobic aryl or alkyl substituents into the α-aminophosphonate framework to prevent water solubility. A styrene-divinylbenzene (DVB-ST) polymer can be functionalized with α-aminophosphonates by first converting the chloromethyl form of the polymer to an amine form.[148] By reacting the resulting amine polymer with

paraformaldehyde and diethyl phosphite, the functionalized polymer can be obtained via the Kabachnik-Fields reaction (Figure 8a). The obtained polymer contains multiple secondary amines and phosphonate groups for metal coordination even via chelation. Functionalization of PGMA (poly(glycidyl-methacrylate)) with α-aminophosphonates was carried out similarly by first reacting polymerized PGMA with amine, and then inserting the phosphonate moiety via the Kabachnik-Fields reaction (Figure 8b).[149] The stoichiometry of phosphorous acid and paraformaldehyde was selected in such a way that the polymer arms contained multiple phosphonic acid groups, in contrast to the DVB-ST–functionalized sorbent. These polymers have been utilized for the separation of Th^{4+} from REEs and for the adsorption of Y^{3+} and La^{3+}. Mono and bisphosphonates were synthesized similarly by varying the ratios of aldehyde and amine (Figure 9).[40,150] The aldehyde and stoichiometry of the amine and phosphonate reagents were chosen in such a way that α-aminophosphonates with aryl moiety in the middle formed. To obtain α-aminomonophosphonates **14** and **15**, 1:1:1 stoichiometry (aldehyde: amine: phosphonate) was used, whereas for α-aminobisphosphonates **16** and **17** the stoichiometry of 1:2:2 was utilized. In both phosphonates, the amine and phosphonate arms are free to coordinate with metals.

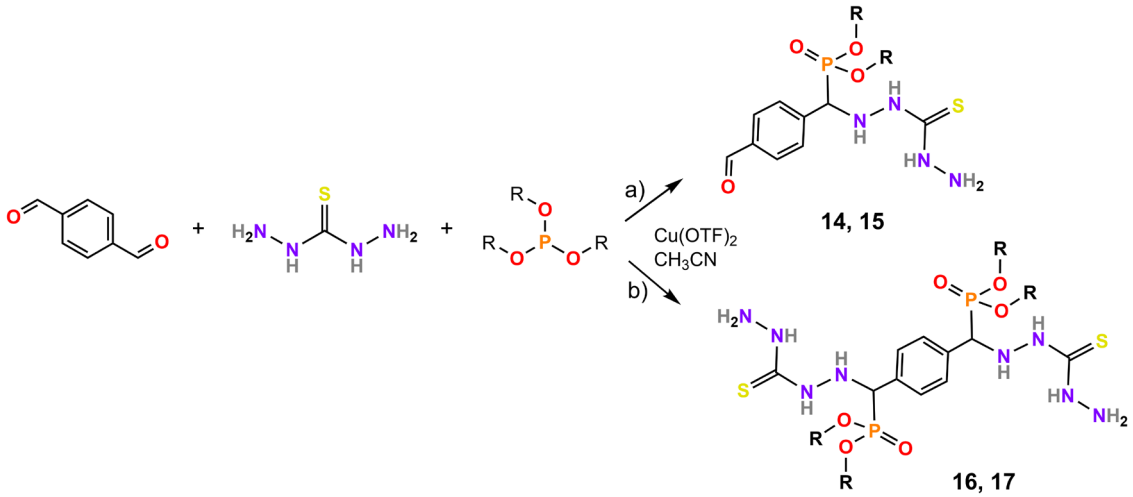

Figure 9. Synthesis routes for mono- and bisphosphonate sorbents utilized in REE recovery. For **14** and **16** R =H, and for **15** and **17** R =Ph. (a) stoichiometry 1:1:1, (b) 1:2:2.

α-Aminophosphonates have also been incorporated into silica particles due to their porous structure and high surface area. The functionalization of silica can be performed by first synthesizing silicon with an α-aminophosphonate arm and reacting with silica gel to obtain silica-based sorbents.[151] Another reported method for α-aminophosphonate-functionalized silica is to synthesize the α-aminophosphonate moiety first. The aminophosphonate is either hydrolyzed to α-aminophosphonic acid or used as it is. The α-aminophosphonate is then reacted with (3-glycidyloxypropyl)trimethoxysilane to obtain silica functionality for the structure, and afterward with silica gel to which the silica-functionalized

α-aminophosphonate can covalently attach (Figure 10).[152] The silica-based materials have been investigated for the adsorption of REEs[151] as well as separating Th from REEs.[152]

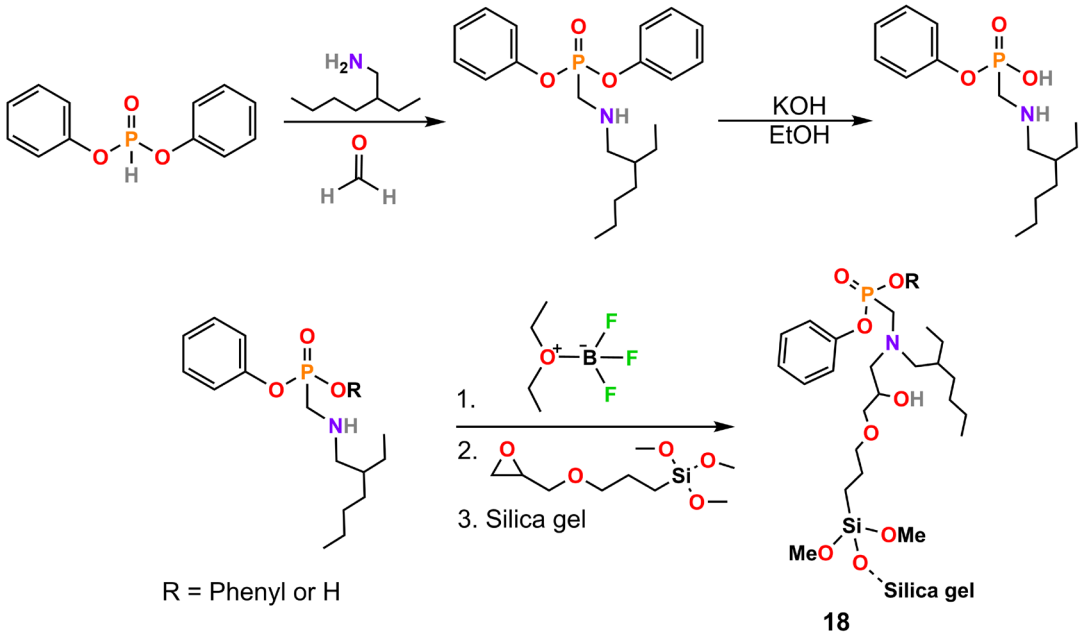

Figure 10. Synthesis route for α-aminophosphonate functionalized silica **18**.

3.2 α-Aminophosphonate-based adsorption materials

Adsorption is a process where compounds, atoms, or ions are transferred to the surface of a solid substance from either a gas or liquid phase.[153] The adsorbed substance is commonly referred to as an adsorbate and the adsorbing material as an adsorbent. Adsorption results in the formation of a film of the adsorbate on the surface of the adsorbent which can be characterized via various methods such as Fourier Transform Infrared Spectroscopy (FTIR), X-ray photoelectron Spectroscopy (XPS) or Scanning Electron Microscope equipped with Energy Dispersive X-ray Spectroscopy (SEM-EDX). The characterization methods are discussed in more detail in section 3.3. The adsorption can proceed through physical adsorption (physisorption) or chemical adsorption (chemisorption) as

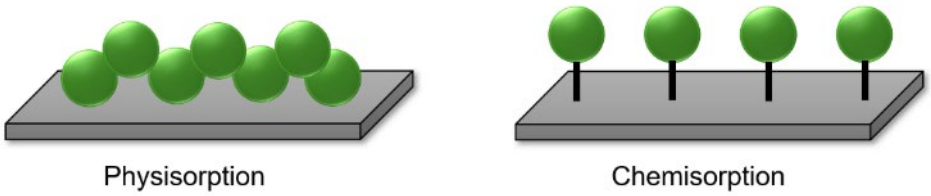

Figure 11. Illustrated adsorption of adsorbate to the surface via different adsorption modes.

illustrated in Figure 11. In physisorption, the adsorbate is retained on the surface by weak Van der Waals forces, and adsorption is typically characterized by the formation of multilayers. Conversely, in chemisorption, chemical bonds (covalent or ionic) between the adsorbate and the adsorbent are formed instead of inter-molecular interactions. Chemisorption typically involves the formation of a monolayer on the surface of the adsorbent. However, physisorption and chemisorption can occur simultaneously as a layer of adsorbates may be physically adsorbed on top of a chemisorbed layer that interacts via van der Waals forces. Depending on the adsorbent, REE binding to adsorption materials can occur via both routes. Ion-adsorbed clays have been studied to contain physiosorbed REEs,[154] whereas α-aminophosphonate ion-exchanger materials adsorb REEs via chemisorption. The adsorption into α-aminophosphonates generally occurs via ion-exchange, in which typically Na^+ (or H^+) is exchanged to REE^{3+}. The adsorption mechanism can be written as

$$\overline{X\text{-}(PO_3^{2-})\ 2Na^+} + REE^{3+}3A^- \rightarrow \overline{X\text{-}(PO_3)\text{-}REE^{3+}A^-} + 2Na^+2A^- \quad (3)$$

in which A is counter anion for dissolved REE, the nature of which depends on the acid background and X is R-NH-CH_2-, in which R is a polymer matrix.[155] The line above the formed α-aminophosphonate denotes the solid resin. Both synthesized and commercial α-aminophosphonate functionalized adsorption materials are known.[40,121,122,146–152] For example, the commercial α-aminophosphonate ion-exchangers are found under the names of Purolite S940 (or S950), Lewatit TP260, and IRC747, whereas adsorbents presented in section 3.1 are illustrative examples of the synthesized materials. The commercial α-aminophosphonate ion-exchangers are usually weakly acidic cation exchangers. Adsorption materials can be prepared either by synthesizing non-soluble (polymer)materials and used as they are, or they can be incorporated into a polymer matrix using 3D printing.

3.2.1 3D-printed adsorbents

3D-printed adsorption materials have become increasingly common over the past decade due to the ease of manufacturing them.[156] This has been strongly influenced by the development of 3D printers and printing techniques. With 3D printing, properties such as surface area, porosity, and pore size distribution of

3D-printed objects with different sizes and shapes can be optimized.[157] All these properties are crucial for adsorption materials, while modifiable shapes and sizes allow for their integration into existing processes. Another advantage of 3D-printed adsorption materials is that various compounds and additives, including ion-exchange materials, metal-organic-frameworks (MOF), and hydrogels, can be incorporated into the polymer matrices of 3D-printed objects as adsorbents.[157,158] These 3D-printed adsorption materials have been applied to a wide range of applications, such as metal recovery,[44–50] gas adsorption (CO_2),[159] metal preconcentration,[51–53] and organic material removal.[54]

The most common 3D printing techniques for adsorption materials are selective laser sintering (SLS), direct ink writing (DIW), fused deposition modeling (FDM), and stereolithography (SLA).[157,158] SLS employs a laser to sinter powdered material, binding it together to create a solid structure. This technique is beneficial for producing porous materials with high surface areas, which are ideal for adsorption applications. Importantly, the porous structure is automatically formed without predesign if partial sintering, in which particles are only partially melted, is used during the manufacturing process. DIW involves the precise deposition of liquid-phase "inks" through small nozzles under controlled flow rates, creating 3D structures layer by layer. It is particularly useful for applications requiring complex geometries and fine details. FDM involves extruding thermoplastic materials layer by layer to form the desired structure. It is widely used due to its simplicity and cost-effectiveness. SLA uses a laser to cure liquid resin into solid layers. This method is known for its high precision and ability to create complex geometries, making it suitable for producing detailed 3D-printed structures.[157,160]

As mentioned above, the rise of 3D printing has accelerated the development of 3D-printed adsorption materials, and many different examples are currently known. Chitosan/metal-organic framework composition coated 3D-printed filters have been utilized in the removal of Pb^{2+} from contaminated water.[161] 3D-printed zeolite-polymer composites have been widely investigated for wastewater treatment.[162] U has been extracted from acidic media with a recovery rate of 90% using quaternary ammonia resin–coated 3D-printed material.[48] The recovery of U from acidic solutions has also been reported with a 3D-printed biopolymer filter.[163] 3D-printed materials have been utilized for Fe, Cr, and Hg preconcentration from low-concentration solutions enhancing the detection of these metals,[51,164,165] and for removing radioactive isotopes of ^{137}Cs and ^{90}Sr from nuclear wastewater.[47] The selective recovery of gold, platinum, and palladium from WEEE has been reported by using SLS 3D-printed filters.[46] Even gases can be separated with 3D-printed materials as illustrated by DIW 3D-printed activated carbon monoliths which can separate methane from N_2.[166] Considering all the above-mentioned, 3D-printed adsorption materials are truly versatile for various applications. However, to the best of our knowledge, 3D-printed filters containing α-aminophosphonate have yet to be utilized for the adsorption of REEs, apart from in Papers **II** and **III**.

3.3 Characterization methods

Adsorption materials, 3D printed or not, can be characterized using a variety of different methods to gain insight into their structural properties, morphology, chemical composition, and adsorption mechanism, all of which affect their adsorption capabilities. Typical characterization methods include Fourier-transform infrared spectroscopy (FTIR), powder X-ray diffraction (PXRD), Scanning electron microscope (SEM), and Brunauer, Emmett, and Teller (BET) surface area measurement. Additionally, X-ray tomography and helium-ion-microscope (HIM) imaging can be used for characterization. For the characterization of the formed α-aminophosphonate complexes, nuclear magnetic resonance (NMR) titrations as well as FTIR are commonly utilized. In the following sections, FTIR and NMR are introduced in more detail as they were the predominant characterization methods for the REE complexes of α-aminophosphonates and for studying complexation and adsorption mechanisms in this dissertation. X-ray tomography is only briefly discussed in this dissertation, as the authors' contribution was minimal in X-ray tomography studies.

3.3.1 Physical characterization

Physical characterization includes the characterization of surface area, porosity, and morphology. Surface area is commonly investigated by utilizing BET surface area measurement, although concerns about its reproducibility have been raised.[167] In this measurement, the adsorbent is exposed to an inert gas, typically nitrogen, by increasing the relative pressure of the sample. The gas is adsorbed by the material and covers the whole structure, forming a monolayer of molecules over the whole area of the sample. After the monolayer is formed, more layers of molecules can be formed through physisorption as the gas pressure increases. An estimate of the specific surface area, pore volume, and pore size distribution of the material can be achieved.[168] These parameters can also be determined with X-ray tomography, in which the attenuation of X-rays is utilized to create detailed 3D images of internal structures. The adsorbent material is scanned with X-rays, data on how the scanned sample attenuates X-rays are collected in different directions, and 3D images are then reconstructed using mathematical algorithms. For example, X-ray tomography has been successfully applied in the determination of the porosity of ZrP/polyacrylonitrile adsorbent[132] and 3D-printed adsorbent containing an additive.[43] The adsorption site of Cu to hemp shives has also been investigated with X-ray tomography.[169]

SEM has been widely utilized for the investigation of the morphology of adsorption materials. It also provides information about topographic features and a variation of the composition. For example, aminophosphonate-functionalized PGMA was characterized with SEM to investigate the size of the particles, which were found to vary from 40 to 100 µm.[149] For functionalized silica, SEM was utilized to confirm that the functionalization did not cause damage to

the porous structure of silica.[151] While SEM is a powerful tool for adsorbent characterization, it usually complements other techniques like BET and FTIR to gain a comprehensive understanding of an adsorbent's properties. The disadvantage of SEM is that it is not applicable to nonconducting samples. Although the samples can be coated with conducting metal, such as gold, important information about the smallest surface structures can be lost. Thus, for nonconduction samples, an alternative characterization method, HIM, can be utilized. For example, 3D-printed adsorbents containing additives such as ion-exchange resin Dowex 21K,[43] thiol-functionalized silica,[165] and MOF[170] have been characterized with HIM, which showed that the additives are attached only to the surface of the polymer matrix.

PXRD can be utilized for the investigation of the crystallinity of the material. Adding functional groups or otherwise modifying the structure changes the material structure. This can be observed by the change in the width of the XRD peaks, angle shifting, changes in intensity, or the appearance of completely new peaks. Aminophosphonate functionalized chitosan was characterized with PXRD, and the functionalization caused the crystallinity to be destroyed and turned it into an amorphous structure as hydrogen bonds were extinct.[171] Aminophosphonate functionalized PGMA was investigated with PXRD and the amorphism of PGMA was observed to increase upon functionalization which increased disorder in the structure.[149]

3.3.2 Chemical characterization

FTIR spectroscopy is a common tool to investigate metal coordination to adsorption materials as well as to characterize their functional groups in the solid state. In the aqueous phase metal complexation can be investigated by using an isothermal calorimeter,[172] potentiometric titrations,[172–176] NMR titrations,[172,173,175,176] and luminescence spectroscopy.[177,178] Out of these methods, the three latter ones have been applied to study REE binding to aminophosphonates.[177–181]

3.3.2.1 FTIR

In FTIR spectroscopy, compounds absorb infrared light, causing them to vibrate at specific frequencies. Different functional groups and bonds present in a material have characteristic vibration bands, making FTIR an informative characterization method. Depending on the studied moiety, vibration bands can arise either from stretching (υ) or bending vibrations (δ). Stretching vibrations require more energy and thus typically appear at higher wavenumbers than bending vibrations. For aminophosphonates, characteristic vibration bands arise from stretching and bending vibrations of NH, C-PO_3. P-OR, P=O and P-OH groups, as illustrated in Figure 12.[182,183]

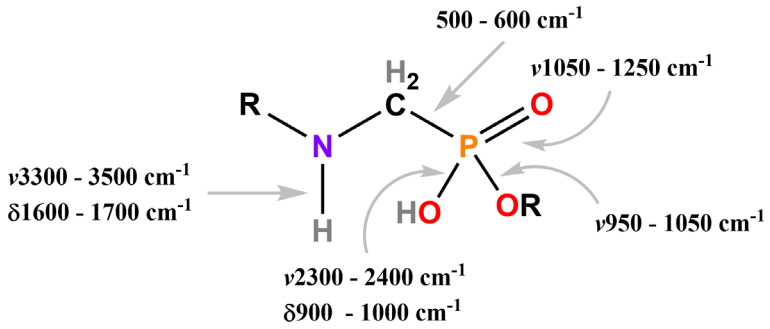

Figure 12. Typical wavenumber regions for the characteristics of stretching and bending vibrations of aminophosphonates.

Upon coordination of a metal ion, shifting or a significant drop in the intensity of the absorption bands of the aminophosphonate moiety is usually detected. For example, mono- and bisaminophosphonates **14** and **16,** presented in section 3.1, have been reported to coordinate to Nd^{3+} through amine moiety as NH and NH_2 vibrations could be detected to shift and/or decrease. Additionally, the intensity of P–O_3 bands at 1043 cm^{-1}, 944 cm^{-1}, and 608 cm^{-1} decreased, and they shifted to 1063 cm^{-1}, 946 cm^{-1}, and 605 cm^{-1} for monoaminophosphonate **14**. Similarly, P=O bands were observed to shift from 1259 cm^{-1} to 1251 cm^{-1}. The results indicated coordination through both phosphonate and amine moieties.[40] For bisphosphonate **16**, no significant shifts were observed for P–O_3, whereas P=O was observed to shift from 1253 cm^{-1} to 1240 cm^{-1}. This shift indicates coordination through the P=O moiety. In the case of PGMA, the P-OH peak at 932 cm^{-1} was observed to disappear upon coordination of Y^{3+} and La^{3+}.[149] Additionally, a new peak was observed to appear at 633 cm^{-1} for both Y^{3+} and La^{3+} coordinated PGMA, which was characterized as the formation of REE–O bond. Similarly, shifting and a decrease of intensity of P=O and P-O_3 were also observed for commercial aminophosphonate ion-exchanger Lewatit TP260 upon coordination of REEs.[41] These observations strongly indicated coordination with the phosphonate moiety. The complexation with liquid-liquid extractants **8–11** was studied to occur from the phosphonate moiety as well. The P-OH stretch at 2300–2400 cm^{-1} was observed to disappear completely and the P=O stretch shifted 10–60 cm^{-1} compared to the uncomplexed reagent.[32,34,36,39] Based on these previous findings, possible coordination modes can be presented for aminobisphosphonates (Figure 13). It is worth noting that in acidic media, in which REE adsorption and complexation typically occurs, aminophosphonates can exist as zwitterions that can show slightly different coordination modes than neutral forms.

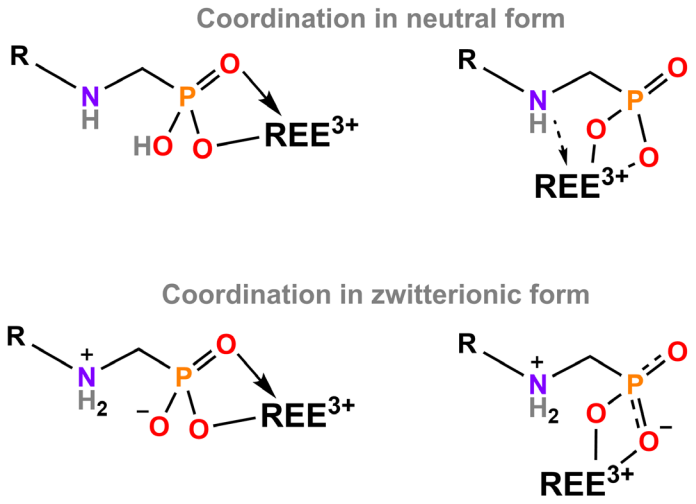

Figure 13. Possible coordination modes for aminophosphonic acids.

3.3.2.2 NMR titration

For the complexation of REEs with aminophosphonates in a liquid state, NMR titrations can be utilized. In short, some atomic nuclei have non-zero spin, and when they are placed in an external magnetic field, these nuclei align with or against the field. When radiofrequency (RF) radiation is applied to the sample, nuclei in the lower energy state can absorb this energy and transfer it to a higher energy state. This transition occurs at a specific frequency, which is unique to each type of nucleus and its chemical environment. As the excited nuclei return to their lower energy state, they emit RF signals. These signals are detected and processed to produce an NMR spectrum, which allows NMR to provide detailed information about the structure, dynamics, and chemical environment of molecules.[184]

The complexation in NMR timescale can either be fast or slow depending on the lifetime of the complex (kinetic stability), which correlates with how strongly the studied metals coordinate to the ligands (thermodynamic stability). When metal binds strongly to a ligand, new peak(s) emerging from the formed complex can be detected in the NMR spectrum, in addition to the free ligand peaks. In this case, the exchange is slow between the metal and ligand and thus both species can be observed. In contrast, fast exchange results from the weaker metal binding to the ligand and in this case, shifting of the NMR peak(s) can be detected. For slow exchange systems, the binding constant can be calculated by knowing NMR peak integrals/areas and the concentration of the complex and free ligand. However, for fast exchanging systems, fitting programs are typically utilized to determine the binding constant.[185] The metal is typically referred to as M and ligand as L. Complexes can form with different M:L ratios, and the equation for the formation can be written as

$$M + L \underset{K_{d1}}{\overset{K_{a1}}{\rightleftharpoons}} ML, \quad ML + L \underset{K_{d2}}{\overset{K_{a2}}{\rightleftharpoons}} ML_2 \ \ldots, \tag{4}$$

where K_a is the binding constant and K_d the dissociation constant for the complex. The binding can continue by adding either ligand or metal to yield M_xL_y complexes. The binding constant is typically presented in logarithmic form if the values are very high.

The complexation with NMR has mainly been studied with divalent metal cations for aminophosphonates and the literature on REEs is scarce. Macrocyclic ligands were found to form 1:1 ML complexes with lanthanoids.[186] Eu^{3+} was shown to coordinate to all of the macrocyclic amine moieties as well as to the phosphonate functionality. Additionally, when ligand was added in excess 1:2 M:L complexes were formed. At low pH values, only phosphonate functionality was found to coordinate into the lanthanoid ions. 7-membered heterocycle containing aminophosphonic acid functionality was found to coordinate to La^{3+} in a 1:1 ML ratio at pH 4 whereas, above pH 8 the formed complexes were mainly 1:2.[187] However, between pH 3 and 5 mixture of free ligand, 1:1 and 1:2 complexes can be detected.

3.3.3 Adsorption isotherms

Adsorption isotherms can be applied to describe the interaction of an adsorbate with an adsorbent at a constant temperature. Among other things, the surface heterogeneity, maximum adsorption capacity, binding mode, and binding energy can be extracted from isotherms by fitting different models to them. Two commonly applied models are the Langmuir and Freundlich isotherms. The Sips model is another frequently used model that aims to address the limitations of the Langmuir and Freundlich models.

The Langmuir adsorption isotherm is based on the assumption that the adsorbate forms a monolayer on the adsorbent, and the adsorption occurs at identical adsorption sites. Additionally, no interaction between the adsorbates on the neighboring sites is assumed to occur. The Langmuir model was invented in 1918 for the adsorption of gas (CO_2) but it has been widely utilized for the adsorption of dissolved ions from a liquid phase as well. The Langmuir model can be either expressed in non-linear (eq. 5) or linear form (eq. 6), although the linear form is more used in the literature due to the easier fitting of experimental data.

$$Q_\mathrm{e} = \frac{Q_\mathrm{max} b C_\mathrm{e}}{1 + bC_\mathrm{e}} \tag{5}$$

$$\frac{C_\mathrm{e}}{Q_\mathrm{e}} = \frac{1}{Q_\mathrm{max} b} + \frac{1}{Q_\mathrm{max}} C_\mathrm{e} \tag{6}$$

In the above equations, Q_e is the amount of adsorbed adsorbate per mass of the adsorbent (mg/g), C_e is the concentration of the solution in equilibrium (mg/l), and b is the Langmuir constant. By fitting experimental data to the equation (linear or non-linear), maximum adsorption capacity Q_{max} (mg/g) can be obtained. Langmuir constant gives information about the adsorbate-adsorbent equilibrium. With low adsorbate concentrations, b is also low, indicating that the equilibrium is on the side of the adsorption. This is in contrast to high adsorbate concentrations in which b is typically high, indicating that more of the free adsorbate is present in the system and the equilibrium is closer to the non-adsorbed adsorbates.

The Freundlich adsorption isotherm is based on the formation of a multilayer to a heterogenous adsorption surface. In contrast to the Langmuir adsorption isotherm, where all adsorption sites are assumed to be identical in energy, the Freundlich adsorption model assumes that adsorption heat and affinities are not uniformly distributed between the adsorption sites. The Freundlich adsorption isotherm was developed in 1907 for the adsorption of contaminants from water.[188] The Freundlich model can similarly be expressed in non-linear (eq. 7) or linear (eq. 8) form:

$$Q_e = K_f C_e^{\frac{1}{n}} \tag{7}$$

$$\ln Q_e = \ln K_f + \frac{1}{n} \ln C_e \tag{8}$$

where K_f is the Freundlich constant and, similar to the Langmuir constant b, it indicates the equilibrium between an adsorbent and adsorbate. The surface heterogeneity is expressed with n. If $1/n$ is closer to zero, the surface is more heterogenous whereas values closer to one indicate a more homogenous adsorption surface.

The Sips adsorption isotherm is the combination of the Langmuir and Freundlich adsorption isotherms in which limitations of both models have been circumvented. Unlike the Langmuir isotherm, the Sips isotherm also fits multilayer adsorption, and high concentrations of adsorbates can be used, unlike in the Freundlich isotherm. The Sips isotherm is expressed in Equation 9 as

$$Q_e = \frac{Q_{max} K_s C_e^{n_s}}{1 + K_s C_e^{n_s}} \tag{9}$$

in which K_s is Sips isotherm constant (l/mg) and n_s Sips isotherm exponent.[189] Sips isotherm can effectively model systems with non-ideal adsorption behaviors.[190] For example, some adsorption systems exhibit sigmoid isotherm shapes, which are difficult to model with Langmuir or Freundlich.

Adsorption isotherms have been utilized for determining the maximum adsorption capacity Q_{max} for various aminophosphonate adsorption materials.[42,149,191] The Langmuir constant b can also indicate the preference of the

adsorbent towards different REEs. Various aminophosphonates have been shown to fit better to the Langmuir adsorption isotherm when investigating the adsorption of REEs.[42,149,191] For aminophosphonate-functionalized PGMA, Langmuir, Freundlich, and Sips isotherms were modelled for Y^{3+} and La^{3+} adsorption, from which Langmuir was found to be the best model.[149] Q_{max} was determined to be 0.79 mmol/g for La^{3+} and 0.77 mmol/g for Y^{3+}. The affinity towards La^{3+} was found to be higher as the coefficient b was 13 l/mmol for La^{3+} and 5 l/mmol for Y^{3+}. In another study, Freundlich and Langmuir isotherms were applied for Nd^{3+} adsorption by aminophosphonate-functionalized chitosan, and the Langmuir model was found to fit the experimental data better than the Freundlich one.[191] Maximum adsorption capacity was found to be 0.22 mmol/g and the Langmuir constant b 8 l/mmol. Thus, a similar preference towards REEs was observed for the aminophosphonate-functionalized chitosan when compared to PGMA (5–13 l/mmol). Commercial ion-exchange resin Purolite S950 was also observed to fit better to the Langmuir isotherm than Freundlich.[42] La^{3+} maximum adsorption capacity Q_{max} was found to be 0.64 mmol/g and Langmuir constant b 12.9 l/mmol similar to the PGMA.

Although adsorption isotherms are commonly used to investigate adsorption mechanisms (such as monolayer vs. multilayer formation), significant uncertainty is associated with mechanism studies if only isotherms are used. For example, for the adsorption of La^{3+} by commercial Lewatit TP260, contradictory results have been found with the different isotherm models.[41,42,192] This issue has also been raised in a review paper focusing on the subject.[193] Indeed, a more accurate picture of the mechanism can be obtained when adsorption isotherms are used in conjunction with other methods like FTIR. Despite the shortcomings of the adsorption isotherm models, there is consensus in the literature that aminophoshonate-based adsorbents tend to follow the Langmuir adsorption isotherm when they adsorb REEs.[42,149,191] This indicates that REEs form a monolayer on the surface of aminophoshonate-based adsorbents rather than a multilayer.

4 RESULTS AND DISCUSSION

This chapter summarizes the main findings of the published Papers **I** and **II** and unpublished Paper **III**. It begins with a discussion on the solubility, acid–base, and complexation properties of synthesized α-aminophosphonic acids, followed by their utilization as precipitation and separation agents for REE, Th, and U (Paper **I**). Following this, the chapter examines the use of self-synthetized and commercial α-aminophosphonate-based additives as adsorbents in 3D-printed filters. This section starts with the characterization of the 3D-printed filters and proceeds to their utilization in REE recovery from two secondary sources, acidic mining wastewater (Paper **II**) and NdFeB magnet (Paper **III**).

4.1 Synthesis and properties of α-aminophosphonic acids

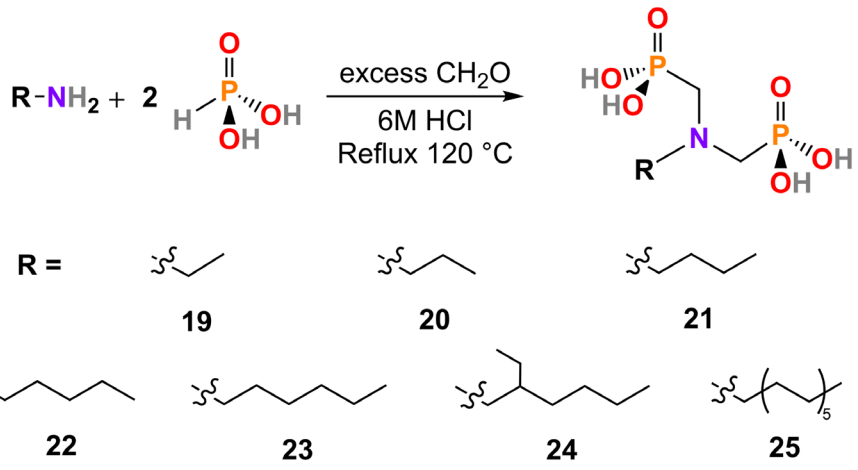

Figure 14. Synthesis procedure for the α-aminophosphonic acids utilized as precipitation agents (**19–24**) and an additive in 3D-printed filters (**25**).

α-Aminophosphonic acids **19–25** were synthesized in a one-pot Kabachnik-Fields reaction described by Moedritzer and Irani (Figure 14).[145] In this reaction, condensation between primary amine, phosphorous acid, and aldehyde occurs

in the presence of an acid catalyst. Typically, HCl is used as an acid catalyst but other acids can also be used as a catalyst, such as *p*-toluenesulfonic acid or copper triflate.[40,148,150] The advantage of HCl is that it also acts as a solvent in the reaction. Water-soluble aminophosphonic acids (**19–24**) were synthetized for precipitation studies, and water-insoluble aminophosphonate (**25**) was utilized as an additive in 3D-printed filters. **19,** with the shortest alkyl chain, was the most water-soluble (326 g/l), but the solubility decreased as the length of the hydrophobic alkyl chain increased, making **24** the least water-soluble precipitation agent (9.5 g/l). As expected, **25** was fully insoluble in neutral or acidic aqueous solutions but dissolved into a basic solution if the pH was over 8. Given the water-insolubility of **25** and the solid-phase separation studies conducted in the pH range of 0–4 to prevent the precipitation of REEs as hydroxides, **25** seemed to be an ideal additive for the 3D-printed filters.

4.1.1 Acid–Base Properties

To figure out the protonation degree of the utilized aminophosphonic acids, ^{1}H and ^{31}P NMR titrations were performed in D_2O. The most water-soluble **19** was chosen for the experiments to avoid precipitation during the NMR measurements. The pH of a solution containing **19** was adjusted from 0.5 to 10.5 with an increment of 0.5, and the shifts of the methylene (N–**CH$_2$**–P) and ^{31}P peaks were monitored in ^{1}H and ^{31}P NMR spectra, respectively. The OH peak could not be observed in the ^{1}H NMR spectrum due to a fast proton deuterium exchange in D_2O. The shifts of ^{1}H and ^{31}P peaks in each pH value were plotted as a function of pH, revealing three equivalent points around pH 1, 5, and 10 in both plots. From these plots, pK_a values of 1.33 and 5.55 were calculated for the first and second protonation of the $P(OH)_2$ group, respectively. No reliable pK_a value could be calculated for the third protonation due to the deprotonation being incomplete in the measured pH range. The calculated p*K*a values of **19** are close to the ones reported for aminophosphonates.[194,195] It was assumed that **19** exists as zwitterion like other aminophosphonates,[195,196] and thus structures depicted in Figure 15 were presented for each protonation degree.

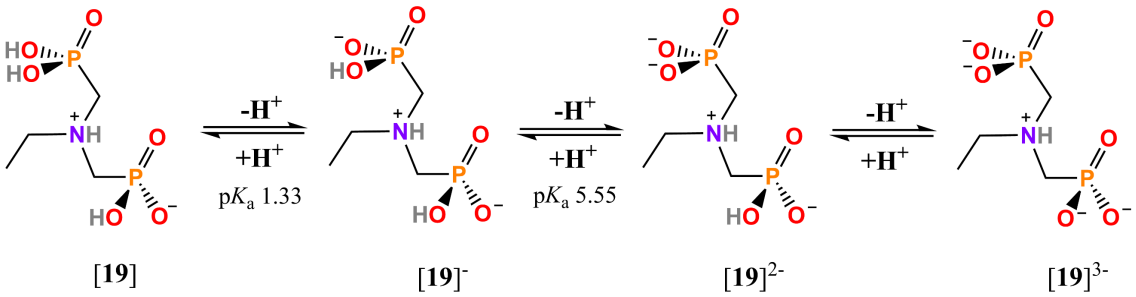

Figure 15. Zwitterionic structure of **19** in different protonation degrees.

4.1.2 Complexation in solution

To understand the complexation properties of **19–24** with REEs in solution, NMR titration studies were conducted for **19** with metals Y, La, or Lu. First, the metal-to-ligand titration was performed by incrementally adding 1 mM of Y, La, or Lu nitrate solution to a 10 mM stock solution of **19** until 1 equivalent was reached. After each addition, ^{1}H and ^{31}P NMR spectra were measured from the resulting solution. Unlike in the pH titration studies, N–**CH$_2$**–P protons of **19** were harder to distinguish under the quartet of CH$_3$–**CH$_2$**–N protons because no apparent peak shift was observed for them. Therefore, only the shift of ^{31}P peaks was followed with an NMR. Second, similarly to metal-to-ligand titration, ligand-to-metal titration was performed by incrementally adding a 3 mM solution of **19** to a 10 mM solution of Y, La, or Lu until 5 equivalent excess was reached. With Lu, however, the solution formed a gel-like structure that prevented completing the ligand-to-metal titration. The data was fitted to binding isotherms with the HypNMR2008 fitting program to investigate the binding models of **19**.

Table 1. Logarithmic binding constants and possible coordination modes for **19** metal complexes. ML = metal to ligand, LM Ligand to metal.

	log*K* 1:1	log*K* 1:2	log*K* 1:3
Y$_{ML}$	2.4 ± 0.2	4.9 ± 0.4	7.3 ± 0.6
Y$_{LM}$	2.6 ± 0.2	4.4 ± 0.4	6.7 ± 0.7
La$_{ML}$	2.6 ± 0.5	4.4 ± 0.1	
La$_{LM}$	2.7 ± 0.5	4.3 ± 0.4	6.8 ± 0.3
Lu$_{ML}$	2.1 ± 0.3		
Lu$_{LM}$	-		

The results indicated that Y and La form 1:1, 1:2, and 1:3 (M:L) complexes with **19** in the solution (Table 1). A 1:4 complex also fitted to the isotherm in one of the replicates for both Y and La. Therefore, the formation of complexes with a higher ligand ratio is possible if enough ligand is present in the solution. For Lu, however, a 1:1 complex already showed the best fit to the binding isotherm and fitting to 1:2 or 1:3 models did not significantly improve the fit.

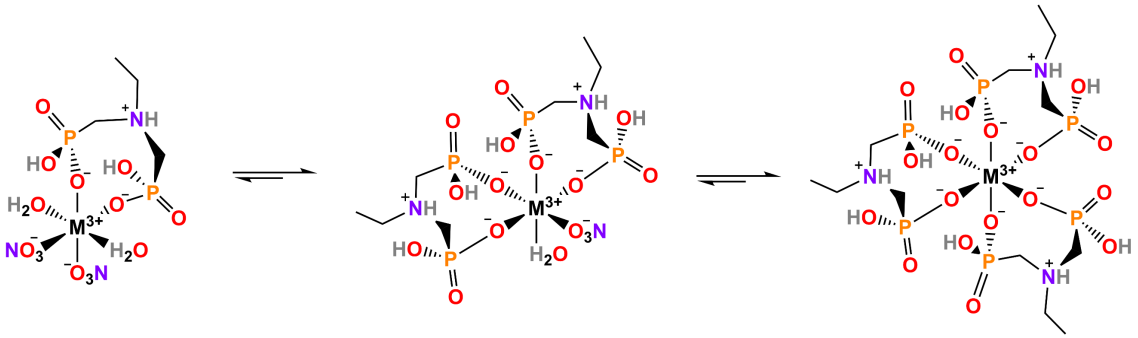

Figure 16. Coordination modes of **19** with REEs 1. M^{3+} = Y, La, Lu.

The determined M:L ratios are similar to the ones obtained for Eu^{3+} and La^{3+} complexes of cyclic aminophosphonates.[186,187] As the complexation was investigated in the pH range of 1.4 to 2.4, ligand **19** likely existed in its deprotonated [**19**]$^-$ form in the solution as suggested by the first measured pK_a value. Based on the NMR titration studies, the plausible metal-ligand coordination was proposed for the investigated aminophosphonates (Figure 16), in which the NO_3^- ions and water are suggested to complete the coordination sphere. Similarly, acidic counterions have been observed in crystal structures of aminophosphonate REE complexes,[197,198] and a coordination of water has been proven by luminescent spectroscopy.[177] Considering all the above-mentioned, the results indicate that REEs with the largest ionic radii bind in a 1:3 ratio with the investigated aminophosphonates, while the smaller REEs prefer 1:1 and 1:2 M:L ratios. Therefore, the results suggest that optimizing the ligand-to-metal ratio could potentially be used to separate LREEs from HREEs.

4.2 Precipitation of REEs, Th, and U with aminophosphonic acids

The separation of REEs, Th, and U was investigated in an acidic aqueous solution using **19–24** as precipitation agents in the function of pH ranging from 0 to 4. pH was not raised above 4 to limit precipitation of REE, Th, or U as hydroxides. It can be observed from Figure 17 that the precipitation percentages increase with increasing pH. This results from the higher protonation degree of the ligands changing from the non-deprotonated state (pH 0) to the first deprotonated state (pH 4) with a minor contribution from the second protonation state. Generally, **22–24** were more efficient precipitating agents than **19–21**, indicating that aminobisphosphonic acids with alkyl chains shorter than five atoms form more soluble complexes with the investigated metals in utilized conditions. However, no clear trend was observed among **19–21**, because **19** precipitated more HREEs, Sc, Th, and U than **20** and **21**. The preference towards Sc and HREEs was expected as aminophosphonates bind more strongly to smaller ions.[41,199] For **22–24**, the separation of Sc and Th from REEs was very efficient already at pH 1. In this pH, REEs remain in the solution, while Sc, and Th almost completely precipitate from the solution. In addition to Sc and Th, **24** also precipitated 100% of U at pH 1, separating all these three elements from REEs. Interestingly, for **22**, a decrease in the precipitation percentage was observed around pH 2.5 every other metal except for Sc and Th, which likely results from the complexes dissolving back to the solution at this specific pH value.

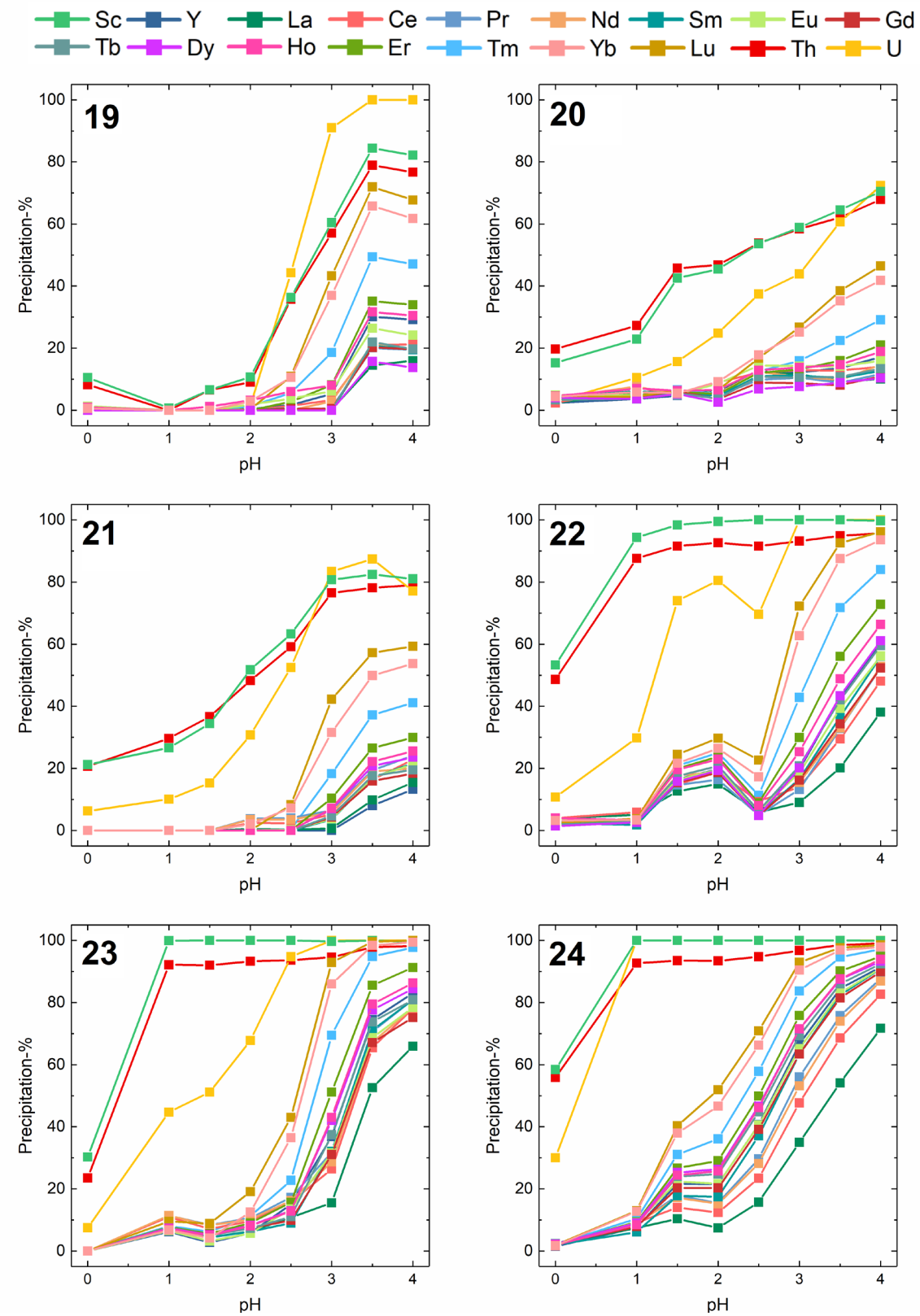

Figure 17. Precipitation percentages in the function of pH for REEs, Th, and U for **19** – **24**.

Although the separation of Sc, Th, and U from REEs was successful, the separation between adjacent REEs was rather poor. The closer inspection of the calculated *SF*s between the adjacent lanthanoids revealed that the *SF*s range from 1.00 to 4.33. Separation factors close to 1.00 were achieved for multiple adjacent pairs generally from Nd to Er, indicating no separation between these pairs, while the adjacent heavier lanthanoids including Y separated better with slightly greater separation factors. For example, the obtained $SF_{Sm/Eu}$ was 1.20 ± 0.05, whereas $SF_{Tm/Yb}$ was 4.33 ± 0.04 when **23** was used as the precipitation agent at pH 4. Compared to DEHPA and EHEHPA, the obtained *SF*s were greater for HREEs, but not for LREEs.[11] In the case of La/Ce separation greater separation factors were achieved with **22** (3.81) compared to the fractional crystallization with borates (1.43) or oxalate precipitation (1.5–2.5).[75,92]

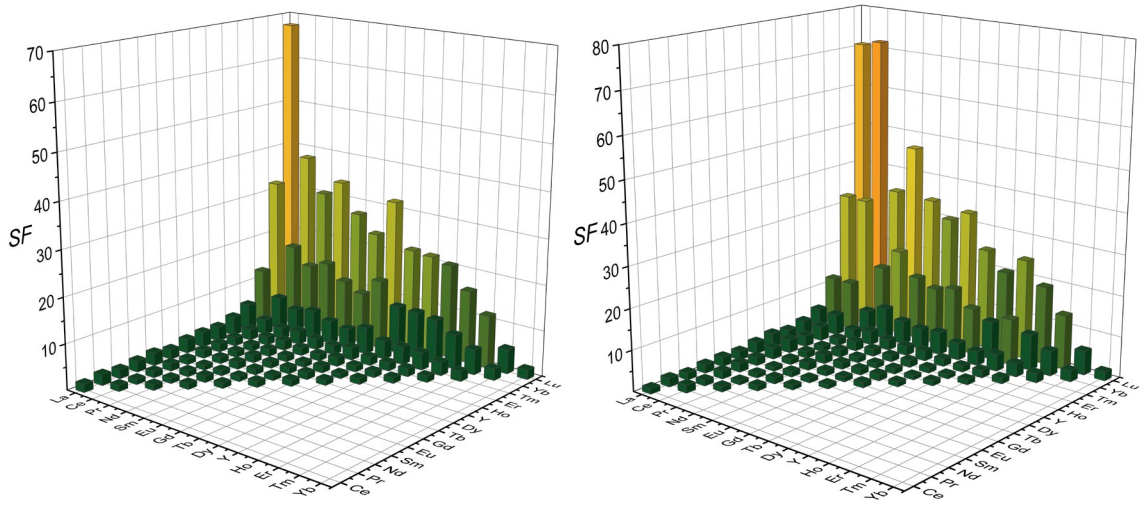

Figure 18. Separation factors for (a) **22** and (b) **23** at pH 3.5 and 3 respectively.

In contrast to the adjacent lanthanoid separation, the separation between HREEs and LREEs was found to be more successful. The best *SF*s were achieved with **22** and **23** at pH 3.5 and 3, respectively (Figure 18). In these pH values the precipitation percentages were considerably higher for HREEs than they were for LREEs. Thus, as the difference in ionic radii between two different REEs increased, the *SF*s simultaneously increased. For example, $SF_{La/Lu}$ was calculated to be 67.7 ± 16.4 for **22** and 71.1 ± 6.9 for **23**. Noticeably, the HREEs were easier to separate from each other than the LREEs were, as the separation factors were observed to be considerably higher for Tm, Yb, and Lu than for the rest of the REEs. This differs from what was observed for DEHPA in liquid-liquid extraction (Figure 3), in which the LREEs were easier to separate. The difference might originate from DEHPA having similar binding constants towards HREEs, which could explain the smaller difference in their extraction (log*K* Dy–Yb 3.63–4.14) and thus lower separation factors for HREEs.[200]

4.3 Solid-phase extraction with 3D-printed filters

4.3.1 Preparation of 3D-printed filters

The 3D-printed filters containing **25** as an additive were prepared by mixing 30 wt% of **25** and 70 wt% of the polymer matrix, nylon-12. From the resulting powder, the filters were printed by SLS printing, where particles are sintered together by a laser. During sintering, most of the additive **25** attaches to the surface of the partially melted nylon-12 matrix and remains intact in the filters during the solid-phase extraction process. The characterization of the 3D-printed filters is discussed in more detail in section 5.3.2. Likewise, filters containing commercial aminophosphonate-functionalized cation exchanger Lewatit TP260 and nylon-12 were printed by SLS printing, but the percentage of additive was varied from 5 wt% to 50 wt%. While the filters containing 30 wt% or less of the additive TP260 were robust, increasing the additive to 40 wt% and 50 wt% led to the partial disintegration of the filters. Thus, no filters with more than 50 wt% of the additive were manufactured, and the 30 wt% filters were primarily used in the solid-phase extraction experiments. The 30 wt% of the additive also enables the easy comparison of the results obtained for the filters containing either **25** or TP260. For clarity, the filters containing 30 wt% of **25** or Lewatit TP260 will be referred to as PA-**25** and PA-TP260, respectively.

4.3.2 Characterization of PA-25 and PA-TP260

The micro-level structures and morphologies of the PA-**25** and PA-TP260 filters were investigated using a helium-ion-microscope (HIM) and X-ray tomography, whereas FTIR spectroscopy was applied to characterize the functional groups of the additives and polymer matrix. HIM images revealed a clear difference between the pure nylon-12 and PA-**25** filters. In the former, the morphology of the particles is round-shaped with no sharp edges, while the latter has a more plate-like morphology indicating that **25** is attached to the surface of the nylon-12 particles (Figure 19). TP260 particles were much harder to distinguish from nylon-12 particles than the plate-like **25**. However, small particles that are unlikely nylon-12 can be observed in the HIM image of the PA-TP260. Moreover, the X-ray tomography images were much more informative for the PA-TP260 than HIM images (see **III**). Importantly, a porous structure can be seen for both filters. This is a crucial property for the adsorption materials because, without voids and flow channels, the solutions would not be able to pass through the filters. The good porosity of the PA-**25** was further confirmed by X-ray tomography, and it was found to be 59 ± 2%. Similar porosity (50 ± 2%) was also measured for the PA-TP260.

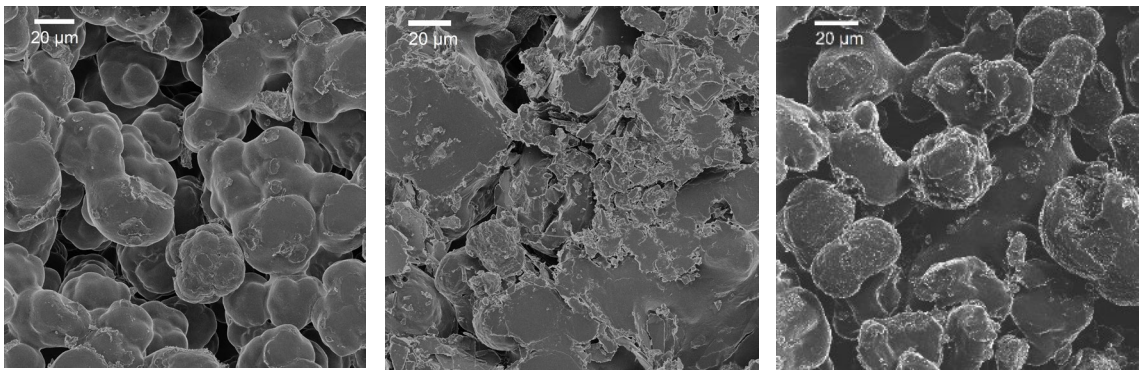

Figure 19. HIM images of the pure nylon-12 (left), PA-**25** (middle), and PA-TP260 (right) filters.

The FTIR spectra of pure nylon-12, **25**, TP260, PA-25, and PA-TP260 were compared to ensure that the additives **25** and T260 were integrated into the polymer matrix and no decomposition occurred during 3D printing. The FTIR spectrum of pure nylon-12 shows the characteristic peaks at 3291 cm^{-1} and 1635 cm^{-1} arising from N-H and C=O stretches, respectively. These peaks, as expected, are also seen in the spectra of the PA-**25** and the PA-TP260 (Figure 20). Two peaks arising from asymmetric and symmetric CH_2 stretching around 2916 cm^{-1} and 2484 cm^{-1}, respectively, are also detected for the nylon-12, PA-**25**, and PA-TP260. The same stretches, but with a small shift (<3 cm^{-1}), are also observed for ligand **25** as it contains a long alkyl chain. The small shift might originate from the CH_3 group of **25,** which can shift C–H stretches towards higher wavenumbers.[182,183] Additionally, CH_2 rocking can be detected around 719 cm^{-1} for nylon-12, PA-**25**, and PA-TP260. For **25**, two very strong peaks are observed at 1154 cm^{-1} and 936 cm^{-1} in the spectrum that can be assigned to the asymmetric and symmetric stretching of the PO_3 moiety, respectively. For the PA-**25**, these peaks are slightly shifted (<3 cm^{-1}), but their intensity remains strong. For TP260, the phosphonate peaks are detected at 1158 cm^{-1} and 916 cm^{-1}, from which the latter shifts 6 cm^{-1} in the spectrum of the PA-TP260. A wide peak between 2500–2000 cm^{-1} is additionally detected for **25**, which arises from the P-OH moiety. For TP260, the OH moiety stretches over a much wider area than it does for **25**, but it is still observable in the spectrum. Given that the FTIR spectra of both the PA-**25** and PA-TP260 filters show characteristic peaks from nylon-12 and their respective additives **25** and TP260, it is evident that the 3D-manufacturing process did not cause decomposition of the additives, and they were successfully integrated into the filters. The main IR peaks of the studied aminophosphonates correspond to similar aminophosphonates reported in the literature, as discussed in section 3.3.2.1.[32,34,36,39–41,149]

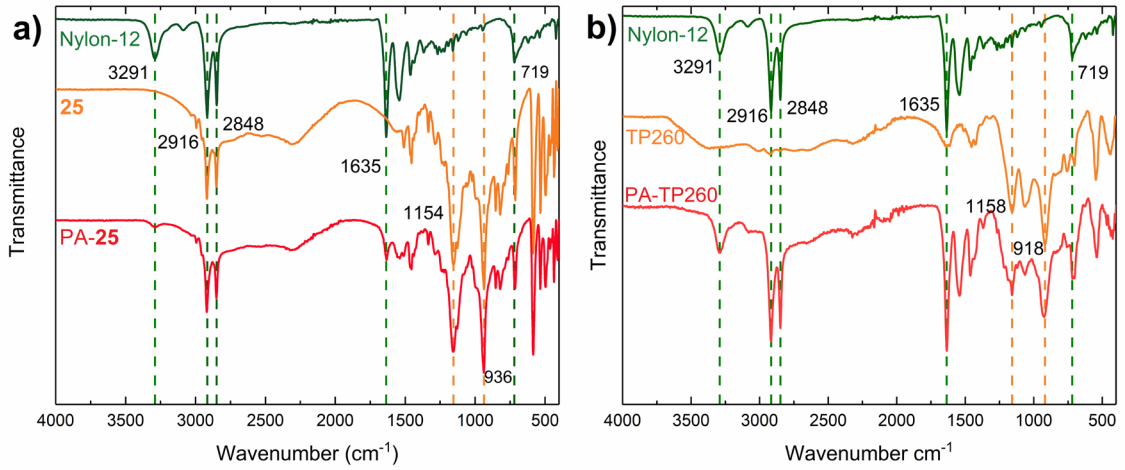

Figure 20. FTIR spectra of (a) the PA-**25** and (b) the PA-TP260. Green dashed lines mark the characteristic peaks of nylon-12, whereas orange dashed lines mark the characteristic peaks of the additives.

4.4 Recovery of REEs from mining wastewater

4.4.1 Adsorption properties of PA-25

The PA-**25** was applied for the recovery of REEs from simulated mining wastewater containing 100 mg/l of Al, K, Ca, and Zn, and 10 mg/l of Sc, Fe, Co, Cu, Y, Nd, Dy, and U in 0.5 M H_2SO_4. Three filters were stacked inside a 10 ml syringe and the flow rate was controlled with a syringe pump. Adsorption was studied as a function of pH at a range of 1 to 4 to limit the precipitation of ions as hydroxides.

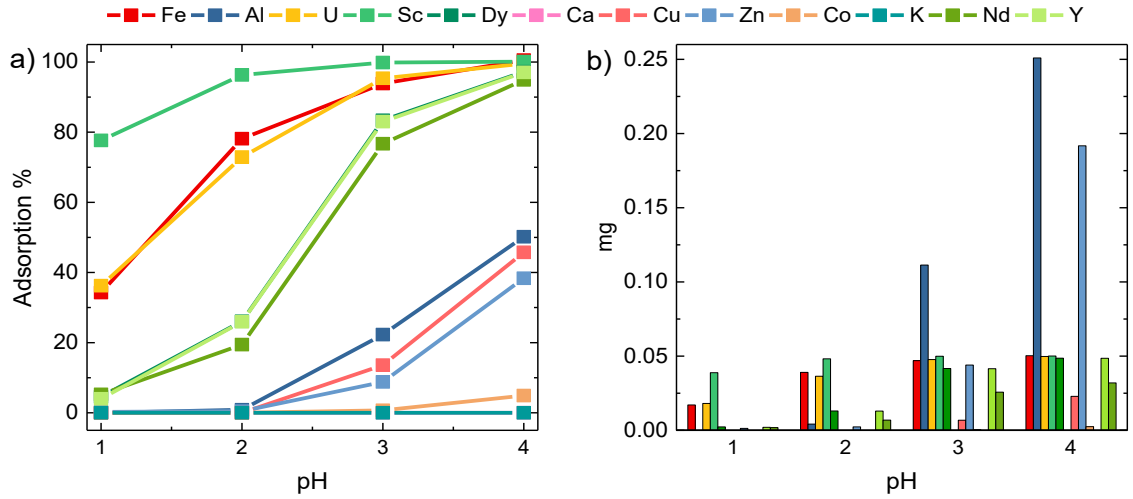

Figure 21. (a) Adsorption percentages for each metal in the function of pH when a 5 ml of solution is passed through the three filters. (b) Adsorbed amount of metals in mg in each pH value.

The adsorption properties of the PA-**25** were first tested with 5 ml of the synthetic mining wastewater solution, which was passed through the filters at a flow rate of 90 ml/h. Figure 21 shows that the adsorption percentages for all metals, except K and Ca, increase with the rising pH, and reach their maximum at pH 4. At pH 1, the PA-**25** filters adsorb almost solely Sc, Fe, and U, and only small amounts of Y, Nd, and Dy. The trend is comparable to the precipitation studies, where the complexes of Sc and U with **19–24** precipitated more efficiently from acidic solutions than REEs at lower pH values. The PA-**25** shows no adsorption towards Al and Zn at pH 1 and 2, but when the pH is increased to 3 and 4, both metals, especially Al, are adsorbed into the filters (Figure 21b). Similar results have been reported in adsorption studies of REEs from acidic mining wastewaters using a commercial aminophosphonate-based adsorbent.[121,122] However, the commercial adsorbents Purolite S950, and Lewatit TP260 have been reported to adsorb significantly more (>80%) of Al, Ca, Co, Cu, and Zn than PA-**25**.[121,122] Thus, PA-**25** is more suitable for concentrating REEs from the studied transition elements and Al. Based on our findings and earlier results, pH 4 is the most suitable pH for the maximum adsorption of metals from mining wastewater. However, if the separation of REEs is the objective, pH 2 is preferable, as only Fe and U are co-adsorbed with REEs at this pH.

The uptake of the PA-**25** as the function of pH was investigated by passing 40 ml of mining wastewater solution through the three stacked filters and collecting samples every 5 ml. The adsorption decreased steeply after the first 5 ml was passed through the filters at the pH range of 1–3. Thus, the uptake limit was almost reached after 25 ml of solution was passed through the filters at pH 1, while more than 30 ml was needed at pH 2 and 3 (Figure 22). At pH 4, however, no saturation was detected even after 40 ml of solution was passed through the filters. At this pH, 60% of Sc and Fe was still adsorbed, followed by 40% of U and 20% of Nd, Dy, and Y. Given that the uptake limits were almost reached at pH 1, 2, and 3, the approximative saturations limits of 0.14 ± 0.03 mg, 0.34 ± 0.11 mg, and 0.75 ± 0.15, respectively, were determined for them. Two other observations were also made from the data. First, the slow accumulation of Al and Zn into the filters was detected at each pH during the adsorption of metals. Second, when the pH was increased, the relative amount of adsorbed Sc decreased when compared to other adsorbed metals.

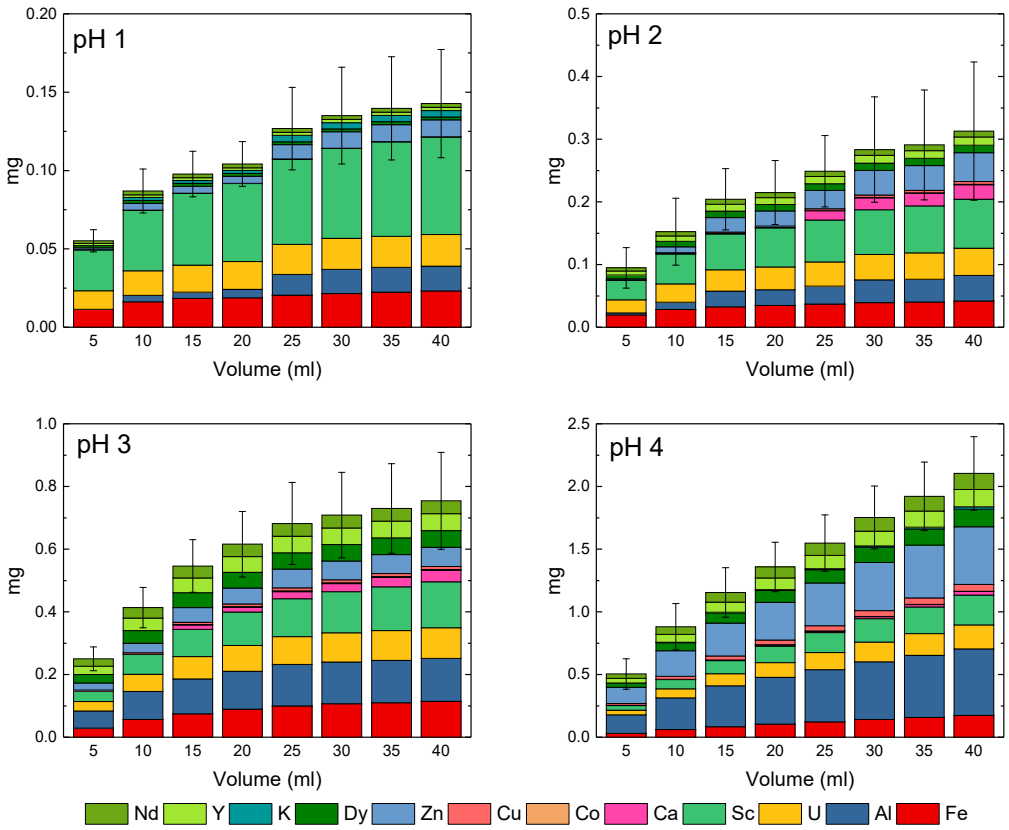

Figure 22. Uptake for the PA-**25** at pH 1, 2, 3, and 4. The amount of metals are given in mg.

4.4.2 Mineral acid elution

A crucial step after adsorbing the metals is their efficient elution from the PA-**25** filters. Three mineral acids (HNO_3, H_2SO_4, and HCl), each with three different molarities (1 M, 3 M, and 6 M), were investigated as eluents. The flow rate of the syringe pump was set to 15 ml/h to ensure a sufficiently long contact time for the acids with the filters.

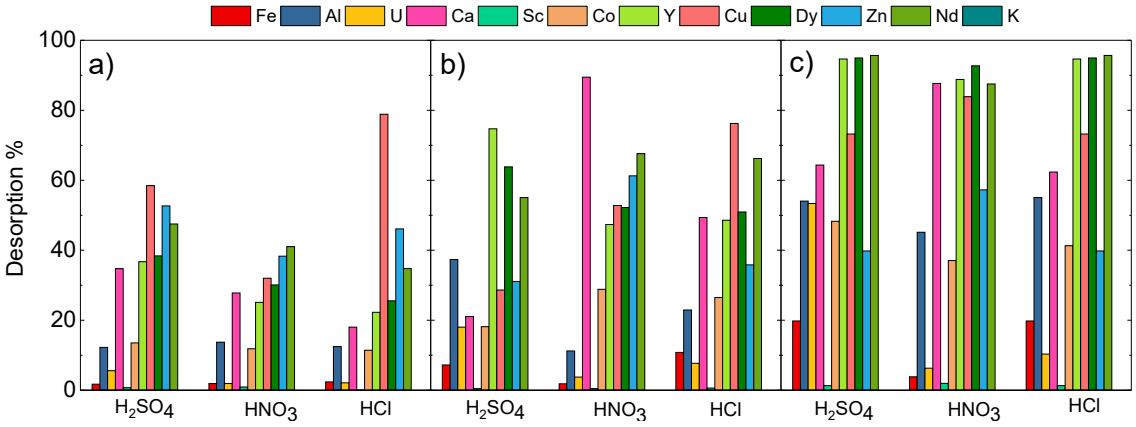

Figure 23. Elution percentages for (a) 1 M, (b) 3 M, and (c) 6 M H_2SO_4, HNO_3, and HCl.

With 1 M HNO_3 and HCl, the elution percentage for Y, Nd, and Dy ranged from 20% to 40%, whereas with H_2SO_4 slightly greater elution percentages were obtained as they were between 40% and 50% (Figure 23). With 1M acids Al, Ca, Cu, and Zn were also eluted, and thus no selectivity towards Y, Nd, and Dy was obtained with 1 M eluents. As the concentration of acids was increased to 3 M, more metals were eluted but the main trends remained the same, with H_2SO_4 as the more efficient eluent for REEs (excluding Sc) than HNO_3 and HCl. With 6 M acids, >90% of REES (excluding Sc) were eluted. However, H_2SO_4 also eluted over 50% of U and 20% of Fe. Interestingly, only a minimal amount of Sc was eluted with the investigated mineral acids. None of the studied acids selectively eluted REEs, but as the co-eluting of the most adsorbed metals, that is Fe and U, was minimal with 6 M HNO_3 it was chosen as the most suitable eluent for REE recovery. In addition to almost completely eluting REEs (excluding Sc), utilizing 6 M HNO_3 ensures that the solution has an acidic background for further processing. However, precautions should always be taken into account when using HNO_3 due to its oxidizing nature.

4.4.3 Recovery scheme

Based on the results of adsorption and elution tests, a recovery scheme for the REE fraction from the mining wastewater was developed. pH 2 was deemed the optimal pH value for the recovery as co-adsorption of other elements, such as Al and Zn, was much smaller compared to higher pH values. Because the adsorption test showed that approximately 20% of Y, Nd, and Dy were adsorbed by the three stacked PA-**25** filters at pH 2, it was assumed that the five sets of

three stacked filters would be enough to adsorb all REEs from the 40 ml of mining wastewater. For eluting REEs from the PA-**25**, 30 ml of 6 M HNO_3 was used to minimize the co-elution of U and Fe.

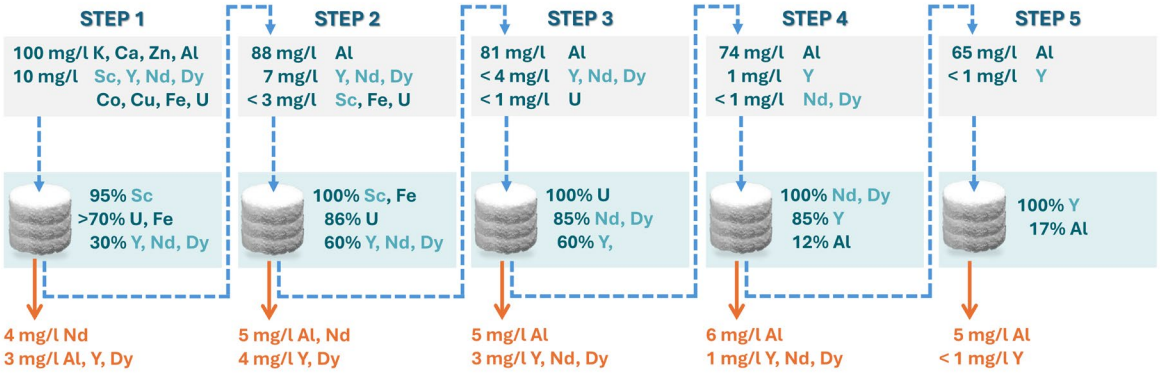

Figure 24. Recovery scheme for REEs from mining wastewater. The adsorbed amounts for each element compared to the starting amount are given in percentages (blue). The eluted amounts for REEs and Al are given in mg/l (orange).

The five-step separation process is illustrated in Figure 24. The initial concentration for Al, K, Ca, and Zn was 100 mg/l, and for Sc, Fe, Co, Cu, Y, Nd, Dy, and U 10 mg/l. During the first step, a majority of Sc, Fe, and U were adsorbed into the filter alongside 30% of Y, Nd, and Dy (Figure 24). The remaining amounts of Sc, Fe, and U were adsorbed in the second and third steps of the process, removing these elements completely from the wastewater. For adsorbing all Nd and Dy, four sets of filters were required, whereas for Y all five were needed. As Fe, REEs, and U were slowly adsorbed from the solution, the adsorption of Al was detected to increase. Thus, the fourth and fifth filters contained significant amounts of Al due to the absence of other strongly adsorbing elements. Because 6 M HNO_3 did not elute Sc, Fe, or U from the filter, the concentrated REE (excluding Sc) fraction was obtained when the first three sets of filters were eluted, yielding a solution containing mainly 9–12 mg/l of REEs (excluding Sc) and 3–5 mg/l of Al. These three fractions contained significantly less Al compared to the initial solution, where the concentration of Al was ten times higher than that of REEs. In contrast to the first three sets of filters, the fourth and fifth sets contained higher amounts of Al than REEs. Thus, to get the REE-rich concentrate, REEs should be eluted only from the first three sets of filters. During the whole process of five adsorption steps, 20% of Co, Ca, K, and Zn, 30% of Cu, and 50% of Al were adsorbed into the filters. The initial, adsorbed, and eluted amounts after the five adsorption steps, as well as stepwise elution amounts in micrograms are presented in Figure 25. With aminophosphonate-based adsorbents, similar results have been obtained for recovering REEs from acidic mining wastewater.[121,122,201]

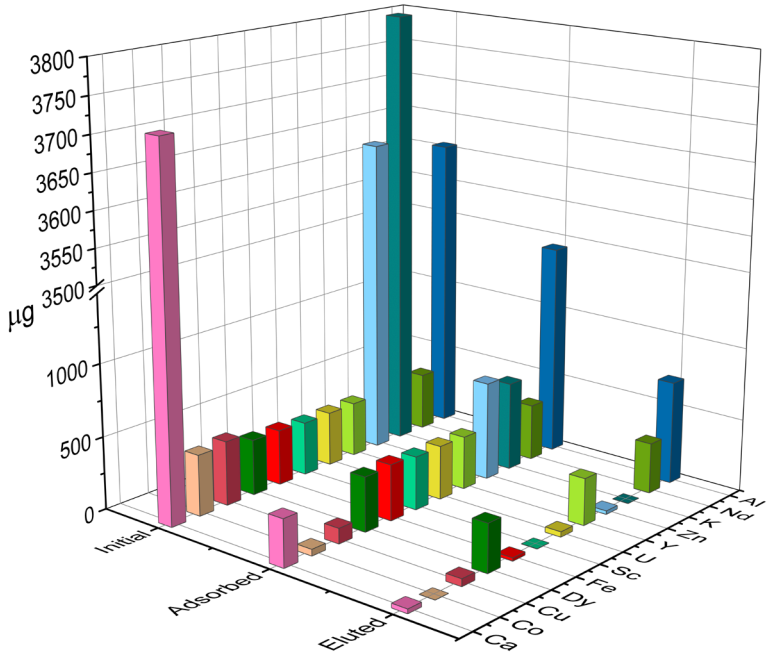

Figure 25. Initial, adsorbed, and eluted amounts of elements after the five-step recovery process.

4.5 Recycling NdFeB magnet

For the recovery of elements from NdFeB magnet waste, both PA-**25** and PA-TP260 filters were utilized. The first step of the process was the leaching of the NdFeB magnet. The organic derivate of sulfuric acid, namely methanesulfonic acid (MSA), was used as a leaching agent as it possesses similar properties to sulfuric acid but has a lower environmental impact.[202] To investigate the leaching efficiency of MSA, the grounded NdFeB magnet was first completely dissolved to aqua regia to obtain its elemental composition (Table 3). Different concentrations (10–100 v/v%) of MSA were then used in the leaching of the magnet while keeping the temperature (60 °C), time (20 h), and S/L ratio (5 g/l) constant. Concentrations of 10 to 60 v/v% MSA were found to dissolve >95% of the magnet. The most effective dilute concentration, that is 10 v/v% MSA, was chosen for further studies to keep the acid consumption to a minimum. This also minimized water consumption because after leaching the solution was diluted to have a 5% MSA background, which was used in the adsorption studies.

Table 2. Elemental composition of the studied NdFeB magnet from aqua regia dissolution (AR) and with 10 v/v% MSA determined using ICP-OES.

	Fe	Nd	Pr	Dy	Al	B, Co, Cu, Sm, Tb, Ho
AR Wt%	63.2 ± 1.3	21.0 ± 0.3	6.2 ± 0.2	2.7 ± 0.1	1.1 ± 0.1	<1
10% Wt%	62.1 ± 1.1	20.8 ± 0.4	6.1 ± 0.2	2.8 ± 0.1	0.9 ± 0.1	<1

As the NdFeB solution contained significant amounts of Fe, which adsorbed readily into the PA-**25** filter (see above), it was first removed via precipitation before the adsorption tests. Due to the non-oxidizing nature of MSA, it was deduced that Fe existed as Fe(II) rather than Fe(III) in the leachate. Fe(II) precipitates as hydroxides around pH 9,[203] which is not an optimal pH for the precipitation if co-precipitation of the other elements must be prevented.[204] Therefore, Fe(II) was first oxidized to Fe(III) by adding an equivalent amount of H_2O_2 to the solution and then precipitated by adjusting the pH to 3.7–4.0 with NH_4OH.[205] This led to the rich brown precipitate and 99.9% removal of Fe from the solution as confirmed by ICP-OES. In addition, 27% of Al and 12% of Cu co-precipitated with Fe, but for all other elements, the precipitation percentages were less than 5%.

4.5.1 Adsorption

Similarly to the mining wastewater, adsorption of ions from the NdFeB magnet leachate was studied in the function of pH using the PA-**25** and PA-TP260 filters. The adsorption properties of the filters were first screened at two different pHs, 0.15 and 4.0. The former is a pH of 5% MSA background in the NdFeB leachate, whereas the latter allows for a higher degree of protonation of the aminophosphonic acids. The adsorption was significantly higher for the PA-TP260 than for the PA-**25** because it adsorbed almost 100% of REEs already at pH 0.15, while the PA-**25** adsorbed less than 10% at this pH (Figure 26). At pH 4, the PA-TP260 completely adsorbed all other elements, except B, whereas the PA-**25** achieved 50% adsorption for all elements except B and Co. As the PA-TP260 was observed to separate REEs from Al, B, Co, and Cu at pH 0.15, additional pH screening was conducted to investigate its ability to separate Al, B, Co, and Cu from each other.

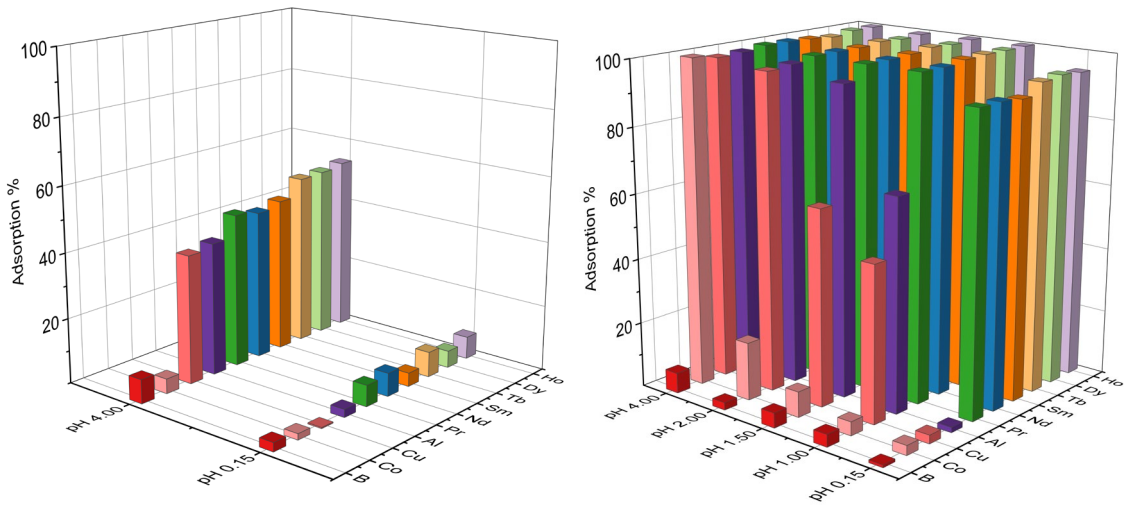

Figure 26. Adsorption percentages of ions for the PA-**25** (left) and the PA-TP260 (right) filters in a function of pH.

Thus, three additional pH values of 1.0, 1.5, and 2.0 were screened for the PA-TP260 to determine the optimal pH range for Al, B, Co, and Cu separation. At pH 1, no Co was adsorbed, while the adsorption of Al and Cu was 65% and 48%, respectively. As the pH was increased to 1.5, the adsorption percentage of Co remained low, but the adsorption of Al reached 100%, and Cu increased to 60%. Finally, at pH 2, the adsorption of Cu was also complete while <20% of Co was adsorbed. The obtained results suggested that the REEs can be separated from other ions at pH 0.15, and from the remaining extract Al and Cu can be separated from Co and B when the pH is set to 1.5.

4.5.2 Elution

The elution of the REEs adsorbed at pH 0.15 into the PA-TP260 was investigated using 3 M and 5 M of MSA and 6 M HNO_3. The latter was used to elute the REEs from PA-**25** when mining wastewater was investigated. The flow rate of the syringe pump was set to 15 ml/h and the amount of the eluent was 30 ml. Surprisingly, compared to the PA-**25**, 6 M HNO_3 was found to be an inefficient eluent for the PA-TP260 as it did not elute the HREEs, (Dy, Tb, and Ho) as efficiently as the LREEs (Nd, Pr, and Sm) (Figure 27). Like 6 M HNO_3, 3 M MSA also eluted Ho and Tb inefficiently, but not Dy. When MSA concentration was raised to 6 M, generally over 90%of the adsorbed REEs were eluted, although the elution of the HREEs was still incomplete.

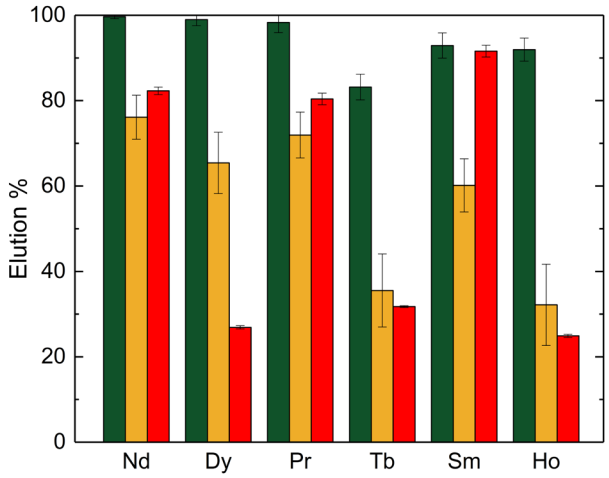

Figure 27. Elution % for REEs with 5 M MSA (green), 3 M MSA (yellow), and 6 M HNO_3 (red)

4.5.3 Recovery process

The recovery process for the NdFeB magnet was developed according to the results of the leaching, adsorption, and desorption studies. The first step was the leaching of the magnet using 10 v/v% MSA (Figure 28, step 1), followed by the removal of Fe by oxidation at pH 3.7 (step 2). Then the pH of the leachate was set to 0.15 and REEs were completely adsorbed from the NdFeB solution using the PA-TP260 filters as an adsorbent (step 3). The REE-containing filters were then eluted first with 1 M NH_4Cl to remove any traces of the co-adsorbed Cu from the filter (step 4), followed by 5 M MSA elution to yield a 99% pure REE fraction, containing only 1% of Al as an impurity (step 5). In the sub-steps of step 3, the solution containing Al, Co, Cu, and B was further processed. The pH of this solution was set to 1.5 and injected through a new set of filters during which Al and Cu were completely adsorbed (step 3.1). During this step, none of B and only half of Co was co-adsorbed separating Co and B into their own fraction. Filters containing Al, Co, and Cu were then eluted first with 1 M NH_4Cl to obtain a Co-

rich fraction (step 3.2), while the subsequent elution of the filters with potassium oxalate yielded an Al-rich intermediate product containing 72% of Al with Co (17%) and Cu (11%) as impurities (step 3.3).

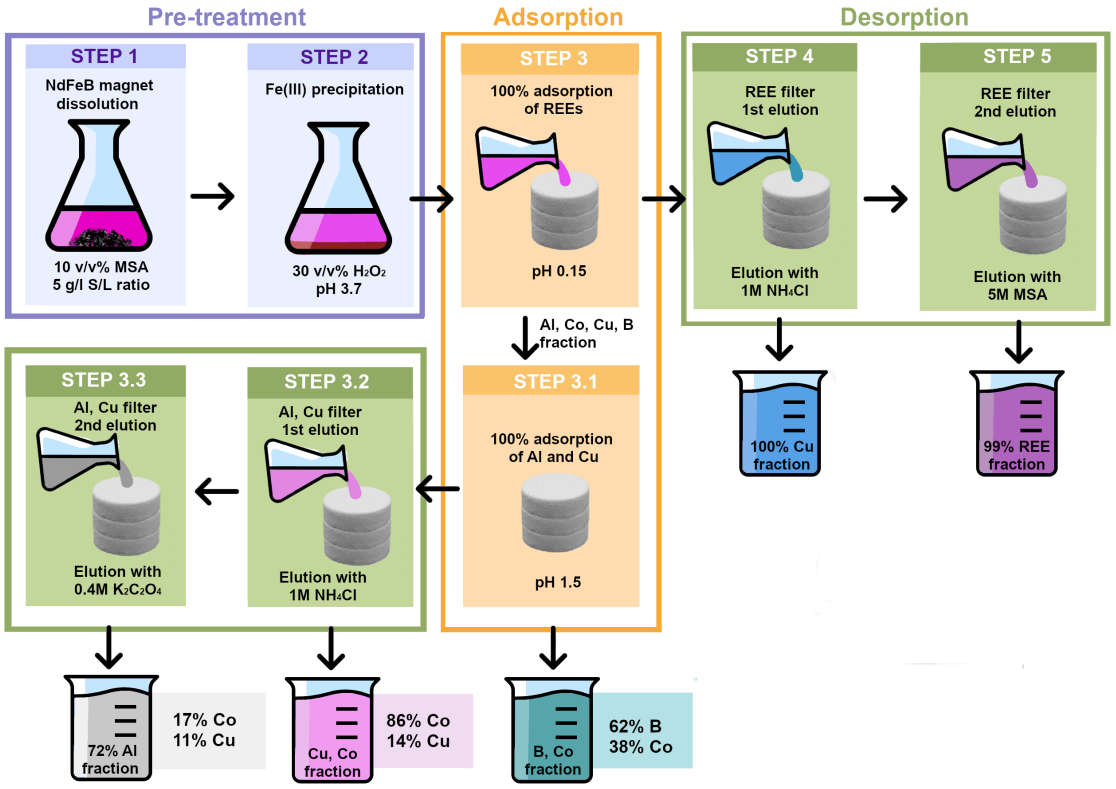

Figure 28. Recovery process for NdFeB magnets utilizing 3D printed PA-TP260 filters

4.6 Reusability of the PA-25 and PA-TP260 filters

The reusability of the 3D-printed filters was tested by performing five and fifty subsequent adsorption-desorption cycles for one PA-**25** and one PA-TP260 filter, respectively. The adsorbed and eluted amounts of metals were measured using ICP-OES. For the PA-**25**, **the** accumulation of strongly adsorbing Sc, Fe, and U was observed as the mineral acids did not efficiently elute these elements (see above) from the filter. However, further tests showed that by removing Sc, Fe, and U from the mining wastewater before adsorption, the PA-**25** filters were reusable, and only Al accumulated in the filters (Figure 29). Sc, Fe, and U can be removed from the solution either by precipitation with aminophosphonates, as was shown in section 5.2 (Sc and U), or as hydroxides (Fe).[205] In contrast to the PA-**25**, adsorbed and desorbed amounts of ions remained rather constant for the PA-TP260 filter and only small ion residues remained in the filter after each elution cycle (Figure 30). A small expectation occurred during the first five cycles

when 3 M MSA was used as an eluent, decreasing the elution percentage. However, this was resolved once the molarity of MSA was increased to 5 M. As the concentration of the eluent was too small during the first five cycles, the more concentrated MSA also slowly eluted the accumulated Nd residual from the filter during subsequent cycles (Figure 30b). Interestingly, the accumulation of HREEs in the filter was observed due to their elution being not 100% complete even with the 5 M MSA. Despite this, the accumulated amounts of ions in the PA-TP260 remained low and no significant reduction in adsorption efficiency was observed.

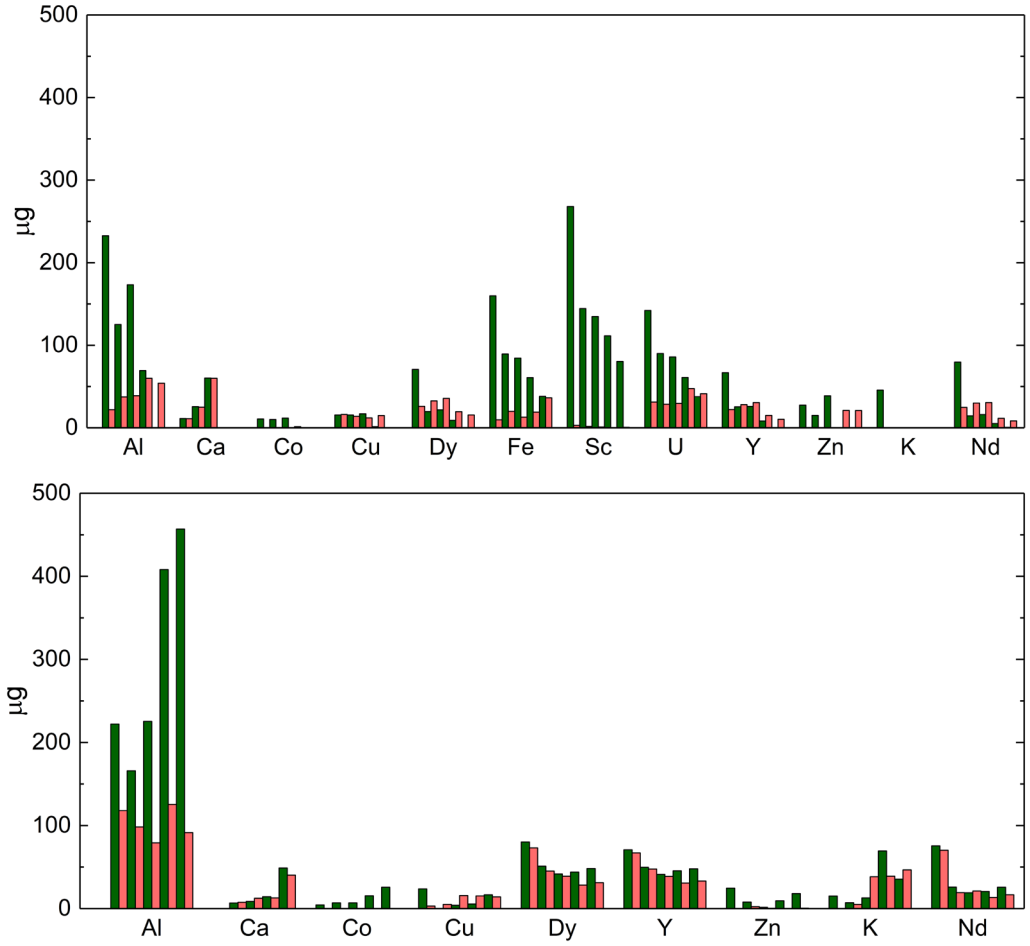

Figure 29. Adsorption (green) and desorption (pink) of the PA-**25** filters during 5 cycles with mining wastewater containing Sc, Fe, and U (above) and without Sc, Fe, and U (below).

Thus, the results suggested that the PA-TP260 filters are fully reusable, underpinning their applicability to industrial applications.

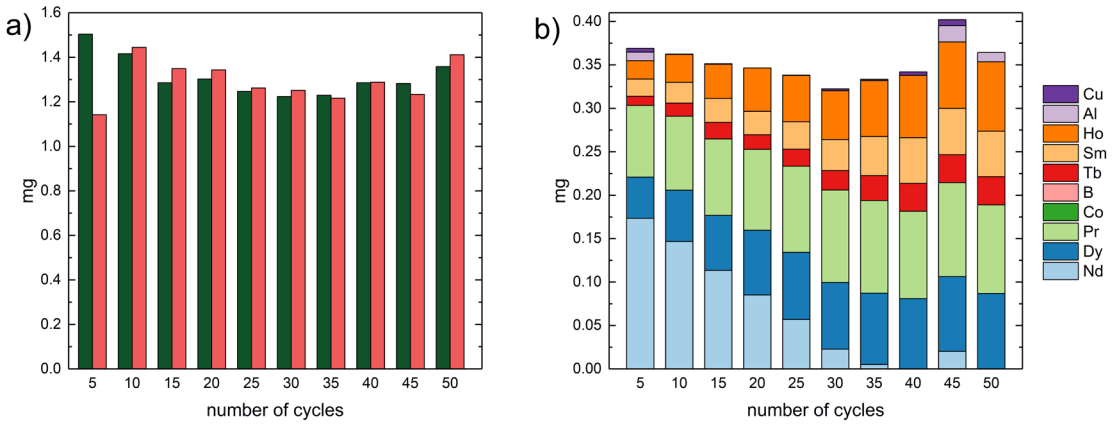

Figure 30. (a) 50 adsorption and elution cycles for the PA-TP260 , and (b) residual amount of ions (mg) after each 5 cycles.

4.7 Adsorption mechanisms and maximum capacities of the filters

FTIR spectra and adsorption isotherms were determined for both PA-**25** and PA-TP260 filters to gain deeper insights into their adsorption mechanisms and maximum capacities. The obtained adsorption isotherms were fit to three different models that were the Langmuir, Freundlich, and Sips models. The best models for each filter were analyzed using the goodness of fits metrics and a statistical F-test. The latter was particularly employed when two or more models gave a similar fit to the data.

4.7.1 FTIR measurements

The FTIR spectra of the unused PA-**25** and PA-TP260 filters were compared to those of the used filters that were saturated with REEs. The PA-**25** filters were saturated with Sc, Nd, or U whereas the PA-TP260 filters with Nd. Interestingly, no significant shifts (<1 cm^{-1}) or changes in the intensity of the peaks were detected for the saturated PA-**25** filters when they were compared to the unused ones (Figure 31). Thus, the majority of the $(PO_3H_2)_2$ remains in the protonated form, and no shifting of NH can be observed due to the masking from the nylon-12 matrix. For the PA-TP260, however, visible changes were detected (Figure 32). The P=O adsorption band at 1156 cm^{-1} slightly shifted and broadened for the saturated filter. The broadening likely occurs due to the coordinating MSA, in which SO_4 group band occurs at the same wavenumber region. The observed coordinating MSA in the spectrum originates from the MSA background. A most

significant change was detected for the P–O stretch, which not only decreased in intensity but also shifted from 924 cm^{-1} to 943 cm^{-1}. This strongly indicated the coordination of Nd to P–O. Additionally, a 10 cm^{-1} shift was observed for the C–P bond, which shifted from 541 cm^{-1} to 551 cm^{-1}. Another band arising from MSA at 523 cm^{-1} appears very close to this band. Coordination of the Nd ion to the nitrogen atom was hard to determine from the spectrum because N–H bands arising from nylon-12 most likely mask all the plausible shifts. The coordination of Nd to TP260 is similar to other reported aminophosphonate complexes with REEs, as similar changes have been observed for them at the spectral region of the PO_3 moiety.[32,34,36,39–41,149]

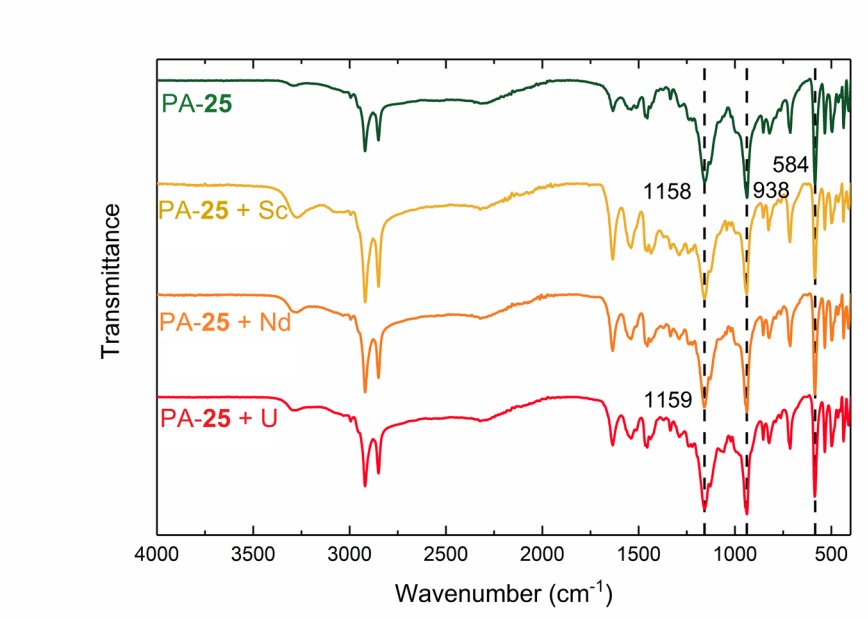

Figure 31. FTIR-spectra for the unused PA-**25** filter, and filter used for the adsorption of Sc (yellow), Nd (orange), and U (red).

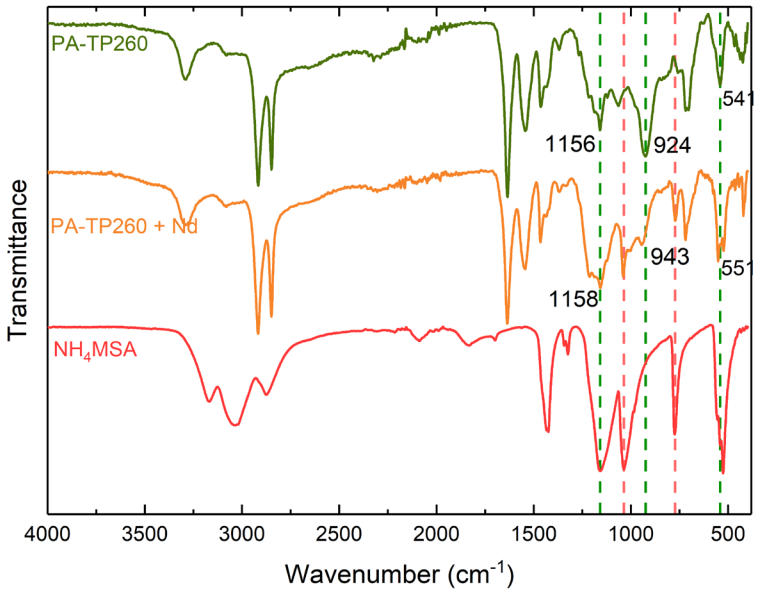

Figure 32. FTIR-spectra for the unused PA-TP260 filter (green), filter used for Nd adsorption (orange), and for NH_4MSA salt.

4.7.2 Adsorption isotherms

For the PA-**25** six different adsorption isotherms were measured using Sc, Fe, Y, Nd, Dy, or U as a metal. For all other metals, except for Fe, the isotherm studies were performed at pH 4. Due to the efficient precipitation of Fe, its isotherm was determined at pH 3. In contrast, for the PA-TP260, the same metal (Nd) was used in all the experiments, but adsorption isotherms were determined for the five different filters containing either 5 wt%, 10 wt%, 20 wt%, 30 wt%, 40 wt%, or 50 wt% of TP260.

The Langmuir adsorption model generally fit well to the adsorption isotherms of the PA-**25** when the metal was Y, Nd, Dy, or U, while Fe fit better to the Freundlich adsorption model (Table 3). The isotherm plots are presented in the supporting information of Paper **II**.[49] As Sc fit well to both models, a statistical F-test was performed to distinguish the performance of the models. According to the F-test, the Freundlich model performed the best. IR did not provide any information about the difference in coordination between Sc and Nd or U to **25**, but the difference of Sc and Fe might be explained by smaller ionic size compared to the other REEs and U. It might be possible for **25** to coordinate two Sc or Fe ions to the same site, which is more unlikely for the bigger ions. However, conclusions about the adsorption mechanism cannot solely be drawn from isotherm fittings.[193] Important additional information could be achieved from adsorption kinetics for example, which could provide information about the type of adsorption, adsorption rate and reversibility.[206]

The maximum capacity Q_{max} was determined for each studied metal using the Langmuir model. The highest capacity of 0.51 mmol/g was obtained for Sc, followed by U with the capacity of 0.47 mmol/g. For Y, Nd, and Dy, the capacities

were 0.17 mmol/g, 0.24 mmol/g, and 0.23 mmol/g, respectively. The Langmuir constant *b*, which indicates the interaction between the adsorbent and the adsorbate, was slightly higher for U than for the REEs. This indicates that **25** binds stronger to U than the REEs. The Freundlich constant K_f, also indicating the interaction between adsorbent and adsorbate, was found to be smaller for Fe than Sc. These results are in line with adsorption tests, as PA-25 adsorbed U stronger than REEs from the mining wastewater, and Sc was more efficiently adsorbed than Fe. Of course, it should be kept in mind that the results for Fe are not directly compared to other metals as a different pH was used in the studies.

Table 3. Langmuir and Freundlich isotherm parameters from linear fittings for each metal.

	Langmuir				**Freundlich**		
	Q_{max} mg/g	Q_{max} mmol/g	b L/mg	R^2	K_f $mg^{1-n}L^n/mg$	n	R^2
Sc	22.86	0.51	0.018	0.970	4.10	4.15	0.994
Fe	-	-	-	-	1.57	1.98	0.997
U	111.65	0.47	0.036	0.985	-	-	0.776
Dy	37.84	0.23	0.030	0.975	-	-	0.743
Nd	34.60	0.24	0.024	0.979	-	-	0.798
Y	14.74	0.17	0.030	0.996	-	-	0.794

In the case of the PA-TP260 filter, the Langmuir isotherm model fit best to the adsorption isotherms of the filters containing 10–30 wt% of TP260, while the 40 wt% and 50 wt% filters fit better to the Freundlich model (Table 4). Interestingly, the 5 wt% filter only fit well to the Sips isotherm model which is a combination of the Langmuir and Freundlich equations. Although the adsorption mechanism of the PA-TP260 filters with different wt% should be the same regardless of the wt% of the additive at the molecular level, the results above suggest that the wt% affects the adsorption mechanism at the macroscale. One possible explanation is that the adsorption material is more heterogeneous when more additive is present in the filter, which affects the observed results.

Table 4. Langmuir, Freundlich, and Sips isotherm parameters for 5–50 wt% of the PA-TP260.

	Langmuir				Freundlich		
Wt%	Q_{max} mg/g (filter)	Q_{max} mg/g (TP260)	b L/mg	R^2	K_f $mg^{1-n}L^n/mg$	n	R^2
5	-	-	-		0.03	1.59	0.938
10	7.64	76.39	1.60	0.992	0.05	1.48	0.975
20	9.71	48.56	2.53	0.987	0.13	1.75	0.982
30	9.12	30.65	5.47	0.985	-	-	-
40	10.09	25.22	7.10	0.972	0.71	2.63	0.997
50	12.18	24.35	11.30	0.957	1.33	3.09	0.993
	Sips						
Wt%	Q_{max} mg/g (filter)	Q_{max} mg/g (TP260)	b L/mg		n $mg^{1-n}L^n/mg$	R^2	
5	2.55	50.92	3.97		1.62	0.989	
10	5.82	58.20	2.60		1.22	0.996	

The maximum capacities were calculated for the mass of TP260 in the filter as well as for the mass of the entire filter. Interestingly, when the former parameter was used, the capacities decreased as a higher wt% of additive was present in the filter. However, as expected, when the capacities were calculated for the mass of the entire filter, they increased from 2.55 mg/g to 12.18 mg/g as the amount of the additive increased from 5 wt% to 50 wt%. This can also be detected from Langmuir and Freundlich constants b and K_f, which can be observed to increase as the wt% increases, further confirming that the higher percentage filters adsorb more Nd. The decrease in capacity calculated towards the amount of TP260 indicates that adding more of the additive into the filter does not enhance its adsorption properties significantly. Whether this is related to the distribution of TP260 particles in the filter and/or their morphology, is hard to conclude with the available data.

CONCLUSIONS

This dissertation focused on investigating α-aminophosphonates in the recovery of REEs by utilizing precipitation and solid-phase–extraction methods. First, self-synthesized water-soluble α-aminophosphonates (**19–24**) with the general formula of $RN[CH_2P(O)(OH)_2]_2$ (**19** R = CH_2CH_3, **20** R = $(CH_2)_2CH_3$, **21** R = $(CH_2)_3CH_3$, **22** R = $(CH_2)_4CH_3$, **23** R = $(CH2)_5CH_3$, **24** R = $CH_2CH(C_2H_5)(CH_2)_3CH_3$) were investigated as precipitants for REEs from a solution containing both REEs and Th and U. The acid–base properties and complexation of **19** were studied by utilizing NMR titrations. The obtained p*K*a values for the phosphonate group $PO(OH)_2$ were 1.3 and 5.6 for the first and second protonation. The studied precipitants were also determined to form 1:1, 1:2, or 1:3 metal:ligand complexes with Lu, La, and Y respectively. In the precipitation experiments, Sc, Th, and U were almost completely precipitated at low pH with the least water-soluble precipitants containing the longest alkyl chains (**22–24)**. This enabled the separation of the REEs from these elements. However, no significant improvements were observed for the separation between adjacent REEs although some separation was obtained between LREEs and HREEs. Therefore, the α-aminophosphonate precipitants were suitable for removing Th, and U from REEs but not for separating REEs.

The non-water-soluble α-aminophosphonate containing long alkyl chain $CH_3(CH_2)_{11}$- (**25**), was investigated as an additive in 3D-printed filters, where nylon-12 was used as the polymer matrix. For the sake of comparison, commercial Lewatit TP260 ion-exchange resin, which contains an α-aminophosphonate functional group, was also investigated as an additive. The filters were referred to as the PA-**25** and PA-TP260 respectively. IR spectroscopy was applied for the chemical characterization of the filters, and it was possible to verify that the additives remained unchanged after 3D printing. PA-**25** filters were studied for the recovery of REEs from mining wastewater which contained 10 mg/l of REEs (Sc, Y Nd, and Dy). The other elements present were 100 mg/l Al, K, Ca, and Zn and 10 mg/l Fe, Co, Cu, and U. By utilizing the PA-**25** filter, it was possible to concentrate the 8% of REEs from the mining wastewater up to 70% by using 6 M HNO_3 as an eluent. Thus, by applying self-synthetized α-aminophosphonate into a 3D-printed filter, mining wastewaters can be processed to a less complex solutions containing enriched amount of REEs.

Finally, both PA-**25** and PA-TP260 filters were investigated for recovery of critical elements from NdFeB magnets. The dissolution of the magnet was first investigated with 10–100 v/v% MSA solutions. It was found that 10 v/v% MSA solution dissolved the magnet almost completely and thus was deemed a good leaching agent. According to the adsorption tests, the PA-**25** filter did not work as efficiently as the PA-TP260 filter and thus was not suitable for recycling NdFeB magnets. With the PA-TP260 filter, the metals in the magnet could be separated into their own fractions by using different environment-friendly eluents, MSA, ammonium chloride, and potassium oxalate. In the precipitation step, 99.9%of Fe could be precipitated with 97.6% purity. REEs could be separated to a 99% pure

fraction at pH 0.15, where the other metals of the magnet did not adsorb to the filter. By eluting the filter with a 5 M MSA, >90% of the rare earth metals could be recovered. In addition, fractions containing mainly Al, Co, Cu, and B were obtained. With PA-TP260 filters, REEs could be recycled from NdFeB magnets with relatively simple adsorption-desorption process.

This dissertation investigated α-aminophosphonates in REE recovery for the first time both as precipitants and as an additive in 3D-printed filters. The findings provided valuable information about the properties of simple aminophosphonates, which can be used in the future to design improved and more efficient precipitants and additives for 3D-printed materials. Additionally, a new separation process for NdFeB magnets was developed utilizing environment-friendly eluents.

SUMMARY IN FINNISH

Tulevaisuudessa harvinaisten maametallien kysynnän arvioidaan kasvavan, kun tietokoneiden, puhelimien ja etenkin sähköisten kulkuvälineiden ja tuulivoimaloiden määrä kasvaa. Harvinaiset maametallit luokitellaan EU:n alueella kriittisiksi, koska niillä ei ole tuotantoa EU:n alueella ja metallit ovat edellä mainittujen käyttötarkoituksiensa vuoksi hyvin kysyttyjä. Viime vuosikymmenenä harvinaisten maametallien kierrätystä on tutkittu laajasti sekundäärisistä lähteistä, kuten esimerkiksi neodyymimagneeteista, kaivosteollisuuden sivuvirroista ja elektroniikkaromusta. Koska sekundäärisillä lähteillä ei voida vielä täysin vastata kasvavaan kysyntään, harvinaisten maametallien tehokkaampaa talteenottoa primäärilähteistä ja erottelua toisistaan on myös tutkittu paljon.

Tässä väitöskirjassa keskityttiin tutkimaan α-aminofosfonaatteja harvinaisten maametallien talteenotossa. Ensimmäisenä tutkittiin itsesyntetisoituja vesiliukoisia aminofosfonaatteja (**19–24**), joiden yleinen molekyylikaava on $RN[CH_2P(O)(OH)_2]_2$ (**19** R = CH_2CH_3, **20** R = $(CH_2)_2CH_3$, **21** R = $(CH_2)_3CH_3$, **22** R = $(CH_2)_4CH_3$, **23** R = $(CH2)_5CH_3$, **24** R = $CH_2CH(C_2H_5)(CH_2)_3CH_3$). α-Aminofosfonaatteja sovellettiin sakkautus-reagensseina liuoksessa, joka sisälsi sekä harvinaisia maametalleja että toriumia ja uraania. Happo-emäs ominaisuuksia ja kompleksoitumista tutkittiin NMR titrausten avulla **19**:lle ja pK_a arvoksi määritettiin fosfonaattiryhmille 1,3 ja 5,6. Tutkittujen sakkautusreagenssien määritettiin myös muodostavan happamissa vesiliuoksissa 1:1, 1:2 tai 1:3 metalli:ligandi komplekseja Lu, La, ja Y kanssa. Kompleksointitutkimukset tehtiin NMR titrausten avulla. Sakkautuskokeissa harvinaisten maametallien erotus onnistui toriumista ja uraanista jo alhaisessa pH:ssa vähemmän vesiliukoisten sakkautusreagenssien **22–24** kanssa. Lisäksi skandium voitiin sakata selektiivisesti erilleen muista harvinaisista maametalleista. Merkittäviä parannuksia vierekkäisten harvinaisten maametallien välille ei kuitenkaan havaittu, vaikka erottumista kevyempien ja raskaampien harvinaisten maametallien välillä voitiin havaita. α-aminofosfonaatti sakkautusreagenssit osoittautuivat sopiviksi Th ja U erottelemiseen REE:stä, mutteivat kuitenkaan REE:n erotteluun toisistaan.

Veteen liukenematonta aminofosfonaattia **25** vuorostaan tutkittiin lisäaineena 3D printatuissa suodattimissa, joissa matriisina käytettiin nailon-12:sta (PA-**25**). Vertailun vuoksi tutkittiin myös kaupallista Lewatit TP260 ioninvaihtohartsia, jossa funktionaalisena ryhmänä toimii myös aminofosfonaatti (PA-TP260). IR-spektroskopian avulla voitiin todentaa, että lisäaineet pysyvät muuttumattomana 3D printtauksen jälkeen. PA-**25** suodattimia tutkittiin harvinaisten maametallien talteenotosta kaivosvesijätteestä, joka sisälsi harvinaisia maametalleja (Sc, Y Nd ja Dy) 10 mg/l. Lisäksi jätteessä oli 100 mg/l Al, K, Ca ja Zn sekä 10 mg/l Fe, Co, Cu ja U. PA-**25** suodattimen avulla voitiin konsentroida harvinaisten maametallien 8 % osuus kaivosvesijätteestä jopa 70 %:n käyttäen eluenttina 6M HNO_3. α-aminofosfonaattia sisältäviä 3D printattuja suodattimia voidaan siten soveltaa harvinaisten maametallien konsentroimisessa liuoksiin, jotka sisältävä huomattavasti vähemmän muita metalleja.

Molempia PA-**25** ja PA-TP260 suodattimia tutkittiin kriittisten alkuaineiden talteenotosta käytetyistä neodyymimagneeteista. Magneettien liuotusta tutkittiin ensin 10–100 v/v% metaanisulfonihappoliuoksilla, ja 10 v/v% happo todettiin tehokkaaksi liuottimeksi, eikä väkevämpien happojen käytölle ollut perustetta. Adsorptiokokeiden mukaan PA-**25** suodatin ei toiminut yhtä tehokkaasti kuin PA-TP260 suodatin, joten PA-**25** suodatin ei soveltunut neodyymimagneettien kierrätykseen. PA-TP260 suodattimella magneetissa olevan metallit voitiin erotella omiin fraktioihinsa käyttämällä ympäristöystävällisiä eluentteja: metaanisulfonihappoa, ammoniumkloridia sekä kaliumoksalaattia. Fe voitiin sakkauttaa 99.9 %:sti liuoksesta 97.6 % puhtausasteella. Harvinaiset maametallit eroteltiin 99 % puhtaasti pH 0.15:ssa, jossa magneetin muut metallit eivät adsorboituneet suodattimeen. Eluoimalla suodatinta 5M metaanisulfonihappoliuoksella voitiin >90 % harvinaisista maametalleista ottaa talteen. Lisäksi saatiin fraktiot, jotka sisälsivät pääasiassa Al, Co, Cu, ja B. PA-TP260 suodattimilla voidaan siis kierrättää neodyymimagneetin sisältämät metallit suhteellisen suoraviivaisella adsorptio-eluointi menetelmällä.

Yhteenvetona tämä väitöskirjatyö tutki aminofosfonaatteja harvinaisten maametallien talteenotossa ensimmäistä kertaa sekä sakkautusreagensseina että adsorboivana lisäaineena 3D printatuissa suodattimissa. Yksinkertaisten aminofosfonaattien tutkimuksella saatiin arvokasta tietoa niiden ominaisuuksista pH:n funktiona, jota voidaan hyödyntää tulevaisuudessa parempien ja tehokkaampien sakkautusreagenssien ja adsorboivien lisäaineiden kehittämisessä. Lisäksi väitöskirjatyössä kehitettiin erotusmenetelmä harvinaisten maametallien talteenottamiseksi neodyymimagneeteista, jossa eluentteina käytettiin ympäristöystävällisiä metaanisulfonihappoa, ammoniumkloridia sekä kaliumoksalaattia.

REFERENCES

1. Balaram, V. Rare earth elements: A review of applications, occurrence, exploration, analysis, recycling, and environmental impact. *Geoscience Frontiers* **10**, 1285–1303 (2019).
2. Binnemans, K. *et al.* Recycling of rare earths: A critical review. *Journal of Cleaner Production* **51**, 1–22 (2013).
3. Binnemans, K., Jones, P. T., Blanpain, B., Van Gerven, T. & Pontikes, Y. Towards zero-waste valorisation of rare-earth-containing industrial process residues: A critical review. *Journal of Cleaner Production* **99**, 17–38 (2015).
4. Wang, S. *et al.* Future demand for electricity generation materials under different climate mitigation scenarios. *Joule* **7**, 309–332 (2023).
5. Bobba, S., Carrara, S., Huisman, J., Mathieux, F. & Pavel, C. *Critical Raw Materials for Strategic Technologies and Sectors in the EU - a Foresight Study*. *European Commission* 100 (2020). doi:10.2873/58081.
6. European Commission, Study on the Critical Raw Materials for the EU 2023 – Final Report.
7. U.S. Geological Survey, Department of Interior. 2022 Final List of Critical Minerals.
8. Barakos, G., Mischo, H. & Gutzmer, J. A forward look into the US rare-earth industry; How potential mines can connect to the global REE market. *Mining Engineering* **70**, 30–37 (2018).
9. EuRare Project | Home. https://www.eurare.org/.
10. Jordens, A., Cheng, Y. P. & Waters, K. E. A review of the beneficiation of rare earth element bearing minerals. *Minerals Engineering* **41**, 97–114 (2013).
11. Gupta, C. K. & Krishnamurthy, N. *Extractive Metallurgy of Rare Earths*. (CRC Press, Boca Raton, 2005).
12. Borra, C. R., Pontikes, Y., Binnemans, K. & Van Gerven, T. Leaching of rare earths from bauxite residue (red mud). *Minerals Engineering* **76**, 20–27 (2015).
13. Buechler, D. T. *et al.* Comprehensive elemental analysis of consumer electronic devices: Rare earth, precious, and critical elements. *Waste Management* **103**, 67–75 (2020).
14. RMIS - Raw materials' profiles. *RMIS - Raw Materials Information System* https://rmis.jrc.ec.europa.eu/rmp/.
15. Liang, Y., Kleijn, R. & van der Voet, E. Increase in demand for critical materials under IEA Net-Zero emission by 2050 scenario. *Applied Energy* **346**, 121400 (2023).
16. Hermassi, M., Granados, M., Valderrama, C., Ayora, C. & Cortina, J. L. Recovery of rare earth elements from acidic mine waters: An unknown secondary resource. *Science of The Total Environment* **810**, 152258 (2022).

17. Waste statistics. https://ec.europa.eu/eurostat/statistics-explained/index.php?title=Waste_statistics#Total_waste_generation.
18. Franks, D. M. *et al.* Tailings facility disclosures reveal stability risks. *Sci Rep* **11**, 5353 (2021).
19. Fortes, J. C. *et al.* Wasted Critical Raw Materials: a Polluted Environmental Scenario as Potential Source of Economic Interest Elements in the Spanish Part of the Iberian Pyrite Belt. *Water Air Soil Pollut* **232**, 88 (2021).
20. Goodman, A. J., Bednar, A. J. & Ranville, J. F. Rare earth element recovery in hard-rock acid mine drainage and mine waste: A case study in Idaho Springs, Colorado. *Applied Geochemistry* **150**, 105584 (2023).
21. Kaya, M. An overview of NdFeB magnets recycling technologies. *Current Opinion in Green and Sustainable Chemistry* **46**, 100884 (2024).
22. Tanvar, H. & Dhawan, N. Extraction of rare earth oxides from discarded compact fluorescent lamps. *Minerals Engineering* **135**, 95–104 (2019).
23. Couto, C. P., van de Ven, J. J. M. M., Yang, Y. & Abrahami, S. T. On the pre-treatment for recycling spent NdFeB permanent magnets: from disassembling, characterisation to de-coating. *Sustainable Materials and Technologies* **41**, e01041 (2024).
24. Lixandru, A. *et al.* Identification and recovery of rare-earth permanent magnets from waste electrical and electronic equipment. *Waste Management* **68**, 482–489 (2017).
25. Zamprogno Rebello, R., Weitzel Dias Carneiro Lima, M. T., Yamane, L. H. & Ribeiro Siman, R. Characterization of end-of-life LED lamps for the recovery of precious metals and rare earth elements. *Resources, Conservation and Recycling* **153**, 104557 (2020).
26. Kumari, A. & Sahu, S. K. A comprehensive review on recycling of critical raw materials from spent neodymium iron boron (NdFeB) magnet. *Separation and Purification Technology* **317**, 123527 (2023).
27. Herak, M. J. & Jagodić, V. Distribution and dimerization of organophosphorus extractants and their extraction efficiency in different solvents. *Journal of Inorganic and Nuclear Chemistry* **35**, 995–1001 (1973).
28. Radošević, J., Jagodić, V. & Herak, M. J. Extraction and complex formation of cerium(III) and praseodymium(III) with monoesters of phosphonic acids. *Journal of Inorganic and Nuclear Chemistry* **39**, 2053–2056 (1977).
29. Jagodić, V., Herak, M. J., Šipalo, B. & Radošević, J. Solvent extraction study of lanthanum and europium by acidic esters of aminophosphonic acids. *Journal of Inorganic and Nuclear Chemistry* **33**, 2651–2659 (1971).
30. Jagodić, V. & Herak, M. J. Synthesis and physical properties of a novel aminophosphonic acid as an extracting agent for metals. *Journal of Inorganic and Nuclear Chemistry* **32**, 1323–1332 (1970).
31. Kukkonen, E., Virtanen, E. J. & Moilanen, J. O. α-Aminophosphonates, -Phosphinates, and -Phosphine Oxides as Extraction and Precipitation Agents for Rare Earth Metals, Thorium, and Uranium: A Review. *Molecules* **27**, 3465 (2022).

32. Kuang, S., Zhang, Z., Li, Y., Wei, H. & Liao, W. Extraction and separation of heavy rare earths from chloride medium by α-aminophosphonic acid HEHAPP. *Journal of Rare Earths* **36**, 304–310 (2018).
33. Kuang, S., Zhang, Z., Li, Y., Wei, H. & Liao, W. Synergistic extraction and separation of rare earths from chloride medium by the mixture of HEHAPP and D2EHPA. *Hydrometallurgy* **174**, 78–83 (2017).
34. Wei, H., Li, Y., Kuang, S., Zhang, Z. & Liao, W. Separation of trivalent rare earths from chloride medium using solvent extraction with heptylaminomethyl phosphonic acid 2-ethylhexyl ester (HEHHAP). *Hydrometallurgy* **188**, 14–21 (2019).
35. Wei, H., Li, Y., Zhang, Z. & Liao, W. Synergistic solvent extraction of heavy rare earths from chloride media using mixture of HEHHAP and Cyanex272. *Hydrometallurgy* **191**, 105240 (2020).
36. Zhao, Q., Zhang, Z., Li, Y., Bian, X. & Liao, W. Solvent extraction and separation of rare earths from chloride media using α-aminophosphonic acid extractant HEHAMP. *Solvent Extraction and Ion Exchange* **36**, 136–149 (2018).
37. Zhao, Q. *et al.* Synergistic extraction of heavy rare earths by mixture of α-aminophosphonic acid HEHAMP and HEHEHP. *Journal of Rare Earths* **37**, 422–428 (2019).
38. Chen, L., Deng, B., Kuang, S. & Liao, W. Efficient extraction and separation of heavy rare earths from chloride medium with N, N′-di(2-ethylhexyl)aminomethyl phosphonic acid mono-2-ethylhexyl ester. *Hydrometallurgy* **222**, 106173 (2023).
39. Fu, Y. *et al.* Separation of trivalent rare earths from nitrate medium using solvent extraction with a novel extractant 2-ethylhexyl ((2-ethylhexylamino)methyl) phosphonic acid. *Journal of Rare Earths* (2021) doi:10.1016/J.JRE.2021.02.009.
40. Imam, E. A. *et al.* Nd(III) sorption using aminophosphonate-based sorbents – Sorption properties and application to the treatment of REE concentrate. *Colloids and Surfaces A: Physicochemical and Engineering Aspects* **685**, 133339 (2024).
41. Sraidi, A., Ait hak, S., Kounbach, S., Khaless, K. & Benhida, R. Extraction of rare earth elements using a chelating amino methyl phosphonic acid resin. *Journal of Molecular Liquids* **402**, 124758 (2024).
42. Kołodyńska, D., Fila, D. & Hubicki, Z. Static and dynamic studies of lanthanum(III) ion adsorption/desorption from acidic solutions using chelating ion exchangers with different functionalities. *Environmental Research* **191**, 110171 (2020).
43. Lahtinen, E. *et al.* Porous 3D Printed Scavenger Filters for Selective Recovery of Precious Metals from Electronic Waste. *Advanced Sustainable Systems* **2**, 1800048 (2018).
44. Ibebunjo, K., El Ouardi, Y., Kwame Bediako, J., Iurchenkova, A. & Repo, E. Functionalization of recycled polymer and 3D printing into porous

structures for selective recovery of copper from copper tailings. *Chemical Engineering Science* **286**, 119664 (2024).
45. Gonçalves, N. P. F., da Silva, E. F., Tarelho, L. A. C., Labrincha, J. A. & Novais, R. M. Simultaneous removal of multiple metal(loid)s and neutralization of acid mine drainage using 3D-printed bauxite-containing geopolymers. *Journal of Hazardous Materials* **462**, 132718 (2024).
46. Lahtinen, E. *et al.* Selective Recovery of Gold from Electronic Waste Using 3D-Printed Scavenger. *ACS Omega* **2**, 7299–7304 (2017).
47. Halevi, O., Chen, T.-Y., See Lee, P., Magdassi, S. & A. Hriljac, J. Nuclear wastewater decontamination by 3D-Printed hierarchical zeolite monoliths. *RSC Advances* **10**, 5766–5776 (2020).
48. Rodas Ceballos, M., González Serra, F., Estela, J. M., Cerdà, V. & Ferrer, L. 3D printed resin-coated device for uranium (VI) extraction. *Talanta* **196**, 510–514 (2019).
49. Virtanen, E. J. *et al.* Recovery of rare earth elements from mining wastewater with aminomethylphosphonic acid functionalized 3D-printed filters. *Separation and Purification Technology* **353**, 128599 (2025).
50. Oliveira, K. G. *et al.* Geopolymer beads and 3D printed lattices containing activated carbon and hydrotalcite for anionic dye removal. *Catalysis Today* **390–391**, 57–68 (2022).
51. Calderilla, C., Maya, F., Cerdà, V. & Leal, L. O. 3D printed device for the automated preconcentration and determination of chromium (VI). *Talanta* **184**, 15–22 (2018).
52. Giret, S. *et al.* Selective Separation and Preconcentration of Scandium with Mesoporous Silica. *ACS Appl. Mater. Interfaces* **10**, 448–457 (2018).
53. Hu, Y. *et al.* Size-Selective Separation of Rare Earth Elements Using Functionalized Mesoporous Silica Materials. *ACS Applied Materials & Interfaces* **11**, 23681–23691 (2019).
54. Frimodig, J. & Haukka, M. Removal of estrogens from aqueous solutions using 3D-printed polymers. *Environ. Sci.: Adv.* **2**, 1739–1745 (2023).
55. Merroune, A. *et al.* A comprehensive review on solvent extraction technologies of rare earth elements from different acidic media: Current challenges and future perspectives. *Journal of Industrial and Engineering Chemistry* **139**, 1–17 (2024).
56. Jha, M. K. *et al.* Review on hydrometallurgical recovery of rare earth metals. *Hydrometallurgy* **165**, 2–26 (2016).
57. Liu, T. & Chen, J. Extraction and separation of heavy rare earth elements: A review. *Separation and Purification Technology* **276**, 119263 (2021).
58. Separation of Rare Earth Elements. *American Chemical Society* https://www.acs.org/education/whatischemistry/landmarks/earthelements.html.
59. Giacalone, J. A. The Market For The 'Not-So-Rare' Rare Earth Elements. *JIEP* **1**, 11–18 (2012).
60. de Boer, M. A. & Lammertsma, K. Scarcity of Rare Earth Elements. *ChemSusChem* **6**, 2045–2055 (2013).

61. Aspinall, H. C. *F-Block Chemistry*. (Oxford University Press, 2020).
62. HIRAI, T. & KOMASAWA, I. Separation of Rare Metals by Solvent Extraction Employing Reductive Stripping Technique. *Mineral Processing and Extractive Metallurgy Review* **17**, 81–107 (1997).
63. Hirai, T. & Komasawa, I. Separation of Europium from Samarium and Gadolinium by Combination of Electrochemical Reduction and Solvent Extraction. *Journal of Chemical Engineering of Japan* **25**, 644–648 (1992).
64. Preston, J. S. & du Preez, A. C. The separation of europium from a middle rare earth concentrate by combined chemical reduction, precipitation and solvent-extraction methods. *Journal of Chemical Technology & Biotechnology* **65**, 93–101 (1996).
65. Rehkämper, M., Gärtner, M., Galer, S. J. G. & Goldstein, S. L. Separation of Ce from other rare-earth elements with application to Sm□Nd and La□Ce chronometry. *Chemical Geology* **129**, 201–208 (1996).
66. Shannon, R. D. Revised effective ionic radii and systematic studies of interatomic distances in halides and chalcogenides. *Acta Cryst A* **32**, 751–767 (1976).
67. Rare Earth Elements. *CRM Alliance* https://www.crmalliance.eu/hrees.
68. D'Angelo, P. *et al.* Revised Ionic Radii of Lanthanoid(III) Ions in Aqueous Solution. *Inorg. Chem.* **50**, 4572–4579 (2011).
69. Zhu, Z., Pranolo, Y. & Cheng, C. Y. Separation of uranium and thorium from rare earths for rare earth production - A review. *Minerals Engineering* **77**, 185–196 (2015).
70. Judge, W. D. & Azimi, G. Recent progress in impurity removal during rare earth element processing: A review. *Hydrometallurgy* **196**, 105435 (2020).
71. Nelson, J. J. M. *et al.* High-throughput screening for discovery of benchtop separations systems for selected rare earth elements. *Communications Chemistry* **3**, (2020).
72. O'Connell-Danes, J. G., Ngwenya, B. T., Morrison, C. A. & Love, J. B. Selective separation of light rare-earth elements by supramolecular encapsulation and precipitation. *Nat Commun* **13**, 4497 (2022).
73. Bogart, J. A., Lippincott, C. A., Carroll, P. J. & Schelter, E. J. An Operationally Simple Method for Separating the Rare-Earth Elements Neodymium and Dysprosium. *Angewandte Chemie International Edition* **54**, 8222–8225 (2015).
74. Gao, Y., Licup, G. L., Bigham, N. P., Cantu, D. C. & Wilson, J. J. Chelator-Assisted Precipitation-Based Separation of the Rare Earth Elements Neodymium and Dysprosium from Aqueous Solutions. *Angewandte Chemie International Edition* **n/a**, e202410233.
75. Yin, X. *et al.* Rare earth separations by selective borate crystallization. *Nature Communications* **8**, 1–8 (2017).
76. Tasaki-Handa, Y. *et al.* Selective Crystallization of Phosphoester Coordination Polymer for the Separation of Neodymium and Dysprosium: A Thermodynamic Approach. *Journal of Physical Chemistry B* **120**, 12730–12735 (2016).

77. Tasaki-Handa, Y. *et al.* Separation of neodymium and dysprosium by forming coordination polymers. *Separation and Purification Technology* **157**, 162–168 (2016).
78. Werner, E. J. & Biros, S. M. Supramolecular ligands for the extraction of lanthanide and actinide ions. *Org. Chem. Front.* **6**, 2067–2094 (2019).
79. Dam, H. H., Reinhoudt, D. N. & Verboom, W. Multicoordinate ligands for actinide/lanthanide separations. *Chem. Soc. Rev.* **36**, 367–377 (2007).
80. Archer, E. M., Galley, S. S., Jackson, J. A. & Shafer, J. C. Investigation of f-Element Interactions with Functionalized Diamides of Phenanthroline-Based Ligands. *Solvent Extraction and Ion Exchange* **41**, 697–740 (2023).
81. Hovey, J. L., Dittrich, T. M. & Allen, M. J. Coordination chemistry of surface-associated ligands for solid–liquid adsorption of rare-earth elements. *Journal of Rare Earths* **41**, 1–18 (2023).
82. Pramanik, S., Kaur, S., Popovs, I., Ivanov, A. S. & Jansone-Popova, S. Emerging Rare Earth Element Separation Technologies. *European Journal of Inorganic Chemistry* **27**, e202400064 (2024).
83. Liu, T., Ivanov, A. S., Popovs, I., Jansone-Popova, S. & Jiang, D. N-oxide ligands for selective separations of lanthanides: insights from computation. *RSC Adv.* **13**, 764–769 (2023).
84. Pramanik, S. *et al.* Tetradentate Ligand's Chameleon-Like Behavior Offers Recognition of Specific Lanthanides. *J. Am. Chem. Soc.* **146**, 25669–25679 (2024).
85. Johnson, K. R., Driscoll, D. M., Damron, J. T., Ivanov, A. S. & Jansone-Popova, S. Size Selective Ligand Tug of War Strategy to Separate Rare Earth Elements. *JACS Au* **3**, 584–591 (2023).
86. Špadina, M., Bohinc, K., Zemb, T. & Dufrêche, J.-F. Synergistic Solvent Extraction Is Driven by Entropy. *ACS Nano* **13**, 13745–13758 (2019).
87. Sarver, L. A. & Brinton, P. H. M.-P. THE SOLUBILITIES OF SOME RARE-EARTH OXALATES1. *ACS Publications* https://pubs.acs.org/doi/pdf/10.1021/ja01403a006 (2002) doi:10.1021/ja01403a006.
88. Feibush, A. M., Rowley, K. & Gordon, L. Solubility of Yttrium Oxalate. *ACS Publications* https://pubs.acs.org/doi/pdf/10.1021/ac60142a008 (2002) doi:10.1021/ac60142a008.
89. Crouthamel, C. E. & Jr, D. S. M. Solubility of the Rare Earth Oxalates and Complex Ion Formation in Oxalate Solution. II. Neodymium and Cerium(III)1. *ACS Publications* https://pubs.acs.org/doi/pdf/10.1021/ja01146a019 (2002) doi:10.1021/ja01146a019.
90. Grenthe, I., Gårdhammar, G. & Rundcrantz, E. Thermodynamic properties of rare earth complexes VI. Stability constants for the oxalate compelxes of Ce (III), Eu (III), Tb (III), and Lu (III). *Acta Chemica Scandinavica* **23**, 93–108 (1969).

91. Chi, R. & Xu, Z. A solution chemistry approach to the study of rare earth element precipitation by oxalic acid. *Metall Mater Trans B* **30**, 189–195 (1999).
92. Weaver, Boyd. Fractional Separation of Rare Earths by Oxalate Precipitation from Homogeneous Solution. *Anal. Chem.* **26**, 479–480 (1954).
93. Effendi, S., Pratomo, U., Anggraeni, A., Mutalib, A. & Bahti, H. H. Optimization of Parameters for Separation of the Medium Rare Earth Element Group from Other Rare Earth Elements by Precipitation Method Using Box-Behken Design. *Analytical and Bioanalytical Chemistry Research* **9**, 221–233 (2022).
94. McNulty, T., Hazen, N. & Park, S. Processing the ores of rare-earth elements. *MRS Bulletin* **47**, 258–266 (2022).
95. Porvali, A., Wilson, B. P. & Lundström, M. Lanthanide-alkali double sulfate precipitation from strong sulfuric acid NiMH battery waste leachate. *Waste Management* **71**, 381–389 (2018).
96. de Vasconcellos, M. E., da Rocha, S. M. R., Pedreira, W. R., da S. Queiroz, C. A. & Abrão, A. Enrichment of yttrium from rare earth concentrate by ammonium carbonate leaching and peroxide precipitation. *Journal of Alloys and Compounds* **418**, 200–203 (2006).
97. Rossmanith, K. Reindarstellung von Neodymoxid in großem Maßstab durch fraktionierte Kristallisation der Ammoniumdoppelnitrate. *Monatsh Chem* **126**, 293–298 (1995).
98. Rossmanith, K. Reindarstellung von Lanthan- und Praseodym-Ammoniumdoppelnitraten durch fraktionierte Kristallisation in großem Maßstab. *Monatsh Chem* **125**, 1027–1031 (1994).
99. James, C. THULIUM I.1. *J. Am. Chem. Soc.* **33**, 1332–1344 (1911).
100. Lu, H. *et al.* Size-dependent selective crystallization using an inorganic mixed-oxoanion system for lanthanide separation. *Dalton Transactions* **48**, 12808–12811 (2019).
101. Kołodyńska, D., Fila, D., Gajda, B., Gęga, J. & Hubicki, Z. Rare Earth Elements—Separation Methods Yesterday and Today. in *Applications of Ion Exchange Materials in the Environment* (eds. Inamuddin, Ahamed, M. I. & Asiri, A. M.) 161–185 (Springer International Publishing, Cham, 2019). doi:10.1007/978-3-030-10430-6_8.
102. Zagorodni, A. A. *Ion Exchange Materials: Properties and Applications*. (Elsevier Science, 2006).
103. Campbell, D. O. & Buxton, S. R. Rapid Ion Exchange Separations. Chromategraphic Lanthanide Separations Using a High-Pressure Ion Exchange Method. *ACS Publications* https://pubs.acs.org/doi/pdf/10.1021/i260033a016 (2002) doi:10.1021/i260033a016.
104. Mosai, A. K., Chimuka, L., Cukrowska, E. M., Kotzé, I. A. & Tutu, H. The Recovery of Rare Earth Elements (REEs) from Aqueous Solutions Using Natural Zeolite and Bentonite. *Water Air Soil Pollut* **230**, 188 (2019).

105. Kurkinen, S., Virolainen, S. & Sainio, T. Chromatographic Separation of Rare Earth Elements as MGDA Complexes on Anion Exchange Resins. *Metals* **13**, 600 (2023).
106. Li, J. *et al.* Selective extraction and column separation for 16 kinds of rare earth element ions by using N, N-dioctyl diglycolacid grafted silica gel particles as the stationary phase. *Journal of Chromatography A* **1627**, 461393 (2020).
107. Colombo, F. *et al.* An insight into REEs recovery from spent fluorescent lamps: Evaluation of the affinity of an NH4-13X zeolite towards Ce, La, Eu and Y. *Waste Management* **175**, 339–347 (2024).
108. El Ouardi, Y. *et al.* The recent progress of ion exchange for the separation of rare earths from secondary resources – A review. *Hydrometallurgy* **218**, 106047 (2023).
109. Rychkov, V. *et al.* Rare Earth Element Preconcentration from Various Primary and Secondary Sources by Polymeric Ion Exchange Resins. *Separation & Purification Reviews* **51**, 468–483 (2022).
110. Swain, N. & Mishra, S. A review on the recovery and separation of rare earths and transition metals from secondary resources. *Journal of Cleaner Production* **220**, 884–898 (2019).
111. Yang, Y. *et al.* REE Recovery from End-of-Life NdFeB Permanent Magnet Scrap: A Critical Review. *J. Sustain. Metall.* **3**, 122–149 (2017).
112. Pan, M. *et al.* Effect of Terbium addition on the coercivity of the sintered NdFeB magnets. *Journal of Rare Earths* **28**, 399–402 (2010).
113. Seo, Y. & Morimoto, S. Comparison of dysprosium security strategies in Japan for 2010–2030. *Resources Policy* **39**, 15–20 (2014).
114. Vo, P. H. N. *et al.* Biomining for sustainable recovery of rare earth elements from mining waste: A comprehensive review. *Science of The Total Environment* **908**, 168210 (2024).
115. Lèbre, É., Corder, G. D. & Golev, A. Sustainable practices in the management of mining waste: A focus on the mineral resource. *Minerals Engineering* **107**, 34–42 (2017).
116. Bian, Z. *et al.* The Challenges of Reusing Mining and Mineral-Processing Wastes. *Science* **337**, 702–703 (2012).
117. Jiao, Y. *et al.* A review of acid mine drainage: Formation mechanism, treatment technology, typical engineering cases and resource utilization. *Process Safety and Environmental Protection* **170**, 1240–1260 (2023).
118. Cánovas, C. R., Chapron, S., Arrachart, G. & Pellet-Rostaing, S. Leaching of rare earth elements (REEs) and impurities from phosphogypsum: A preliminary insight for further recovery of critical raw materials. *Journal of Cleaner Production* **219**, 225–235 (2019).
119. Salo, M., Knauf, O., Mäkinen, J., Yang, X. & Koukkari, P. Integrated acid leaching and biological sulfate reduction of phosphogypsum for REE recovery. *Minerals Engineering* **155**, 106408 (2020).

120. Virolainen, S., Repo, E. & Sainio, T. Recovering rare earth elements from phosphogypsum using a resin-in-leach process: Selection of resin, leaching agent, and eluent. *Hydrometallurgy* **189**, 105125 (2019).
121. Hermassi, M., Granados, M., Valderrama, C., Ayora, C. & Cortina, J. L. Recovery of Rare Earth Elements from acidic mine waters by integration of a selective chelating ion-exchanger and a solvent impregnated resin. *Journal of Environmental Chemical Engineering* **9**, 105906 (2021).
122. Hermassi, M. *et al.* Impact of functional group types in ion exchange resins on rare earth element recovery from treated acid mine waters. *Journal of Cleaner Production* **379**, 134742 (2022).
123. Bernardo José, L., Cordeiro Silva, G. & Cláudia Queiroz Ladeira, A. Pre-concentration and partial fractionation of rare earth elements by ion exchange. *Minerals Engineering* **205**, 108477 (2024).
124. Wang, Y. *et al.* Selective recovery of rare earth metals from acid mine drainage by pyrrolidine diglycolamide silica column. *Journal of Environmental Chemical Engineering* **11**, 110091 (2023).
125. Beltrami, D., Deblonde, G. J.-P., Bélair, S. & Weigel, V. Recovery of yttrium and lanthanides from sulfate solutions with high concentration of iron and low rare earth content. *Hydrometallurgy* **157**, 356–362 (2015).
126. Hassas, B. V., Rezaee, M. & Pisupati, S. V. Effect of various ligands on the selective precipitation of critical and rare earth elements from acid mine drainage. *Chemosphere* **280**, 130684 (2021).
127. Maani, T., Mathur, N., Singh, S., Rong, C. & Sutherland, J. W. Potential for Nd and Dy Recovery from End-of-Life Products to Meet Future Electric Vehicle Demand in the U.S. *Procedia CIRP* **98**, 109–114 (2021).
128. Ding, A., Liu, C., Zhang, X., Lei, L. & Xiao, C. ZnCl2: A Green Brønsted Acid for Selectively Recovering Rare Earth Elements from Spent NdFeB Permanent Magnets. *Environ. Sci. Technol.* **56**, 4404–4412 (2022).
129. Dewulf, B., Batchu, N. K. & Binnemans, K. Enhanced Separation of Neodymium and Dysprosium by Nonaqueous Solvent Extraction from a Polyethylene Glycol 200 Phase Using the Neutral Extractant Cyanex 923. *ACS Sustainable Chem. Eng.* **8**, 19032–19039 (2020).
130. Sun, P., Huang, K., Song, W., Gao, Z. & Liu, H. Separation of Rare Earths from the Transition Metals Using a Novel Ionic-Liquid-Based Aqueous Two-Phase System: Toward Green and Efficient Recycling of Rare Earths from the NdFeB Magnets. *Ind. Eng. Chem. Res.* **57**, 16934–16943 (2018).
131. Xu, J. *et al.* Separation of cobalt, neodymium and dysprosium using amorphous zirconium phosphate. *Hydrometallurgy* **175**, 170–178 (2018).
132. Xu, J. *et al.* Polyacrylonitrile-encapsulated amorphous zirconium phosphate composite adsorbent for Co, Nd and Dy separations. *Chemical Engineering Journal* **351**, 832–840 (2018).
133. Cole, B. E. *et al.* A molecular basis to rare earth separations for recycling: tuning the TriNOx ligand properties for improved performance. *Chem. Commun.* **54**, 10276–10279 (2018).

134. Cheisson, T., Cole, B. E., Manor, B. C., Carroll, P. J. & Schelter, E. J. Phosphoryl-Ligand Adducts of Rare Earth-TriNOx Complexes: Systematic Studies and Implications for Separations Chemistry. *ACS Sustainable Chem. Eng.* **7**, 4993–5001 (2019).
135. Onoda, H. & Iinuma, A. Selective preparation of neodymium phosphates from iron mixed solution by two-step precipitation. *Journal of Environmental Chemical Engineering* **8**, 104083 (2020).
136. Önal, M. A. R., Riaño, S. & Binnemans, K. Alkali baking and solvometallurgical leaching of NdFeB magnets. *Hydrometallurgy* **191**, 105213 (2020).
137. Dupont, D. & Binnemans, K. Recycling of rare earths from NdFeB magnets using a combined leaching/extraction system based on the acidity and thermomorphism of the ionic liquid [Hbet][Tf2N]. *Green Chem.* **17**, 2150–2163 (2015).
138. Liu, F. *et al.* Recovery and separation of rare earths and boron from spent Nd-Fe-B magnets. *Minerals Engineering* **145**, 106097 (2020).
139. Kumari, A., Sinha, M. K., Pramanik, S. & Sahu, S. K. Recovery of rare earths from spent NdFeB magnets of wind turbine: Leaching and kinetic aspects. *Waste Management* **75**, 486–498 (2018).
140. O'Connell-Danes, J. G. *et al.* A Simple Supramolecular Approach to Recycling Rare Earth Elements. *ACS Sustainable Chem. Eng.* **12**, 9301–9305 (2024).
141. Amira, A. *et al.* Recent Advances in the Synthesis of α-Aminophosphonates: A Review. *ChemistrySelect* **6**, 6137–6149 (2021).
142. Fedorenko, S. V. *et al.* Sodium picrate effect on extraction of lanthanum and lutetium by aminophosphonate calix[4]resorcinarenes. *Russian Chemical Bulletin* **52**, 562–566 (2003).
143. Ziganshina, A. Yu., Kazakova, E. H., Fedorenko, S. V., Mustafina, A. R. & Konovalov, A. I. Aminomethylphosphonate Derivatives of Tetramethylcalix[4]resorcinolarene. Synthesis and Some Extraction Properties in Relation to the Lantane Ions. *Russian Journal of General Chemistry* **71**, 1422–1425 (2001).
144. Varga, P. R. & Keglevich, G. Synthesis of α-Aminophosphonates and Related Derivatives; The Last Decade of the Kabachnik–Fields Reaction. *Molecules* **26**, 2511 (2021).
145. Moedritzer, K. & Irani, R. R. The Direct Synthesis of α-Aminomethylphosphonic Acids. Mannich-Type Reactions with Orthophosphorous Acid. *Journal of Organic Chemistry* **31**, 1603–1607 (1966).
146. Neiber, R. R. *et al.* Selective lead (II) sorption using aminophosphonate-based sorbents: Effect of amine linker, characterization and sorption performance. *Chemical Engineering Journal* **442**, 136300 (2022).
147. Rashad, M. M. *et al.* Synthesis of α-aminophosphonate based sorbents – Influence of inserted groups (carboxylic vs. amine) on uranyl sorption. *Chemical Engineering Journal* **421**, 127830 (2021).

148. Zhou, Z., Fu, Y., Wang, X., Si, X. & Lu, Y. Separation of thorium from radioactive rare-earth waste residue using aminophosphonate-functionalized polymer resin. *J Radioanal Nucl Chem* **332**, 607–616 (2023).
149. Galhoum, A. A. *et al.* Synthesis of polyaminophosphonic acid-functionalized poly(glycidyl methacrylate) for the efficient sorption of La(III) and Y(III). *Chemical Engineering Journal* **375**, 121932 (2019).
150. Imam, E. A. *et al.* Effect of mono- vs. bi-functionality of aminophosphonate derivatives on the enhancement of U(VI) sorption: physicochemical properties and sorption performance. *Journal of Environmental Chemical Engineering* **11**, 109951 (2023).
151. Artiushenko, O. *et al.* Recovery of rare earth elements from waste phosphors using phosphonic acid-functionalized silica adsorbent. *Separation and Purification Technology* **330**, 125525 (2024).
152. Yang, B. *et al.* Ultra-selective removal of thorium from rare earths by aminophosphonic acid-modified porous silica. *Separation and Purification Technology* **341**, 126952 (2024).
153. Dąbrowski, A. Adsorption — from theory to practice. *Advances in Colloid and Interface Science* **93**, 135–224 (2001).
154. Borst, A. M. *et al.* Adsorption of rare earth elements in regolith-hosted clay deposits. *Nat Commun* **11**, 4386 (2020).
155. de Dardel, F. & Arden, T. V. Ion Exchangers. in *Ullmann's Encyclopedia of Industrial Chemistry* (John Wiley & Sons, Ltd, 2008). doi:10.1002/14356007.a14_393.pub2.
156. Mohd Yusoff, N. H. *et al.* Recent Advances in Polymer-based 3D Printing for Wastewater Treatment Application: An Overview. *Chemical Engineering Journal* **429**, 132311 (2022).
157. Yu, J. *et al.* A review of adsorption materials and their application of 3D printing technology in the separation process. *Chemical Engineering Journal* **475**, 146247 (2023).
158. Gao, Y., Lalevée, J. & Simon-Masseron, A. An Overview on 3D Printing of Structured Porous Materials and Their Applications. *Advanced Materials Technologies* **8**, 2300377 (2023).
159. Jivrakh, K. B. *et al.* A critical review on 3D-printed adsorbents, membranes, and catalysts for carbon dioxide capture, separation, and conversion. *Journal of Cleaner Production* **472**, 143522 (2024).
160. Zhou, L.-Y., Fu, J. & He, Y. A Review of 3D Printing Technologies for Soft Polymer Materials. *Advanced Functional Materials* **30**, 2000187 (2020).
161. Wu, T. *et al.* 3D printed porous chitosan/metal–organic framework composites as effective adsorbents to remove heavy metals from wastewater. *Chemical Engineering Journal* **493**, 152780 (2024).
162. Setiawan, T., Alvin Setiadi, G. & Mukti, R. R. Deployable and Retrievable 3D-Printed Zeolite–Polymer Composites for Wastewater Treatment: A Review. *Ind. Eng. Chem. Res.* **62**, 18159–18177 (2023).

163. Fuxiang, S., Na, W., Qiangqiang, Z., Jie, W. & Bin, L. 3D printing calcium alginate adsorbents for highly efficient recovery of U(VI) in acidic conditions. *Journal of Hazardous Materials* **440**, 129774 (2022).
164. Calderilla, C., Maya, F., Cerdà, V. & Leal, L. O. 3D printed device including disk-based solid-phase extraction for the automated speciation of iron using the multisyringe flow injection analysis technique. *Talanta* **175**, 463–469 (2017).
165. Kulomäki, S., Lahtinen, E., Perämäki, S. & Väisänen, A. Determination of mercury at picogram level in natural waters with inductively coupled plasma mass spectrometry by using 3D printed metal scavengers. *Analytica Chimica Acta* **1092**, 24–31 (2019).
166. Pereira, A., Ferreira, A. F. P., Rodrigues, A., Ribeiro, A. M. & Regufe, M. J. Study of methane upgrading using an activated carbon 3D-printed adsorbent. *Journal of Environmental Chemical Engineering* **12**, 111730 (2024).
167. Osterrieth, J. W. M. *et al.* How Reproducible are Surface Areas Calculated from the BET Equation? *Advanced Materials* **34**, 2201502 (2022).
168. Brunauer, S., Emmett, P. H. & Teller, E. Adsorption of Gases in Multimolecular Layers. *J. Am. Chem. Soc.* **60**, 309–319 (1938).
169. Mongioví, C. *et al.* Adsorption location of copper on hemp shives revealed by combination of K-edge subtraction X-ray micro-tomography and X-ray micro-fluorescence. *Cellulose* **31**, 809–822 (2024).
170. Lahtinen, E., Precker, R. L. M., Lahtinen, M., Hey-Hawkins, E. & Haukka, M. Selective Laser Sintering of Metal-Organic Frameworks: Production of Highly Porous Filters by 3D Printing onto a Polymeric Matrix. *ChemPlusChem* **84**, 222–225 (2019).
171. Imam, E. A. *et al.* Synthesis of α-aminophosphonate functionalized chitosan sorbents: Effect of methyl vs phenyl group on uranium sorption. *Chemical Engineering Journal* **352**, 1022–1034 (2018).
172. Sawada, K., Miyagawa, T., Sakaguchi, T. & Doi, K. Structure and thermodynamic properties of aminopoly-phosphonate complexes of the alkaline-earth metal lons. *J. Chem. Soc., Dalton Trans.* 3777–3784 (1993) doi:10.1039/DT9930003777.
173. Sawada, K., Araki, T. & Suzuki, T. Complex formation of amino polyphosphonates. 1. Potentiometric and nuclear magnetic resonance studies of nitrilotris(methylenephosphonato) complexes of the alkaline-earth-metal ions. *Inorg. Chem.* **26**, 1199–1204 (1987).
174. Kubíček, V., Kotek, J., Hermann, P. & Lukeš, I. Aminoalkylbis(phosphonates): Their Complexation Properties in Solution and in the Solid State. *European Journal of Inorganic Chemistry* **2007**, 333–344 (2007).
175. Sawada, K., Kanda, T., Naganuma, Y. & Suzuki, T. Formation and protonation of aminopolyphosphonate complexes of alkaline-earth and divalent transition-metal ions in aqueous solution. *J. Chem. Soc., Dalton Trans.* 2557–2562 (1993) doi:10.1039/DT9930002557.

176. Rostášová, I. *et al.* Interaction of the Zn(ii)–cyclen complex with aminomethylphosphonic acid: original simultaneous potentiometric and 31 P NMR data treatment. *New Journal of Chemistry* **41**, 7253–7259 (2017).
177. Holz, R. C., Meister, G. E. & Horrocks, W. D. Spectroscopic characterization of a series of europium(III) amino phosphonate complexes in solution. *Inorg. Chem.* **29**, 5183–5189 (1990).
178. Frey, S. T. & Horrocks, W. D. Complexation, luminescence, and energy transfer of cerium(3+) with a series of multidentate aminophosphonic acids in aqueous solution. *Inorg. Chem.* **30**, 1073–1079 (1991).
179. Virtanen, E. J., Perämäki, S., Helttunen, K., Väisänen, A. & Moilanen, J. O. Alkyl-Substituted Aminobis(phosphonates)—Efficient Precipitating Agents for Rare Earth Elements, Thorium, and Uranium in Aqueous Solutions. *ACS Omega* **6**, 23977–23987 (2021).
180. Kaboudin, B., Saadati, F., Golshan, A., Abdollahi, H. & Yokomatsu, T. Synthesis and Complexation Properties of N,N-Bis(phosphinomethyl)amine as a New Class of 1-Aminophosphinic Acids with Transition Metals and Lanthanide Ions in Aqueous Solution. *J. Chem. Eng. Data* **56**, 3651–3656 (2011).
181. Bollinger, J. E. & Roundhill, D. M. Complexation of indium(III), gallium(III), iron(III), gadolinium(III), and neodymium(III) ions with amino diphosphonic acids in aqueous solution. *Inorg. Chem.* **32**, 2821–2826 (1993).
182. Stuart, B. H. *Infrared Spectroscopy: Fundamentals and Applications*. (John Wiley & Sons, Incorporated, Newark, UNITED KINGDOM, 2004).
183. Larkin, P. *Infrared and Raman Spectroscopy: Principles and Spectral Interpretation*. (Elsevier, San Diego, UNITED STATES, 2011).
184. Günther, H. *NMR Spectroscopy: Basic Principles, Concepts and Applications in Chemistry*. (John Wiley & Sons, Incorporated, Newark, UNITED STATES, 2013).
185. Macomber, R. S. An introduction to NMR titration for studying rapid reversible complexation. *J. Chem. Educ.* **69**, 375 (1992).
186. Burai, L., Ren, J., Kovacs, Z., Brücher, E. & Sherry, A. D. Synthesis, Potentiometry, and NMR Studies of Two New 1,7-Disubstituted Tetraazacyclododecanes and Their Complexes Formed with Lanthanide, Alkaline Earth Metal, Mn2+, and Zn2+ Ions. *Inorg. Chem.* **37**, 69–75 (1998).
187. Weekes, D. M., Jaraquemada-Peláez, M. de G., Kostelnik, T. I., Patrick, B. O. & Orvig, C. Di- and Trivalent Metal-Ion Solution Studies with the Phosphinate-Containing Heterocycle DEDA-(PO). *Inorg. Chem.* **56**, 10155–10161 (2017).
188. Freundlich, H. & Losev, G. Über die Adsorption der Farbstoffe durch Kohle und Fasern. *Zeitschrift für Physikalische Chemie* **59U**, 284–312 (1907).
189. Ayawei, N., Ebelegi, A. N. & Wankasi, D. Modelling and Interpretation of Adsorption Isotherms. *Journal of Chemistry* **2017**, 3039817 (2017).

190. de Vargas Brião, G., Hashim, M. A. & Chu, K. H. The Sips isotherm equation: Often used and sometimes misused. *Separation Science and Technology* **58**, 884–892 (2023).
191. Elsalamouny, A. R., Desouky, O. A., Mohamed, S. A., Galhoum, A. A. & Guibal, E. Uranium and neodymium biosorption using novel chelating polysaccharide. *International Journal of Biological Macromolecules* **104**, 963–968 (2017).
192. Esma, B., Omar, A. & Amine, D. M. Comparative study on lanthanum(III) sorption onto Lewatit TP 207 and Lewatit TP 260. *J Radioanal Nucl Chem* **299**, 439–446 (2014).
193. Hu, Q., Lan, R., He, L., Liu, H. & Pei, X. A critical review of adsorption isotherm models for aqueous contaminants: Curve characteristics, site energy distribution and common controversies. *Journal of Environmental Management* **329**, 117104 (2023).
194. Villemin, D. & Didi, M. A. Aminomethylenephosphonic Acids Syntheses and Applications (A Review). *Oriental Journal of Chemistry* **31**, 1–12 (2015).
195. Nesterenko, P. N., Shaw, M. J., Hill, S. J. & Jones, P. Aminophosphonate-Functionalized Silica: A Versatile Chromatographic Stationary Phase for High-Performance Chelation Ion Chromatography. *Microchemical Journal* **62**, 58–69 (1999).
196. Boichenko, A. P., Markov, V. V., Kong, H., Matveeva, A. G. & Loginova, L. P. Re-evaluated data of dissociation constants of alendronic, pamidronic and olpadronic acids. *Central European Journal of Chemistry* **7**, 8–13 (2009).
197. Yang, X. *et al.* Effect of Counteranions on the Extraction and Complexation of Trivalent Lanthanides with Tetradentate Phenanthroline-Derived Phosphonate Ligands. *Inorg. Chem.* **59**, 17453–17463 (2020).
198. Bligh, S. W. A. *et al.* Lanthanide and Transition Metal Complexes of Dialkyl α-Hydroxyiminophosphonates. *Phosphorus, Sulfur, and Silicon and the Related Elements* **111**, 49–49 (1996).
199. Archer, W. R., Iftekhar, N., Fiorito, A., Winn, S. A. & Schulz, M. D. Synthesis of Phosphonated Polymer Resins for the Extraction of Rare-Earth Elements. *ACS Appl. Polym. Mater.* **4**, 2506–2512 (2022).
200. Tsurubou, Shigekazu. *et al.* Solvent extraction of alkaline earths and lanthanides using crown ethers as ion size selective masking reagents: A macrocycle application. *Anal. Chem.* **67**, 1465–1469 (1995).
201. Fonseka, C. *et al.* Selective recovery of europium from real acid mine drainage by using novel amine based modified SBA15 adsorbent and membrane distillation system. *Journal of Water Process Engineering* **56**, 104551 (2023).
202. Binnemans, K. & Tom Jones, P. Methanesulfonic acid (MSA) in clean processes and applications: a tutorial review. *Green Chemistry* **26**, 8583–8614 (2024).
203. Belous, A. G., Pashkova, E. V., Elshanskii, V. A. & Ivanitskii, V. P. Effect of precipitation conditions on the phase composition, particle morphology,

and properties of iron(III,II) hydroxide precipitates. *Inorg Mater* **36**, 343–351 (2000).
204. Vaziri Hassas, B., Rezaee, M. & Pisupati, S. V. Precipitation of rare earth elements from acid mine drainage by CO2 mineralization process. *Chemical Engineering Journal* **399**, 125716 (2020).
205. Hu, X. *et al.* Treatment and recovery of iron from acid mine drainage: a pilot-scale study. *Journal of Environmental Chemical Engineering* **10**, 106974 (2022).
206. Wang, J. & Guo, X. Adsorption kinetic models: Physical meanings, applications, and solving methods. *Journal of Hazardous Materials* **390**, 122156 (2020).

ORIGINAL PAPERS

I

ALKYL-SUBSTITUTED AMINOBIS(PHOSPHONATES)—EFFICIENT PRECIPITATING AGENTS FOR RARE EARTH ELEMENTS, THORIUM, AND URANIUM IN AQUEOUS SOLUTIONS

by

Virtanen, E.J., Perämäki S., Helttunen K., Väisänen A. & Moilanen J.O. 2021

ACS Omega vol 6, 23977-23987

https://doi.org/10.1021/acsomega.1c02982

ACS OMEGA

http://pubs.acs.org/journal/acsodf

Article

Alkyl-Substituted Aminobis(phosphonates)—Efficient Precipitating Agents for Rare Earth Elements, Thorium, and Uranium in Aqueous Solutions

Emilia J. Virtanen, Siiri Perämäki, Kaisa Helttunen, Ari Väisänen,* and Jani O. Moilanen*

Cite This: *ACS Omega* 2021, 6, 23977−23987

Read Online

ACCESS | Metrics & More | Article Recommendations | Supporting Information

ABSTRACT: The efficient and environmentally sustainable separation process for rare earth elements (REE), especially for adjacent lanthanoids, remains a challenge due to the chemical similarity of REEs. Tetravalent actinoids, thorium, and traces of uranium are also present in concentrates of REEs, making their separation relevant. This study reports six simple water-soluble aminobis(phosphonate) ligands, $RN[CH_2P(O)(OH)_2]_2$ (**1** R = CH_2CH_3, **2** R = $(CH_2)_2CH_3$, **3** R = $(CH_2)_3CH_3$, **4** R = $(CH_2)_4CH_3$, **5** R = $(CH_2)_5CH_3$, **6** R = $CH_2CH(C_2H_5)$-$(CH_2)_3CH_3$) as precipitating agents for REEs, Th, and U, as well as gives insight into the coordination modes of the utilized ligands with REEs at the molecular level. Aminobis(phosphonates) **4**−**6** with longer carbon chains were found to separate selectively thorium, uranium, and scandium from REEs with short precipitation time (15 min) and excellent separation factors that generally range from 100 to 2000 in acidic aqueous solution. Ligands **1**−**6** also improved separation factors for adjacent lanthanoids in comparison to traditional oxalate precipitation agents. Importantly, precipitated metals can be recovered from the ligands with 3 molar HNO_3 with no observed ligand decomposition enabling the possibility of recycling the ligands in the separation process. NMR-monitored pH titrations for **1** showed deprotonation steps at pK_a 1.3, 5.55, and >10.5, which indicate that the ligands remain in a deprotonated $[L]^{-1}$ form in the pH range of 0−4 used in the precipitation studies. ^{31}P NMR titration studies between **1** and $M(NO_3)_3$ (M = Y, La, Lu) gave satisfactory fits for 1:3, 1:2, and 1:1 metal−ligand stoichiometries for Y, La, and Lu, respectively, according to an F-test. Therefore, aminobis(phosphonate) precipitation agents **1**−**6** are likely to form metal complexes with fewer ligands than traditional separation agents like DEHPA, which coordinates to REEs in 1:6 metal−ligand ratio.

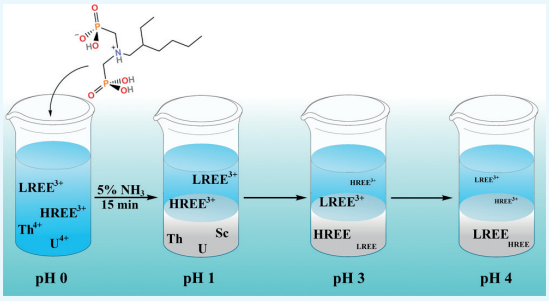

INTRODUCTION

Rare earth elements (REE) consisting of lanthanoids, scandium, and yttrium are widely used in crucial technological applications such as computers, catalysts, batteries of electric cars, and renewable energy production; latter two play an important role in a shift toward greener technologies.[1] Thus, the demand of REEs has been estimated to increase considerably in the future. In EU alone, e-mobility and renewable energy production could increase the demand for dysprosium and neodymium up to 12- and 4-fold by 2050 from the current demand of 200 and 4000 tons, respectively.[2] Globally, the demand for all REEs has been estimated to grow annually 4.4% until 2026, raising concerns for the sufficiency of primary production of REEs from ores, which is not an environmentally sustainable process (see below).[3] Ores of REEs also contain radioactive elements like thorium and uranium that complicate the separation process of REEs.[4] Therefore, it is not only important to investigate the recycling and recovery of REEs from secondary sources, where the concentration of REEs is relatively high,[5−7] but also to develop new separation processes for REE concentrates that allow the efficient and environmentally friendly separation of REEs from each other and other metals.

The most common separation process for lanthanoids includes liquid−liquid extraction with organophosphorous extracting agents, while Th and U are typically separated from lanthanoids first by selective dissolution and further purificated by liquid−liquid extraction.[4] The most commonly used extracting agents for lanthanoids are di(2-ethylhexyl)-phosphoric acid (DEHPA) and 2-ethylhexylphosphonic acid mono-2-ethylhexyl ester (EHEHPA) due to their robustness and good recyclability, whereas Th and U can be separated from REEs, and further from each other using tributylphos-

Received: June 7, 2021
Published: September 13, 2021

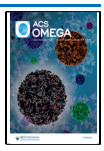

phate (TBP) or secondary and tertiary amines.[8] However, lanthanoids are chemically a very similar group of elements, and especially the separation of adjacent lanthanoids is challenging even with the commercial extracting agents. Although a liquid−liquid extraction process is the most suitable for industrial scale, one of the challenges has been to reduce the amount of used organic solvents to make the process more sustainable.[4] The liquid−liquid extraction utilizing commercial extraction agents, such as DEHPA and EHEHPA, can be improved by replacing organic solvents with ionic liquids.[9−13] This replacement has shown improvements in the separation of heavy and light adjacent lanthanoids,[9,10] selectivity to Nd over transition metals,[11] and high La/Ce separation.[12] Ionic liquids have also been used in Th/U separation with a success as very good separation factor is obtained ($SF_{Th/U}$ 793).[13] However, the high viscosity of ionic liquids still remains a challenge in the extraction processes.

Apart from the liquid−liquid extraction, separation for REEs and Th can also be done solely in water solution with no need for the organic phase, either by precipitation or fractional crystallization. Traditional precipitation agents, oxalates, have been reported to separate light lanthanoids from heavy ones by selective dissolution of rare earth oxalates.[14] Fractional crystallization from water solutions with borates[15] or coordination polymers[16,17] have yielded good separation factors, especially for Nd/Dy separation ($SF_{Nd/Dy}$ > 300). Furthermore, selective crystallization with the iodate−sulfate system has been reported to separate efficiently lighter lanthanoids from heavier ones,[18] and selenite crystallization has yielded good Th/Ln separations.[19] Nevertheless, the crystallization method with borates, iodate−sulfate, and selenite systems requires long reaction times of 5 days, hydrothermal conditions (>453 K), and in the case of borate systems, environmentally hazardous bromoform for the final separation step.[15]

Aminophosphonates have gathered attention in the medical field due to their pharmaceutical properties[20] and good binding affinity toward medically relevant lanthanoids, such as gadolinium (common MRI contrasting agent) and samarium (nuclear medicine).[21] Despite the good coordination properties of aminophosphonates toward REEs, their utilization in REE recovery and separation has been initiated only recently, yielding promising results. For example, the separation factors of (2-ethylhexylamino)methylphosphonic acid mono-2-ethylhexyl ester (HEHAMP) and 2-ethylhexyl-3-(2-ethylhexylamino)pentan-3-yl-phosphonic acid (HEHAPP) in the liquid−liquid extraction process of REEs are larger in comparison to the separation factors of two conventional extracting agents, DEHPA and EHEHPA.[22−26] Similarly, tetravalent Th/Ce separation in a liquid−liquid extraction with an aminophosphonate-based extracting agent Cextrant 230 gives a good separation factor of 14.7.[27]

Depending on the nature of organic moiety and the number of phosphonate groups in the aminophosphonate framework, aminophosphonates can be designed to be water soluble,[28] which would enable their use as precipitation agents for metals in acidic aqueous solutions, similar to oxalates.[20] Furthermore, by varying the number of phosphonate group and/or organic moiety, precipitation abilities of aminophosphonates toward different metal ions can be tuned. For example, by increasing the number of phosphonate groups in the ligand framework, more binding sites are available for metal ions in a single ligand. With that being said, we investigated the complexation and precipitation properties of simple aminobis(phosphonates) **1**−**6** (Scheme 1) toward REEs, Th and U in

Scheme 1. General Synthesis Route for Aminomethylphoshonate Ligands 1−6

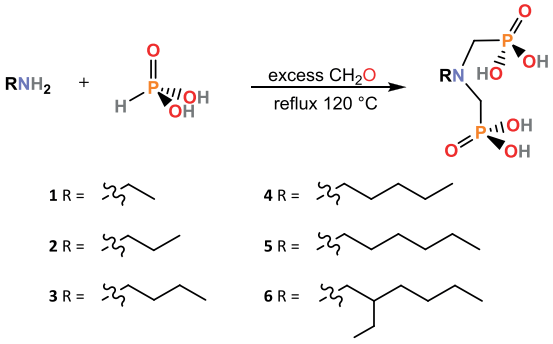

NMR, and larger (∼100 mg) scale in different pH values ranging from 1 to 4. We also determined the acid−base properties of synthesized aminobis(phosphonate) ligands utilizing NMR spectroscopy and carried out computational analysis for the most plausible complexes in the aqueous solution to get further insight into their solution behavior. To the best of our knowledge, this study demonstrates for the first time that simple aminobis(phosphonates), which can be synthesized by straightforward addition reactions, can be used as efficient precipitation agents with short precipitation times for REEs, Th, and U in aqueous solutions.

RESULTS AND DISCUSSION

Ligands **1**−**6** were prepared using a modified reported one-pot synthesis, where a condensation reaction between an amine and formaldehyde is followed by nucleophilic addition of phosphorous acid under reflux condition in an acidic water solution (Scheme 1).[28] Crude products were purified by recrystallization either from ethanol, water, or water:ethanol (2:1) mixture. The purity of the recrystallized products was ensured by ^{1}H NMR, IR, and elemental analysis (Figures S1−S12).

As expected, the ligands with shorter carbon chains (**1**−**3**) showed higher solubility in water compared to ligands with longer (**4** and **5**) and branched (**6**) chains (Table S1). For example, the water solubility of ligands **1**, **3**, and **6** were 327, 184, and 9.5 g/L, respectively.

Acid−Base Properties. The deprotonation processes of the most water-soluble ligand **1** were investigated to assess the protonation state of ligands in metal complexes. Dependence of the deprotonation steps of **1** on the pH was determined by NMR titrations in D_2O at 295 K. The pH of the 0.14 M solution of **1** was adjusted between 0.5 and 10.5 with the addition of a 5% NH_3 solution, and ^{31}P and ^{1}H NMR spectra were measured at 0.5 pH unit intervals. Figure S13 shows the measured ^{31}P NMR and ^{1}H NMR shifts as a function of pH for the P atom and N−CH_2−P protons, respectively. ^{1}H NMR shifts of OH protons were not used in the determination since they cannot be directly observed in D_2O due to the fast proton−deuterium exchange. Three equivalent points for the deprotonation steps of **1** were observed at pH 1, pH 5, and around pH 10. The observed shift for the first deprotonation is

https://doi.org/10.1021/acsomega.1c02982
ACS Omega 2021, 6, 23977−23987

Scheme 2. Structures of Ligand 1 (L1) after Each Deprotonation Step

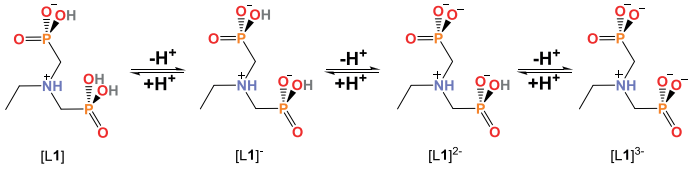

slightly different for ^{31}P nucleus than for the ^{1}H nuclei, but otherwise, the data obtained from ^{31}P and ^{1}H experiments are consistent. pK_a values for the first two deprotonations were calculated from the observed chemical shifts according to a previously reported method.[29] In contrast, the third deprotonation step at 10.5 takes place at the end of the titration (pH of ammonia is ∼10.6). Thus, the pK_a could not be calculated for the third deprotonation step. For the first and second deprotonation steps, the calculated pK_{a1} and pK_{a2} values are 1.33 and 5.55, respectively.

The deprotonation steps of **1** can be further elaborated by comparing the determined pK_a values to the pK_a values of two polyprotic phosphoric acids, namely pyrophosphoric acid (pK_{a1} = 0.91, pK_{a2} = 2.10, pK_{a3} = 6.70, and pK_{a4} = 9.32)[30] and pamidronic acid (pK_{a1} = 1.85, pK_{a2} = 5.85, and pK_{a3} = 10.30).[31] Assuming that **1** exists as a zwitterion, the determined pK_{a1} value 1.33 suggests that the first deprotonation likely occurs from the fully protonated $P(OH)_2(O)$ group forming structure $[L1]^-$ (Scheme 2), similar to pamidronic acid, which is known to exist as a zwitterion in a low pH regime.[32] The zwitterionic nature of **1** is further supported by the fact that it has only one low pK_a value (<2.50), arising from the deprotonation of one of the $P(OH)_2(O)$ groups, in contrast to pyrophosphoric acid which has two low pK_a values due to the two fully protonated $P(OH)_2(O)$ groups. By comparing the pK_{a2} value (5.55) of **1** to the pK_{a3} (6.70) and pK_{a2} (5.85) values of pyrophosphoric acid and pamidronic acid, respectively, it can be concluded that the second deprotonation step originates from either of the $P(OH)(O^-)$ groups forming a twice deprotonated structure $[L1]^{2-}$. The third deprotonation step takes place either from the $P(OH)(O^-)$ or the R_3NH^+ group. However, aminophosphonates have been reported to deprotonate first fully from the phosphorous groups before the NH^+ deprotonation is observed to occur.[31,33] Therefore, the third observed deprotonation is most likely to occur from the last $P(OH)(O^-)$ proton forming a structure $[L1]_3^-$ in pH > 10.5.

Complexation Studies. The binding affinity of ligand **1** toward REEs was investigated by performing NMR titrations in D_2O with three different metal salts—$Y(NO_3)_3$, $La(NO_3)_3$, and $Lu(NO_3)_3$—at low pH values (∼1.4−2.4), where **1** exists as a monoanion. These metal salts were chosen because of their different ionic radii and diamagnetic nature (no unpaired electrons). NMR titrations were also attempted for **1** with $Sc(NO_3)_3$ and $Th(NO_3)_4$ by adding 1 mM metal to 10 mM ligand. Unfortunately, Sc and Th complexes of **1** precipitated out from D_2O during titrations even at low pH values, preventing further analysis of the titration data.

First, metal-to-ligand titrations were carried out for Y by adding incremental amounts of $Y(NO_3)_3$ into 10 mM solution of **1** in D_2O. After each addition of the metal salt, ^{31}P and ^{1}H NMR spectra were measured. The ^{31}P NMR spectrum of the free ligand displayed one triplet for the P atoms at 8.54 ppm, and the ^{1}H spectrum showed doublet, quartet, and triplet for $N-CH_2-P$, $C-CH_2-N$, and CH_3 protons, respectively. Since ^{1}H resonances overlapped strongly in metal-to-ligand (Figure S14) and also in reverse ligand-to-metal titrations (see below and Figure S15), the chemical shift change of the ^{31}P signal was followed. During the titration, the ^{31}P signal shifted 2.54 ppm upfield, indicating that the free ligand and complexed species experienced fast exchange dynamics on the NMR timescale (Figure S16). Saturation of the chemical shift changes of phosphorus was observed after the addition of 1 equiv of metal. However, when **1** was titrated with La and Lu, smaller, <1 ppm upfield shift in ^{31}P signal was observed without saturation of the chemical shift changes at 1 equiv of metal (Figures S17 and S18). Additionally, the precipitate was observed during Lu titration; therefore, pH was set to 1.0 to prevent Lu complex from precipitating.

For Y, analysis of the titration data to theoretical 1:1 and 1:2 (M/L) binding isotherms provided unsatisfactory fits with relatively large errors of fit (Figure S19), whereas the addition of a third binding constant K_3 for the 1:3 binding model improved the fit significantly (Figure 1). Data was also fitted to a theoretical 1:4 binding isotherm (Figure S19). Because a small improvement of fit was observed by introducing more variables to the model, statistical F-tests were carried out for all fits to assign the preferential binding model. Based on the F-tests, the 1:3 binding model provided the best fit for the titration data at this range of concentrations for Y (Table S2). Similar fits to theoretical 1:1, 1:2, 1:3, and 1:4 binding isotherms were obtained for La as for Y (Figures 1 and S20);

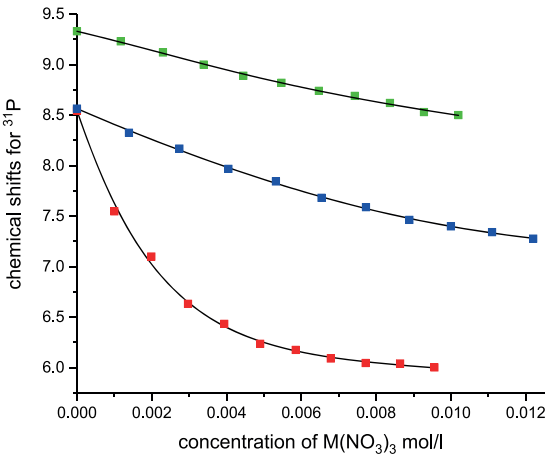

Figure 1. ^{31}P NMR shift changes as a function of the concentration of $M(NO_3)_3$ when ligand **1** is titrated with $Y(NO_3)_3$ (red) and $La(NO_3)_3$ at pH 1.8 (blue), and $Lu(NO_3)_3$ at pH 1.0 (green). Fittings for 1:3, 1:2, and 1:1 (M/L) binding models are presented for Y, La, and Lu, respectively (black solid lines).

https://doi.org/10.1021/acsomega.1c02982
ACS Omega 2021, 6, 23977−23987

however, the F-tests indicated that the 1:2 binding model was slightly better than the 1:3 model (Table S3). Interestingly, for Lu, analysis of the titration data to a theoretical 1:1 binding isotherm already provided a satisfactory fit (Figures 1 and S20), which was confirmed by the F-test (Table S4). The binding constants obtained for the 1:1, 1:2, and 1:3 metal complexes (Table 1) indicate that all M/L complexes are being formed in the solution when the ligand is titrated with Y or La.

Table 1. Overall Logarithmic Binding Constants (log *K*) for 1:1, 1:2, and 1:3 (Metal:Ligand) Binding Models[a]

	log *K* 1:1	log *K* 1:2	log *K* 1:3
Y_{ML}	2.4 ± 0.2	4.9 ± 0.4	7.3 ± 0.6
Y_{LM}	2.6 ± 0.2	4.4 ± 0.4	6.7 ± 0.7
La_{ML}	2.6 ± 0.5	4.4 ± 0.1	
La_{LM}	2.7 ± 0.5	4.3 ± 0.4	6.8 ± 0.3
Lu_{ML}	2.1± 0.3		
Lu_{LM}	N.D.[b]		

[a]M_{ML} represents the metal-to-ligand titration and M_{LM} the ligand-to-metal titration (M = Y, La, Lu). Errors are derived from standard deviation. [b]Sample formed a gel.

Reverse ligand-to-metal titrations were also performed by titrating 10 mM $M(NO_3)_3$ with incremental addition of **1**. However, the addition of 3 equiv of **1** to the NMR tube containing $Lu(NO_3)_3$ promoted the formation of a gel-like structure, thus preventing the determination of the binding constant for Lu. For Y and La, the first spectra were recorded after the addition of 0.3 eq of ligand, where phosphorus nuclei resonated at 6.25 and 7.02 ppm for Y and La, respectively (Figures S21 and S22). The titration was continued until the concentration of **1** reached 5 equiv, at which point, the chemical shift of the phosphorus signal had changed to 8.16 ppm for Y and 8.25 ppm for La without saturation of the chemical shift changes.

Analysis of the titration data to a 1:1 binding model provided unsatisfactory fits for both Y and La, whereas the addition of 1:2 and 1:3 binding models showed a slight improvement to the fits (Figures 2, S23, and S24). Similarly, to

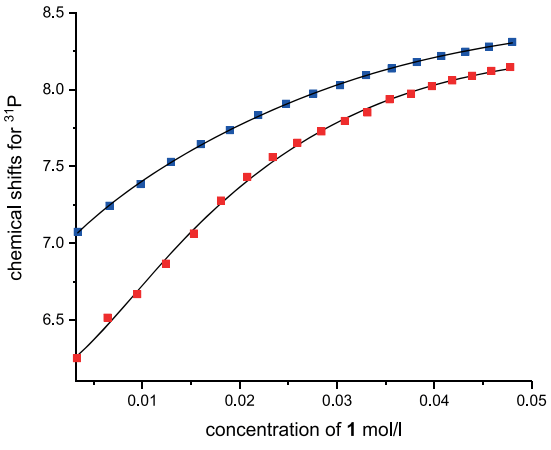

Figure 2. ^{31}P NMR shift change as a function of the concentration of **1** when $Y(NO_3)_3$ (red) and $La(NO_3)_3$ (blue) are titrated with **1**. Fittings for 1:3 (M/L) binding models are presented as black lines.

the metal-to-ligand titration, fourth binding constant K_4 was also fitted to the titration data of Y and La where it provided the best fit for one of the repeats in both cases (Tables S5 and S6). Based on the unsaturation observed in the titration data and partial success in the fitting of the 1:4 model, it is possible that higher-order complexes are formed in the solution when the concentration of the ligand is high enough. Overall, the binding constants obtained from the reverse ligand-to-metal titrations are similar to the metal-to-ligand binding constants for Y and La, although small differences can be observed (Table 1). The differences most likely arise from the different forming order of the complexes in the titrations, as in the reverse ligand-to-metal titration, the 1:1 complex forms first followed by the 1:2 and 1:3 complexes.

Proposed complexation structures based on the titrations for Y, La, and Lu complexes are illustrated in Scheme 3. As the pH was between 1.4 and 2.4 during titrations, **1** is expected to coordinate to the metals in the deprotonated $[L\mathbf{1}]^{-1}$ form (Scheme 2), which is the most likely form of **1** at the lower pH region. This protonation state also provides neutral 1:3 complexes.

Further insight into the coordination properties of ligands was obtained from the density functional theory calculations, which were carried out for the 1:3 complex of Y^{3+} and three $[L]^-$ (**L** = $CH_3N[CH_2P(O)(OH)_2]_2$) in the neutral and zwitterionic form in the solution state. The calculations predicted the zwitterionic form to be significantly more stable (76 kJ mol^{-1}) than the neutral one, which is consistent with the NMR studies. As illustrated with the space-filling model of the most stable optimized 1:3 complex, three $[L]^-$ ligands do not entirely complete the coordination sphere of Y^{3+} (Figure S25). Thus, it is likely that in the aqueous solution coordinated water molecules and/or other species present in the solution might coordinate Y^{3+} ion in 1:3 complex. The results further support that 1:4 complexes cannot be fully ruled out due to steric reasons, although 1:3 complexes are the most likely species in the aqueous solution at least for the REEs with larger ionic radii based on the NMR studies.

The 1:3 M/L stoichiometry proposed for M:**1** complexes was compared with other phosphonate−metal complexes reported in the literature. The 1:3 metal−ligand stoichiometry has also been reported for the complexes of lanthanoids and nitrilotris(methylphosphonic acid), whereas commercial extraction agent DEHPA, which contains only one phosphonate group, forms 1:6 complexes with REEs and actinoids.[34−37] Although NMR titration data with Th could not be analyzed, the literature suggests that bisphosphonates bind into Th and U either with similar 1:3 or 1:2 stoichiometry, and depending on the medium, nitrate or sulfate ions fulfill the coordination sphere.[38−42] As uranium is commonly precipitated as an ammonium salt by injecting NH_3 and CO_2 gases into a uranium-containing solution, it is therefore highly possible for uranium to also form insoluble ammonium salts at higher pH values.[43,44] Also, Th forms insoluble ammonium salts in the solution with higher pH (see below). Taken together, the obtained results indicate that a smaller amount of **1**−**6** is needed for the REE separation process compared to the commercial liquid−liquid extraction (DEHPA and EHEHPA), which form 1:6 complexes with REEs.[34−37] On the other hand, commercial precipitation agents (oxalates) are needed in smaller quantities than ligands **1**−**6** since oxalates have been reported to bind with 2:3 metal−ligand ratio.[45,46]

https://doi.org/10.1021/acsomega.1c02982
ACS Omega 2021, 6, 23977−23987

Scheme 3. Proposed Zwitterionic Structures for 1:1, 1:2, and 1:3 M/L Metal Complexes (M = Y, La, Lu) with Ligand 1

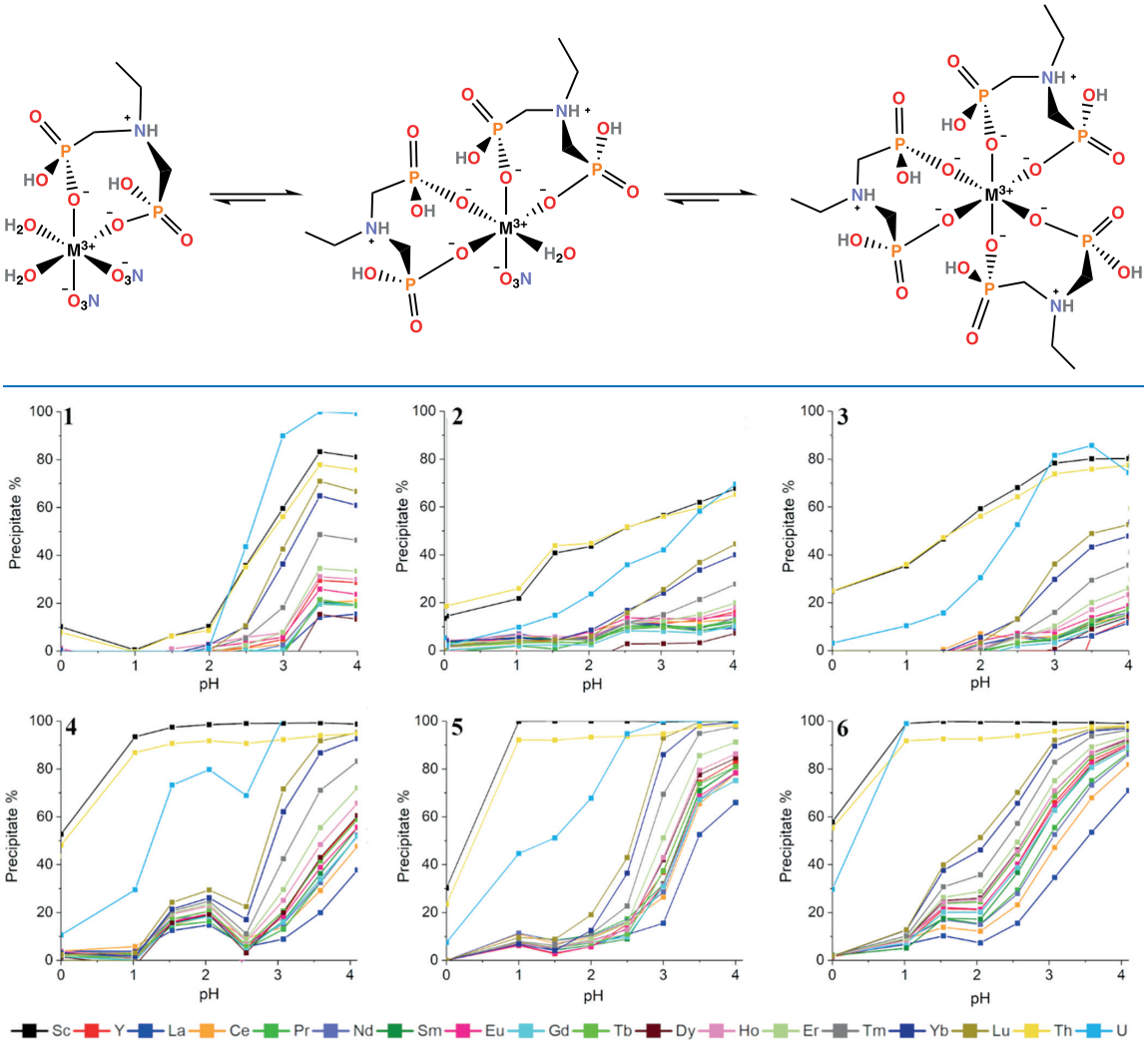

Figure 3. Precipitation percentages of REEs, Th, and U in different pH for ligands **1**–**6** (from the top left to the bottom right). For clarity, the error bars are omitted from the figure, but the standard deviation errors for precipitation percentages are given in Tables S8–S13.

Precipitation Studies. The precipitation properties of ligands **1**–**6** toward REEs, Th, and U in 5% HNO_3 solution were investigated in a pH range of 0–4. The pH was not increased above 4 to avoid precipitation of lanthanoid hydroxides.[47] pH was set with 5% NH_3 solution and the precipitation percentages were determined by taking into account the dilution of the added base, calculating the precipitated amount for each metal, and dividing the precipitated amount by the concentration at the beginning. As the expected stoichiometry for the metal–ligand ratio is 1:3, solutions were prepared with a 6-fold excess of the ligands to ensure sufficient amount of the precipitation agents. From each pH, the sample was taken aside, filtrated, and diluted with 5% HNO_3 for the inductively coupled plasma optical emission spectrometer (ICP-OES) measurements. Precipitation studies were also performed without the presence of ligands to ensure that the metal complexes do not precipitate out from the solution as ammonia salts (Table S7). No precipitation or minimal precipitation was observed for REEs and U with ammonia, whereas Th precipitated out from the solution at pH higher than 2.5.

Figure 3 shows the precipitated percentages for ligands **1**–**6** in the pH range of 0–4, and five main trends can be observed from it. First, the deprotonated form of ligand $[\mathbf{L}]^-$ increases when the pH of the solution increases, resulting in higher precipitation percentages of REEs, Th, and U. Second, ligands **4**–**6** with longer carbon chains precipitate more metals out from the solution than **1**–**3** with shorter carbon chains, with the exception of ligand **1**, which unexpectedly precipitates out more some of the metals (Er–Lu, Th, and U) than ligands **2** and **3**. Third, ligand **6** precipitates U, Th, and Sc selectively at pH 1 leaving all of the lanthanoids and Y in the solution.

https://doi.org/10.1021/acsomega.1c02982
ACS Omega 2021, 6, 23977–23987

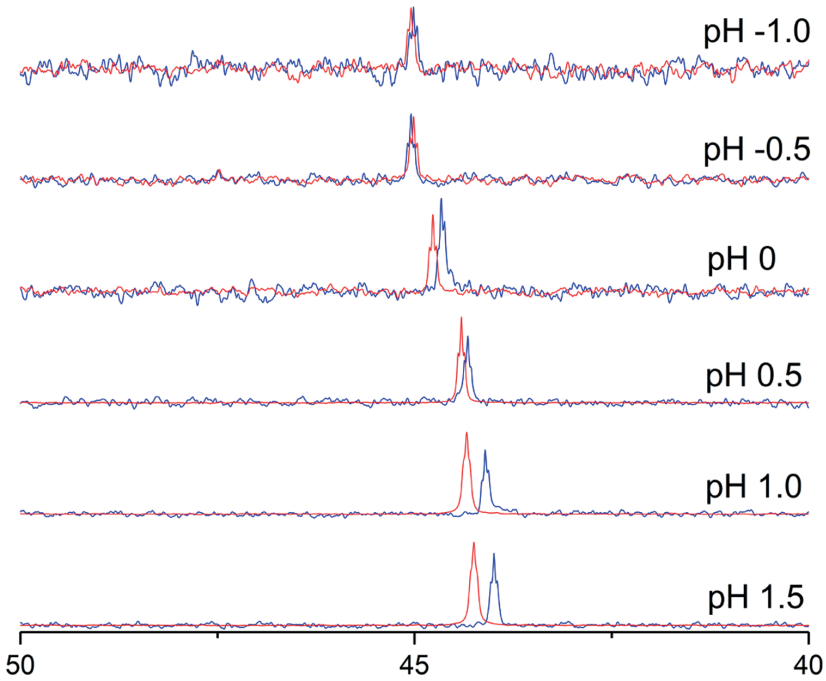

Figure 4. Three hundred megahertz ^{31}P NMR spectra of ligand **1** Y complex (blue) and free ligand **1** (red) in different pH values.

Fourth, ligands **4** and **5** are also selective precipitating agents for Sc and Th over other investigated REEs at pH 1, but a decrease in the U precipitation rate can be observed when compared to ligand **6**. Fifth, with ligand **4**, a dip in the precipitation percentages for most of the metals can be observed at pH 2.5, which is most likely resulting from the metal complexes dissolving back into the solution.

Separation Factors. The ability to separate two elements from each other is expressed by separation factor (*SF*), which is calculated by adapting calculations from a liquid−liquid extraction as presented by Nelson et al.[48] The ratio of precipitated metals and metals left in the solution on each pH is expressed as *D* (distribution factor) and can be determined according to the following eq 1, where $[M]_p$ expresses the precipitated metals and $[M]_s$ the metals in solution.

$$D = \frac{[M]_p}{[M]_s} \quad (1)$$

Separation factors between two elements can be determined with eq 2 by comparing their distribution factors.

$$SF_{1/2} = \frac{D_1}{D_2} \quad (2)$$

If metals precipitate completely from the solution or reversely, no precipitation occurs, it is not possible to determine the distribution factor and separation factor for the metal. Separation factors between adjacent lanthanoids, Sc, Th, and U were calculated for all of the ligands **1**−**6** (Tables S14−S19). Ionic radius (3+) of Y lies between the radii of Er and Tm, and therefore, Y was positioned between these two elements.

All ligands **16** have almost equal ability to separate adjacent lanthanoid pairs at each pH, meaning that no ligand was considerably better than the other. Additionally, separation factors between heavy adjacent lanthanoids from Er to Lu are calculated to be slightly better for all of the ligands **1**−**6** when compared to other adjacent lanthanoid pairs. For example, the best value for heavy lanthanoid pairs $SF_{Tm/Yb}$ and $SF_{Yb/Lu}$ arecalculated to be 4.33 ± 0.04 and 2.32 ± 0.02 with ligands **5** and **4**, respectively. These separation factors are higher than the reported separation factors for DEHPA and EHEHPA ($SF_{Tm/Yb}$= 1.12−2.12, $SF_{Yb/Lu}$ = 1.03−1.44) in the conventional liquid-liquid separation processes.[4] For lighter lanthanoids separation factors are generally under two for the adjacent lanthanoids, with the exception of ligand **4** which has separation factor of 3.81 (±0.86) for Ce/La separation, which is in the same range with the conventional liquid-liquid method ($SF_{Ce/La}$ 1.30−4.55), but shows improvement to the previously reported fractional crystallization with borates[15] ($SF_{Ce/La}$ 1.43) or oxalates[49] ($SF_{Ce/La}$ 1.5−2.5). With ligand **5**, albeit the obtained $SF_{Ce/La}$ is lower, 2.11 ± 0.21, it is still in par with other separation systems reported above. For the other adjacent lanthanoids (Nd−Er), separation factors are calculated to be rather low for all of the ligands as they range from 1 to 1.7. When compared to other precipitation agents such as oxalates, the ligands **1**−**6** perform either similarly or slightly better, for example $SF_{Nd/Sm}$ of 1.6 has been reported for oxalates,[49] whereas for ligand **5**, a slightly better value is obtained ($SF_{Nd/Sm}$ 2.0 ± 0.1). Compared to the hydrothermal borate crystallization, ligands **16** perform either similar or worse. However, a notable fact is that the borate crystallization requires high temperatures of 473 K for 3 days and additional 2 days for slow crystallization,[15] whereas the precipitation of REEs and studied actinoids takes only 15 min at 295 K in

https://doi.org/10.1021/acsomega.1c02982
ACS Omega 2021, 6, 23977−23987

acidic water solutions. As Y is positioned between Er and Tm, separation factors between these elements were also calculated. Good separation factors can be calculated for all of the ligands **16** for Tm/Y separation ranging from 2.06 to 8.88, of which the highest separation factor is obtained with ligand **1**. Smaller separation values (1.00−3.33) are obtained for Er/Y separation, the highest one (3.33 ± 1.17) is observed for ligand **3**.

Overall best separation factors are obtained when distribution factors of Sc, Th, or U are compared to the distribution factors of lanthanoids, for example, with ligand **5** $SF_{Sc/La}$ is calculated to be over 15 000 at pH 1 as Sc precipitates out from the solution almost quantitatively. In fact, with ligands **4**−**6**, *SF* cannot be calculated for Sc in most cases as it completely precipitates from the solution already at a low pH value (pH 1−2.5). Similar results are obtained for U and Th. For example, $SF_{Th/Lu}$ is calculated to be 44.41 ± 6.34, 48.32 ± 6.04, and 33.62 ± 32.13 for ligands **4**−**6**, respectively, at low pH (2−2.5). These $SF_{Th/Lu}$ are similar to $SF_{Th/Ln}$ obtained from the fractional SeO_2 crystallization in hydrothermal conditions.[19] U precipitates completely from the solution with **6** at pH 1 and no separation factor can be calculated for U/Lu separation, whereas with **4** and **5**, the best separation factors are 9.45 ± 1.26 and 23.79 ± 0.24, respectively.

In general, ligands **1**−**6** provide improved separation factors in mild conditions especially for heavy adjacent lanthanoids and Y, when compared to oxalates or liquid−liquid extracting agents, and excellent selectivity toward Sc, Th, and U is observed with ligands **4**−**6**. Even though separation factor-wise the system is no better than the fractional crystallization with borates, the advantage is the simple and fast precipitation of the metals directly from the water solution at 295 K.

Ligand and Metal Recovery. Recovery of the ligands was investigated with the 1:3 complex of Y^{3+} and ligand **1** by measuring ^{31}P NMR shifts of the complex in low pH values (1.5−(−1)) set with 65% HNO_3, and comparing spectra to the NMR spectra of free ligand. It can be observed from Figure 4 that **1** is substituted for NO_3^- around pH −0.5 because the ^{31}P NMR shift of the Y-containing sample matches the shift of the free ligand **1** at this pH.

Importantly, no decomposition of the ligand can be observed in the ^1H NMR spectrum of ligand during the recovery process. As the molarity of nitric acid in pH −0.5 can be calculated to be 3 molar, these findings not only show that the precipitated metals can be recovered from the complexes with 3 molar HNO_3, but they also indicate that the investigated ligands **1**−**6** are recyclable and could be utilized more than once in the separation process.

CONCLUSIONS

NMR and large-scale complexation and precipitation studies were performed for six different simple aminobis(phosphonates) ligands **1**−**6** with REEs, Th, and U. These studies were complemented by quantum chemical calculations and the acid−base titration in NMR scale to determine the protonation steps of the utilized ligands. The determined pK_a values of 1.3 and 5.6 for **1** suggested that **1**−**6** exist mainly as monoanionic ($[\mathbf{L}]^-$) form in the pH range used in the complexation and precipitation studies, whereas NMR titration studies in conjunction with computational data indicated that **1**−**6** preferably form either 1:1, 1:2, or 1:3 (metal−ligand) complexes in zwitterionic form with Lu, La, and Y, respectively. log*K* values for 1:1, 1:2, and 1:3 complexes, respectively, are calculated to be 2.4 ± 0.2, 4.9 ± 0.4, and 7.3 ± 0.3 for Y, 2.6 ± 0.5 and 4.4 ± 0.1 for La, and 2.1 ± 0.3 for Lu, in aqueous acidic solutions. Importantly, the precipitation studies showed that **4**−**6** are very selective precipitation agents to recover radioactive elements (Th and U) from REE concentrates in a short period of time (15 min). The performance of **1**−**6** to separate adjacent lanthanides was comparable or in some cases more efficient compared to other precipitation methods (borates and oxalates) reported so far. Additionally, the precipitation agents are recyclable in the separation process, as shown by the NMR study, and the metals could be recovered from the ligands by dissolving the formed complexes to 3 molar HNO_3 without any decomposition of the ligands **1**−**6**. Considering all the abovementioned and the fact that aminobis(phosphonates) are relatively easy to synthesize with simple addition reaction, aminobis(phosphonates) are promising precipitation agents for REEs, Th, and U. Importantly, the selectivity of aminobis(phosphonates) toward adjacent lanthanoids could be increased by modification of ligand frameworks, which underpin their potential as alternative precipitation agents.

EXPERIMENTAL SECTION

Materials and Methods. Formaldehyde (36%) was purchased from VWR; phosphorous acid (99%) and hexylamine (98%) from Fluka Chemical Co.; 2-ethylhexylamine (98%), $La(NO_3)_3{\cdot}6H_2O$, and propylamine hydrochloride from Sigma-Aldrich; ethylamine hydrochloride (98%), butylamine (99%), and $Y(NO_3)_3{\cdot}6H_2O$ (99.8%) from Merck; and $Lu(NO_3)_3{\cdot}H_2O$ from abcr and amylamine (98%) from TCI chemicals. All of the chemicals were reagent grade and used without further purification. NMR measurements and titrations were performed on a Bruker Avance III 300 MHz-spectrometer, and NMR data was processed with Bruker TopSpin 4.0.8. IR spectra were measured by Bruker Alpha FT-IR. Elemental analyses were done by an Elementar Vario EL III-analysator. Lanthanoid concentrations were determined by a Perkin Elmer Optima 8300 DV ICP-OES- spectrometer.

Syntheses. [(Ethylimino)bis(methylene)]bis(phosphonic acid) (**1**) was synthesized by dissolving phosphorous acid (19.35 g, 0.24 mol) and ethylamine (10.1 g, 0.05 mol) into a mixture of 100 mL of deionized water and 100 mL of 37% HCl. An excess of 36% formaldehyde (36 mL, 0.48 mol) was added dropwise to the solution for an hour, after which the solution was refluxed overnight at 120 °C. The solvent was removed under vacuum resulting in an oily product of which **1** was precipitated out with ethanol. The crude product was purified by recrystallization from hot ethanol to obtain it as a white solid. Yield 12.81 g, 46%. ^1H NMR (D_2O 300 MHz): δ 3.65−3.51 (m, 6H), and 1.39 (t, 3H). ^{31}P NMR (D_2O 300 MHz): δ 8.90. Elemental analysis Calcd for $C_4H_{13}NO_6P_2$: N, 6.01; C, 20.61; and H, 5.62. Found: C, 20.42; H, 5.68; and N, 5.92.

[(Propylimino)bis(methylene)]bis(phosphonic acid) (**2**) was prepared following the same procedure. The solvent was removed under vacuum resulting in a pale yellow oily product. A white precipitate was obtained after adding ethanol and heating up the solution. The crude product was purified by recrystallization from hot ethanol. Yield 7.27 g, 46%. ^1H NMR (D_2O 300 MHz δ): 3.60 (d, 4H), 3.51(m, 2H), 1.84 (m, 2H), and 1.02 (t, 3H). ^{31}P NMR (D_2O 300 MHz): δ 8.79. Elemental analysis calcd for $C_5H_{15}NO_6P_2$: C, 24.3; H, 6.12; and N, 5.67. Found: C, 24.3; H, 6.00; and N, 5.78.

https://doi.org/10.1021/acsomega.1c02982
ACS Omega 2021, 6, 23977−23987

[(Butylimino)bis(methylene)]bis(phosphonic acid) (**3**) was prepared following the same procedure. The solvent was removed under vacuum resulting in a yellow oily product. A white precipitate was obtained from adding ethanol and heating the solution. The crude product was purified by recrystallization from the water−ethanol solution. Yield 6.51 g, 41%. ^{1}H NMR (D_2O 300 MHz): δ 3.66−3.53 (m, 6H), 1.83 (m, 2H), 1.46 (m, 2H), and 1.01 (t, 3H). ^{31}P NMR (D_2O 300 MHz): δ 8.65. Elemental analysis calcd for $C_6H_{17}NO_6P_2$: C, 27.6; H, 6.56; and N, 5.36. Found: C, 27.1; H, 6.46; and N, 5.43.

[(Pentylimino)bis(methylene)]bis(phosphonic acid) (**4**) was prepared following the same procedure. The product precipitated out after cooling down. The white crude product was purified by recrystallization from water. Yield 5.83 g, 31%. ^{1}H NMR (D_2O 300 MHz): δ 3.66−3.52 (m, 6H), 1.85 (m, 2H), 1.41 (m, 4H), and 0.96 (t, 3H). ^{31}P NMR (D_2O 300 MHz): δ 8.56. Elemental analysis calcd for $C_7H_{19}NO_6P_2$: C, 30.55; H, 6.96; and N, 5.09. Found: C, 29.74; H, 6.91; and N, 5.02.

[(Hexylimino)bis(methylene)]bis(phosphonic acid) (**5**) was prepared following the same procedure. Around 1 h, after starting the refluxing, brown solid started forming into the solution. After cooling down and stirring the solution for ∼15 min, white solid precipitated heavily out, and it was isolated by suction filtration. The crude product contained still some brown impurities, which were removed by dissolving the product in hot water and filtrating while hot. The crude product was purified by recrystallization from hot water, and colorless needles were obtained. Yield 6.36 g, 36%. ^{1}H NMR (D_2O 300 MHz): δ 3.71−3.50 (m, 6H), 1.84 (m, 2H), 1.52−1.29 (m, 6H), and 0.93 (t, 3H). ^{31}P NMR (D_2O 300 MHz): δ 8.66. Elemental analysis calcd for $C_8H_{21}NO_6P_2$: C, 33.22; H, 7.32; and N, 4.84. Found: C, 32.79; H, 7.23; and N, 4.82.

[(2-Ethylhexylimino)bis(methylene)]bis(phosphonic acid) (**6**) was prepared by refluxing the reaction mixture for 3 h instead of 12 h at 120 °C. The solution was concentrated and the left stand at the room temperature overnight. The precipitated white solid was filtrated, washed with cold water, and purified by recrystallization from hot water. Yield 11.46 g, 46%. ^{1}H NMR (D_2O 300 MHz): δ 3.61 (d, 4H), 3.54 (m, 2H), 1.98 (m, 1H), 1.59−1.29 (m, 8H), and 0.95 (m, 6H). ^{31}P NMR (D_2O 300 MHz): δ 8.37. Elemental analysis calc. (%): N: 4.42, C: 37.86, and H: 7.94; meas. (%): N: 4.173, C: 37.12, and H: 7.972. Elemental analysis calcd for $C_{10}H_{25}NO_6P_2$: C, 37.86; H, 7.94; and N, 4.42. Found: C, 37.12; H, 7.97; and N, 4.17.

Deprotonation Titration. Three hundred milligrams of **1** was dissolved into 9 mL of D_2O to obtain a 0.14 M solution. Nondeuterated 5% NH_3 solution was added to the stock solution, and from each 0.5 pH, the NMR sample was taken aside. The pH was measured in the range of 0.5 to 10.5.

NMR Titrations. Titrating **1** with $Y(NO_3)_3$: 0.01 M solution of ligand **1** was prepared by dissolving ligand **1** (10.249 mg, 0.044 mmol) into 4.4 mL of D_2O. Typically, 0.6 mL of analyte was taken aside, and roughly 20 times excess of $Y(NO_3)_3{\cdot}6\ H_2O$ (303.07 mg, 0.791 mmol) was added to the titrant. The analyte was titrated by adding 0.1 equiv of the titrant (4 μL) to the analyte, and ^{31}P NMR spectra was measured after each addition. The analyte was titrated until the concentration reached 1 equiv. Titrations were performed similarly with $La(NO_3)_3$ and $Lu(NO_3)_3$ by preparing 0.01 M solution of **1** into 3 mL of D_2O, taking 0.6 mL analyte aside and adding excess $La(NO_3)_3$ (88.00 mg, 0.203 mmol) or $Lu(NO_3)_3$ (61.64 mg, 0.17 mmol) into the titrant. Analyte was titrated by adding 0.1 equiv (10 μL) to the titrant until 1 equiv was reached. pH for the Lu titration was set to 1.0 to prevent the complex from precipitating. All titrations were replicated three times.

Titrating $Y(NO_3)_3$, $La(NO_3)_3$ with **1**: Titrations were done by following the same procedure. The analyte was titrated by adding 0.3 equiv of the titrant (7 μL) to the analyte until the concentration reached 5 equiv.

All titrations were replicated three times and pH was monitored during titrations. Binding models were fitted with HypNMR2008 programme Version 4.0.71.[50]

Precipitation Experiments. Two hundred fifty milligrams of ligands **1**−**6** were dissolved into 100 mL of 5% HNO_3 prepared from ultrapure water to avoid any unwanted element contaminations. Typically, 1 g/L uranium standard solution was diluted (10/100 mL 5% HNO_3) to obtain 100 mg/L solution, and 1.7 mL of the solution was combined with 17.3 mL of the 10 mg/L REE multistandard solution (Ln, Sc, Y, Th) to obtain roughly 9 mg/L solution for the inspected metals. For each of the ligands **1**−**6**, 3 mL of the metal solution and 3 mL of the ligand solution were combined and pH was set with 5% NH_3, prepared in ultrapure water. From each pH increment of 0.5 in the pH range of 1−4, and before adding ammonia (pH 0), 0.5 mL of the sample was taken aside, filtrated with syringe, and diluted to 5 mL with 5% HNO_3 for the ICP-OES measurements. The measurements were replicated three times. Precipitation experiments were also performed for the solutions without ligands **1**−**6**, to investigate the precipitation of metals in the absence of ligands.

Ligand Recovery. Roughly 0.01 M solution of the 1:3 metal−ligand complex of Y with**1** was prepared by dissolving 16.45 mg of **1** and 9.07 mg of $Y(NO_3)_3$ into 6 mL of D_2O. The pH of the solution was set with 65% HNO_3, and samples were taken from the solution every 0.5 change in pH within the pH range of 1.5 to −1. For comparision, roughly 0.01 M solution of free ligand **1** was prepared by dissolving 4.97 mg of **1** into the 1 −2 mL of D_2O. pH was set similarly with 65% HNO_3 and samples were taken aside every 0.5 pH. ^{31}P NMR spectra of each sample were measured.

Computational Details. The lowest energy structure for the 1:3 complex of Y^{3+} and three $[L1]^-$ in the neutral and zwitterionic form was obtained from the conformational sampling, which were followed by the three different separate DFT calculations. The conformational sampling was carried out employing the Merck Molecular Force Field (MMFF)[51] with Monte-Carlo search as implemented in Spartan' 18 molecular modeling software.[52] The same software was also used in the subsequent PBE-D3/def2-SV(P)[53−59] single-point energy calculations that were carried out for all 1483 and 901 unique structures of neutral and zwitterionic forms, respectively, obtained from the conformational sampling. Out of these structures, 277 (198) lowest energy structures of the neutral (zwitterionic) form were selected to the full geometry optimizations performed at the PBE1PBE-D3/def2-SV(P)[57−61] level of theory in the gas-phase because no clear energy cut-off value could be determined from the results of the single-point energy calculations. These calculations were carried out with Gaussian 16 quantum chemistry program.[62] For both forms, the subsequent final geometry optimizations were performed for the 10 lowest energy structures obtained from the previous step at the PBE1PBE-D3/def2-TZVP[57−61]

https://doi.org/10.1021/acsomega.1c02982
ACS Omega 2021, 6, 23977−23987

level in a solution state. In the solution-state calculations, water was used as a solvent and it was modeled using the integral equation formalism variant of the polarizable continuum model as implement in the Gaussian 16.[63−66] The frequency analyses were calculated for all of the final optimized structures to ensure that they correspond to a true minimum on the potential energy hypersurface (no negative frequencies).

■ ASSOCIATED CONTENT

Supporting Information

The Supporting Information is available free of charge at https://pubs.acs.org/doi/10.1021/acsomega.1c02982.

> Characterization for the aminobis(phosphonates) **1**−**6** (^{1}H NMR and IR spectra) NMR titration curve for ligand **1**, spectra, and plotted shifts for the complexation studies; Tables for the separation factors between adjacent lanthanoids and ^{31}P NMR spectra for the ligand recovery (PDF)

■ AUTHOR INFORMATION

Corresponding Authors

Ari Väisänen − *Department of Chemistry, University of Jyväskylä, FI-40014 Jyväskylä, Finland*; Email: ari.o.vaisanen@jyu.fi

Jani O. Moilanen − *Department of Chemistry, Nanoscience Center, University of Jyväskylä, FI-40014 Jyväskylä, Finland*; orcid.org/0000-0002-2096-593X; Email: jani.o.moilanen@jyu.fi

Authors

Emilia J. Virtanen − *Department of Chemistry, Nanoscience Center, University of Jyväskylä, FI-40014 Jyväskylä, Finland*

Siiri Perämäki − *Department of Chemistry, University of Jyväskylä, FI-40014 Jyväskylä, Finland*; orcid.org/0000-0002-3983-186X

Kaisa Helttunen − *Department of Chemistry, Nanoscience Center, University of Jyväskylä, FI-40014 Jyväskylä, Finland*; orcid.org/0000-0001-7455-4207

Complete contact information is available at: https://pubs.acs.org/10.1021/acsomega.1c02982

Author Contributions

All authors have given approval to the final version of the manuscript.

Notes

The authors declare no competing financial interest.

■ ACKNOWLEDGMENTS

The authors would like to acknowledge the financial support provided by the University of Jyväskylä and the Academy of Finland (projects 315829, 320015, 309910, 314287). CSC-IT Center for Science in Finland, the Finnish Grid and Cloud Infrastructure (persistent identifier urn:nbn:fi:research-infras-2016072533), and Prof. H. M. Tuononen (University of Jyväskylä) are acknowledged for providing computational resources for the project. Laboratory engineering Elina Hautakangas is acknowledged for carrying out elemental analyses for the samples.

■ REFERENCES

(1) Balaram, V. Rare earth elements: A review of applications, occurrence, exploration, analysis, recycling, and environmental impact. *Geosci. Front.* **2019**, *10*, 1285−1303.

(2) Bobba, S.; Carrara, S.; Huisman, J.; Mathieux, F.; Pavel, C. *Critical Raw Materials for Strategic Technologies and Sectors in the EU - a Foresight Study*; European Commission, 2020.

(3) Goodenough, K. M.; Wall, F.; Merriman, D. The Rare Earth Elements: Demand, Global Resources, and Challenges for Resourcing Future Generations. *Nat. Resour. Res.* **2018**, *27*, 201−216.

(4) Gupta, C. K.; Krishnamurthy, N. *Extractive Metallurgy of Rare Earths*; CRC Press, 2005.

(5) Borra, C. R.; Pontikes, Y.; Binnemans, K.; Van Gerven, T. Leaching of rare earths from bauxite residue (red mud). *Miner. Eng.* **2015**, *76*, 20−27.

(6) Buechler, D. T.; et al. Comprehensive elemental analysis of consumer electronic devices: Rare earth, precious, and critical elements. *Waste Manage.* **2020**, *103*, 67−75.

(7) Binnemans, K.; et al. Recycling of rare earths: A critical review. *J. Cleaner Prod.* **2013**, *51*, 1−22.

(8) Zhu, Z.; Pranolo, Y.; Cheng, C. Y. Separation of uranium and thorium from rare earths for rare earth production - A review. *Miner. Eng.* **2015**, *77*, 185−196.

(9) Sun, X.; Waters, K. E. Synergistic effect between bifunctional ionic liquids and a molecular extractant for lanthanide separation. *ACS Sustainable Chem. Eng.* **2014**, *2*, 2758−2764.

(10) Guo, L.; et al. Highly Selective Extraction and Separation of Rare Earths(III) Using Bifunctional Ionic Liquid Extractant. *ACS Sustainable Chem. Eng.* **2014**, *2*, 1968−1975.

(11) Sun, P.; Huang, K.; Song, W.; Gao, Z.; Liu, H. Separation of Rare Earths from the Transition Metals Using a Novel Ionic-Liquid-Based Aqueous Two-Phase System: Toward Green and Efficient Recycling of Rare Earths from the NdFeB Magnets. *Ind. Eng. Chem. Res.* **2018**, *57*, 16934−16943.

(12) Vargas, S. J. R.; Quintão, J. C.; Ferreira, G. M. D.; Da Silva, L. H. M.; Hespanhol, M. C. Lanthanum and Cerium Separation Using an Aqueous Two-Phase System with Ionic Liquid. *J. Chem. Eng. Data* **2019**, *64*, 4239−4246.

(13) He, Y.; et al. "Super moiety"-phosphoramidate in task-specific ionic liquids for effcient thorium separation through hybrid interaction. *Sep. Purif. Technol.* **2020**, *252*, No. 117466.

(14) Prodius, D.; et al. Rationally designed rare earth separation by selective oxalate solubilization. *Chem. Commun.* **2020**, *56*, 11386−11389.

(15) Yin, X.; et al. Rare earth separations by selective borate crystallization. *Nat. Commun.* **2017**, *8*, No. 14438.

(16) Tasaki-Handa, Y.; et al. Separation of neodymium and dysprosium by forming coordination polymers. *Sep. Purif. Technol.* **2016**, *157*, 162−168.

(17) Tasaki-Handa, Y.; et al. Selective Crystallization of Phosphoester Coordination Polymer for the Separation of Neodymium and Dysprosium: A Thermodynamic Approach. *J. Phys. Chem. B* **2016**, *120*, 12730−12735.

(18) Lu, H.; et al. Size-dependent selective crystallization using an inorganic mixed-oxoanion system for lanthanide separation. *Dalton Trans.* **2019**, *48*, 12808−12811.

(19) Wang, Y.; et al. Facile and Efficient Decontamination of Thorium from Rare Earths Based on Selective Selenite Crystallization. *Inorg. Chem.* **2018**, *57*, 1880−1887.

(20) Galezowska, J.; Gumienna-Kontecka, E. Phosphonates, their complexes and bio-applications: A spectrum of surprising diversity. *Coord. Chem. Rev.* **2012**, *256*, 105−124.

(21) Amoroso, A. J.; Fallis, I. A.; Pope, S. J. A. Chelating agents for radiolanthanides: Applications to imaging and therapy. *Coord. Chem. Rev.* **2017**, *340*, 198−219.

(22) Zhao, Q.; et al. Synergistic extraction of heavy rare earths by mixture of α-aminophosphonic acid HEHAMP and HEHEHP. *J. Rare Earths* **2019**, *37*, 422−428.

(23) Kuang, S.; Zhang, Z.; Li, Y.; Wei, H.; Liao, W. Extraction and separation of heavy rare earths from chloride medium by α-aminophosphonic acid HEHAPP. *J. Rare Earths* **2018**, *36*, 304−310.
(24) Wei, H.; Li, Y.; Zhang, Z.; Liao, W. Synergistic solvent extraction of heavy rare earths from chloride media using mixture of HEHHAP and Cyanex272. *Hydrometallurgy* **2020**, *191*, No. 105240.
(25) Wei, H.; Li, Y.; Kuang, S.; Zhang, Z.; Liao, W. Separation of trivalent rare earths from chloride medium using solvent extraction with heptylaminomethyl phosphonic acid 2-ethylhexyl ester (HEH-HAP). *Hydrometallurgy* **2019**, *188*, 14−21.
(26) Kuang, S.; Zhang, Z.; Li, Y.; Wei, H.; Liao, W. Synergistic extraction and separation of rare earths from chloride medium by the mixture of HEHAPP and D2EHPA. *Hydrometallurgy* **2017**, *174*, 78−83.
(27) Lu, Y.; Zhang, Z.; Li, Y.; Liao, W. Extraction and recovery of cerium(IV) and thorium(IV) from sulphate medium by an α-aminophosphonate extractant. *J. Rare Earths* **2017**, *35*, 34−40.
(28) Moedritzer, K.; Irani, R. R. The Direct Synthesis of α-Aminomethylphosphonic Acids. Mannich-Type Reactions with Orthophosphorous Acid. *J. Org. Chem.* **1966**, *31*, 1603−1607.
(29) Gift, A. D.; Stewart, S. M.; Kwete Bokashanga, P. Experimental determination of pK a values by use of NMR chemical shifts, revisited. *J. Chem. Educ.* **2012**, *89*, 1458−1460.
(30) Lide, D. R. *CRC Handbook of Chemistry and Physics*; CRC Press, 2004.
(31) Kubíček, V.; Kotek, J.; Hermann, P.; Lukeš, I. Aminoalkylbis-(phosphonates): Their complexation properties in solution and in the solid state. *Eur. J. Inorg. Chem.* **2007**, *2007*, 333−344.
(32) Boichenko, A. P.; Markov, V. V.; Kong, H.; Matveeva, A. G.; Loginova, L. P. Re-evaluated data of dissociation constants of alendronic, pamidronic and olpadronic acids. *Open Chem.* **2009**, *7*, 8−13.
(33) David, T.; et al. Aminoalkyl-1,1-bis(phosphinic acids): Stability, Acid-Base, and Coordination Properties. *Eur. J. Inorg. Chem.* **2014**, *2014*, 4357−4368.
(34) Nash, K. L. The Chemistry of TALSPEAK: A Review of the Science. *Solvent Extr. Ion Exch.* **2015**, *33*, 1−55.
(35) Mathur, J. N. Extraction of thorium with 2-ethyl hexyl phosphonic acid mono-2- ethyl hexyl ester (PC-88A). *J. Radioanal. Nucl. Chem.* **2001**, *250*, 123−128.
(36) Bazaga-García, M.; et al. Luminescent and Proton Conducting Lanthanide Coordination Networks Based on a Zwitterionic Tripodal Triphosphonate. *Inorg. Chem.* **2016**, *55*, 7414−7424.
(37) Cunha-Silva, L.; et al. Photoluminescent lanthanide-organic 2D networks: A combined synchrotron powder X-ray diffraction and solid-state NMR study. *Chem. Mater.* **2007**, *19*, 3527−3538.
(38) Das, D.; Brahmmananda Rao, C. V. S.; Sivaraman, N.; Sivaramakrishna, A.; Vijayakrishna, K. Synthesis and extraction behavior of alkyl and cyclic aminophosphonates towards actinides. *Inorg. Chim. Acta* **2018**, *482*, 597−604.
(39) Goud, E. V.; et al. Unexpected Coordination Modes of Bisphosphoramides with Lanthanum(III) and Thorium(IV) Salts: Synthesis, Structural Characterization, Stability, and Extraction Studies. *ChemistrySelect* **2021**, *6*, 2085−2093.
(40) Reed, W. A.; et al. Complexation of UVI with 1-hydroxyethane-1,1-diphosphonic acid in acidic to basic solutions. *Inorg. Chem.* **2007**, *46*, 2870−2876.
(41) Jacopin, C.; et al. Investigation of the interaction between 1-hydroxyethane-1,1′-diphosphonic acid (HEDP) and uranium(VI). *Inorg. Chem.* **2003**, *42*, 5015−5022.
(42) Wu, Q. Y.; Wang, C. Z.; Lan, J. H.; Chai, Z. F.; Shi, W. Q. Theoretical insight into the binding affinity enhancement of serine with the uranyl ion through phosphorylation. *RSC Adv.* **2016**, *6*, 69773−69781.
(43) Sadeghi, M. H.; Outokesh, M.; Zare, M. H. Production of high quality ammonium uranyl carbonate from "uranyl nitrate + carbonate" precursor solution. *Prog. Nucl. Energy* **2020**, *122*, No. 103270.
(44) Mellah, A.; Chegrouche, S.; Barkat, M. The precipitation of ammonium uranyl carbonate (AUC): Thermodynamic and kinetic investigations. *Hydrometallurgy* **2007**, *85*, 163−171.
(45) Battsengel, A.; et al. Recovery of light and heavy rare earth elements from apatite ore using sulphuric acid leaching, solvent extraction and precipitation. *Hydrometallurgy* **2018**, *179*, 100−109.
(46) Tunsu, C.; Petranikova, M.; Ekberg, C.; Retegan, T. A hydrometallurgical process for the recovery of rare earth elements from fluorescent lamp waste fractions. *Sep. Purif. Technol.* **2016**, *161*, 172−186.
(47) Suzuki, Y.; Nagayama, T.; Sekine, M.; Mizuno, A.; Yamaguchi, K. Precipitation incidence of the lanthanoid(III) hydroxides. *J. Less-Common Met.* **1986**, *126*, 351−356.
(48) Nelson, J. J. M.; et al. High-throughput screening for discovery of benchtop separations systems for selected rare earth elements. *Commun. Chem.* **2020**, *3*, No. 7.
(49) Weaver, B. Fractional Separation of Rare Earths by Oxalate Precipitation from Homogeneous Solution. *Anal. Chem.* **1954**, *26*, 479−480.
(50) Frassineti, C.; et al. Nuclear magnetic resonance as a tool for determining protonation constants of natural polyprotic bases in solution. *Anal. Biochem.* **1995**, *231*, 374−382.
(51) Halgren, T. A. Force Fields for Conformational Interaction Energies and Geometries. *J. Comput. Chem.* **1999**, *20*, 730−748.
(52) *Spartan 18*; Wavefunction Inc.: Irvivine CA, 2019.
(53) Perdew, J. P.; Burke, K.; Ernzerhof, M. Generalized gradient approximation made simple. *Phys. Rev. Lett.* **1996**, *77*, 3865−3868.
(54) Perdew, J. P.; Wang, Y. Accurate and simple analytic representation of the electron-gas correlation energy. *Phys. Rev. B* **1992**, *45*, 13244−13249.
(55) Grimme, S.; Antony, J.; Ehrlich, S.; Krieg, H. A consistent and accurate ab initio parametrization of density functional dispersion correction (DFT-D) for the 94 elements H-Pu. *J. Chem. Phys.* **2010**, *132*, No. 241733.
(56) Grimme, S.; Ehrlich, S.; Goerigk, L. Effect of the damping function in dispersion corrected density functional theory. *J. Comput. Chem.* **2011**, *32*, 1456−1465.
(57) Andrae, D.; Häußermann, U.; Dolg, M.; Stoll, H.; Preuß, H. Energy-adjusted ab initio pseudopotentials for the second and third row transition elements. *Theor. Chim. Acta* **1990**, *77*, 123−141.
(58) Weigend, F. Hartree-fock exchange fitting basis sets for H to Rn. *J. Comput. Chem.* **2008**, *29*, 167−175.
(59) Weigend, F.; Ahlrichs, R. Balanced basis sets of split valence, triple zeta valence and quadruple zeta valence quality for H to Rn: Design and assessment of accuracy. *Phys. Chem. Chem. Phys.* **2005**, *7*, 3297−3305.
(60) Ernzerhof, M.; Scuseria, G. E. Assessment of the Perdew-Burke-Ernzerhof exchange-correlation functional. *J. Chem. Phys.* **1999**, *110*, 5029−5036.
(61) Adamo, C.; Barone, V. Toward reliable density functional methods without adjustable parameters: The PBE0 model. *J. Chem. Phys.* **1999**, *110*, 6158−6170.
(62) Frisch, M. J.; Trucks, G. W.; Schlegel, H. B.; Scuseria, G. E.; Robb, M. A.; Cheeseman, J. R.; Scalmani, G.; Barone, V.; Petersson, G. A.; Nakatsuji, H.; Li, X.; Caricato, M.; Marenich, A. V.; Bloino, J.; Janesko, B. G.; Gomperts, R.; Mennucci, B.; Hratchian, H. P.; Farkas, J. B.; Foresman, J. V.; Fox, D. J. et al. *Gaussian 16*; Gaussian, Inc.: Wallingford CT, 2016.
(63) Miertuš, S.; Scrocco, E.; Tomasi, J. Electrostatic interaction of a solute with a continuum. A direct utilizaion of AB initio molecular potentials for the prevision of solvent effects. *Chem. Phys.* **1981**, *55*, 117−129.
(64) Pascual-ahuir, J. L.; Silla, E.; Tuñon, I. GEPOL: An improved description of molecular surfaces. III. A new algorithm for the computation of a solvent-excluding surface. *J. Comput. Chem.* **1994**, *15*, 1127−1138.
(65) Miertuš, S.; Tomasi, J. Approximate evaluations of the electrostatic free energy and internal energy changes in solution processes. *Chem. Phys.* **1982**, *65*, 239−245.

https://doi.org/10.1021/acsomega.1c02982
ACS Omega 2021, 6, 23977−23987

(66) Tomasi, J.; Mennucci, B.; Cancès, E. The IEF version of the PCM solvation method: An overview of a new method addressed to study molecular solutes at the QM ab initio level. *J. Mol. Struct.: THEOCHEM* **1999**, *464*, 211−226.

https://doi.org/10.1021/acsomega.1c02982
ACS Omega 2021, 6, 23977−23987

II

RECOVERY OF RARE EARTH ELEMENTS FROM MINING WASTEWATER WITH AMINOMETHYLPHOSPHONIC ACID FUNCTIONALIZED 3D-PRINTED FILTERS

by

Virtanen, E. J., Kukkonen, E., Yliharju, J., Tuomisto, M., Frimodig, J., Kinnunen, K., Lahtinen, E., Hänninen, M. M., Väisänen, A., Haukka, M. & Moilanen, J. O. 2024

Separation and purification technology vol 353, 128599

https://doi.org/10.1016/j.seppur.2024.128599

Separation and Purification Technology 353 (2025) 128599

Contents lists available at ScienceDirect

Separation and Purification Technology

journal homepage: www.elsevier.com/locate/seppur

Recovery of rare earth elements from mining wastewater with aminomethylphosphonic acid functionalized 3D-printed filters

Emilia J. Virtanen [a,c], Esa Kukkonen [a,c], Janne Yliharju [b,c,d], Minnea Tuomisto [e], Janne Frimodig [a], Kimmo Kinnunen [b,c], Elmeri Lahtinen [a,1], Mikko M. Hänninen [a,1], Ari Väisänen [a], Matti Haukka [a], Jani O. Moilanen [a,c,*]

[a] Department of Chemistry, University of Jyväskylä, P.O. Box 35, FI-40014 Jyväskylä, Finland
[b] Department of Physics, University of Jyväskylä, P.O. Box 35, FI-40014 Jyväskylä, Finland
[c] Nanoscience Center, University of Jyväskylä, P.O. Box 35, FI-40014 Jyväskylä, Finland
[d] School of Resource Wisdom, University of Jyväskylä, P.O. Box 35, FI-40014 Jyväskylä, Finland
[e] Department of Chemistry, University of Turku, FI-20014 Turku, Finland

ARTICLE INFO

Editor: Kuo-Lun Tung

Keywords:
Rare earth elements
3D printing
Mining waste
Recovery
Separation

ABSTRACT

Herein we report the use of nylon-12-based 3D-printed filters incorporating α-aminomethylphosphonic acid as an active additive for the recovery of Y, Nd, and Dy from the mining waste solution containing Al, K, Ca, Sc, Fe, Co, Cu, Zn, Y, Nd, Dy, and U. Nylon-12 was chosen for the polymer matrix of the filter due to its inactivity towards the studied metals. The micrometer-level structure of the filters was studied with a scanning helium ion microscope and X-ray tomography to reveal the porosity, pore size, and active additive distribution in the filters. Furthermore, FTIR spectroscopy was used to analyze the compositional changes in the 3D-printed filters after the printing and adsorption processes. Adsorption of the metals was studied at a pH range of 1–4, and the following adsorption trend Sc > Fe > U > Y, Nd, Dy > Al, Cu, Zn > K, Ca, Co was observed in each of the studied pH values. The sequential recovery process for metals was studied at pH 2, and desorption of the metals from the filters was performed with 6 M HNO_3. 100 % adsorption of REEs, Fe, and U was achieved during the recovery process, and on average, over 88 % of the adsorbed Y, Nd, and Dy were desorbed from the filters. In contrast to Y, Nd, and Dy, the desorption of Sc, Fe, and U was minimal (Fe and U) or negligible (Sc) with 6 M HNO_3 due to their strong coordination to the active additive. Maximum adsorption capacities for Y, Nd, Dy, and U were determined by using linear Langmuir adsorption isotherm. The best maximum adsorption capacity was determined for Sc, Q_{max} = 0.51 mmol/g followed by U, Nd, Dy, and Y with capacities of 0.47, 0.24, 0.23, and 0.17 mmol/g, respectively. Overall, this study achieved a complete removal of Sc, Fe, and U from the simulated mining waste solution leaving a final eluate that mainly contained Y (320 μg), Nd (350 μg), Dy (330 μg), and Al (710 μg) demonstrating the applicability of the 3D-printed filters in the recovery of Y, Nd, and Dy from the multimetal solution.

1. Introduction

Mining waste, which is a by-product of extracting and processing of mineral resources, is one of the largest waste streams in the European Union with roughly 500 megatons produced in 2020 [1]. Mining waste includes topsoil material, such as sedimentary rocks which are removed to access mineral resources, as well as waste rocks and tailings which are left behind after valuable metals are extracted from minerals [2,3]. It has been estimated that the annual production of tailings alone is up to 13 gigatons globally [4]. When sulphide-rich mineral waste is exposed to air and water, it oxidizes and forms sulfuric acid causing acid mine drainages (AMD). These drainages can be concentrated with metals, not only because of the sulphide ores but also due to the acid leaching of the surrounding minerals [5]. Depending on the types of minerals and the target metals in a main extraction process, the (metal) composition of the mining waste varies greatly. For example, mine tailings from Pb, Ag, and Zn mining activity in Mazarron, Spain, consist of high amounts of Al, Mn, Fe, Cu, Zn, As, Cd, and Pb along with elevated amounts of Ge,

* Corresponding author at: Department of Chemistry, Nanoscience Center University of Jyväskylä, P.O. Box 35, Jyväskylä FI-40014, Finland.
E-mail address: jani.o.moilanen@jyu.fi (J.O. Moilanen).
[1] Present address: Weeefiner Oy, 40530 Jyväskylä, Finland.

https://doi.org/10.1016/j.seppur.2024.128599
Received 20 March 2024; Received in revised form 16 June 2024; Accepted 26 June 2024
Available online 28 June 2024

Mo, Sn, Cs, La, Ce, Bi, Th, and U [6]. Out of these metals, Al, Mn, Ge, As, La, Ce, and Bi are classified as critical raw materials, for example, in the EU and US, due to their economic importance and supply risk [7,8]. Especially rare earth elements (REEs) are needed in a variety of modern technological applications and renewable energy production [9], whereas Al, Mn, and Bi are used in a variety of alloys. Tailings from quartzite and quarzitic sandstone mines in Kielce, Poland, consist of elevated amounts of As and REEs due to the AMD leaching the metal (loid)s from the surrounding minerals [10]. Valuable sources for REEs can additionally be found in the mining waste of apatite ores, phosphogypsum, from which up to 80 % of REEs can be leached out for further recovery processes [11,12]. Lixiviates from the Iberian Pyrite Belt could account for the production of 24 t/year of REEs, 34 t/year of Co, and 7000 t/year of Mg [13], all of which are classified as critical elements, whereas from Idaho Springs mine tailings up to 985 kg of REEs could be recovered annually [14].

The recovery of elements from mining waste typically includes a combination of hydrometallurgical processes such as leaching the target metals from the mining waste [15,16], precipitating the metals out from leachate or mine wastewater [17–19], and/or ion exchange [20,21] to separate the elements from other metals and impurities. In ion exchange, a solution containing metals is passed through a resin containing functional groups that selectively coordinate to one or more of the target metals [22]. Commercial ion exchange resins typically contain sulfonic, carboxylic, (amino)phosphonic, or iminodiacetic acids as functional groups that are capable of cation exchange [23]. Silica-based materials have also been studied for the recovery of REEs [24]. Aminophosphonates have shown great promise as chelating agents in ion-exchange resins due to their generally low toxicity [25–27], ability to coordinate with metals, such as Cu, Zr, REEs, Th, and U [28], and robustness in acidic conditions [29,30]. Virolainen *et al.* have studied REE extraction from phosphogypsum with aminophosphoric acid functionalized resin and obtained recovery rates up to 75 % for REEs. However, the reported purity of the REE fraction was 20 % due to the strong coadsorption of Ca [31]. Phosphonate functionalized mesoporous silica was found to be a selective adsorbent for U at pH 3, and U-containing solutions could be enriched up to 15-fold [32]. With the commercial aminophosphonate-functionalized resin TP260, REEs were completely extracted from the acidic solution even at a low pH value of 0.5, but Al coextracted completely with REEs [33]. Hermassi *et al.* have studied three commercial resins functionalized with sulfonic, aminophosphonic, and sulfonic/phosphonic groups for treating acidic mine waters containing Mg, Al, Ca, Mn, Fe, Co, Ni, Cu, Zn, Cd, and REEs. Although aminophosphonic-functionalized resin extracted over 90 % of the REEs present in the solution at pH 2, the best separation between the REEs and transition metals was achieved with the sulfonic resin [34]. Coextraction of Al, Fe Th, and U in conjunction with REEs has also been reported to occur with other commercial aminophosphonate resins [35,36].

3D-printed adsorption and ion exchange materials have increased their utilization in the solid phase extraction of metals because they are easy to manufacture, their sizes and shapes can be customized, and their active additives can be readily changed [37–39]. Thus, they can be adapted for a variety of different recovery and removal processes. For example, 90 % of U has been extracted from acidic media by 3D-printed material which has been coated with adsorbing quaternary ammonia resins [40], or 98 % from acidic solutions by a 3D-printed biopolymer filter with a solid/liquid ratio of 2 g/l [41]. 3D-printed devices have also been utilized for the preconcentration of Fe and Cr from low concentration-solutions enhancing the detection of these metals [42,43], and for removing radioactive ^{137}Cs and ^{90}Sr species from nuclear wastewater [44]. The selective recovery of Pd, Pt, and Au from waste electrical and electronic equipment (WEEE) by using the patented SLS 3D-printed filters has also been reported [45,46]. In these filters, the printing material consisted of either a functional polymer or hybrid material where a polymeric resin was used as the active additive. Another illustrative example was the selective removal of Cu from multimetal solutions using 3D-printed filters that were manufactured from a recycled polymer [38].

In the current work, we report a process for recovering Y, Nd, and Dy from a multimetal mining waste solution with the α-aminomethylphosphonic acid functionalized 3D-printed filters. The developed recovery process shows a reasonably good selectivity towards Y, Dy, and Nd among the investigated metals, while simultaneously minimize the amount of problematic coadsorbed metals, such as Al and Ca, in the final eluate. We demonstrate that 100 % of Fe, REEs, and U are adsorbed from the simulated mining waste solution with the 3D-printed filters in a low pH regime, and 88 % of adsorbed Y, Nd, and Dy can be desorbed, alongside some amount of Al, from the filters by acid elution. We also show that the 3D-printed filters are reusable in sequential adsorption–desorption cycles if the best adsorbing and accumulating metals, namely Sc, Fe, and U, are removed from the mining waste before the filtering process. Overall, the results demonstrate that the 3D-printed filters are robust and reusable for the recovery of critical rare earth metals from the multimetal mining waste solution.

2. Experimental

2.1. Materials and methods

Formaldehyde (36 %) was purchased from VWR, phosphorous acid (99 %) from Fluka Chemical Co., and dodecylamine (98 %) from Merck. All the chemicals were reagent grade and used without any further purification. 1000 mg/l standard solutions used for ICP-OES calibration of Al, K, Ca, Sc, Fe, Co, Cu, Zn, Y, Nd, Dy, and U in 5 % HNO_3 were purchased from Perkin Elmer. NMR measurements were performed on Bruker Avance III 300 MHz-spectrometer, and the obtained NMR data was processed with Bruker TopSpin 4.0.8. FTIR spectra were measured by Bruker Alpha FT-IR. Elemental analyses were conducted by Elementar Vario EL III- CHN analyser. Powder X-ray diffraction measurements were conducted with PANalytical Aeris. Flowrate for the adsorption/desorption experiments was controlled with Aladdin AL-1000 syringe pumps. Metal concentrations were determined by PerkinElmer ICP-OES Optima 8300 spectrometer. The filters were printed with ShareBot SnowWhite SLS 3D printer. X-ray tomography was performed by using an in-house-built X-ray microtomographic scanner JTomo in the X-ray tomography laboratory of the Department of Physics.

2.2. Synthesis of additive 1

[(Dodecylimino)bis(methylene)]bisphosphonic acid **1** was synthesized in three batches by dissolving phosphorous acid (44.5 g, 0.54 mol) and dodecylamine (50 g, 0.27 mol) into 400 ml of 6 M HCl. After heating the solution to reflux (>120 °C), an excess of 36 % formaldehyde (90 ml, 1.17 mol) was added to the solution dropwise within an hour after which the solution was refluxed for two more hours. The resulting white precipitate was filtered out and washed with ethanol. Because **1** is only soluble in basic aqueous solutions, NMR was measured in the presence of NaOH. Yield: 75 g, 46 %. Melting point: 210 °C. ^{1}H NMR (D_2O 300 MHz): δ 3.09–3.04 (m, 4H), 2.93 (d, 2H), 1.69–1.56 (m, 2H), 1.43–1.23 (m, 18H), 0.89 (t, 3H). ^{31}P NMR (D_2O 300 MHz): δ 14.16. Elemental analysis Calcd. for $C_{14}H_{33}NO_6P_2$: C, 45.04; H, 8.91; N 3.75. Found: C, 44.92; H, 9.21; N, 3.76.

2.3. 3D printing

The 3D model of the filters was designed using FreeCAD v. 0.16 and further processed into 0.1 mm layers with Slic3r v. 1.2.9. The 3D-printed filters were manufactured from the mechanically mixed powder, consisting of 70 wt-% of a powderous nylon-12 (particle size ca. 50 μm) and 30 wt-% of a finely grounded additive **1** (<125 μm), using selective laser

sintering 3D printing, which is a robust method to manufacture porous 3D-printed filters [37,45,47–49]. The laser power, speed, and printing temperature were set to 40 % (of 14 W), 1600 mm/s, and 172 °C, respectively. These parameters were selected to prevent the melting of the active additive **1** (mp 210 °C) while enabling the partial melting of nylon-12 particles in the printing process. Prior to the recovering and imaging experiments, the 3D-printed filters were thoroughly washed with water to remove any unsintered powder.

2.4. X-ray tomography

A filter was scanned inside a syringe before and after the adsorption tests. The voxel size of the 3D image was set to 8.1 × 8.1 × 8.1 µm to estimate the properties of the structure of the filter and simultaneously obtain a representative volume of the sample. The current and the voltage of the X-ray tube were set to 0.2 mA and 40 kV, respectively, and no additional filtering was used in the X-ray source to minimize the average energy of the X-ray spectrum of the source. The image size was 1374 × 1314 × 444 voxels in both cases, i.e., before and after the adsorption tests. In the reconstruction of the tomographic image, pi2 software was used [50]. The noise of the reconstructed images was reduced by using bilateral filtering and the segmentation of the pores was performed utilizing the Otsu thresholding method [51]. The pore size distribution of the sample was analysed within a selected 11.1 × 10.6 × 3.6 mm^3 volume using the tmap -function of the pi2 software, which calculates the local thickness map of the image [52].

2.5. Adsorption and desorption

The metals and their concentrations in the simulated mining waste solution were adjusted with a small modification according to the reported concentrations of metals observed in the biggest mine in Finland [53] and in aqueous mining waste [10,54]. Because REEs were of particular interest in the study, and because the AMDs of coal and ore mines typically contain 0–5 mg/l (0–5 ppm) and 5–25 mg/l (5–25 ppm) of REEs, respectively [55,56], the REE content of the analyte was set to 10 mg/l (10 ppm). The investigated mining waste solution was prepared by diluting the 10 000 mg/l stock solutions of Al, K, Cs, and Zn and 1000 mg/l standard solution of Sc, Fe, Co, Cu, Y, Nd, Dy, and U with 0.5 M H_2SO_4 to obtain an analyte solution containing 100 mg/l of Al, K, Ca, and Zn as well as 10 mg/l of Sc, Fe, Co, Cu, Y, Nd, Dy, and U. pH for the adsorption tests was set to 1–4 with 25 % ammonia solution. In the initial tests 5 ml of the solution, and in the longer adsorption tests 40 ml of the solution was withdrawn into a 60 ml syringe that was attached to a syringe pump. The flow rate of the pump was set to 90 ml/h and the simulated mining waste solution was passed through three stacked filters. Samples were taken every 5 ml to monitor the adsorption process, and pH was measured from each sample to confirm the stability of adsorption conditions. The amount of adsorbed metals was determined with Perkin Elmer ICP-OES Optima 8300 by measuring the metal concentration in the solution before and after passing the solutions through the 3D-printed filters. From these values, adsorption percentages were calculated with Eq. (1)

$$\text{Adsorption-\%} = \frac{c_i - c_f}{c_i} \times 100\% \quad (1)$$

where c_i is the metal concentration (mg/l) in the solution before adsorption tests, and c_f is the concentration (mg/l) in the solution after tests.

Desorption of the metals from the used filters was studied with 1, 3, and 6 M HCl, H_2SO_4, and HNO_3 by passing 30 ml of the acids through the filters with a flow rate of 15 ml/h. Desorption percentages were calculated with Eq. (2)

$$\text{Desorption-\%} = \frac{C_d \times V}{m_a} \times 100\% \quad (2)$$

in which C_d is the concentration of desorbed metals in the solution (mg/l), V is the volume of the acid passed through the filters (l), and m_a is the adsorbed amount of metals in the filters (mg).

2.6. Adsorption isotherms

The adsorption mechanism and capacity of the filters for Sc, Fe, U, Nd, Dy, and Y were determined by fitting their adsorption isotherms to linear Langmuir and Freundlich models [57,58]. Adsorption isotherms were determined in 0.5 M H_2SO_4 at pH 2 for Sc, Y, Nd, Dy, and U, and at pH 3 for Fe. For each metal 10, 50, 100, 250, 500, and 1000 mg/l solutions were passed through one filter at a time and the concentrations of both the initial eluent and final eluate were measured with ICP-OES. The total contact time for the adsorption isotherm tests was 1.5 h. All the tests were performed in triplicate. The results were plotted to the linear Langmuir adsorption isotherm Eq. (3) [57].

$$\frac{C_e}{Q_e} = \frac{1}{Q_{max}} C_e + \frac{1}{bQ_{max}} \quad (3)$$

where C_e is the concentration of the metals in the solution at equilibrium (mg/l), Q_e is the equilibrium loading of the metals (mg/g), b is Langmuir constant (l/mg), and Q_{max} is the maximum adsorption capacity (mg/g). The results were also fitted to the linear Freundlich adsorption isotherm Eq. (4) [58]

$$\log Q_e = \log K_f + \frac{1}{n} \log C_e \quad (4)$$

where K_f is the Freundlich isotherm constant (L/g) and n is constant indicating adsorption intensity. The capacity was calculated with respected to the amount of active material **1** in the filter.

2.7. Adsorption-desorption cycles

The reusability of the 3D printed filters was studied at pH 2 by performing five sequentially adsorption–desorption cycles for the three stacked filters. In the adsorption step, 40 ml of the mining waste solution was injected through the filters with a flowrate of 90 ml/h. The following desorption step was performed by injecting 30 ml of 6 M HNO_3 into the filters with a flowrate of 15 ml/h. Between the adsorption and desorption steps, the filters were washed with 10 ml of ultrapure water to remove metal and acid residuals on the surface of a syringe and tubing that could cause errors to the results and change the value of pH, respectively. The adsorbed and desorbed amount of metals in each cycle were determined as described above.

3. Results and discussion

3.1. Preparation, characterization, and structure of the 3D-printed filters

[(Dodecylimino)bis(methylene)]bisphosphonic acid **1** was synthesized by following the previously reported method by Moedritzer and Irani, where dodecylamine is reacted with phosphorous acid and formaldehyde in a one-pot acid-catalyzed reaction (Scheme 1) [29,59]. The resulting white solid, which started precipitating out from the

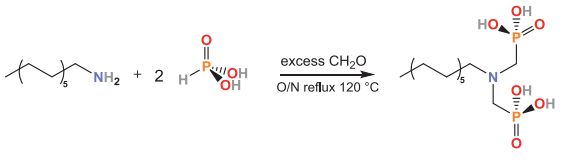

Scheme 1. Synthesis route for the [(dodecylimino)bis(methylene)] bisphosphonic acid **1** that was used as the active additive in the investigated 3D-printed filters.

solution when the heating was turned off, was filtered and washed with ethanol to remove HCl residuals. The purity of the compound was confirmed with ^{1}H and ^{31}P NMR (Figs. S1 and S2), elemental analysis (see above), and FTIR (see below). The active additive **1** was insoluble in both neutral and acidic aqueous solutions, in which the adsorption and desorption processes take place, but **1** dissolved into basic aqueous solutions (pH > 8).

The printing material for SLS printing was prepared by mixing 30 wt-% of the active additive **1** with the commercial nylon-12 powder. Nylon-12 was selected for the polymer matrix because it adsorbed only negligible amounts of the studied metals from the mining waste solution without the active additive (Table S1). A similar finding has previously been reported for nylon-12 although it adsorbed strongly and selectively Au [45]. The round 5 mm thick filters with a diameter of 16.6 mm (Fig. S3) were prepared using ShareBot SnowWhite SLS 3D printer. Each filter was cleaned thoroughly with deionized water to remove any unsintered powder before the experiments. Although the filters were 3D-printed the same way each time, variation in the distribution of the active additive inside filters may exist.

The micrometer-level structure and the distribution of the active additive inside the prewashed 3D-printed filter were analyzed by Helium Ion Microscopy (HIM) and X-ray tomography. The HIM images show that the porosity is homogeneous throughout the 3D-printed filter which is particularly visible from the HIM picture taken from the pure nylon-12 (Fig. 1). The porosity ensures that 3D-printed filters manufactured by the selective laser sintering contain voids and flow channels along which solutions can flow-through as previously reported [45,47,60]. Fig. 1 also shows that the aminomethylphosphonate additive **1** formed an adsorption layer on the surface of nylon-12 particles causing them to look more like plate-like particles than round-shaped ones as observed for the pure nylon-12. Importantly, prewash with the deionized water before imaging did not leach the active additive out from the filters. The negligible solubility of **1** in mineral acids and water at room temperature can contribute to its minimal dissolution during the adsorption and desorption steps, but it is more likely that the partially melting nylon-12 particles attached **1** to their surfaces during the 3D-printing process as depicted in Fig. 1. These are important findings because it is crucial that the active additive of the 3D-printed filters will remain intact during the recovery process and forms the adsorption layer which metal can coordinate to.

With X-ray tomography, the average porosity of the whole filter was determined to be 59 ± 2 % before the adsorption process and 60 ± 2 % after the adsorption indicating that there was no significant loss of material during the metal recovery process although leaching of some solids could sometimes be detected during the first millilitres of the adsorption tests. The average pore size was determined to be 95 ± 5 μm with a standard deviation of 50 μm and no significant difference was found in the pore size before and after using the filter. Similar pore sizes have previously been reported for 3D-printed filters utilized for recovering precious metals from electronic waste [37]. Fig. 2 shows that there were no significant changes in the structures of the unused and used filters. The ring-like structure was only marginally smaller in the used one, but otherwise no significant changes were detected. It should also be noted that the filter possibly moved a little during the adsorption process, and thus the image was not taken from the exactly same spot. Overall, HIM and X-ray tomography studies indicated that the filter has good porosity for the adsorption and desorption tests and the additive **1** is not leached from the filters in acidic aqueous solutions.

The 3D-printed filter was further characterized by a powder X-ray diffractometer (PXRD) and a FTIR-spectrometer, and its measured diffractogram and spectrum were compared to ones of the pure nylon-12 and the active additive **1**. The PXRD diffractogram of the pure nylon-12 filter was similar to the previously reported one [61], whereas the diffractogram of the 3D-printed filter containing both nylon-12 and **1** showed characteristic peaks of nylon-12 and **1** although some characteristic peaks of **1** were masked by the peaks of nylon-12 (Fig. S4). In the IR spectra of nylon-12 and the filter, the N—H stretch of the amide group was observed at 3291 cm^{-1} (Fig. 3). The less intense band at 3090 cm^{-1} in the IR spectrum of nylon-12 is the overtone of the C—N—H bend which was observed at 1540 cm^{-1}. This band was only barely visible in the spectrum of the filter, and no band was observed for **1**. The latter should not show the C—N—H bend because it is a tertiary amine [62,63], but depending on the pH, **1** can exist as a zwitterion [29]. The characteristic C═O stretch of nylon-12 at 1635 cm^{-1} was slightly shifted to 1633 cm^{-1} in the IR spectrum of the filter. Also, the asymmetric (2916 cm^{-1}) and symmetric (2848 cm^{-1}) stretching bands of CH_2 groups of nylon-12 shifted to 2919 cm^{-1} and 2850 cm^{-1} for the additive **1** and filter, respectively. The slight shifts of the CH_2 bands are expected because the additive and, therefore, the filter contain CH_3 groups which typically are observed at slightly higher wavenumbers than CH_2 groups [62,63]. The rocking of CH_2 group occurred at 719 cm^{-1} for nylon-12 and at 713 cm^{-1} for the additive **1** and filter [62,63]. Vibrations associated with P—OH stretch were observed at 2309 cm^{-1} for the additive **1** and at 2324 cm^{-1} for the filter. The additive **1** showed strong bands at 1154 cm^{-1} and 936 cm^{-1} which could be attributed to the asymmetric and symmetric stretch of the PO_3 group, respectively [64]. For the filter, these bands were shifted to 1157 cm^{-1} and 938 cm^{-1}. The bending of C—PO_3 groups was observed as a strong band at 585 cm^{-1} for the additive **1** and filter [65]. Overall, these findings supported the results obtained from the HIM and X-ray tomography studies and indicated that

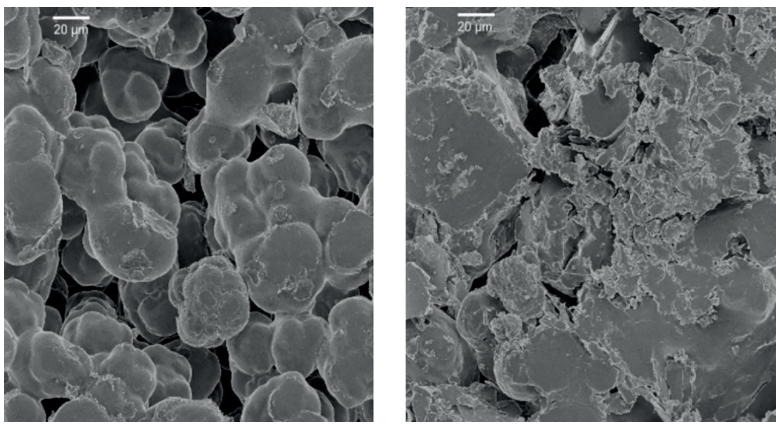

Fig. 1. HIM picture of the pure nylon-12 filter (left) and the filter with the additive **1** (right).

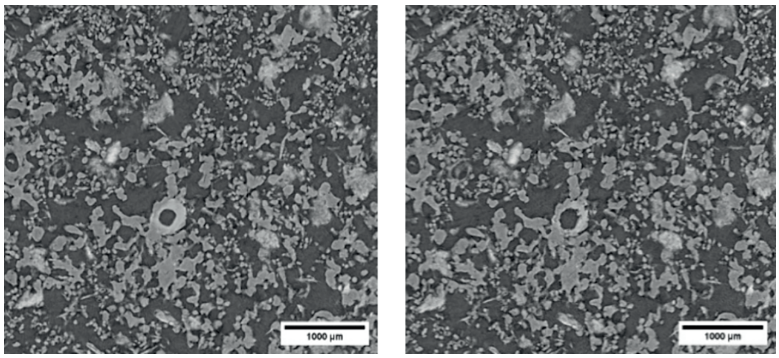

Fig. 2. X-ray tomography of the filter with the active additive **1** before metal adsorption test (left) and the same filter after the test (right).

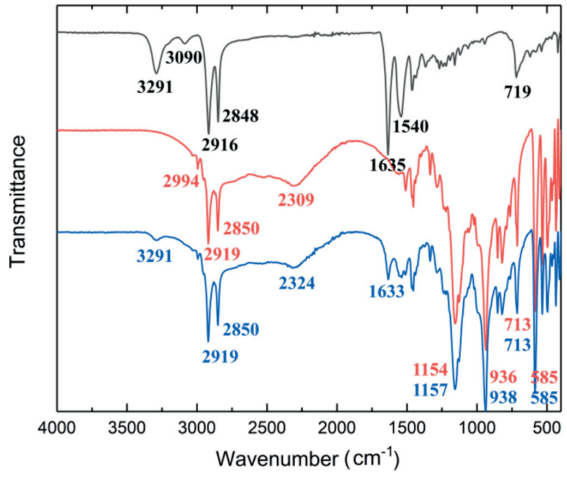

Fig. 3. FTIR spectra of nylon-12 (black), aminobisphosphonate additive **1** (red), and the 3D-printed filter (blue). (For interpretation of the references to colour in this figure legend, the reader is referred to the web version of this article.)

the active additive **1** inside in the 3D-printed filters did not decompose in the manufacturing process. In contrast to mineral acids and water, 2 M NaOH can leach a small amount of **1** out from the filters. Thus, the stability of **1** was further confirmed by recording the ^{1}H (Fig. S5) and ^{31}P (Fig. S6) NMR spectra of the leached active additive **1**. No signs of decomposition were observed in the recorded NMR spectra.

3.2. Metal adsorption

The adsorption tests were performed for the simulated mining waste solution containing 100 mg/l of Al, K, Ca, and Zn and 10 mg/l of Sc, Fe, Co, Cu, Y, Nd, Dy, and U in 0.5 M H_2SO_4. The solid-phase extraction system utilized in the study contained three stacked 3D-printed filters inside a 10 ml syringe and a syringe pump that was equipped with a 60 ml syringe (Fig. S7). The initial adsorption tests of the filters were performed by withdrawing 5 ml of the synthetic solution into the syringe and then injecting it through the three stacked filters with a flow rate of 90 ml/h. A pH range of 1 to 4 with an increment of 1 was studied to find out the effect of pH on adsorption. In this pH range, the protonation degree of the hydroxy groups (—OP(**OH**^{x})$_2$, x = 1 or 2) of phosphoric acid **1** varies from 0 % to 100 % which was determined by using the Henderson-Hasselbalch equation [66] and the previously reported pKa values of 1.33 and 5.55 for the first and second protonation, respectively, of the similar aminobisphosphonic acid (Table 1) [29]. The leaching of **1** was monitored by measuring the phosphorus concentration of the samples during the adsorption studies. It was found to be minimal (<1 %) indicating no loss of the active additive **1** in the process.

The adsorption of each metal increased with increasing pH value (Fig. 4). Of all adsorbed metals, Sc adsorbed most strongly. Roughly 80 % of Sc was already adsorbed at pH 1, whereas the adsorption percentages for Fe and U were ~ 35 %, and for Y, Nd, and Dy they were less than 10 % at the same pH value (Fig. 4). No adsorption of Al, K, Ca, Co, Cu, or Zn was detected at pH 1. A similar but stronger trend was observed at pH 2, where 96 % of Sc, ~75 % of U and Fe, and >20 % of Y, Nd, and Dy were adsorbed by the filters, but no significant adsorption of other metals was observed. However, when the pH value was increased from 3 to 4, the adsorption percentages increased from 22 % to 50 % for Al, from 14 % to 46 % for Cu, from 9 % to 35 % for Zn, and from 1 % to 5 % for Co. No significant adsorption of K and Ca was detected at pH 3 or pH 4. The adsorptions of Sc, Fe, Y, Nd, Dy, and U were strong at pH 3 and practically quantitative at pH 4. The efficient and selective adsorption of Sc and U by bisphosphonic acid-based adsorption materials in the presence of other metals has been reported before [32,67], but the above results demonstrated that the 3D-printed filters can also effectively adsorb other REEs (Y, Nd, and Dy) like commercial aminophosphonic acid resin, Purolite S950, that adsorbs La, Sm, and Ho well [35]. However, the coadsorption of Al with REEs (Sc, Y, Nd, and Dy) in percentages was much smaller for the investigated 3D-printed filters than for Purolite S950, which adsorbed Al equally or stronger if compared to the adsorption of Ho and La, respectively. It should be mentioned that the result obtained for Fe at pH 4 should be interpreted with caution because roughly 30 % of Fe precipitated out from the solution as a brown solid (most likely as FeOOH) [68] when the value of pH was increased to 4. This solid was filtered from the solution before the adsorption tests were continued. Moreover, while the adsorption percentages for Al and Zn were not high in the studied pH range, their adsorbed amounts in micrograms were high due to their high initial concentrations in the mining waste solution. For example, the adsorption for Al at pH 3 was 56.7 ± 12.5 µg, whereas for Sc and Dy they were 32.3 ± 9.1 µg and 26.8 ± 5.8 µg, respectively.

To investigate the saturation limit of the three stacked 3D-printed filters, 40 ml of the synthetic solution was passed through them, and samples were taken every 5 ml. As already explained above the filters

Table 1
Degree of protonation for the P-OH groups of **1** at pH values of 1–4.

pH	1	2	3	4
OH^1	68 %	18 %	2 %	0 %
OH^2	100 %	100 %	100 %	97 %

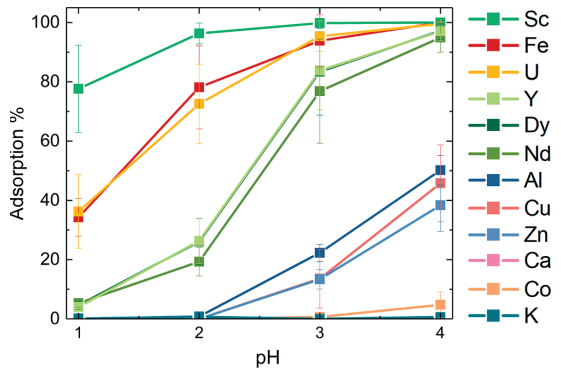

Fig. 4. Avarage adsorption percentages and their standard errors for the eluted metals in a function of pH (1–4) when 5 ml of synthetic solution is passed through the filters.

adsorbed Sc, Fe, and U better than the rest of the investigated metals. However, the adsorption of these three metals quickly decreased after the first 5 ml of the mining waste solution was passed through the three filters in the pH regime of 1–3 and passing more than 40 ml of the solution through the filters decreased the adsorption percentages below 20 % for each metal (Fig. 5). In contrast to this, at pH 4, the saturation was not achieved even after 40 ml of the solution was passed through the three filters and the adsorption percentages remained over 60 % for Sc and Fe, over 40 % for U, and over 20 % for Y, Nd, and Dy. The adsorption percentages of the less adsorbed metals, namely Al, Cu, and Zn followed by K, Ca, and Co, also increased in pH 4 if compared to the lower pH values, but their adsorption percentages were ~10 % or less when more than 20 ml of the mining waste solution was passed through the filters.

Overall, the results of adsorption studies indicated that in a low pH value of ~1, Sc, U, and Fe could be selectively recovered from the investigated mining wastewater, although their total adsorption percentages remained rather low and passing more than 40 ml of the solution through the three filters in the pH regime of 1–3 was not reasonable. However, if the aim is to recover Y, Nd, and Dy from the mining waste solution, higher than pH 1 should be used in the adsorption process.

3.3. *Adsorption isotherms and adsorption capacities for Sc, Fe, Y, Nd, Dy, and U*

The adsorption isotherms were fitted to linear Langmuir (Eq. (3)) and Freundlich (Eq. (4)) models to get more insight into the capacities of the filters and the adsorption mechanism of the studied metals. The Langmuir adsorption isotherm describes the equilibrium between an adsorbate and a monolayer adsorbent surface with equal binding sites and energies [57], whereas the Freundlich adsorption isotherm describes multilayer adsorption to a heterogenous surface which binding sites and energies can differ from one to other [58,69]. The adsorption isotherms were determined for Sc, Fe, Y, Nd, Dy, and U from samples whose concentrations ranged from 10 to 1000 mg/l either at pH 4 (Sc, Y, Nd, Dy, and U) or at pH 3 (Fe), due to the excessive precipitation of Fe at pH 4. This means that the results obtained for Fe are not directly comparable to the results of other metals. The maximum adsorption capacities (Q_{max}) determined from the Langmuir adsorption isotherms were calculated with respect to the amount of the active additive **1** in the filter. All tests were performed with three replicates and the results were displayed as a mean with a standard deviation of the replicates. For all other metals, except for Fe, the adsorption isotherms were fitted to the Langmuir model with decent correlations of $R^2 = 0.97–0.99$, while the correlation of Fe was only $R^2 = 0.89$ (Table 2 and Fig. S8). However, the adsorption isotherms of Fe were well fitted to the Freundlich model with the correlation of $R^2 = 0.99$ (Table 2 and Fig. S9). The Freundlich model also showed an equally good correlation for Sc than for Fe, while for Y, Nd, Dy, and U statistically meaningful results were not obtained according to the F-tests. All determined parameters along with their errors from the adsorption isotherm fits are presented in Table 2.

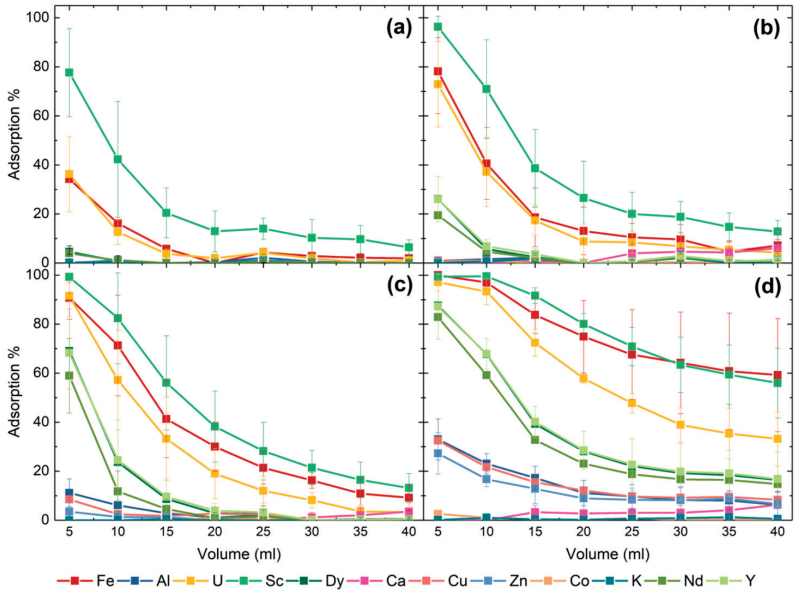

Fig. 5. Average adsorption percentages and their standard errors at pH values of 1–4 for every 5 ml of the synthetic solution passed through the filters at pH 1 (a) pH 2 (b), pH 3 (c), and pH 4 (d). The adsorption tests were performed in triplicate.

Table 2
Calculated maximum adsorption capacities Q_{max}, Langmuir constants b, Freundlich constants K_f and n, and correlation coefficients for the linear fittings for Sc, Fe, U, Dy, Nd, and Y.

Element	Langmuir					Freundlich	
	Q_{max}mg/g	Q_{max}mmol/g	bL/mg	R^2	K_f $mg^{1-n}L^n/mg$	n	R^2
Sc	22.86 ± 3.61	0.51 ± 0.08	0,018 ± 0,002	0.970 ± 0.006	4.10 ± 1.01	4.15 ± 0.71	0.994 ± 0.005
Fe*	–	–	–	0.887 ± 0.041	1.57 ± 0.41	1.98 ± 0.18	0.997 ± 0.003
U	111.65 ± 3.77	0.47 ± 0.02	0.036 ± 0.004	0.985 ± 0.001	–	–	0.776 ± 0.028
Dy	37.84 ± 6.45	0.23 ± 0.04	0.030 ± 0.018	0.975 ± 0.018	–	–	0.743 ± 0.033
Nd	34.60 ± 2.11	0.24 ± 0.01	0.024 ± 0.005	0.979 ± 0.003	–	–	0.798 ± 0.023
Y	14.74 ± 2.84	0.17 ± 0.03	0.030 ± 0.008	0.996 ± 0.004	–	–	0.794 ± 0.019

* Determined at pH 3.

The highest adsorption capacity was determined for U (111.65 mg/g), followed by Dy (37.84 mg/g), Nd (34.60 mg/g), Sc (22.86 mg/g), and Y (14.74 mg/g). No adsorption capacity was determined for Fe because the Langmuir model did not fit well the adsorption isotherms of Fe. Because elements with higher molar masses have naturally higher capacities in mg per g than lighter ones, the adsorption capacities were also converted to mmol per g. When the values in mmol per g were examined, it was found that Sc had the highest adsorption capacity of 0.51 mmol/g among all investigated metals, whereas the values for U, Nd, Dy, and Y were 0.47, 0.24, 0.23, and 0.17 mmol/g, respectively. The data indicates that the 3D-printed filters can adsorb U almost as effectively as Sc in mmol per g. Although the determined maximum adsorption capacities for the investigated 3D-printed filters are decent, they are smaller than the highest ones reported for other similar adsorbents and ion-exchange resins. For example, almost three times larger maximum adsorption capacity of U (1.31 mmol/g) has been reported for synthesized aminophosphonate resins [70]. The capacity for Sc is higher than what has been reported for mesoporous silica (1 mg/g) [71], but lower than the capacity of commercial aminophosphonate functionalized resin that is 35.5 mg/g (dry resin) at pH 1.5 [72]. The adsorption capacity of Nd was 70.1 mg/g for aminophosphonate functionalized metal–organic framework [73], and the adsorption capacities of 104.1, 118.0 and 63.9 mg/g were reported for Nd, Dy, and Y, respectively, when phosphorylated phenolic resins where used as adsorbents [74]. Theoretical adsorption maximums for the 3D-printed filters containing 30-wt% of the active additive **1** were calculated by assuming that metals bind to **1** with 1:1 ratio. The calculated values were 120.4 mg/g for Sc, 238.0 mg/g for Y, 386,0 mg/g for Nd, 435,3 mg/g for Dy and 637.4 mg/g for U which were considerable higher amounts than what were obtained from the experimental data. The differences between the 3D-printed filters and previously reported adsorbents and ion-exchange resins most likely originate from the fact that there is only 30-wt% of the active additive **1** in the 3D-printed filters and/or likely only some of the active additives on the surfaces of nylon-12 particles are available for binding as suggested by the theoretical maximum capacities.

3.4. Adsorption mechanism and selectivity of 3D-printed filters

Given that the 3D-printed filters contain aminophosphonic acid **1** as an active additive, they should function like a chelating ion exchange resin in which adsorption kinetics are dictated by the formation of a coordination bond between the functional groups of an active additive and metal ions [35,75–77]. To get more insight into the adsorption mechanism and selectivity of the 3D-printed filters, we utilized the above-described Langmuir (Eq. (3)) and Freundlich (Eq. (4)) models as well as FTIR spectroscopy.

The good fits of adsorption isotherms of Y, Nd, Dy, and U to the Langmuir model indicated that they likely bind only to one adsorbent site of the active additive **1**. The result is in par with the assumption that the active additive **1** forms (mono)layer on the surfaces of nylon-12 particles to which metals can coordinate. The data also showed that the 3D-printed filters adsorbed U stronger than Y, Dy, and Nd because the determined Langmuir constants b for U, Y, Dy, and Nd were in descending order: 0.036, 0.030, 0.030, and 0.024 L/mg, respectively. Because the larger Langmuir constant b is associated with the stronger interaction between the adsorbate and the adsorbent [78], the above data also explained the stronger selectivity of the 3D-printed filters towards U over Y, Nd, and Dy. Contrast to Y, Nd, Dy, and U, the adsorption isotherms of Sc and Fe fitted better to the Freundlich than to the Langmuir model implying that the adsorption mechanism of Sc, and in particular of Fe, might differ from Y, Nd, Dy, and U. It should be noted that the fit of the adsorption isotherm of Sc to the Langmuir model was reasonably good, so the nature of the adsorption mechanism of Sc cannot be unambiguously determined from two different fits. Because the metal–ligand coordination is controlled by several factors, such as the geometry and energy of the bonding orbitals [77], it is difficult to say a specific reason for the different adsorption mechanisms. Because the Freundlich model indicates the multilayer adsorption mechanism, the active additive **1** could bind more than one Sc or Fe ion per adsorbent site, due to their smaller ionic radii compared to Y, Nd, Dy, and U [79], and/or the coordination mode of **1** with Sc and Fe could differ from Y, Nd, Dy, and U. Although aminophosphonic acids usually bind the trivalent metal ions via the phosphonate oxygen atoms, their coordination modes with different metals can differ [80,81]. Unfortunately, no direct evidence was obtained for either case from FTIR spectroscopy studies (see below). Importantly, the fitted Freundlich constant K_f, the distribution coefficient which indicates similarly to b the interaction between the adsorbate and the adsorbent [82], was larger for Sc than for Fe. The result was in line with the adsorption studies and proved that the 3D-printed filters adsorbed stronger and more selectively Sc than Fe.

Because the adsorption isotherms were only determined for the best adsorbing metals, the stronger selectivity of the 3D-printed filters towards Fe, REEs, and U over other investigated metals will only be discussed at a qualitative level. The adsorption percentages and capacities of the studied metals mainly followed the strength of their effective Lewis acidities whether they are determined from Gutmann–Beckett-type [83], fluorescent [84,85], or ESR [86] measurements. The Lewis acidity of the two strongest adsorbed metals, Sc and U, is strong which is further augmented by their strong oxophilicity [87]. Unfortunately, references 83–86 report no data for Fe, which was adsorbed as strongly as U by the 3D-printed filters. However, a previous study has shown that the simple aminobisphosphonates coordinate stronger to Fe than Nd in aqueous media [81], although Fe is not calculated to be as oxophilic as lanthanoids [65]. For the remaining well-adsorbed metals—Al, Cu, Zn, Y, Nd, and Dy—the reported effective Lewis acidities are similar in strength [83–86], but REEs are more oxophilic than Al, Cu, and Zn, which most likely facilitates their adsorption to the investigated filters over Al, Cu, and Zn [87], if the phosphonic acid groups of **1** play the largest role in the adsorption mechanism. To find out this, FTIR spectroscopic studies were carried out for the unused and used filters.

The FTIR spectra of the 3D-printed filters were measured after passing the mining waste solution and the solutions containing either Sc, Nd, or U through the filters at pH 4 until the capacity of the filters was reached (~100 ml). Unfortunately, only small shifts (less than 1 cm^{-1})

were observed in the vibration bands when the measured spectra of the used and unused filters were compared together (Figs. S10–S13). Although the shifts associated with the vibration bands of phosphonate groups upon coordination can be very small for aminophosphonate and aminophosphonic acids [80], the role of the phosphonate groups in the adsorption mechanism cannot be determined based on such small shifts. Zhao *et al.* have reported the FTIR spectra of aminophosphonate extractant where the shifts of vibration bands were only detected when the extractant was fully loaded with Yb^{3+} [88]. Given that the maximum adsorption capacity of the 3D-printed filters is reached before the full deprotonation of phosphonic acid groups and the amount of the active additive is only 30-wt% in the filters (see above), it is possible that more intense vibration bands of the nylon-12 matrix and/or unoccupied phosphonic acid groups mask the characteristic shifts arising from the coordination of metal ions to the phosphonic acid groups. A slightly more indicative proof of the metal coordination to the phosphonic acid groups of **1** was observed in the intensity of P-OH stretches observed at ~ 2324 cm^{-1}; it slightly decreased upon metal coordination (Fig. S14). Indeed, a similar decrease in the intensity or complete removal of P-OH stretches has been reported for aminophosphonates and aminophosphonic acids upon coordination to a metal ion [80].

Although the direct shifts of the functional groups and changes in the intensities of vibration bands were rather uninformative, three facts supported the role of the phosphonate groups in the adsorption mechanism. First, the adsorption tests performed for the 3D-printed filters consisting only of pure nylon-12 showed very limited adsorption, almost negligible within the margin of errors, towards any of the investigated metals (Table S1). Second, the adsorption of all investigated metals increased in tandem with the increasing pH as the deprotonation degree of the phosphonic acid group increased (Table 1). The ion exchange mechanism is pH-dependent [89,90]. Third, XPS measurements performed for the aminophosphonate-based sorbents showed that phosphonate groups in conjunction with amine groups play an important role in the sorption process of REEs [91]. Taking into account all the above mentioned, it is highly likely that the adsorption process is dictated by the phosphonic acid groups of the active additive **1** in the investigated 3D-printed filters and that the functional groups of nylon-12 play only a minor role.

3.5. Mineral acid elutions

Three different mineral acids, namely HNO_3, H_2SO_4, and HCl, with three different molarities 1, 3, and 6 M were investigated as eluents in desorption studies. 30 ml of the eluent was used in each desorption experiment and the experiments were performed for the filters utilized in adsorption tests at pH 3 and 4, where the adsorptions of metals were stronger compared to pH 1 and 2. With 1 M acids generally less than 50 % of the adsorbed metals were eluted out from the filters and the desorption of Y, Nd, and Dy was only 30–40 % (Fig. S15). Minimal amounts (~6 %) of Fe and U were eluted out from the filters with 1 M acids. Increasing the molarity from 1 M to 3 M resulted in higher elution percentages. For example, 50–75 % of Y, Nd, and Dy were eluted with all 3 M acids, and the percentages for Fe and U increased to 11 % and 7 %, respectively, with 3 M HCl, whereas with 3 M H_2SO_4 increase were 18 % and 8 %, respectively. In contrast to 3 M HCl and H_2SO_4, the elution percentages of 3 M HNO_3 for Fe and U remained rather low (<5 %). With 6 M mineral acids over 90 % of Y, Nd, and Dy were desorbed from the filter, while the desorption of Fe and U remained low. For Fe and U, the best-performing 6 M acid was H_2SO_4 which was able to recover 20 % of Fe and 50 % of U from the filter indicating that these metals can also be eluted to some extent. All the used acids also eluted a significant amount of Zn and Ca from the filters in terms of milligrams and percentages. Therefore, the adsorption of these two metals should be minimized if the aim is obtain a high-purity REE fraction. The elution percentages of Al and Co also improved when the molarity of the acid was increased. However, the total amount of eluted Co in milligrams was low because it was poorly adsorbed by the filters (see above). The eluted amount of Cu increased with increasing molarity of HNO_3 but with HCl, it remained similar (73–78 %) despite the increase in molarity. H_2SO_4 was also able to remove Cu effectively from the filters. In contrast to all other metals, Sc remained in the filter regardless of the used eluent most likely because of its strong Lewis acidity and oxophilicity. Only 6 M HCl was able to desorb a small amount of Sc (~2 %), but with all other acids, the elution percentage for Sc was less than 1 %. Overall, Y, Nd, and Dy were desorbed from the filters well, but no clear selectivity towards metals or any group of metals was observed in the elution studies. In principle, only Fe and U could be eluted to their own fraction with H_2SO_4 if other metals are first washed out with HNO_3 or HCl.

3.6. The recovery process for REEs

The adsorption and desorption studies described above demonstrated that the 3D-printed filters selectively adsorbed Sc, Fe, Y, Nd, Dy, and U below pH 2, but no selectivity was observed in the desorption studies, except for Fe and U. The three tested mineral acids particularly eluted Al, Ca, and Zn, which were adsorbed by the filters over pH 2. Thus, to minimize the contamination of the final REE-rich eluate with other metals, the sequential recovery process for Y, Nd, and Dy was developed at pH 2. The flow chart of the developed recovery process is depicted in Fig. 6, and the amounts of adsorbed and desorbed metals in each step of the process are also given in Tables S2 and S3. In the recovery process, 40 ml of the synthetic mining waste solution in 0.5 M H_2SO_4 was passed through five sets of the three stacked 3D-printed filters and samples for ICP-OES measurements were taken from each fraction. The adsorbed metals were eluted with 6 M HNO_3 to minimize the amount of Fe and U in the final eluate that mainly consisted of Al, Y, Nd, and Dy.

During the first two steps of the process, Sc and Fe were completely removed from the mining waste solution. Already at the first step, 350 ± 10 μg (95 %) of Sc and 290 ± 50 μg (76 %) of Fe were adsorbed from the solution, and the second step recovered the rest of Fe and traces of Sc. For U, however, three steps were necessary for its complete removal from the solution. During the first two steps, 250 ± 30 μg (69 %) and 100 ± 40 μg (86 %) of U were adsorbed, and the rest of it (~20 μg, 100 %) was finally adsorbed in the third step. The first three steps also adsorbed 318 ± 6 μg of Y (84 %), 372 ± 6 μg of Nd (93 %), and 352 ± 1 μg Dy (92 %). However, for complete removal of Nd and Dy, four steps were required, whereas for Y all five steps were needed. Most of K, Ca, Co, Cu, and Zn passed through the filters during the five adsorption steps because less than 20 % of K, Ca, and Co, 25 % of Zn, and 30 % of Cu were adsorbed into the filters. Interestingly, K starts to adsorb only in the last (i.e. fifth) step of the process, after stronger adsorbed metals are removed from the mining waste solution. In contrast to K, Ca, Co, Cu, and Zn, the adsorption of Al was significant, and particularly increased after Sc was removed from the mining waste solution. In total, 1460 ± 197 μg (48 %) of Al was adsorbed in the process. The high adsorbed amount of Al could be problematic in the elution steps because it can contaminate the final REE-rich eluate. Fortunately, the strong adsorption of Al is compensated by its weaker desorption if compared to Y, Nd, and Dy in the desorption steps (see below).

When the first-step filters were eluted with 6 M HNO_3, 110 ± 26 μg of Nd (84 %), 94 ± 20 μg of Dy (77 %) and 80 ± 16 μg (77 %) of Y were desorbed from the filters along with 90 ± 15 μg (52 %) of Al. Eluting the second-step filters yielded to similar results because 90 % of adsorbed Y, Nd, and Dy as well as 54 % of adsorbed Al were eluted from the filters. The coadsorption and desorption of Al alongside REEs has been reported to be an issue in the separation processes when aminophosphonic acids have been utilized [33–35]. However, it is worth mentioning that the two sequenced adsorption and desorption steps result in the elute in which equal amounts of Nd, Dy, Y, and Al are present. This is a significant result because the concentration of Al in the unprocessed simulated mining waste solution is ten times higher than the concentrations

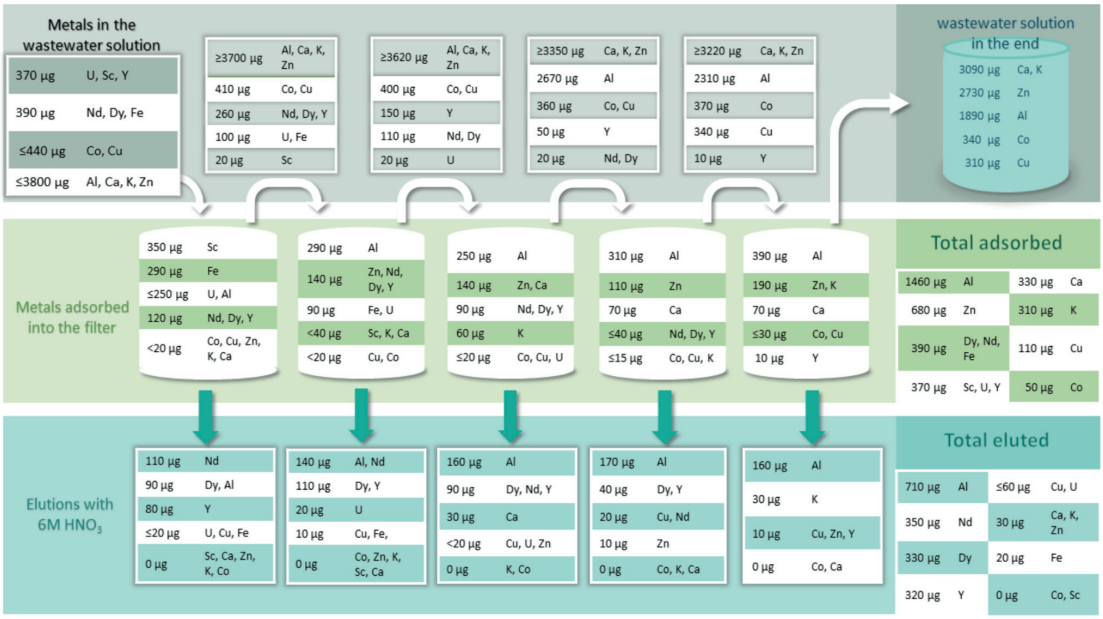

Fig. 6. Sequential five-step adsorption and desorption process developed for recovering Sc, Fe, and U as well as concentrating Y, Nd, and Dy into their own less complex fractions at pH 2. The top, middle, and bottom figures show the concentrations of metals in the solution, in the 3D-filters, and in eluate, respectively, after each step of the process along with the total amounts.

of Y, Nd, and Dy. Only a small amount (<20 µg) of each Cu, Fe, and U was washed out from the filters with 6 M HNO_3 in the first and second elution steps, as expected.

Over 95 % of the adsorbed Y, Nd, and Dy was desorbed during the elution of the third-step filters, but unfortunately, the amount of desorbed Al also increased and exceeded the amount of Y, Nd, and Dy. Eluting the fourth and fifth sets of filters yielded elutes that mostly contained 170 ± 20 µg and 160 ± 10 µg of Al, respectively. Only minor amounts of other metals than Al, Y, Nd, and Dy were desorbed during the third, fourth, and fifth elution steps. Fig. 7 summarizes the amount of adsorbed and desorbed metals in the sequential five-step recovery process. It is evident from Fig. 7 that complete adsorption of Sc, Fe, U, Nd, Dy, and Y was achieved and that Y, Nd, and Dy were desorbed from the filters alongside Al with 6 M HNO_3. This yielded the final eluate which consisted of 91 % of three REEs (Y, Nd, and Dy; 53 %) and Al (38 %) as well as 9 % of other metals (Fig. S17).

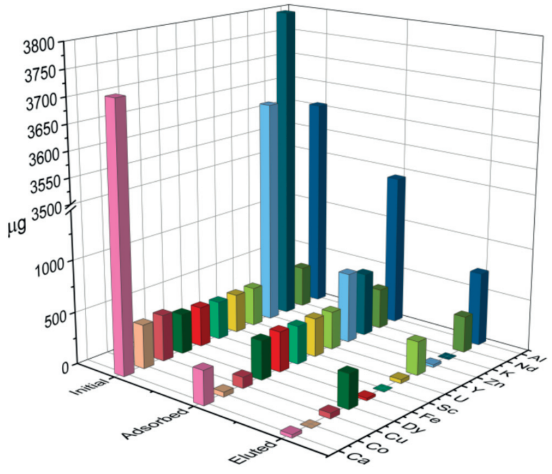

Fig. 7. The total amount of metals adsorbed and eluted during the sequential five-step recovery process. Close-up view of initial, adsorbed, and eluted amounts of metals with the lower initial concentrations are given in Fig. S16 and total percentages in Fig. S17.

Based on the results above, to obtain the pure REE fraction from the mining waste solution, three sequential sets of three stacked 3D-printed filters would be enough because these adsorb as much as 84–100 % of REEs from the mining waste solution. Only two sequential adsorption steps could also be considered if Al desorption must be minimized in the subsequent elution steps. Even though Fe and U were adsorbed strongly in the first steps of the process, they did not extensively contaminate the final REE-rich fraction because only a minimal amount of these two metals was desorbed from the filters with 6 M HNO_3. However, Fe and U can, to some extent, be desorbed from the filters with 6 M H_2SO_4 after elution with 6 M HNO_3, unlike Sc which was not desorbed in significant amounts from the filters with any of the investigated acids. When the total amounts of the most desorbed metals—Al, Y, Nd, and Dy—in the final eluates are compared to their initial concentrations, the results showed that 17 % of Al, 82 % of Y, 85 % of Nd, and 89 % of Dy were recovered with the investigated sequential five-step recovery process. Moreover, no coadsorption of Ca, which has been an issue in the previously reported study, was observed [31].

Because of the accumulation of Sc, Fe, and U into the filters, it was necessary to study the reusability of the filters. Thus, five sequential adsorption–desorption cycles were performed for the three stacked filters by injecting 40 ml of the mining waste solution with pH 2 through them with a flowrate of 90 ml/h followed by the elution step with 30 ml of 6 M HNO_3 similar to the five-step recovery process. It was evident from the results that the adsorption of Y, Nd, and Dy already decreased after the first cycle and was non-existent in the fifth cycle due to the accumulation of Sc, Fe, and U into the filters (Fig. S18). Thus, the presence of Sc, Fe, and U in the mining waste solution compromised the

Table 3
Selected adsorbents used for the recovery of the REEs from acidic mining waste solutions.

Adsorbent	REE adsorption %	REE desorption %	Ref
Aminobisphosphonate	100 %	>82 % (−Sc)	This work
TP260(aminophosphonic)	80–100 %	>95 %	[33]
S950(aminophosphonic)	100 %	<80 %	[34]
Aminophosphonate functionalized silica	<80 % (Eu)	90 %	[93]
Lewatit MDS200H(Sulfonic acid)	85 %	89 %	[94]
Lewatit MDS200H(Sulfonic acid)	78 %	75–100 %	[95]
Amide functionalized silica	>75 %	>75 %	[96]

reusability of the filters. However, these three metals can be removed from a multimetal solution by a simple precipitation step leaving most of Y, Nd or Dy in the solution as demonstrated in the previous studies [29,92]. When the reusability test was performed for the mining waste solution containing no Sc, Fe, and U, a small increase in the adsorption of Y, Nd, and Dy was observed in the first cycle, but it levelled out at the same level as in the five-step recovery process over the next four cycles (Fig. S19). The better adsorption rate of Y, Nd, and Dy in the first cycle most likely originated from the absence of Sc, Fe, and U in the solution. Although the accumulation of Al was also detected in the data (Fig. S19), it did not affect the adsorption and desorption of Y, Nd, and Dy during the five sequential cycles. The result confirmed that the filters are reusable if the most accumulating metals are removed from the multimetal mining waste solution.

Comparing the recovery rate of the developed five-step recovery process to other adsorption methods developed for the recovery of the REEs from acidic mine waste waters, it can be concluded that the obtained recovery rates of the 3D-printed filters are similar to the selected adsorbents functionalized with aminophosphonic acid and/or sulfonic acid and/or amide groups (Table 3).

Overall, the results obtained in this study not only highlighted the efficient recovery of the REEs from the mining waste solution but also confirmed that the amount of Al can be significantly decreased in the final REE-rich eluate of the mining waste solution, while the coadsorption and desorption of Ca can be eliminated. These novel results are important because the coadsorption and desorption of Al and Ca alongside with REEs have been reported to be an issue in previous studies [33–35].

4. Conclusions

Recovery of Y, Nd, and Dy from the simulated mining waste solution containing multiple metals was studied with the aminophosphonic acid **1** functionalized 3D-printed filters. The structure of the filters was studied in detail with HIM and X-ray tomography imaging which revealed that the filters have uniform structure, even distribution of the additive **1**, and a good porosity for the recovery process. The FTIR, powder X-ray, and NMR studies performed for the pure nylon-12, the active additive **1,** and the 3D-printed filters showed that the active additive stays intact in the printing process as well as during the recovery process. The adsorption of the investigated metals from the simulated mining waste solution was studied at pH 1–4 in which additive **1** exists in two different protonation states. The highest recovery rates were obtained at pH 4. However, the separation between REEs and the other elements present in the mining waste solution was best at pH 2. Desorbing the metals from the filters was studied with 1, 3, and 6 M HNO_3, HCl, and H_2SO_4. In general, the 6 M acids were the best eluents as they desorbed $\geq$ 90 % of the adsorbed Y, Nd, and Dy. The sequential five-step recovery process for Y, Nd, and Dy worked the best at pH 2 and yielded the final eluate that mainly contained Al, Y, Nd, and Dy. Importantly, the recovery process significantly decreased the amount of Al in the final eluate compared to its initial concentration in the mining waste solution and fully eliminated the coadsorption and desorption of Ca with Y, Nd, and Dy. The reusability tests showed that the accumulation of the best adsorbing metals, Sc, Fe, and U, into the filters compromised their reusability in the recovery of Y, Nd, and Dy, but by removing these three accumulating metals from the solution before the recovery process, the reusability of the filters can be maintained. The capacity of the filters towards Sc, Y, Nd, Dy, and U was determined by fitting their adsorption isotherms to the Langmuir model. The best capacity was determined for Sc (Q_{max} = 0.51 mmol/g) followed by U, Nd, Dy, and Y with capacities of 0.47, 0.24, 0.23, and 0.17 mmol/g, respectively. Interestingly, the fitting of the adsorption isotherms to the Langmuir and Freundlich models indicated that the adsorption mechanism of Fe (and also Sc) might be different from the one of Y, Nd, Dy, and U. Considering all the abovementioned, the 3D-printed filters with aminophosphonic acid **1** as an active additive showed promise for the recovery and separation of Y, Nd, and Dy from the multimetal mining waste solution. The next logical step is to improve the capacity and selectivity of the developed 3D-printed filters towards REEs as well as to develop better elution methods for Sc, Fe, and U.

Author contributions

All authors have given approval to the final version of the manuscript.

CRediT authorship contribution statement

Emilia J. Virtanen: Writing – review & editing, Writing – original draft, Visualization, Validation, Investigation, Formal analysis, Conceptualization. **Esa Kukkonen:** Writing – review & editing, Resources, Investigation. **Janne Yliharju:** Formal analysis, Investigation, Resources, Visualization, Writing – original draft, Writing – review & editing. **Minnea Tuomisto:** Formal analysis, Investigation. **Janne Frimodig:** Resources. **Kimmo Kinnunen:** Visualization, Resources, Investigation. **Elmeri Lahtinen:** Writing – review & editing, Conceptualization. **Mikko M. Hänninen:** Writing – review & editing, Conceptualization. **Ari Väisänen:** Writing – review & editing, Supervision, Funding acquisition, Conceptualization. **Matti Haukka:** Writing – review & editing, Supervision, Resources, Conceptualization. **Jani O. Moilanen:** Writing – review & editing, Writing – original draft, Visualization, Supervision, Resources, Project administration, Funding acquisition, Data curation, Conceptualization.

Declaration of competing interest

The authors declare that they have no known competing financial interests or personal relationships that could have appeared to influence the work reported in this paper.

Data availability

Data will be made available on request.

Acknowledgment

We thank the University of Jyväskylä, the Research Council of Finland (projects 315829 and 338733), the Technology Industries of Finland Centennial Foundation and Jane and Aatos Erkko Foundation for their financial support. We would like to acknowledge laboratory engineer Elina Hautakangas for carrying out elemental analyses for the samples and research assistant Tia Christiansen for performing part of the ICP-OES measurements and laboratory work, and Anssi Peuronen (University of Turku) for the useful discussions related to the subject.

Appendix A. Supplementary material

Supplementary data to this article can be found online at https://doi.org/10.1016/j.seppur.2024.128599.

References

[1] Waste statistics, n.d., https://ec.europa.eu/eurostat/statistics-explained/index.php?title=Waste_statistics#Total_waste_generation (accessed October 26, 2023).
[2] É. Lèbre, G.D. Corder, A. Golev, Sustainable practices in the management of mining waste: a focus on the mineral resource, Miner. Eng. 107 (2017) 34–42, https://doi.org/10.1016/j.mineng.2016.12.004.
[3] Z. Bian, X. Miao, S. Lei, S. Chen, W. Wang, S. Struthers, The challenges of reusing mining and mineral-processing wastes, Science 337 (2012) 702–703, https://doi.org/10.1126/science.1224757.
[4] D.M. Franks, M. Stringer, L.A. Torres-Cruz, E. Baker, R. Valenta, K. Thygesen, A. Matthews, J. Howchin, S. Barrie, Tailings facility disclosures reveal stability risks, Sci. Rep. 11 (2021) 5353, https://doi.org/10.1038/s41598-021-84897-0.
[5] Y. Jiao, C. Zhang, P. Su, Y. Tang, Z. Huang, T. Ma, A review of acid mine drainage: Formation mechanism, treatment technology, typical engineering cases and resource utilization, Process Saf. Environ. Prot. 170 (2023) 1240–1260, https://doi.org/10.1016/j.psep.2022.12.083.
[6] M. Azizi, A. Faz, R. Zornoza, S. Martínez-Martínez, V. Shahrokh, J.A. Acosta, Environmental pollution and depth distribution of metal(loid)s and rare earth elements in mine tailing, J. Environ. Chem. Eng. 10 (2022) 107526, https://doi.org/10.1016/j.jece.2022.107526.
[7] European Commission, Study on the Critical Raw Materials for the EU 2023 – Final Report, n.d.
[8] U.S. Geological Survey, Department of Interior, 2022 Final List of Critical Minerals, n.d.
[9] V. Balaram, Rare earth elements: a review of applications, occurrence, exploration, analysis, recycling, and environmental impact, Geosci. Front. 10 (2019) 1285–1303, https://doi.org/10.1016/j.gsf.2018.12.005.
[10] Z.M. Migaszewski, A. Gałuszka, S. Dołęgowska, Extreme enrichment of arsenic and rare earth elements in acid mine drainage: Case study of Wiśniówka mining area (south-central Poland), Environ. Pollut. 244 (2019) 898–906, https://doi.org/10.1016/j.envpol.2018.10.106.
[11] C.R. Cánovas, S. Chapron, G. Arrachart, S. Pellet-Rostaing, Leaching of rare earth elements (REEs) and impurities from phosphogypsum: a preliminary insight for further recovery of critical raw materials, J. Clean. Prod. 219 (2019) 225–235, https://doi.org/10.1016/j.jclepro.2019.02.104.
[12] M. Salo, O. Knauf, J. Mäkinen, X. Yang, P. Koukkari, Integrated acid leaching and biological sulfate reduction of phosphogypsum for REE recovery, Miner. Eng. 155 (2020) 106408, https://doi.org/10.1016/j.mineng.2020.106408.
[13] J.C. Fortes, A.M. Sarmiento, A.T. Luis, M. Santisteban, J.M. Davila, F. Córdoba, J. A. Grande, Wasted critical raw materials: a polluted environmental scenario as potential source of economic interest elements in the Spanish part of the Iberian pyrite belt, Water Air Soil Pollut. 232 (2021) 88, https://doi.org/10.1007/s11270-021-05018-1.
[14] A.J. Goodman, A.J. Bednar, J.F. Ranville, Rare earth element recovery in hard-rock acid mine drainage and mine waste: a case study in Idaho Springs, Colorado, Appl. Geochem. 150 (2023) 105584, https://doi.org/10.1016/j.apgeochem.2023.105584.
[15] T. Chen, C. Lei, B. Yan, X. Xiao, Metal recovery from the copper sulfide tailing with leaching and fractional precipitation technology, Hydrometall. 147–148 (2014) 178–182, https://doi.org/10.1016/j.hydromet.2014.05.018.
[16] B. Zhang, C. Liu, C. Li, M. Jiang, A novel approach for recovery of rare earths and niobium from Bayan Obo tailings, Miner. Eng. 65 (2014) 17–23, https://doi.org/10.1016/j.mineng.2014.04.011.
[17] K. Menzel, L. Barros, A. García, R. Ruby-Figueroa, H. Estay, Metal sulfide precipitation coupled with membrane filtration process for recovering copper from acid mine drainage, Sep. Purif. Technol. 270 (2021) 118721, https://doi.org/10.1016/j.seppur.2021.118721.
[18] B.V. Hassas, M. Rezaee, S.V. Pisupati, Effect of various ligands on the selective precipitation of critical and rare earth elements from acid mine drainage, Chemosphere 280 (2021) 130684, https://doi.org/10.1016/j.chemosphere.2021.130684.
[19] Q. Li, W. Zhang, Process development for recovering critical elements from acid mine drainage, Resour. Conserv. Recycl. 180 (2022) 106214, https://doi.org/10.1016/j.resconrec.2022.106214.
[20] A.B. Botelho Junior, D.B. Dreisinger, D.C.R. Espinosa, A review of nickel, copper, and cobalt recovery by chelating ion exchange resins from mining processes and mining tailings, Min. Metall. Explor. 36 (2019) 199–213, https://doi.org/10.1007/s42461-018-0016-8.
[21] M. Hermassi, M. Granados, C. Valderrama, C. Ayora, J.L. Cortina, Recovery of rare earth elements from acidic mine waters: an unknown secondary resource, Sci. Total Environ. 810 (2022) 152258, https://doi.org/10.1016/j.scitotenv.2021.152258.
[22] R.A. Silva, K. Hawboldt, Y. Zhang, Application of resins with functional groups in the separation of metal ions/species – a review, Miner. Process. Extr. Metall. Rev. 39 (2018) 395–413, https://doi.org/10.1080/08827508.2018.1459619.
[23] F. de Dardel, T.V. Arden, Ion Exchangers, in: Ullmanns Encycl. Ind. Chem., John Wiley & Sons, Ltd, 2008, doi: 10.1002/14356007.a14_393.pub2.
[24] W.C. Wilfong, T. Ji, Y. Duan, F. Shi, Q. Wang, M.L. Gray, Critical review of functionalized silica sorbent strategies for selective extraction of rare earth elements from acid mine drainage, J. Hazard. Mater. 424 (2022) 127625, https://doi.org/10.1016/j.jhazmat.2021.127625.
[25] R. Damiche, S. Chafaa, Synthesis of new bioactive aminophosphonates and study of their antioxidant, anti-inflammatory and antibacterial activities as well the assessment of their toxicological activity, J. Mol. Struct. 1130 (2017) 1009–1017, https://doi.org/10.1016/j.molstruc.2016.10.054.
[26] A. Mucha, P. Kafarski, Ł. Berlicki, Remarkable potential of the α-aminophosphonate/phosphinate structural motif in medicinal chemistry, J. Med. Chem. 54 (2011) 5955–5980, https://doi.org/10.1021/jm200587f.
[27] L. Liu, C. Liu, L. Nie, T. Jiang, J. Hong, X. Zhang, L. Luo, X. Wang, Study on the synergistic antibacterial effect of silver-carried layered zirconium alkyl-N, N-dimethylenephosphonate, Inorganica Chim. Acta 435 (2015) 66–72, https://doi.org/10.1016/j.ica.2015.06.002.
[28] S. Kuang, W. Liao, Progress in the extraction and separation of rare earths and related metals with novel extractants: a review, Sci. China Technol. Sci. 61 (2018) 1319–1328, https://doi.org/10.1007/s11431-018-9295-0.
[29] E.J. Virtanen, S. Perämäki, K. Helttunen, A. Väisänen, J.O. Moilanen, Alkyl-substituted aminobis(phosphonates)—efficient precipitating agents for rare earth elements, thorium, and uranium in aqueous solutions, ACS Omega 6 (2021) 23977–23987, https://doi.org/10.1021/acsomega.1c02982.
[30] M.H. Kudzin, J. Drabowicz, F. Jordan, Z.H. Kudzin, P. Urbaniak, Reactivity of aminophosphonic acids. 2. Stability in solutions of acids and bases, Phosphorus Sulfur Silicon Relat. Elem. 194 (2019) 326–328, https://doi.org/10.1080/10426507.2018.1540002.
[31] S. Virolainen, E. Repo, T. Sainio, Recovering rare earth elements from phosphogypsum using a resin-in-leach process: selection of resin, leaching agent, and eluent, Hydrometall. 189 (2019) 105125, https://doi.org/10.1016/j.hydromet.2019.105125.
[32] R. Thapa, A. Rahmani, P. Turhanen, A. Taskinen, T. Nissinen, R. Neitola, J. Vepsäläinen, V.-P. Lehto, J. Riikonen, Recovery of uranium with bisphosphonate modified mesoporous silicon, Sep. Purif. Technol. 272 (2021) 118913, https://doi.org/10.1016/j.seppur.2021.118913.
[33] M. Hermassi, M. Granados, C. Valderrama, C. Ayora, J.L. Cortina, Recovery of Rare Earth Elements from acidic mine waters by integration of a selective chelating ion-exchanger and a solvent impregnated resin, J. Environ. Chem. Eng. 9 (2021) 105906, https://doi.org/10.1016/j.jece.2021.105906.
[34] M. Hermassi, M. Granados, C. Valderrama, N. Skoglund, C. Ayora, J.L. Cortina, Impact of functional group types in ion exchange resins on rare earth element recovery from treated acid mine waters, J. Clean. Prod. 379 (2022) 134742, https://doi.org/10.1016/j.jclepro.2022.134742.
[35] M.J. Page, K. Soldenhoff, M.D. Ogden, Comparative study of the application of chelating resins for rare earth recovery, Hydrometall. 169 (2017) 275–281, https://doi.org/10.1016/j.hydromet.2017.02.006.
[36] K.L. Ang, D. Li, A.N. Nikoloski, The effectiveness of ion exchange resins in separating uranium and thorium from rare earth elements in acidic aqueous sulfate media. Part 2. Chelating resins, Miner. Eng. 123 (2018) 8–15, https://doi.org/10.1016/j.mineng.2018.04.017.
[37] E. Lahtinen, M.M. Hänninen, K. Kinnunen, H.M. Tuononen, A. Väisänen, K. Rissanen, M. Haukka, Porous 3D printed scavenger filters for selective recovery of precious metals from electronic waste, Adv. Sustain. Syst. 2 (2018) 1800048, https://doi.org/10.1002/adsu.201800048.
[38] K. Ibebunjo, Y. El Ouardi, J. Kwame Bediako, A. Iurchenkova, E. Repo, Functionalization of recycled polymer and 3D printing into porous structures for selective recovery of copper from copper tailings, Chem. Eng. Sci. 286 (2024) 119664, https://doi.org/10.1016/j.ces.2023.119664.
[39] N.P.F. Gonçalves, E.F. da Silva, L.A.C. Tarelho, J.A. Labrincha, R.M. Novais, Simultaneous removal of multiple metal(loid)s and neutralization of acid mine drainage using 3D-printed bauxite-containing geopolymers, J. Hazard. Mater. 462 (2024) 132718, https://doi.org/10.1016/j.jhazmat.2023.132718.
[40] M. Rodas Ceballos, F. González Serra, J.M. Estela, V. Cerdà, L. Ferrer, 3D printed resin-coated device for uranium (VI) extraction, Talanta 196 (2019) 510–514, https://doi.org/10.1016/j.talanta.2018.12.055.
[41] S. Fuxiang, W. Na, Z. Qiangqiang, W. Jie, L. Bin, 3D printing calcium alginate adsorbents for highly efficient recovery of U(VI) in acidic conditions, J. Hazard. Mater. 440 (2022) 129774, https://doi.org/10.1016/j.jhazmat.2022.129774.
[42] C. Calderilla, F. Maya, V. Cerdà, L.O. Leal, 3D printed device including disk-based solid-phase extraction for the automated speciation of iron using the multisyringe flow injection analysis technique, Talanta 175 (2017) 463–469, https://doi.org/10.1016/j.talanta.2017.07.028.
[43] C. Calderilla, F. Maya, V. Cerdà, L.O. Leal, 3D printed device for the automated preconcentration and determination of chromium (VI), Talanta 184 (2018) 15–22, https://doi.org/10.1016/j.talanta.2018.02.065.
[44] O. Halevi, T.-Y. Chen, P. See Lee, S. Magdassi, J.A. Hriljac, Nuclear wastewater decontamination by 3D-Printed hierarchical zeolite monoliths, RSC Adv. 10 (2020) 5766–5776, https://doi.org/10.1039/C9RA09967K.
[45] E. Lahtinen, L. Kivijärvi, R. Tatikonda, A. Väisänen, K. Rissanen, M. Haukka, Selective recovery of gold from electronic waste using 3D-printed scavenger, ACS Omega 2 (2017) 7299–7304, https://doi.org/10.1021/acsomega.7b01215.
[46] M. Haukka, K. Rissanen, A. Väisänen, E. Lahtinen, L. Kivijärvi, A porous body, method for manufacturing it and its use for collecting substance from source material, PCT Pat application No 050533, 2018.
[47] J. Frimodig, M. Haukka, Removal of estrogens from aqueous solutions using 3D-printed polymers, Environ. Sci. Adv. 2 (2023) 1739–1745, https://doi.org/10.1039/D3VA00159H.
[48] S. Dupin, O. Lame, C. Barrès, J.-Y. Charmeau, Microstructural origin of physical and mechanical properties of polyamide 12 processed by laser sintering, Eur.

Polym. J. 48 (2012) 1611–1621, https://doi.org/10.1016/j.eurpolymj.2012.06.007.
[49] T. Stichel, T. Frick, T. Laumer, F. Tenner, T. Hausotte, M. Merklein, M. Schmidt, A Round Robin study for selective laser sintering of polymers: back tracing of the pore morphology to the process parameters, J. Mater. Process. Technol. 252 (2018) 537–545, https://doi.org/10.1016/j.jmatprotec.2017.10.013.
[50] Available at https://github.com/arttumiettinen/pi2, n.d.
[51] N. Otsu, A threshold selection method from gray-level histograms, IEEE Trans. Syst. Man Cybern. 9 (1979) 62–66, https://doi.org/10.1109/TSMC.1979.4310076.
[52] T. Hildebrand, P. Rüegsegger, A new method for the model-independent assessment of thickness in three-dimensional images, J. Microsc. 185 (1997) 67–75, https://doi.org/10.1046/j.1365-2818.1997.1340694.x.
[53] A. Hubau, A.-G. Guezennec, C. Joulian, C. Falagán, D. Dew, K.A. Hudson-Edwards, Bioleaching to reprocess sulfidic polymetallic primary mining residues: determination of metal leaching mechanisms, Hydrometall. 197 (2020) 105484, https://doi.org/10.1016/j.hydromet.2020.105484.
[54] S. Peelman, D. Kooijman, J. Sietsma, Y. Yang, Hydrometallurgical recovery of rare earth elements from mine tailings and WEEE, J. Sustain. Metall. 4 (2018) 367–377, https://doi.org/10.1007/s40831-018-0178-0.
[55] K. Pyrgaki, V. Gemeni, C. Karkalis, N. Koukouzas, P. Koutsovitis, P. Petrounias, Geochemical occurrence of rare earth elements in mining waste and mine water: a review, Minerals 11 (2021) 860, https://doi.org/10.3390/min11080860.
[56] P.H.N. Vo, S. Danaee, H.T.N. Hai, L.N. Huy, T.A.H. Nguyen, H.T.M. Nguyen, U. Kuzhiumparambil, M. Kim, L.D. Nghiem, P.J. Ralph, Biomining for sustainable recovery of rare earth elements from mining waste: a comprehensive review, Sci. Total Environ. 908 (2024) 168210, https://doi.org/10.1016/j.scitotenv.2023.168210.
[57] I. Langmuir, The constitution and fundamental properties of solids and liquids. Part I. Solids, J. Am. Chem. Soc. 38 (1916) 2221–2295, https://doi.org/10.1021/ja02268a002.
[58] H. Freundlich, G. Losev, Über die Adsorption der Farbstoffe durch Kohle und Fasern, Z. Für Phys. Chem. 59U (1907) 284–312, https://doi.org/10.1515/zpch-1907-5916.
[59] K. Moedritzer, R.R. Irani, The direct synthesis of α-aminomethylphosphonic acids. mannich-type reactions with orthophosphorous acid, J. Org. Chem. 31 (1966) 1603–1607, https://doi.org/10.1021/jo01343a067.
[60] E. Lahtinen, E. Kukkonen, V. Kinnunen, M. Lahtinen, K. Kinnunen, S. Suvanto, A. Väisänen, M. Haukka, Gold nanoparticles on 3D-printed filters: from waste to catalysts, ACS Omega 4 (2019) 16891–16898, https://doi.org/10.1021/acsomega.9b02113.
[61] R. Dai, M. Huang, L. Ma, W. Liu, S. He, H. Liu, C. Zhu, Y. Wang, Z. Zhang, A. Sun, Study on crystal structure and phase transitions of polyamide 12 via wide-angle X-ray diffraction with variable temperature, Adv. Compos. Hybrid Mater. 3 (2020) 522–529, https://doi.org/10.1007/s42114-020-00192-y.
[62] B.H. Stuart, Infrared Spectroscopy: Fundamentals and Applications, John Wiley & Sons, Incorporated, Newark, UNITED KINGDOM, 2004, http://ebookcentral.proquest.com/lib/jyvaskyla-ebooks/detail.action?docID=194354 (accessed January 24, 2024).
[63] P. Larkin, Infrared and Raman Spectroscopy: Principles and Spectral Interpretation, Elsevier, San Diego, United States, 2011, http://ebookcentral.proquest.com/lib/jyvaskyla-ebooks/detail.action?docID=692432 (accessed January 24, 2024).
[64] S. Kuang, Z. Zhang, Y. Li, H. Wei, W. Liao, Extraction and separation of heavy rare earths from chloride medium by α-aminophosphonic acid HEHAPP, J. Rare Earths 36 (2018) 304–310, https://doi.org/10.1016/j.jre.2017.09.007.
[65] K. Gholivand, R. Yaghoubi, A. Farrokhi, S. Khoddami, Two new supramolecular metal diphosphonates: synthesis, characterization, crystal structure and inhibiting effects on metallic corrosion, J. Solid State Chem. 243 (2016) 23–30, https://doi.org/10.1016/j.jssc.2016.07.027.
[66] H.N. Po, N.M. Senozan, The Henderson-Hasselbalch equation: its history and limitations, J. Chem. Educ. 78 (2001) 1499, https://doi.org/10.1021/ed078p1499.
[67] R. Thapa, T. Nissinen, P. Turhanen, J. Määttä, J. Vepsäläinen, V.-P. Lehto, J. Riikonen, Bisphosphonate modified mesoporous silicon for scandium adsorption, Microporous Mesoporous Mater. 296 (2020) 109980, https://doi.org/10.1016/j.micromeso.2019.109980.
[68] N.N.N. Mahasti, Y.-J. Shih, Y.-H. Huang, Removal of iron as oxyhydroxide (FeOOH) from aqueous solution by fluidized-bed homogeneous crystallization, J. Taiwan Inst. Chem. Eng. 96 (2019) 496–502, https://doi.org/10.1016/j.jtice.2018.12.022.
[69] K.Y. Foo, B.H. Hameed, Insights into the modeling of adsorption isotherm systems, Chem. Eng. J. 156 (2010) 2–10, https://doi.org/10.1016/j.cej.2009.09.013.
[70] M.M. Rashad, I.E. El-Sayed, A.A. Galhoum, M.M. Abdeen, H.I. Mira, E.A. Elshehy, S. Zhang, X. Lu, J. Xin, E. Guibal, Synthesis of α-aminophosphonate based sorbents – influence of inserted groups (carboxylic vs. amine) on uranyl sorption, Chem. Eng. J. 421 (2021) 127830, https://doi.org/10.1016/j.cej.2020.127830.
[71] S. Giret, Y. Hu, N. Masoumifard, J.-F. Boulanger, F. Estelle Juère, D.L. Kleitz, Selective separation and preconcentration of scandium with mesoporous silica, ACS Appl. Mater. Interfaces 10 (2018) 448–457, https://doi.org/10.1021/acsami.7b13336.
[72] S. Bao, W. Hawker, J. Vaughan, Scandium loading on chelating and solvent impregnated resin from sulfate solution, Solvent Extr. Ion Exch. 36 (2018) 100–113, https://doi.org/10.1080/07366299.2017.1412917.
[73] Y.-R. Lee, K. Yu, S. Ravi, W.-S. Ahn, Selective adsorption of rare earth elements over functionalized Cr-MIL-101, ACS Appl. Mater. Interfaces 10 (2018) 23918–23927, https://doi.org/10.1021/acsami.8b07130.
[74] Z. Liu, M. Rong, Y. Mi, H. Cai, L. Yang, Phosphorylated porous phenolic resin for efficient extraction of low-concentration rare earth elements from tailing wastewater, Sep. Purif. Technol. 346 (2024) 127502, https://doi.org/10.1016/j.seppur.2024.127502.
[75] R. Turse, W.I. Rieman, Kinetics of ion exchange in a chelating resin, J. Phys. Chem. 65 (1961) 1821–1824, https://doi.org/10.1021/j100827a031.
[76] C. Heitner-Wirguin, J. Kendler, Kinetic behaviour of chelating resins with phosphonic functional groups, J. Inorg. Nucl. Chem. 33 (1971) 3119–3129, https://doi.org/10.1016/0022-1902(71)80078-7.
[77] A.A. Zagorodni, Ion Exchange Materials: Properties and Applications, first edition, Elsevier Science, 2006.
[78] K. Vijayaraghavan, T.V.N. Padmesh, K. Palanivelu, M. Velan, Biosorption of nickel (II) ions onto *Sargassum wightii*: application of two-parameter and three-parameter isotherm models, J. Hazard. Mater. 133 (2006) 304–308, https://doi.org/10.1016/j.jhazmat.2005.10.016.
[79] R.D. Shannon, Revised effective ionic radii and systematic studies of interatomic distances in halides and chalcogenides, Acta Crystallogr. A 32 (1976) 751–767, https://doi.org/10.1107/S0567739476001551.
[80] E. Kukkonen, E.J. Virtanen, J.O. Moilanen, α-Aminophosphonates, -phosphinates, and -phosphine oxides as extraction and precipitation agents for rare earth metals, thorium, and uranium: a review, Molecules 27 (2022) 3465, https://doi.org/10.3390/molecules27113465.
[81] J.E. Bollinger, D.M. Roundhill, Complexation of indium(III), gallium(III), iron(III), gadolinium(III), and neodymium(III) ions with amino diphosphonic acids in aqueous solution, Inorg. Chem. 32 (1993) 2821–2826, https://doi.org/10.1021/ic00065a007.
[82] T.S. Khayyun, A.H. Mseer, Comparison of the experimental results with the Langmuir and Freundlich models for copper removal on limestone adsorbent, Appl. Water Sci. 9 (2019) 170, https://doi.org/10.1007/s13201-019-1061-2.
[83] R.R. Golwankar, T.D.I. Curry, C.J. Paranjothi, J.D. Blakemore, Molecular influences on the quantification of Lewis acidity with phosphine oxide probes, Inorg. Chem. 62 (2023) 9765–9780, https://doi.org/10.1021/acs.inorgchem.3c00084.
[84] J.N. Bentley, S.A. Elgadi, J.R. Gaffen, P. Demay-Drouhard, T. Baumgartner, C. B. Caputo, Fluorescent Lewis adducts: a practical guide to relative Lewis acidity, Organometallics 39 (2020) 3645–3655, https://doi.org/10.1021/acs.organomet.0c00389.
[85] J.R. Gaffen, J.N. Bentley, L.C. Torres, C. Chu, T. Baumgartner, C.B. Caputo, A simple and effective method of determining Lewis acidity by using fluorescence, Chem 5 (2019) 1567–1583, https://doi.org/10.1016/j.chempr.2019.03.022.
[86] K. Ohkubo, S.C. Menon, A. Orita, J. Otera, S. Fukuzumi, Quantitative evaluation of Lewis acidity of metal ions with different ligands and counterions in relation to the promoting effects of Lewis acids on electron transfer reduction of oxygen, J. Org. Chem. 68 (2003) 4720–4726, https://doi.org/10.1021/jo034258u.
[87] K.P. Kepp, A quantitative scale of oxophilicity and thiophilicity, Inorg. Chem. 55 (2016) 9461–9470, https://doi.org/10.1021/acs.inorgchem.6b01702.
[88] Q. Zhao, Z. Zhang, Y. Li, X. Bian, W. Liao, Solvent extraction and separation of rare earths from chloride media using α-aminophosphonic acid extractant HEHAMP, Solvent Extr. Ion Exch. 36 (2018) 136–149, https://doi.org/10.1080/07366299.2018.1431079.
[89] Q. He, J. Chen, L. Gan, M. Gao, M. Zan, Y. Xiao, Insight into leaching of rare earth and aluminum from ion adsorption type rare earth ore: adsorption and desorption, J. Rare Earths 41 (2023) 1398–1407, https://doi.org/10.1016/j.jre.2022.08.009.
[90] M. Traore, A. Gong, Y. Wang, L. Qiu, Y. Bai, W. Zhao, Y. Liu, Y. Chen, Y. Liu, H. Wu, S. Li, Y. You, Research progress of rare earth separation methods and technologies, J. Rare Earths 41 (2023) 182–189, https://doi.org/10.1016/j.jre.2022.04.009.
[91] E.A. Imam, A.I. Hashem, X. Lu, A.A. Tolba, M.G. Mahfouz, J. Xin, I.-E.-T. El-Sayed, S.I. Mohamady, A.A.S. Ahmed, A.A. Galhoum, E. Guibal, Nd(III) sorption using aminophosphonate-based sorbents – sorption properties and application to the treatment of REE concentrate, Colloids Surf. Physicochem. Eng. Asp. 685 (2024) 133339, https://doi.org/10.1016/j.colsurfa.2024.133339.
[92] X. Hu, H. Yang, K. Tan, S. Hou, J. Cai, X. Yuan, Q. Lan, J. Cao, S. Yan, Treatment and recovery of iron from acid mine drainage: a pilot-scale study, J. Environ. Chem. Eng. 10 (2022) 106974, https://doi.org/10.1016/j.jece.2021.106974.
[93] C. Fonseka, S. Ryu, Y. Choo, G. Naidu, J. Kandasamy, R. Thiruvenkatachari, L. Foseid, H. Ratnaweera, S. Vigneswaran, Selective recovery of europium from real acid mine drainage by using novel amine based modified SBA15 adsorbent and membrane distillation system, J. Water Process Eng. 56 (2023) 104551, https://doi.org/10.1016/j.jwpe.2023.104551.
[94] L.B. José, A.C.Q. Ladeira, Recovery and separation of rare earth elements from an acid mine drainage-like solution using a strong acid resin, J. Water Process Eng. 41 (2021) 102052, https://doi.org/10.1016/j.jwpe.2021.102052.
[95] L. Bernardo José, G. Cordeiro Silva, A. Cláudia Queiroz Ladeira, Pre-concentration and partial fractionation of rare earth elements by ion exchange, Miner. Eng. 205 (2024) 108477, https://doi.org/10.1016/j.mineng.2023.108477.
[96] Y. Wang, Y. He, A. Gong, L. Qiu, M. Zhang, M. Traore, X. Zhan, Y. Li, Y. Bai, Y. Liu, G. Gao, W. Zhao, Selective recovery of rare earth metals from acid mine drainage by pyrrolidine diglycolamide silica column, J. Environ. Chem. Eng. 11 (2023) 110091, https://doi.org/10.1016/j.jece.2023.110091.

III

SEPARATING CRITICAL ELEMENTS FROM A NDFEB MAGNET WITH AMINOPHOSPHONIC ACID FUNCTIONALISED 3D PRINTED FILTERS AND THEIR DETAILED STRUCTURAL CHARACTERISATION WITH X-RAY TOMOGRAPHY

by

Virtanen, E. J., Yliharju, J., Kukkonen, E., Christiansen, T., Tuomisto, M., Miettinen, A., Väisänen, A. & Moilanen J. O. 2024

Manuscript

Request a copy from the author.

DEPARTMENT OF CHEMISTRY, UNIVERSITY OF JYVÄSKYLÄ
RESEARCH REPORT SERIES

1. Vuolle, Mikko: Electron paramagnetic resonance and molecular orbital study of radical ions generated from (2.2)metacyclophane, pyrene and its hydrogenated compounds by alkali metal reduction and by thallium(III)trifluoroacetate oxidation. (99 pp.) 1976
2. Pasanen, Kaija: Electron paramagnetic resonance study of cation radical generated from various chlorinated biphenyls. (66 pp.) 1977
3. Carbon-13 Workshop, September 6-8, 1977. (91 pp.) 1977
4. Laihia, Katri: On the structure determination of norbornane polyols by NMR spectroscopy. (111 pp.) 1979
5. Nyrönen, Timo: On the EPR, ENDOR and visible absorption spectra of some nitrogen containing heterocyclic compounds in liquid ammonia. (76 pp.) 1978
6. Talvitie, Antti: Structure determination of some sesquiterpenoids by shift reagent NMR. (54 pp.) 1979
7. Häkli, Harri: Structure analysis and molecular dynamics of cyclic compounds by shift reagent NMR. (48 pp.) 1979
8. Pitkänen, Ilkka: Thermodynamics of complexation of 1,2,4-triazole with divalent manganese, cobalt, nickel, copper, zinc, cadmium and lead ions in aqueous sodium perchlorate solutions. (89 pp.) 1980
9. Asunta, Tuula: Preparation and characterization of new organometallic compounds synthesized by using metal vapours. (91 pp.) 1980
10. Sattar, Mohammad Abdus: Analyses of MCPA and its metabolites in soil. (57 pp.) 1980
11. Bibliography 1980. (31 pp.) 1981
12. Knuuttila, Pekka: X-Ray structural studies on some divalent 3d metal compounds of picolinic and isonicotinic acid N-oxides. (77 pp.) 1981
13. Bibliography 1981. (33 pp.) 1982
14. 6^{th} National NMR Symposium, September 9-10, 1982, Abstracts. (49 pp.) 1982
15. Bibliography 1982. (38 pp.) 1983
16. Knuuttila, Hilkka: X-Ray structural studies on some Cu(II), Co(II) and Ni(II) complexes with nicotinic and isonicotinic acid N-oxides. (54 pp.) 1983
17. Symposium on inorganic and analytical chemistry May 18, 1984, Program and Abstracts. (100 pp.) 1984
18. Knuutinen, Juha: On the synthesis, structure verification and gas chromatographic determination of chlorinated catechols and guaiacols occuring in spent bleach liquors of kraft pulp mill. (30 pp.) 1984
19. Bibliography 1983. (47 pp.) 1984
20. Pitkänen, Maija: Addition of BrCl, B_2 and Cl_2 to methyl esters of propenoic and 2-butenoic acid derivatives and ^{13}C NMR studies on methyl esters of saturated aliphatic mono- and dichlorocarboxylic acids. (56 pp.) 1985
21. Bibliography 1984. (39 pp.) 1985
22. Salo, Esa: EPR, ENDOR and TRIPLE spectroscopy of some nitrogen heteroaromatics in liquid ammonia. (111 pp.) 1985

23. Humppi, Tarmo: Synthesis, identification and analysis of dimeric impurities of chlorophenols. (39 pp.) 1985
24. Aho, Martti: The ion exchange and adsorption properties of sphagnum peat under acid conditions. (90 pp.) 1985
25. Bibliography 1985 (61 pp.) 1986
26. Bibliography 1986. (23 pp.) 1987
27. Bibliography 1987. (26 pp.) 1988
28. Paasivirta, Jaakko (Ed.): Structures of organic environmental chemicals. (67 pp.) 1988
29. Paasivirta, Jaakko (Ed.): Chemistry and ecology of organo-element compounds. (93 pp.) 1989
30. Sinkkonen, Seija: Determination of crude oil alkylated dibenzothiophenes in environment. (35 pp.) 1989
31. Kolehmainen, Erkki (Ed.): XII National NMR Symposium Program and Abstracts. (75 pp.) 1989
32. Kuokkanen, Tauno: Chlorocymenes and Chlorocymenenes: Persistent chlorocompounds in spent bleach liquors of kraft pulp mills. (40 pp.) 1989
33. Mäkelä, Reijo: ESR, ENDOR and TRIPLE resonance study on substituted 9,10-anthraquinone radicals in solution. (35 pp.) 1990
34. Veijanen, Anja: An integrated sensory and analytical method for identification of off-flavour compounds. (70 pp.) 1990
35. Kasa, Seppo: EPR, ENDOR and TRIPLE resonance and molecular orbital studies on a substitution reaction of anthracene induced by thallium(III) in two fluorinated carboxylic acids. (114 pp.) 1990
36. Herve, Sirpa: Mussel incubation method for monitoring organochlorine compounds in freshwater recipients of pulp and paper industry. (145 pp.) 1991
37. Pohjola, Pekka: The electron paramagnetic resonance method for characterization of Finnish peat types and iron (III) complexes in the process of peat decomposition. (77 pp.) 1991
38. Paasivirta, Jaakko (Ed.): Organochlorines from pulp mills and other sources. Research methodology studies 1988-91. (120 pp.) 1992
39. Veijanen, Anja (Ed.): VI National Symposium on Mass Spectrometry, May 13-15, 1992, Abstracts. (55 pp.) 1992
40. Rissanen, Kari (Ed.): The 7. National Symposium on Inorganic and Analytical Chemistry, May 22, 1992, Abstracts and Program. (153 pp.) 1992
41. Paasivirta, Jaakko (Ed.): CEOEC'92, Second Finnish-Russian Seminar: Chemistry and Ecology of Organo-Element Compounds. (93 pp.) 1992
42. Koistinen, Jaana: Persistent polychloroaromatic compounds in the environment: structure-specific analyses. (50 pp.) 1993
43. Virkki, Liisa: Structural characterization of chlorolignins by spectroscopic and liquid chromatographic methods and a comparison with humic substances. (62 pp.) 1993
44. Helenius, Vesa: Electronic and vibrational excitations in some

biologically relevant molecules. (30 pp.) 1993

45. Leppä-aho, Jaakko: Thermal behaviour, infrared spectra and x-ray structures of some new rare earth chromates(VI). (64 pp.) 1994
46. Kotila, Sirpa: Synthesis, structure and thermal behavior of solid copper(II) complexes of 2-amino-2- hydroxymethyl-1,3-propanediol. (111 pp.) 1994
47. Mikkonen, Anneli: Retention of molybdenum(VI), vanadium(V) and tungsten(VI) by kaolin and three Finnish mineral soils. (90 pp.) 1995
48. Suontamo, Reijo: Molecular orbital studies of small molecules containing sulfur and selenium. (42 pp.) 1995
49. Hämäläinen, Jouni: Effect of fuel composition on the conversion of fuel-N to nitrogen oxides in the combustion of small single particles. (50 pp.) 1995
50. Nevalainen, Tapio: Polychlorinated diphenyl ethers: synthesis, NMR spectroscopy, structural properties, and estimated toxicity. (76 pp.) 1995
51. Aittola, Jussi-Pekka: Organochloro compounds in the stack emission. (35 pp.) 1995
52. Harju, Timo: Ultrafast polar molecular photophysics of (dibenzylmethine)borondifluoride and 4-aminophthalimide in solution. (61 pp.) 1995
53. Maatela, Paula: Determination of organically bound chlorine in industrial and environmental samples. (83 pp.) 1995
54. Paasivirta, Jaakko (Ed.): CEOEC'95, Third Finnish-Russian Seminar: Chemistry and Ecology of Organo-Element Compounds. (109 pp.) 1995
55. Huuskonen, Juhani: Synthesis and structural studies of some supramolecular compounds. (54 pp.) 1995
56. Palm, Helena: Fate of chlorophenols and their derivatives in sawmill soil and pulp mill recipient environments. (52 pp.) 1995
57. Rantio, Tiina: Chlorohydrocarbons in pulp mill effluents and their fate in the environment. (89 pp.) 1997
58. Ratilainen, Jari: Covalent and non-covalent interactions in molecular recognition. (37 pp.) 1997
59. Kolehmainen, Erkki (Ed.): XIX National NMR Symposium, June 4-6, 1997, Abstracts. (89 pp.) 1997
60. Matilainen, Rose: Development of methods for fertilizer analysis by inductively coupled plasma atomic emission spectrometry. (41 pp.) 1997
61. Koistinen, Jari (Ed.): Spring Meeting on the Division of Synthetic Chemistry, May 15-16, 1997, Program and Abstracts. (36 pp.) 1997
62. Lappalainen, Kari: Monomeric and cyclic bile acid derivatives: syntheses, NMR spectroscopy and molecular recognition properties. (50 pp.) 1997
63. Laitinen, Eira: Molecular dynamics of cyanine dyes and phthalimides in solution: picosecond laser studies. (62 pp.) 1997
64. Eloranta, Jussi: Experimental and theoretical studies on some

quinone and quinol radicals. (40 pp.) 1997

65. Oksanen, Jari: Spectroscopic characterization of some monomeric and aggregated chlorophylls. (43 pp.) 1998
66. Häkkänen, Heikki: Development of a method based on laser-induced plasma spectrometry for rapid spatial analysis of material distributions in paper coatings. (60 pp.) 1998
67. Virtapohja, Janne: Fate of chelating agents used in the pulp and paper industries. (58 pp.) 1998
68. Airola, Karri: X-ray structural studies of supramolecular and organic compounds. (39 pp.) 1998
69. Hyötyläinen, Juha: Transport of lignin–type compounds in the receiving waters of pulp mills. (40 pp.) 1999
70. Ristolainen, Matti: Analysis of the organic material dissolved during totally chlorine-free bleaching. (40 pp.) 1999
71. Eklin, Tero: Development of analytical procedures with industrial samples for atomic emission and atomic absorption spectrometry. (43 pp.) 1999
72. Välisaari, Jouni: Hygiene properties of resol-type phenolic resin laminates. (129 pp.) 1999
73. Hu, Jiwei: Persistent polyhalogenated diphenyl ethers: model compounds syntheses, characterization and molecular orbital studies. (59 pp.) 1999
74. Malkavaara, Petteri: Chemometric adaptations in wood processing chemistry. (56 pp.) 2000
75. Kujala Elena, Laihia Katri, Nieminen Kari (Eds.): NBC 2000, Symposium on Nuclear, Biological and Chemical Threats in the 21st Century. (299 pp.) 2000
76. Rantalainen, Anna-Lea: Semipermeable membrane devices in monitoring persistent organic pollutants in the environment. (58 pp.) 2000
77. Lahtinen, Manu: *In situ* X-ray powder diffraction studies of Pt/C, CuCl/C and Cu_2O/C catalysts at elevated temperatures in various reaction conditions. (92 pp.) 2000
78. Tamminen, Jari: Syntheses, empirical and theoretical characterization, and metal cation complexation of bile acid-based monomers and open/closed dimers. (54 pp.) 2000
79. Vatanen, Virpi: Experimental studies by EPR and theoretical studies by DFT calculations of α-amino-9,10-anthraquinone radical anions and cations in solution. (37 pp.) 2000
80. Kotilainen, Risto: Chemical changes in wood during heating at 150-260 °C. (57 pp.) 2000
81. Nissinen, Maija: X-ray structural studies on weak, non-covalent interactions in supramolecular compounds. (69 pp.) 2001
82. Wegelius, Elina: X-ray structural studies on self-assembled hydrogen-bonded networks and metallosupramolecular complexes. (84 pp.) 2001
83. Paasivirta, Jaakko (Ed.): CEOEC'2001, Fifth Finnish-Russian Seminar: Chemistry and Ecology of Organo-Element Compounds. (163 pp.) 2001
84. Kiljunen, Toni: Theoretical studies on spectroscopy and

atomic dynamics in rare gas solids. (56 pp.) 2001

85. Du, Jin: Derivatives of dextran: synthesis and applications in oncology. (48 pp.) 2001
86. Koivisto, Jari: Structural analysis of selected polychlorinated persistent organic pollutants (POPs) and related compounds. (88 pp.) 2001
87. Feng, Zhinan: Alkaline pulping of non-wood feedstocks and characterization of black liquors. (54 pp.) 2001
88. Halonen, Markku: Lahon havupuun käyttö sulfaattiprosessin raaka-aineena sekä havupuun lahontorjunta. (90 pp.) 2002
89. Falábu, Dezsö: Synthesis, conformational analysis and complexation studies of resorcarene derivatives. (212 pp.) 2001
90. Lehtovuori, Pekka: EMR spectroscopic studies on radicals of ubiquinones Q-*n*, vitamin K_3 and vitamine E in liquid solution. (40 pp.) 2002
91. Perkkalainen, Paula: Polymorphism of sugar alcohols and effect of grinding on thermal behavior on binary sugar alcohol mixtures. (53 pp.) 2002
92. Ihalainen, Janne: Spectroscopic studies on light-harvesting complexes of green plants and purple bacteria. (42 pp.) 2002
93. Kunttu, Henrik, Kiljunen, Toni (Eds.): 4th International Conference on Low Temperature Chemistry. (159 pp.) 2002
94. Väisänen, Ari: Development of methods for toxic element analysis in samples with environmental concern by ICP-AES and ETAAS. (54 pp.) 2002
95. Luostarinen, Minna: Synthesis and characterisation of novel resorcarene derivatives. (200 pp.) 2002
96. Louhelainen, Jarmo: Changes in the chemical composition and physical properties of wood and nonwood black liquors during heating. (68 pp.) 2003
97. Lahtinen, Tanja: Concave hydrocarbon cyclophane π-prismands. (65 pp.) 2003
98. Laihia, Katri (Ed.): NBC 2003, Symposium on Nuclear, Biological and Chemical Threats – A Crisis Management Challenge. (245 pp.) 2003
99. Oasmaa, Anja: Fuel oil quality properties of wood-based pyrolysis liquids. (32 pp.) 2003
100. Virtanen, Elina: Syntheses, structural characterisation, and cation/anion recognition properties of nano-sized bile acid-based host molecules and their precursors. (123 pp.) 2003
101. Nättinen, Kalle: Synthesis and X-ray structural studies of organic and metallo-organic supramolecular systems. (79 pp.) 2003
102. Lampiselkä, Jarkko: Demonstraatio lukion kemian opetuksessa. (285 pp.) 2003
103. Kallioinen, Jani: Photoinduced dynamics of $Ru(dcbpy)_2(NCS)_2$ – in solution and on nanocrystalline titanium dioxide thin films. (47 pp.) 2004
104. Valkonen, Arto (Ed.): VII Synthetic Chemistry Meeting and XXVI Finnish NMR Symposium. (103 pp.) 2004

105. Vaskonen, Kari: Spectroscopic studies on atoms and small molecules isolated in low temperature rare gas matrices. (65 pp.) 2004
106. Lehtovuori, Viivi: Ultrafast light induced dissociation of $Ru(dcbpy)(CO)_2I_2$ in solution. (49 pp.) 2004
107. Saarenketo, Pauli: Structural studies of metal complexing Schiff bases, Schiff base derived *N*-glycosides and cyclophane π-prismands. (95 pp.) 2004
108. Paasivirta, Jaakko (Ed.): CEOEC'2004, Sixth Finnish-Russian Seminar: Chemistry and Ecology of Organo-Element Compounds. (147 pp.) 2004
109. Suontamo, Tuula: Development of a test method for evaluating the cleaning efficiency of hard-surface cleaning agents. (96 pp.) 2004
110. Güneş, Minna: Studies of thiocyanates of silver for nonlinear optics. (48 pp.) 2004
111. Ropponen, Jarmo: Aliphatic polyester dendrimers and dendrons. (81 pp.) 2004
112. Vu, Mân Thi Hong: Alkaline pulping and the subsequent elemental chlorine-free bleaching of bamboo (*Bambusa procera*). (69 pp.) 2004
113. Mansikkamäki, Heidi: Self-assembly of resorcinarenes. (77 pp.) 2006
114. Tuononen, Heikki M.: EPR spectroscopic and quantum chemical studies of some inorganic main group radicals. (79 pp.) 2005
115. Kaski, Saara: Development of methods and applications of laser-induced plasma spectroscopy in vacuum ultraviolet. (44 pp.) 2005
116. Mäkinen, Riika-Mari: Synthesis, crystal structure and thermal decomposition of certain metal thiocyanates and organic thiocyanates. (119 pp.) 2006
117. Ahokas, Jussi: Spectroscopic studies of atoms and small molecules isolated in rare gas solids: photodissociation and thermal reactions. (53 pp.) 2006
118. Busi, Sara: Synthesis, characterization and thermal properties of new quaternary ammonium compounds: new materials for electrolytes, ionic liquids and complexation studies. (102 pp.) 2006
119. Mäntykoski, Keijo: PCBs in processes, products and environment of paper mills using wastepaper as their raw material. (73 pp.) 2006
120. Laamanen, Pirkko-Leena: Simultaneous determination of industrially and environmentally relevant aminopolycarboxylic and hydroxycarboxylic acids by capillary zone electrophoresis. (54 pp.) 2007
121. Salmela, Maria: Description of oxygen-alkali delignification of kraft pulp using analysis of dissolved material. (71 pp.) 2007
122. Lehtovaara, Lauri: Theoretical studies of atomic scale impurities in superfluid ^{4}He. (87 pp.) 2007
123. Rautiainen, J. Mikko: Quantum chemical calculations of structures, bonding, and spectroscopic properties of some sulphur and selenium iodine cations. (71 pp.) 2007
124. Nummelin, Sami: Synthesis, characterization, structural and

retrostructural analysis of self-assembling pore forming dendrimers. (286 pp.) 2008

125. Sopo, Harri: Uranyl(VI) ion complexes of some organic aminobisphenolate ligands: syntheses, structures and extraction studies. (57 pp.) 2008
126. Valkonen, Arto: Structural characteristics and properties of substituted cholanoates and *N*-substituted cholanamides. (80 pp.) 2008
127. Lähde, Anna: Production and surface modification of pharmaceutical nano- and microparticles with the aerosol flow reactor. (43 pp.) 2008
128. Beyeh, Ngong Kodiah: Resorcinarenes and their derivatives: synthesis, characterization and complexation in gas phase and in solution. (75 pp.) 2008
129. Välisaari, Jouni, Lundell, Jan (Eds.): Kemian opetuksen päivät 2008: uusia oppimisympäristöjä ja ongelmalähtöistä opetusta. (118 pp.) 2008
130. Myllyperkiö, Pasi: Ultrafast electron transfer from potential organic and metal containing solar cell sensitizers. (69 pp.) 2009
131. Käkölä, Jaana: Fast chromatographic methods for determining aliphatic carboxylic acids in black liquors. (82 pp.) 2009
132. Koivukorpi, Juha: Bile acid-arene conjugates: from photoswitchability to cancer cell detection. (67 pp.) 2009
133. Tuuttila, Tero: Functional dendritic polyester compounds: synthesis and characterization of small bifunctional dendrimers and dyes. (74 pp.) 2009
134. Salorinne, Kirsi: Tetramethoxy resorcinarene based cation and anion receptors: synthesis, characterization and binding properties. (79 pp.) 2009
135. Rautiainen, Riikka: The use of first-thinning Scots pine (*Pinus sylvestris*) as fiber raw material for the kraft pulp and paper industry. (73 pp.) 2010
136. Ilander, Laura: Uranyl salophens: synthesis and use as ditopic receptors. (199 pp.) 2010
137. Kiviniemi, Tiina: Vibrational dynamics of iodine molecule and its complexes in solid krypton - Towards coherent control of bimolecular reactions? (73 pp.) 2010
138. Ikonen, Satu: Synthesis, characterization and structural properties of various covalent and non-covalent bile acid derivatives of N/O-heterocycles and their precursors. (105 pp.) 2010
139. Siitonen, Anni: Spectroscopic studies of semiconducting single-walled carbon nanotubes. (56 pp.) 2010
140. Raatikainen, Kari: Synthesis and structural studies of piperazine cyclophanes – Supramolecular systems through Halogen and Hydrogen bonding and metal ion coordination. (69 pp.) 2010
141. Leivo, Kimmo: Gelation and gel properties of two- and three-component Pyrene based low molecular weight organogelators. (116 pp.) 2011
142. Martiskainen, Jari: Electronic energy transfer in light-harvesting complexes isolated from *Spinacia oleracea* and from three

photosynthetic green bacteria *Chloroflexus aurantiacus*, *Chlorobium tepidum*, and *Prosthecochloris aestuarii*. (55 pp.) 2011

143. Wichmann, Oula: Syntheses, characterization and structural properties of [O,N,O,X´] aminobisphenolate metal complexes. (101 pp.) 2011
144. Ilander, Aki: Development of ultrasound-assisted digestion methods for the determination of toxic element concentrations in ash samples by ICP-OES. (58 pp.) 2011
145. The Combined XII Spring Meeting of the Division of Synthetic Chemistry and XXXIII Finnish NMR Symposium. Book of Abstracts. (90 pp.) 2011
146. Valto, Piia: Development of fast analysis methods for extractives in papermaking process waters. (73 pp.) 2011
147. Andersin, Jenni: Catalytic activity of palladium-based nanostructures in the conversion of simple olefinic hydro- and chlorohydrocarbons from first principles. (78 pp.) 2011
148. Aumanen, Jukka: Photophysical properties of dansylated poly(propylene amine) dendrimers. (55 pp.) 2011
149. Kärnä, Minna: Ether-functionalized quaternary ammonium ionic liquids – synthesis, characterization and physicochemical properties. (76 pp.) 2011
150. Jurček, Ondřej: Steroid conjugates for applications in pharmacology and biology. (57 pp.) 2011
151. Nauha, Elisa: Crystalline forms of selected Agrochemical actives: design and synthesis of cocrystals. (77 pp.) 2012
152. Ahkola, Heidi: Passive sampling in monitoring of nonylphenol ethoxylates and nonylphenol in aquatic environments. (92 pp.) 2012
153. Helttunen, Kaisa: Exploring the self-assembly of resorcinarenes: from molecular level interactions to mesoscopic structures. (78 pp.) 2012
154. Linnanto, Juha: Light excitation transfer in photosynthesis revealed by quantum chemical calculations and exiton theory. (179 pp.) 2012
155. Roiko-Jokela, Veikko: Digital imaging and infrared measurements of soil adhesion and cleanability of semihard and hard surfaces. (122 pp.) 2012
156. Noponen, Virpi: Amides of bile acids and biologically important small molecules: properties and applications. (85 pp.) 2012
157. Hulkko, Eero: Spectroscopic signatures as a probe of structure and dynamics in condensed-phase systems – studies of iodine and gold ranging from isolated molecules to nanoclusters. (69 pp.) 2012
158. Lappi, Hanna: Production of Hydrocarbon-rich biofuels from extractives-derived materials. (95 pp.) 2012
159. Nykänen, Lauri: Computational studies of Carbon chemistry on transition metal surfaces. (76 pp.) 2012
160. Ahonen, Kari: Solid state studies of pharmaceutically important molecules and their derivatives. (65 pp.) 2012

161. Pakkanen, Hannu: Characterization of organic material dissolved during alkaline pulping of wood and non-wood feedstocks. (76 pp.) 2012
162. Moilanen, Jani: Theoretical and experimental studies of some main group compounds: from closed shell interactions to singlet diradicals and stable radicals. (80 pp.) 2012
163. Himanen, Jatta: Stereoselective synthesis of Oligosaccharides by *De Novo* Saccharide welding. (133 pp.) 2012
164. Bunzen, Hana: Steroidal derivatives of nitrogen containing compounds as potential gelators. (76 pp.) 2013
165. Seppälä, Petri: Structural diversity of copper(II) amino alcohol complexes. Syntheses, structural and magnetic properties of bidentate amino alcohol copper(II) complexes. (67 pp.) 2013
166. Lindgren, Johan: Computational investigations on rotational and vibrational spectroscopies of some diatomics in solid environment. (77 pp.) 2013
167. Giri, Chandan: Sub-component self-assembly of linear and non-linear diamines and diacylhydrazines, formulpyridine and transition metal cations. (145 pp.) 2013
168. Riisiö, Antti: Synthesis, Characterization and Properties of Cu(II)-, Mo(VI)- and U(VI) Complexes With Diaminotetraphenolate Ligands. (51 pp.) 2013
169. Kiljunen, Toni (Ed.): Chemistry and Physics at Low Temperatures. Book of Abstracts. (103 pp.) 2013
170. Hänninen, Mikko: Experimental and Computational Studies of Transition Metal Complexes with Polydentate Amino- and Aminophenolate Ligands: Synthesis, Structure, Reactivity and Magnetic Properties. (66 pp.) 2013
171. Antila, Liisa: Spectroscopic studies of electron transfer reactions at the photoactive electrode of dye-sensitized solar cells. (53 pp.) 2013
172. Kemppainen, Eeva: Mukaiyama-Michael reactions with α-substituted acroleins – a useful tool for the synthesis of the pectenotoxins and other natural product targets. (190 pp.) 2013
173. Virtanen, Suvi: Structural Studies of Dielectric Polymer Nanocomposites. (49 pp.) 2013
174. Yliniemelä-Sipari, Sanna: Understanding The Structural Requirements for Optimal Hydrogen Bond Catalyzed Enolization – A Biomimetic Approach.(160 pp.) 2013
175. Leskinen, Mikko V: Remote β-functionalization of β'-keto esters. (105 pp.) 2014
176. 12th European Conference on Research in Chemistry Education (ECRICE2014). Book of Abstracts. (166 pp.) 2014
177. Peuronen, Anssi: N-Monoalkylated DABCO-Based N-Donors as Versatile Building Blocks in Crystal Engineering and Supramolecular Chemistry. (54 pp.) 2014
178. Perämäki, Siiri: Method development for determination and recovery of rare earth elements from industrial fly ash. (88 pp.) 2014

179. Chernyshev, Alexander, N.: Nitrogen-containing ligands and their platinum(IV) and gold(III) complexes: investigation and basicity and nucleophilicity, luminescence, and aurophilic interactions. (64 pp.) 2014
180. Lehto, Joni: Advanced Biorefinery Concepts Integrated to Chemical Pulping. (142 pp.) 2015
181. Tero, Tiia-Riikka: Tetramethoxy resorcinarenes as platforms for fluorescent and halogen bonding systems. (61 pp.) 2015
182. Löfman, Miika: Bile acid amides as components of microcrystalline organogels. (62 pp.) 2015
183. Selin, Jukka: Adsorption of softwood-derived organic material onto various fillers during papermaking. (169 pp.) 2015
184. Piisola, Antti: Challenges in the stereoselective synthesis of allylic alcohols. (210 pp.) 2015
185. Bonakdarzadeh, Pia: Supramolecular coordination polyhedra based on achiral and chiral pyridyl ligands: design, preparation, and characterization. (65 pp.) 2015
186. Vasko, Petra: Synthesis, characterization, and reactivity of heavier group 13 and 14 metallylenes and metalloid clusters: small molecule activation and more. (66 pp.) 2015
187. Topić, Filip: Structural Studies of Nano-sized Supramolecular Assemblies. (79 pp.) 2015
188. Mustalahti, Satu: Photodynamics Studies of Ligand-Protected Gold Nanoclusters by using Ultrafast Transient Infrared Spectroscopy. (58 pp.) 2015
189. Koivisto, Jaakko: Electronic and vibrational spectroscopic studies of gold-nanoclusters. (63 pp.) 2015
190. Suhonen, Aku: Solid state conformational behavior and interactions of series of aromatis oligoamide foldamers. (68 pp.) 2016
191. Soikkeli, Ville: Hydrometallurgical recovery and leaching studies for selected valuable metals from fly ash samples by ultrasound-assisted extraction followed by ICP-OES determination. (107 pp.) 2016
192. XXXVIII Finnish NMR Symposium. Book of Abstracts. (51 pp.) 2016
193. Mäkelä, Toni: Ion Pair Recognition by Ditopic Crown Ether Based bis-Urea and Uranyl Salophen Receptors. (75 pp.) 2016
194. Lindholm-Lehto, Petra: Occurrence of pharmaceuticals in municipal wastewater treatment plants and receiving surface waters in Central and Southern Finland. (98 pp.) 2016
195. Härkönen, Ville: Computational and Theoretical studies on Lattice Thermal conductivity and Thermal properties of Silicon Clathrates. (89 pp.) 2016
196. Tuokko, Sakari: Understanding selective reduction reactions with heterogeneous Pd and Pt: climbing out of the black box. (85 pp.) 2016
197. Nuora, Piia: Monitapaustutkimus LUMA-Toimintaan liittyvissä oppimisympäristöissä tapahtuvista kemian oppimiskokemuksista. (171 pp.) 2016

198. Kumar, Hemanathan: Novel Concepts on The Recovery of By-Products from Alkaline Pulping. (61 pp.) 2016
199. Arnedo-Sánchez, Leticia: Lanthanide and Transition Metal Complexes as Building Blocks for Supramolecular Functional Materials. (227 pp.) 2016
200. Gell, Lars: Theoretical Investigations of Ligand Protected Silver Nanoclusters. (134 pp.) 2016
201. Vaskuri, Juhani: Oppiennätyksistä opetussuunnitelman perusteisiin - lukion kemian kansallisen opetussuunnitelman kehittyminen Suomessa vuosina 1918-2016. (314 pp.) 2017
202. Lundell Jan, Kiljunen Toni (Eds.): 22nd Horizons in Hydrogen Bond Research. Book of Abstracts. 2017
203. Turunen, Lotta: Design and construction of halogen-bonded capsules and cages. (61 pp.) 2017
204. Hurmalainen, Juha: Experimental and computational studies of unconventional main group compounds: stable radicals and reactive intermediates. (88 pp.) 2017
205. Koivistoinen Juha: Non-linear interactions of femtosecond laser pulses with graphene: photo-oxidation, imaging and photodynamics. (68 pp.) 2017
206. Chen, Chengcong: Combustion behavior of black liquors: droplet swelling and influence of liquor composition. (39 pp.) 2017
207. Mansikkamäki, Akseli: Theoretical and Computational Studies of Magnetic Anisotropy and Exchange Coupling in Molecular Systems. (190 p. + included articles) 2018.
208. Tatikonda, Rajendhraprasad: Multivalent N-donor ligands for the construction of coordination polymers and coordination polymer gels. (62 pp.) 2018
209. Budhathoki, Roshan: Beneficiation, desilication and selective precipitation techniques for phosphorus refining from biomass derived fly ash. (64 pp.) 2018
210. Siitonen, Juha: Synthetic Studies on 1-azabicyclo[5.3.0]decane Alkaloids. (140 pp.) 2018
211. Ullah, Saleem: Advanced Biorefinery Concepts Related to Non-wood Feedstocks. (57 pp.) 2018
212. Ghalibaf, Maryam: Analytical Pyrolysis of Wood and Non-Wood Materials from Integrated Biorefinery Concepts. (106 pp.) 2018

DEPARTMENT OF CHEMISTRY, UNIVERSITY OF JYVÄSKYLÄ
DISSERTATIONS PUBLISHED IN THE JYU DISSERTATIONS RESEARCH SERIES

1. Bulatov, Evgeny: Synthetic and structural studies of covalent and non-covalent interactions of ligands and metal center in platinum(II) complexes containing 2,2′-dipyridylamine or oxime ligands. (58 pp.) 2019. JYU Dissertations 70.
2. Annala, Riia: Conformational Properties and Anion Complexes of Aromatic Oligoamide Foldamers. (80 pp.) 2019. JYU Dissertations 84.
3. Isoaho, Jukka Pekka: Dithionite Bleaching of Thermomechanical Pulp - Chemistry and Optimal Conditions. (73 pp.) 2019. JYU Dissertations 85.
4. Nygrén, Enni: Recovery of rubidium from power plant fly ash. (98 pp.) 2019. JYU Dissertations 136.
5. Kiesilä, Anniina: Supramolecular chemistry of anion-binding receptors based on concave macromolecules. (68 pp.) 2019. JYU Dissertations 137.
6. Sokolowska, Karolina: Study of water-soluble p-MBA-protected gold nanoclusters and their superstructures. (60 pp.) 2019. JYU Dissertations 167.
7. Lahtinen, Elmeri: Chemically Functional 3D Printing: Selective Laser Sintering of Customizable Metal Scavengers. (71 pp.) 2019. JYU Dissertations 175.
8. Larijani, Amir: Oxidative reactions of cellulose under alkaline conditions. (102 pp.) 2020. JYU Dissertations 217.
9. Kolari, Kalle: Metal-metal contacts in late transition metal polymers. (60 pp.) 2020. JYU Dissertations 220.
10. Kauppinen, Minttu: Multiscale computational investigation of catalytic properties of zirconia supported noble metals. (87 pp.) 2020. JYU Dissertations 231.
11. Ding, Xin: Halogen Bond in Crystal Engineering: Structural Studies on Crystals with Ruthenium Centered Complexes and 1-(4-Pyridyl)-4-thiopyridine Zwitterion as Halogen Bond Acceptors. (59 pp.) 2020. JYU Dissertations 323.
12. Neuvonen, Antti: Toward an Understanding of Hydrogen-Bonding Bifunctional Organocatalyst Conformations and Their Activity in Asymmetric Mannich Reactions. (77 pp.) 2020. JYU Dissertations 336.
13. Kortet, Sami: 2,5-Diarylpyrrolidines and Pyroglutamic-Acid-Derived 2-Diarylmethyl-5-Aryl-Pyrrolidines: Their Synthesis and Use in Asymmetric Synthesis. (221 pp.) 2020. JYU Dissertations 337.
14. Saarnio, Ville: Fluorescent probes, noble metal nanoparticles and their nanocomposites: detection of nucleic acids and other biological targets. (80 pp.) 2021. JYU Dissertations 361.
15. Chernysheva, Maria: σ-hole interactions: the effect of the donors and acceptors nature in selenoureas, thioureas, halogenated species, substituted benzenes, and their adducts. (72 pp.) 2021. JYU Dissertations 370.
16. Bulatova, Margarita: Noncovalent interactions as a tool for supramolecular self-assembly of metallopolymers. (62 pp.) 2021. JYU Dissertations 377.

17. Romppanen, Sari: Laser-spectroscopic studies of rare earth element- and lithium-bearing minerals and rocks. (66 pp.) 2021. JYU Dissertations 393.
18. Kukkonen, Esa: Nonlinear optical materials through weak interactions and their application in 3D printing. (58 pp.) 2021. JYU Dissertations 441.
19. Kuosmanen, Riikka: The Effect of Structure on the Gel Formation Ability and the Properties of Bile Acid Based Supramolecular Organogels. (68 pp.) 2021. JYU Dissertations 465.
20. Reuna, Sini: Development of a Method for Phosphorus Recovery from Wastewaters. (67 pp.) 2022. JYU Dissertations 486.
21. Taipale, Essi: Synthetic and Structural Studies on the Effect of Non-Covalent Interactions on N(*sp2*)-Heterocyclic Molecules. (67 pp.) 2022. JYU Dissertations 496.
22. Järvinen, Teemu: Molecular Dynamics View on Matrix Isolation. (143 pp.) 2022. JYU Dissertations 544.
23. Kumar, Parveen: Synthesis and Structural Studies on Halogen(I) Complexes. (160 pp.) 2022. JYU Dissertations 549.
24. Forsblom, Samu: Design and Construction of Metal-Organic Polyhedra. (212 pp.) 2022. JYU Dissertations 569.
25. Korpelin, Ville: Computational Studies of Catalytic Active Site Properties and Reactions at the Metal–Oxide Interface. (78 pp.) 2022. JYU Dissertations 578.
26. Vuori, Hannu: Extending Benson Group Increment Theory to Compounds of Phosphorus, Silicon, and Boron with Computational Chemistry. (59 pp.) 2022. JYU Dissertations 581.
27. Pallerla, Rajanish: Studies Towards Synthesis of Favipiravir & Humilisin E. (139 pp.) 2023. JYU Dissertations 611.
28. Taponen, Anni: Radical-Ion Salts based on Thiazyls and Tetracyanoquinodimethane: Hysteretic Magnetic Bistability in a Multicomponent System. (66 pp.) 2023. JYU Dissertations 613.
29. Aho, Noora: Molecular Dynamics Simulations of Acids and Bases in Biomolecular Environments. (78 pp.) 2023. JYU Dissertations 614.
30. Sabooni Asre Hazer, Maryam: Electronic and Optical Properties of Gold Clusters with Carbene Ligands using Density Functional Theory Calculations. (68 pp.) 2023. JYU Dissertations 650.
31. Kinnunen, Virva-Tuuli: Improving the Accuracy of Single Particle ICP-MS Analyses of Au and Ag Nanoparticles. (67 pp.) 2023. JYU Dissertations 689.
32. Kulomäki, Suvi: Preconcentration, Speciation, and Determination of Mercury in Natural Waters by Inductively Coupled Plasma Mass Spectrometry. (61 pp.) 2023. JYU Dissertations 725.
33. Schirmer, Johanna: Effects of Two-Photon Oxidation for the Development of Graphene-Bio Interfaces. (69 pp.) 2023. JYU Dissertations 726.
34. Halmemies, Eelis: Chemical Changes in the Industrial Extractive-Containing Sidestreams of Norway Spruce (*Picea abies*) during Storage. (84 pp.) 2024. JYU Dissertations 737.

35. Alaranta, Johanna: Synthesis of Monomethine Cyanine Dyes and Gold Nanoclusters and their Applications as Fluorescent Probes. (67 pp.) 2024. JYU Dissertations 766.
36. Chevigny, Romain: Out-of-equilibrium and in-equilibrium amino acid-based supramolecular gels: Transient self-assembly and hybrid materials. (79 pp.) 2024. JYU Dissertations 768.
37. Mahajan, Shreya: Exploring the Applicability of Amine-Containing Metal–Organic Frameworks on Direct Air Capture of Carbon Dioxide. (69 pp.) 2024. JYU Dissertations 819.
38. Lehmann, Annika: Experimental and Computational Studies of Reactive Main Group Species: Low-Coordinate Complexes, Multiple Bonding, and Hydrometallation. (65 pp.) 2024. JYU Dissertations 829.
39. Lempelto, Aku: Computational modelling of carbon dioxide reduction to methanol on heterogeneous zirconia-supported copper catalysts. (78 pp.) 2024. JYU Dissertations 839.
40. Sokolovskii, Ilia: Multiscale Molecular Dynamics Simulations of Enhanced Excitation Energy Transport in Organic Microcavities. (82 pp.) 2024. JYU Dissertations 844.
41. Pamula, Malgorzata: Diverse roles of noncovalent interactions in supramolecular systems based on resorcinarenes and calix[4]pyrroles. (92 pp.) 2024. JYU Dissertations 851.